UNIVERSITY OF CALIFORNIA SAN DIEGO

Channel Estimation for Massive MIMO Systems Based on Sparse Representation and Sparse Signal Recovery

A dissertation submitted in partial satisfaction of the
requirements for the degree
Doctor of Philosophy

in

Electrical Engineering
(Communication Theory and Systems)

by

Yacong Ding

Committee in charge:

Professor Bhaskar D. Rao, Chair
Professor Sanjoy Dasgupta
Professor William S. Hodgkiss
Professor Ken Kreutz-Delgado
Professor Laurence B. Milstein

2018

The dissertation of Yacong Ding is approved, and it is acceptable in quality and form for publication on microfilm and electronically:

Chair

University of California San Diego

2018

DEDICATION

To my family.

TABLE OF CONTENTS

LIST OF FIGURES

LIST OF TABLES

ACKNOWLEDGEMENTS

First and foremost, I am greatly indebted to my advisor, Professor Bhaskar D. Rao, for his patience and encouragement at the beginning of my PhD study, and for his support and guidance during my exploration of new research topics. I deeply thank him for introducing me into the fields of wireless communication and sparse signal recovery, based on which this dissertation is developed. I would also like to thank him for always believing in me, which helps me to build the confidence to overcome difficulties and achieve higher goals in the research.

I would like to thank Prof. Sanjoy Dasgupta, Prof. William S. Hodgkiss, Prof. Ken Kreutz-Delgado, and Prof. Laurence B. Milstein for serving on my committee. I have learned a lot from their lectures and their feedback during my PhD progress. Also, I would like to thank Prof. Robert Lugannani, Prof. Gert Lanckriet, Prof. Alon Orlitsky, Prof. Piya Pal, Prof. Paul H. Siegel, Prof. Lawrence K. Saul, Prof. Rayan Saab, Prof. Mohan M. Trivedi and Prof. Nuno M. Vasconcelos, from whom I have taken or audited classes. What I have learned in those courses have laid the foundation for my research and would continue to benefit me in the future.

I would like to express my thanks to my collaborators in UCSD DSP Lab, Sung-En Chiu, Yonghee Han, and Jing Liu. I have gained many helpful suggestions and insights from the discussion with them. I am also thankful to other former and current colleagues at UCSD DSP Lab, Yichao Huang, Zhilin Zhang, Sheu-Sheu Tan, Nandan Das, Eddy Kwon, Anh Nguyen, PhuongBang Nguyen, Furkan Kovasoglu, Ritwik Giri, Elina Nayebi, David Ho, Maher Al-Shoukairi, Igor Fedorov, Alican Nalci, Govind Gopal, Richard Bell, and Tharun Srikrishnan. Their kindness and friendship make the UCSD DSP Lab a wonderful place to work in.

During my PhD study, I am fortunate to be supported by Dr. Huang Memorial Scholarship at UCSD, National Science Foundation under Grant CCF-1617365, King Abdulaziz City for Science and Technology, and Center for Wireless Communications at UCSD.

Many thanks to my supervisor, Dr. Kyeong Jin Kim, and other colleagues, Dr. Toshiaki Koike-Akino, Dr. Milutin Pajovic, Dr. Pu Wang, Dr. Philip Orlik, and Dr. Chen Feng, during my

internship at Mitsubishi Electric Research Laboratories. I would also like to thank Dr. Scott R. Velazquez for supervising me during my internship at Innovation Digital, LLC. I am thankful to my supervisors and other colleagues for providing me a lot of help during my internships.

I would like to thank my friends, who have made my time in San Diego a most enjoyable experience, including Bing Fan, Shiyang Gao, Xueshi Hou, Pengfei Huang, Yihan Jiang, Han Li, Xing Li, Yao Liu, Yao Lu, Weiheng Ni, Jiechun Sun, Zhongen Tao, Jiance Tong, Peizhi Wu, Xichang Wu, Xiang Xu, Bentao Zhang, and Chicheng Zhang.

Finally, I want to thank my mother, Guangqin Zhang, and my father, Qihong Ding, for their endless love and unconditional support. I also want to thank my beloved wife, Shunan Qiao, for her love and company. This dissertation is dedicated to them.

Chapter 2, in part, is a reprint of the material as it appears in the paper: Y. Ding and B. D. Rao, "Dictionary learning-based sparse channel representation and estimation for FDD massive MIMO systems," *IEEE Trans. Wireless Commun.*, in press. The dissertation author was the primary investigator and author of this paper.

Chapter 3, in part, is a reprint of the material as it appears in the papers: Y. Ding and B. D. Rao, "Compressed downlink channel estimation based on dictionary learning in FDD massive MIMO systems," In *Proc. IEEE Global Commun. Conf. (GLOBECOM)*, Dec. 2015, pp. 1-6, Y. Ding and B. D. Rao, "Channel estimation using joint dictionary learning in FDD massive MIMO systems," In *Proc. IEEE Glob. Conf. Signal Inf. Process. (GlobalSIP)* , Dec. 2015, pp. 185-189, and Y. Ding and B. D. Rao, "Dictionary learning-based sparse channel representation and estimation for FDD massive MIMO systems," *IEEE Trans. Wireless Commun.*, in press. The dissertation author was the primary investigator and author of these papers.

Chapter 4, in part, is a reprint of the material as it appears in the paper: Y. Ding, S. Chiu, and B. D. Rao, "Bayesian channel estimation algorithms for massive MIMO systems with hybrid analog-digital processing and low resolution ADCs," *IEEE J. Sel. Topics Signal Process.*, vol. 12, no. 3, pp. 499-513, June 2018. The dissertation author was the primary investigator and author of this paper.

Chapter 5, in part is currently being prepared for submission for publication of the material. The dissertation author was the primary investigator and author of this material, and Bhaskar D. Rao supervised the research.

VITA

2012	Bachelor of Engineering, Xiamen University, China
2015	Master of Science, University of California San Diego
2018	Doctor of Philosophy, University of California San Diego

PUBLICATIONS

Y. Ding and B. D. Rao, “Dictionary learning-based sparse channel representation and estimation for FDD massive MIMO systems,” *IEEE Trans. Wireless Commun.*, in press.

Y. Ding, S. Chiu, and B. D. Rao, “Bayesian channel estimation algorithms for massive MIMO systems with hybrid analog-digital processing and low resolution ADCs,” *IEEE J. Sel. Topics Signal Process.*, vol. 12, no. 3, pp. 499-513, June 2018.

Y. Ding, S. Chiu, and B. D. Rao, “Sparse recovery with quantized multiple measurement vectors,” In *Proc. 51st Asilomar Conf. Signals Syst. Comput.*, Oct. 2017, pp. 845-849.

J. W. Choi, B. Shim, Y. Ding, B. D. Rao, and D. I. Kim, “Compressed sensing for wireless communications: Useful tips and tricks,” *IEEE Commun. Surveys Tuts.*, vol. 19, no. 3, pp. 1527-1550, Feb. 2017.

Y. Ding and B. D. Rao, “Channel estimation using joint dictionary learning in FDD massive MIMO systems,” In *Proc. IEEE Glob. Conf. Signal Inf. Process. (GlobalSIP)* , Dec. 2015, pp. 185-189.

Y. Ding and B. D. Rao, “Compressed downlink channel estimation based on dictionary learning in FDD massive MIMO systems,” In *Proc. IEEE Global Commun. Conf. (GLOBECOM)*, Dec. 2015, pp. 1-6.

Y. Ding and B. D. Rao, “Joint dictionary learning and recovery algorithms in a jointly sparse framework,” In *Proc. 49th Asilomar Conf. Signals Syst. Comput.*, Nov. 2015, pp. 1482-1486.

J. Liu, Y. Ding, B. D. Rao, “Sparse Bayesian learning for robust PCA,” Submitted.

S. Alzeer, S. Almatrudi, H. A. Bukhari, Y. Han, Y. Ding, B. D. Rao, “Millimeter wave channel estimation using data-aided DoA estimation,” Submitted.

Y. Ding, K. J. Kim, T. Koike-Akino, M. Pajovic, P. Wang, and P. Orlik, “Spatial scattering modulation for uplink millimeter-wave systems,” *IEEE Commun. Lett.*, vol. 21, no. 7, pp. 1493-1496, July 2017.

Y. Ding, K. J. Kim, T. Koike-Akino, M. Pajovic, P. Wang, and P. Orlik, “Millimeter wave adaptive transmission using spatial scattering modulation,” In *Proc. IEEE Int. Conf. on Commun. (ICC)*, May 2017, pp. 1-6.

ABSTRACT OF THE DISSERTATION

Channel Estimation for Massive MIMO Systems Based on Sparse Representation and Sparse Signal Recovery

by

Yacong Ding

Doctor of Philosophy in Electrical Engineering
(Communication Theory and Systems)

University of California San Diego, 2018

Professor Bhaskar D. Rao, Chair

Massive multiple-input multiple-output (MIMO) is a promising technology for next generation communication systems, where the base station (BS) is equipped with a large number of antenna elements to serve multiple user equipments. With the large number of antenna elements, the BS can perform multi-user beamforming with much narrower beamwidth, thereby simultaneously serving more users with less interference among them. Furthermore, the large antenna array results in large array gain which lowers the radiated energy. However, efficient beamforming relies on the availability of channel state information at the BS. In a frequency-division duplexing massive MIMO system, the channel estimation is challenging due to the need to estimate a high dimensional unknown channel vector, which requires large training and feedback overhead for the conventional channel estimation algorithms. Moreover, massive MIMO system with fully digital architecture, where a dedicated radio frequency chain and a high-resolution analog-to-digital converter (ADC) are connected to each antenna element, will cause too much power and hardware cost as the size of the antenna array becomes large.

To reduce the training and feedback overhead, compressive sensing methods and sparse recovery algorithms are proposed to robustly estimate the downlink and uplink channel by exploiting the sparse representation of the massive MIMO channel. Previous works model this sparse representation by some predefined matrix, while in this dissertation, a dictionary learning based channel model is proposed which learns an efficient and robust representation from the data. Furthermore, a joint uplink/downlink dictionary learning framework is proposed by observing the reciprocity between the angle of arrival in uplink and the angel of departure in downlink, which enables a joint channel estimation algorithm. To save the power and hardware cost, a hardware-efficient architecture which contains both hybrid analog-digital processing and low-resolution ADCs is proposed. This hardware-efficient architecture poses significant challenges to channel estimation due to the reduced dimension and precision of the measured signal. To address the problem, the sparse nature of the channel is exploited and the transmitted data symbols are utilized as the virtual pilots, both of which are treated in a unified Bayesian formulation. We formulate the channel estimation into a quantized compressive sensing problem utilizing the sparse Bayesian learning framework, and develop a variational Bayesian algorithm for inference. The performance of the compressive sensing can be further improved by applying a well structured sensing matrix, and we propose a sensing matrix design algorithm which can exploit the partial knowledge of the support.

Chapter 1

Introduction

1.1 Massive MIMO Systems

Massive multiple-input multiple-output (MIMO) systems have been considered as a key technology for the next generation wireless communication system, which scale up MIMO by possibly orders of magnitude compared to the current state of the art. As shown in Fig. 1.1, in a massive MIMO system, the base station (BS) is equipped with a large antenna array and simultaneously serves multiple user equipments (UEs) in the same time-frequency resource, enabling significant gains in the capacity and the energy efficiency. With the large number of antenna elements, the BS can perform multi-user beamforming with much narrower beamwidth, thereby serving more UEs with less interference among them. Moreover, a large antenna array also leads to larger antenna gains. In Fig. 1.2, we compare the beampattern of the uniform linear array (ULA) with different number of antennas, all pointing to the array broadside. It can be clearly seen from the plot that as the number of antenna elements increases, the beamwidth becomes narrower and the beamforming gain becomes larger. As a result, the BS can focus the power towards the desired direction and reduce the interference to other directions, leading to an increase in the capacity (by spatial multiplexing) and energy efficiency (by energy concentration).

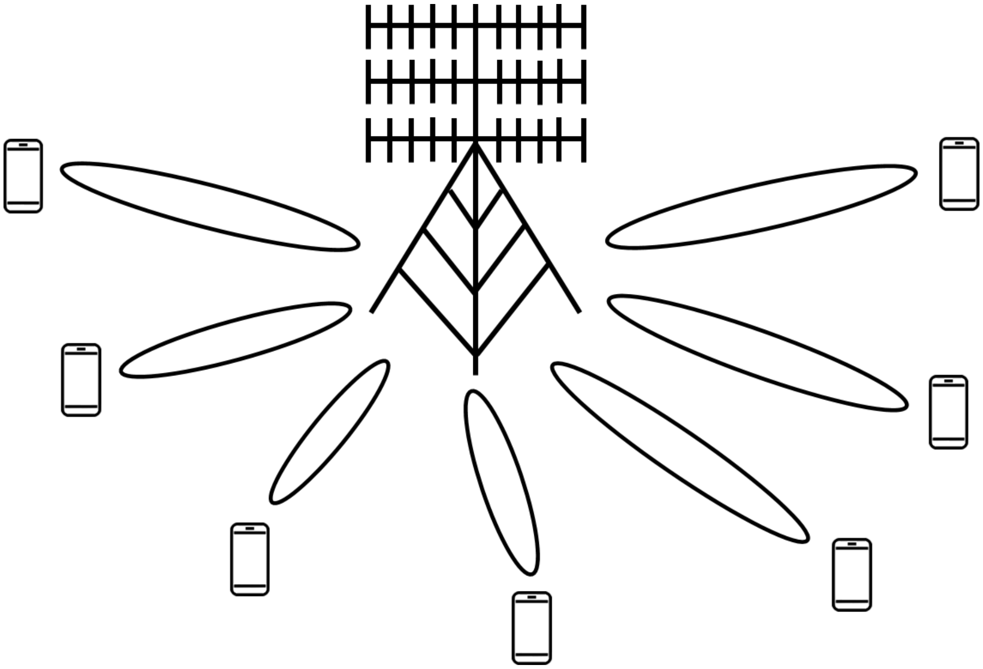

Figure 1.1: A typical illustration of a massive MIMO system.

Many other benefits of massive MIMO have been shown in the literature [1, 2], e.g., massive MIMO can be built with inexpensive and low-power components, the large antenna array in the massive MIMO system provides a large surplus of degree of freedoms, and the massive MIMO increases the robustness against both unintended man-made interference and intentional jamming.

However, efficient beamforming relies on the availability of channel state information (CSI) at the BS for both the uplink and the downlink. To obtain the uplink channel, the UEs transmit the pilot symbols and the BS perform the channel estimation. Since the channel is estimated at the BS, there is no feedback needed. On the other hand, to estimate the downlink channel, the BS sends out pilot symbols, and the downlink channel is estimated at UEs and then fed back to the BS. For the optimal downlink channel estimation, the pilots should be mutually orthogonal between the antennas, which means that the number of pilots scales with the number of antennas at the BS. Moreover, each UE needs to feed back the estimated channel information to the BS, so the feedback overhead is also proportional to the number of antennas. In a massive MIMO system, the number of antennas is large, implying a large training and feedback

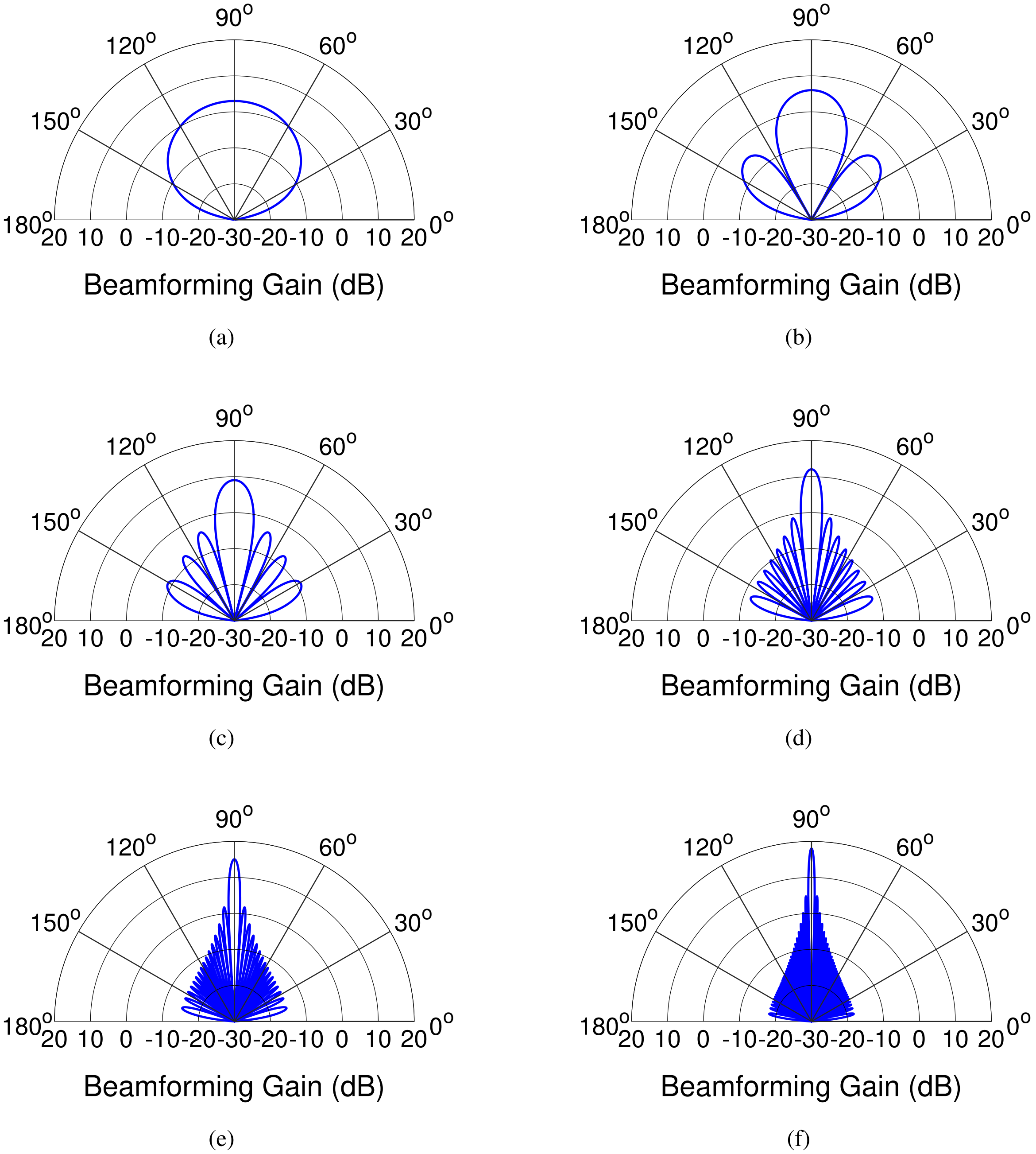

Figure 1.2: Beampattern comparison for uniform linear array with different number of antennas. (a) 2 antennas. (b) 4 antenna. (c) 8 antenna. (d) 16 antenna. (e) 32 antenna. (f) 64 antennas.

overhead. Furthermore, the downlink training and feedback have to be performed within the coherence time of the channel. As a result, the downlink channel estimation is very challenging in a massive MIMO system, especially with limited coherence time. On the contrary, uplink channel estimation is relatively easy since typically the UE is assumed to have a single antenna or very small number of antennas, so the training overhead for the uplink channel estimation only scales with the number of UEs, which is assumed to be much smaller than the number of antennas at the BS. Moreover, there is no feedback overhead since the channel estimation is performed at the BS.

Due to the challenges of downlink channel estimation, massive MIMO systems are assumed to be operated in time-division duplexing (TDD) mode [1, 2], where the reciprocity between the uplink and downlink channels is assumed. Therefore, only the uplink channel is estimated at the BS, and the estimated channel response is directly applied for the downlink beamforming, so the difficult downlink channel estimation can be completely avoided. However, many current networks are operating in frequency-division duplexing (FDD) mode where the uplink and the downlink use different frequency band, so the channel reciprocity between the uplink and downlink is no longer valid and the downlink training and feedback are required, imposing big challenges to the use of massive MIMO in a FDD system. With respect to the wide deployment of the FDD system, the adoption of the massive MIMO would be much faster if the downlink channel can be efficiently estimated. This dissertation will shed some light on this direction by utilizing the sparse structure of the massive MIMO channel to reduce the training and feedback overhead in the downlink channel estimation.

In a conventional MIMO system, fully digital architecture is assumed where each antenna is equipped with a dedicated RF chain. Furthermore, a high-resolution analog-to-digital converter (ADC) is typically used to transform the signal from the analog domain to the digital domain for baseband processing. In a massive MIMO system, utilizing fully digital architecture and high-resolution ADCs would incur a large power and hardware cost, since the number of RF chains and the high-resolution ADCs would scale up with the number of antennas. To deal with the problem, one option is to apply hybrid analog-digital (AD) processing, where only a limited number of RF chains are used and each RF chain is connected to antennas through a group of phase shifters [3], so the total number of RF chains is no longer scaling with the number of antennas. Another option is to replace high-resolution ADCs with low-resolution ADCs [4], which can greatly reduce the power consumption. However, despite their hardware effectiveness, such architectures also pose significant challenges to the channel estimation due to the reduced dimension and precision of the received signal. In this dissertation, a hardware-efficient architecture is proposed which combines both the hybrid AD processing and the low-resolution ADCs, and a Bayesian channel estimation algorithm is developed to deal with the challenges posed by the hardware constraints.

1.2 Compressive Sensing

Compressive sensing, or more generally speaking, sparse signal recovery, is a powerful technique which utilizes the sparse structure of the signal to reduce the number of measurements that is required to robustly estimate the signal. More specifically, when the signal can be sparsely represented in some basis or dictionary, which we call the sparsifying matrix, the number of measurements required to robustly estimate the signal no longer scales with the ambient dimension of the signal, but only scales with the sparsity level of the corresponding representation, if some conditions on the measurement matrix and the sparsity level are satisfied. Moreover, such recovery process can be performed using some convex optimization algorithms, or other highly efficient algorithms. Over the past two decades, many theoretical results as well as practical algorithms have been developed to show what performance can be achieved by compressive sensing and sparse recovery methods, how to achieve that performance, and they have been successfully applied in many different areas. Readers are referred to interesting tutorial papers [5,6] and useful books [7–9] for more details. In the following, we will briefly review the basic concept of the compressive sensing in a setup related to our specific channel estimation problem.

Denote the interested signal as $\boldsymbol{x} \in \mathbb{C}^{N\times 1}$, and the measurement matrix as $\boldsymbol{A} \in \mathbb{C}^{T\times N}$. Each measurement is performed by correlating one row of $\boldsymbol{A}$ with the signal $\boldsymbol{x}$. After performing

T such measurements, the measured signal is given by

$$\boldsymbol{y} = \boldsymbol{A}\boldsymbol{x} + \boldsymbol{n} \tag{1.1}$$

where $\boldsymbol{n} \in \mathbb{C}^{T\times 1}$ denotes the measurement noise. Given $\boldsymbol{y}$ and $\boldsymbol{A}$, the goal is to robustly estimate $\boldsymbol{x}$. Notice that $\boldsymbol{x}$ is an N dimensional signal and the number of measurements is T. Even without the measurement noise $\boldsymbol{n}$, it is required that $T \geq N$ such that (1.1) has a unique solution for $\boldsymbol{x}$. In other words, the number of measurements required to estimate the signal scales with the dimension of the signal. For a high-dimensional signal $\boldsymbol{x}$, the required number of measurements is also large, which is impractical for many applications.

However, in practice, many high-dimensional signal actually resides in a low-dimensional space, and there exists some basis or dictionary on which the high dimensional signal can be much more efficiently represented. Assume there is a sparsifying matrix $\boldsymbol{D} \in \mathbb{C}^{N\times M}$ such that $\boldsymbol{x} = \boldsymbol{D}\boldsymbol{\beta}$, where the coefficient vector $\boldsymbol{\beta}$ satisfies $||\boldsymbol{\beta}||_0 = s \ll N$. Here the ℓ_0 norm $||\boldsymbol{\beta}||_0$ denotes the number of nonzero elements in $\boldsymbol{\beta}$. The measurement scheme in (1.1) can then be written as

$$\boldsymbol{y} = \boldsymbol{A}\boldsymbol{x} + \boldsymbol{n} = \boldsymbol{A}\boldsymbol{D}\boldsymbol{\beta} + \boldsymbol{n}, \tag{1.2}$$

and now the goal is to estimate $\boldsymbol{\beta}$ given the knowledge of $\boldsymbol{y}$, $\boldsymbol{A}$ and $\boldsymbol{D}$. Notice that if the locations of nonzero elements in $\boldsymbol{\beta}$ are known, then based on the same arguments as before the required number of measurements is $T \geq s$. Compared to $T \geq N$, the number of measurements is greatly reduced if s is much less than N, and it only scales with the underlying sparsity level of the signal rather than the ambient dimension of the signal.

The requirements of knowing the sparsity level s and the locations of s nonzero elements in $\boldsymbol{\beta}$ are hard to satisfy in practical applications, since they depend on the specific unknown signal $\boldsymbol{x}$. But with the prior knowledge that $\boldsymbol{\beta}$ is sparse, i.e., $s = ||\boldsymbol{\beta}||_0$ is small, the problem in (1.2) can be regularized such that we aim to find the sparsest representation of $\boldsymbol{x}$ that is consistent with the measurement $\boldsymbol{y}$ by solving the following problem

$$\arg\min_{\boldsymbol{\beta}} \|\boldsymbol{\beta}\|_0 \quad \text{s.t.} \quad \|\boldsymbol{y} - \boldsymbol{A}\boldsymbol{D}\boldsymbol{\beta}\|_2 \leq \epsilon \tag{1.3}$$

where ϵ is the parameter that bounds the energy in the measurement noise. Notice that the ℓ_0 norm is not a convex function, so solving (1.3) is very difficult. One has to exhaustively enumerate all $\binom{M}{k}$ possible locations of nonzero elements in $\boldsymbol{\beta}$, starting with $k = 1$ and increasing k by 1 if no solution is found. The complexity is prohibitive even for a moderate problem size. Fortunately, many practical algorithms have been proposed to approximately solve the problem, and we briefly list several types of algorithms which are commonly used in practice:

- Greedy algorithms: orthogonal matching pursuit (OMP) [10] and compressive sampling matching pursuit (CoSaMP) [11].

- Convex relaxation algorithms: basis pursuit (BP) [12] and fast iterative shrinkage-thresholding algorithm (FISTA) [13].

- Iteratively re-weighted algorithms: reweighted ℓ_1 algorithm [14], reweighted ℓ_2 algorithm [15] and focal underdetermined system solver (FOCUSS) [16].

- Graphical model based algorithms: approximated message passing (AMP) [17] and generalized approximated message passing (GAMP) [18].

- Bayesian algorithms: relevance vector machine (RVM) [19], sparse Bayesian learning (SBL) [20, 21], and other Bayesian-based algorithms [22, 23].

Besides the algorithms listed above, there are many other algorithms [7–9]. Each algorithm has its own advantages and disadvantages in terms of performance guarantee, complexity, and recovery accuracy. In practice, trade-offs among those factors have to be made in order to choose the appropriate algorithm.

In addition to those practical algorithms, many theoretical results have been developed to provide conditions on the equivalent sensing matrix $\mathbf{\Phi} = \boldsymbol{AD}$ and the sparsity level of $\boldsymbol{\beta}$, such that the problem in (1.3) (or its convex relaxation form by replacing $\|\boldsymbol{\beta}\|_0$ with $\|\boldsymbol{\beta}\|_1$) can be solved. Generally speaking, the columns of $\mathbf{\Phi}$ are expected to be as incoherent as possible, since two highly correlated columns would mislead any recovery algorithms. Many useful measures, such as mutual coherence [7], Spark [24], null space property (NSP) [8] and restricted isometry property (RIP) [25], have been proposed to describe the incoherent property of $\mathbf{\Phi}$. And based on those measures, the conditions imposed on the sparsity level s are provided to indicate when specific algorithm can succeed, revealing (either explicitly or implicitly) the relationship between the number of measurements T and the sparsity level s. One of the most notable results is that, when specific conditions on $\mathbf{\Phi}$ and s are satisfied, the required number of measurements T to obtain a robust estimate of $\boldsymbol{\beta}$ is only proportional to the sparsity level s rather than the signal dimension N [6]. So when the signal is very sparse, i.e., $s \ll N$, the required number of measurements can be greatly reduced. This result shows the advantage of exploring the sparse representation of the signal and applying compressive sensing algorithms to estimate the signal, in terms of reducing the number of measurements.

1.3 Dissertation Overview

This dissertation is organized as follows.

In Chapter 2, we present the massive MIMO system model and formulate the channel estimation problem for both the downlink and the uplink. For the downlink, we discuss the challenges of using conventional channel estimation algorithm due to the large training and feedback overhead that scale with the number of antennas at the BS. Then we utilize the compressive sensing-based channel estimation which exploits the sparse structure of the massive MIMO channel to reduce the number of pilots. For the uplink, we show the benefit of utilizing the channel sparse structure and propose sparse recovery-based channel estimation. With this new formulation, robust channel estimate can be obtained with number of uplink pilots less than the number of UEs, which is an underdetermined problem if one is using a conventional channel estimation algorithm. A well structured sensing matrix can improve the performance of the sparse recovery-based uplink channel estimation, indicating the importance of pilots design and user scheduling.

In Chapter 3, we propose the dictionary learning-based channel model which learns an efficient and robust channel representation from collected measurements. Compared to the predefined sparsifying matrix, the learned dictionary leads to a more sparse channel representation and is robust to any antenna uncertainties, which in turn can improve the performance of compressive sensing-based channel estimation. Then we generalize the downlink sparse channel model to a joint uplink/downlink sparse channel model based on joint uplink/downlink dictionary learning. We discuss the motivation and present the optimization problem. A joint uplink/downlink channel estimation algorithm is proposed by utilizing the jointly learned dictionaries, which further improves the performance compared to the downlink only channel estimation.

In Chapter 4, we consider the hardware-efficient architecture which applies both hybrid analog-digital processing and low-resolution ADCs. Although this architecture can reduce the hardware cost and power consumption, it also makes channel estimation challenging due to the reduced number of measurements and the high quantization error in each measurement. We formulate the channel estimation problem utilizing the sparse structure of the massive MIMO channel, so the required number of measurements is decreased. Furthermore, part of the transmitted data is jointly estimated with the channel, acting as the virtual pilots to improve the channel estimation accuracy. We formulate the problem in a sparse Bayesian learning framework, and apply the variational Bayesian method to solve the problem.

In Chapter 5, we study the sensing matrix design problem in compressive sensing, where partial knowledge of support is assumed. When the signal can be sparsely represented using an overcomplete dictionary, a carefully designed sensing matrix can improve the performance of compressive sensing algorithms. In this dissertation, we further assume the partial knowledge of the support, and propose an algorithm to utilize such knowledge for sensing matrix design. Simulation results show better recovery performance of the proposed algorithm compared to previous sensing matrix design algorithms. The algorithm proposed in this chapter can be used to design the pilots in the massive MIMO system, since the supports of the transformed domain channel in two consecutive blocks of coherence time are similar when the channel changes slowly. As a result, partial knowledge of the support of the transformed domain channel in the current block of coherence time can be obtained from the estimated channel in the previous block of coherence time. Therefore, better pilots can be designed using the proposed algorithm when the compressive sensing method is applied for channel estimation.

Chapter 2

Channel Estimation Utilizing Sparse Channel Structure

Massive multiple-input multiple-output (MIMO) is a promising technology for next generation communication systems, which can achieve significant gains in the capacity and the energy efficiency by performing multi-user beamforming. However, efficient beamforming relies on the availability of channel state information at the BS. In a frequency-division duplexing massive MIMO system, the channel estimation is challenging due to the need to estimate a high dimensional unknown channel vector, which requires large training and feedback overhead when conventional channel estimation algorithms are used. Furthermore, the channel coherence time may make the feedback delay unacceptably high. In this chapter, the compressive sensing and sparse recovery algorithms are used to robustly estimate the downlink and uplink channel with reduced overhead. We illustrate the intuition behind the sparse channel structure for massive MIMO system, and utilize such structure for efficient channel estimation.

2.1 Introduction

Massive multiple-input multiple-output (MIMO) systems have been proposed for the next generation of communication systems [1, 2]. By deploying a large antenna array at the base station (BS), both receive combining and transmit beamforming can be performed with narrow beams, thereby eliminating multiuser interference and increasing the cell throughput. For effective uplink (UL) combining and downlink (DL) precoding, it is essential to have accurate knowledge of the channel state information (CSI) at BS. The common assumption in massive MIMO is that each user equipment (UE) only has a small number of antennas, therefore it is relatively easy to have the uplink CSI since the uplink training overhead is only proportional to the number of users [26]. In a time-division duplexing (TDD) system, downlink CSI can also be easily obtained by exploiting the uplink/downlink channel reciprocity. On the other hand, channel reciprocity is no longer valid in a frequency-division duplexing (FDD) system because the uplink and downlink transmission are operated at different frequencies. In order to have downlink CSI, the BS has to perform downlink training. Subsequently, the user needs to estimate, quantize and feedback the channel state information. When conventional channel estimation and feedback schemes are used, the downlink training and feedback overhead are proportional to the number of antennas at the base station. The large antenna array in the massive MIMO system makes such training impractical due to the high overhead and infeasible when the coherence time of the channel is limited. However, since FDD system is generally considered to be more effective for systems with symmetric traffic and delay-sensitive applications, most cellular systems today employ FDD [27, 28]. And the adopt of massive MIMO system would be much faster if the large antenna array can also be applied in current FDD system.

To alleviate the overhead of downlink channel training and feedback in a FDD massive MIMO system, one option is to explore possible underlying channel structure whereby the high dimensional channel vector has a low dimensional representation [27–29]. Motivated by the framework of compressive sensing (CS), if the desired signal (channel response) can be sparsely represented in some basis or dictionary, then it can be robustly recovered with the number of measurements (downlink pilot symbols) only proportional to the number of nonzero entries in the representation [6]. This indicates that when such basis or dictionary does exist and leads to a very sparse representation, we are able to greatly reduce the downlink training overhead. Fortunately, the limited scattering environment implies the low dimensionality of the channel, and the large antenna array provides finer angular resolution to resolve the limited scattering and represent channel sparsely [30, 31]. Many previous works have proposed efficient downlink channel estimation and feedback algorithms based on this sparse assumption [27–29, 32]. Besides the downlink channel estimation, we further formulate the uplink channel estimation explicitly into a sparse recovery problem. Although the compressive sensing formulation has been applied widely in the downlink channel estimation, utilizing sparse property for the uplink has only received limited attention [33, 34]. We show that with both appropriate pilots design and non-overlapping (or limited overlapping in practice) sparse supports of users, good estimation accuracy can be achieved even with pilot symbols *less* than the number of users, which is the underdetermined case for the conventional least square channel estimation.

The chapter is organized as follows. In Section 2.2, we introduce the system model. In Section 2.3, we review the conventional channel estimation algorithms. The compressive sensing-based downlink channel estimation algorithm is provided in Section 2.4, and we develop the sparse recovery-based uplink channel estimation algorithm in Section 2.5. The chapter is concluded in Section 2.6

Notations used in this chapter are as follows. Upper (lower) bold face letters are used throughout to denote matrices (column vectors). $(\cdot)^T$, $(\cdot)^H$ $(\cdot)^\dagger$ denotes the transpose, Hermitian transpose, and the Moore-Penrose pseudo-inverse. $\boldsymbol{A}_{i\cdot}$ and $\boldsymbol{A}_{\cdot j}$ represents the i-th row and j-th column of $\boldsymbol{A}$, and for a set $\mathcal{S}$ we denote $\boldsymbol{A}_{\mathcal{S}}$ to be the submatrix of $\boldsymbol{A}$ that contains columns indexed by elements of $\mathcal{S}$. For a vector $\boldsymbol{x}$, $\text{diag}(\boldsymbol{x})$ is a diagonal matrix with entries of $\boldsymbol{x}$ along its diagonal. $\|\boldsymbol{x}\|_1, \|\boldsymbol{x}\|_2$ denotes the ℓ_1 and ℓ_2 norm. $\|\boldsymbol{x}\|_0$ represents the number of nonzero entries in $\boldsymbol{x}$ and is referred to as the ℓ_0 norm. $\mathrm{supp}(\boldsymbol{x})$ denotes the set of indices such that the corresponding entries of $\boldsymbol{x}$ are nonzero.

2.2 System Model

We consider a single cell massive MIMO system operated in FDD mode. The BS is equipped with N antennas and each UE has a single antenna. Assume a narrowband block fading channel, we adopt a simplified spatial channel model which captures the physical propagation structure of the uplink and the downlink transmission as

$$\begin{aligned} \boldsymbol{h}^u &= \sum_{i=1}^{N_c} \sum_{l=1}^{N_s} \alpha_{il}^u \boldsymbol{a}^u(\Omega_{il}^u) \\ \boldsymbol{h}^d &= \sum_{i=1}^{N_c} \sum_{l=1}^{N_s} \alpha_{il}^d \boldsymbol{a}^d(\Omega_{il}^d) \end{aligned} \tag{2.1}$$

where the superscript u and d denotes the uplink and downlink. N_c is the number of scattering clusters, each of which contains N_s propagation subpaths. α_{il}^u and α_{il}^d are the complex gains of the l-th subpath in the i-th scattering cluster for the uplink and downlink. For 2D channel model [30, 31, 35], $\Omega_{il}^u = \{\theta_{il}^u\}$ denotes the angle of arrival (AOA) for the uplink transmission and $\Omega_{il}^d = \{\theta_{il}^d\}$ is angle of departure (AOD) for the downlink. $\boldsymbol{a}^u(\Omega_{il}^u)$ and $\boldsymbol{a}^d(\Omega_{il}^d)$ are the array response vectors for the uplink and downlink, and for a uniform linear array (ULA)

$$\begin{aligned} \boldsymbol{a}^u(\theta) &= [1, e^{j2\pi \frac{d}{\lambda^u} \sin(\theta)}, \dots, e^{j2\pi \frac{d}{\lambda^u} \sin(\theta) \cdot (N-1)}]^T \\ \boldsymbol{a}^d(\theta) &= [1, e^{j2\pi \frac{d}{\lambda^d} \sin(\theta)}, \dots, e^{j2\pi \frac{d}{\lambda^d} \sin(\theta) \cdot (N-1)}]^T \end{aligned} \tag{2.2}$$

where d is the antenna spacing and λ^u (λ^d) is the wavelength of uplink (downlink) propagation. For 3D channel model [36, 37], $\Omega_{il}^u = \{\theta_{il}^u, \phi_{il}^u\}$, $\Omega_{il}^d = \{\theta_{il}^d, \phi_{il}^d\}$, where $\theta_{il}^u, \phi_{il}^u$ are zenith angle of arrival (ZOA) and azimuth angle of arrival (AOA) for the uplink, and $\theta^d_{il}, \phi^d_{il}$ are zenith angle of departure (ZOD) and azimuth angle of departure (AOD) for the downlink. For a uniform rectangular array (URA) with N_1 vertical antennas spaced by d_1 and N_2 horizontal antennas with d_2 spacing, $N_1 N_2 = N$, the array response vectors is given as [36]

$$\begin{aligned} \boldsymbol{a}^u(\theta, \phi) &= \boldsymbol{q}(v^u) \otimes \boldsymbol{p}(w^u) \\ \boldsymbol{a}^d(\theta, \phi) &= \boldsymbol{q}(v^d) \otimes \boldsymbol{p}(w^d) \end{aligned} \tag{2.3}$$

where we have

$$\begin{aligned} \boldsymbol{p}(w) &= [1, e^{jw}, \dots, e^{j(N_1-1)w}]^T \\ \boldsymbol{q}(v) &= [1, e^{jv}, \dots, e^{j(N_2-1)v}]^T \end{aligned} \tag{2.4}$$

and $w^u = 2\pi d_1 \text{cos}(\theta)/\lambda^u$, $w^d = 2\pi d_1 \text{cos}(\theta)/\lambda^d$, $v^u = 2\pi d_2 \text{sin}(\theta)\text{cos}(\phi)/\lambda^u$, and $v^d = 2\pi d_2 \text{sin}(\theta)\text{cos}(\phi)/\lambda^d$.

In order to model the scattering clusters, we consider the principles of *Geometry-Based Stochastic Channel Model* (GSCM) [38], as illustrated in Fig. 2.1. For a specific cell, the locations of the dominant scattering clusters are determined by cell specific attributes such as the buildings, and are common to all the users irrespective of user position. We assume such scattering clusters are far away from the base station, so the subpaths associated with a specific scattering cluster will be concentrated in a small range, i.e., having a small angular spread (AS). While modeling the scattering effects which are user-location dependent, for example the ground reflection close to the user, or some moving physical scatterers near the user, we assume the UE is far away from the base station, so subpaths associated with the user-location dependent scattering cluster also have small angular spread. Since the BS is far away and is commonly assumed to be mounted at a height, the number of scattering clusters that contribute to the channel responses is limited, i.e., N_c is small. Because the number of scattering clusters is limited and each of them spans a small AS, there are only limited dimensions being occupied when viewed from the angular domain. Furthermore, the large antenna array at the BS leads to narrower beamwidth, resulting in smaller

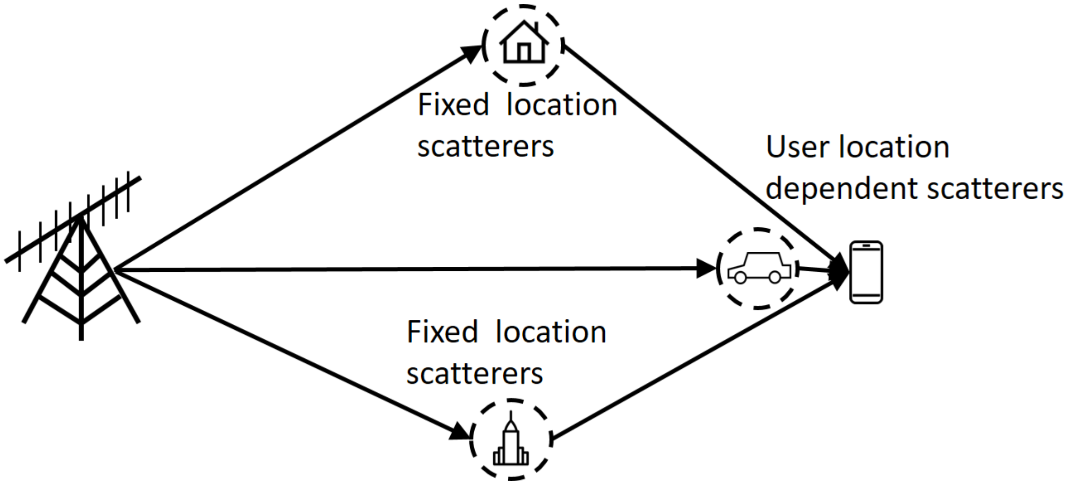
Fixed location scatterers
User location dependent scatterers
Fixed location scatterers

Figure 2.1: Illustration of signal propagation in a typical cell

leakage effect of some scattering cluster to the other angular bins. Due to the limited scattering effect and the large antenna array, it is reasonable to assume a low dimensional representation for the large massive MIMO channel [27–29, 32].

2.3 Conventional Channel Estimation

For the downlink channel estimation in FDD system, the BS transmits training pilots. The UE estimates the channel and feed back the channel state information to the BS. The received signal $\boldsymbol{y}^d$ at the UE is given as

$$\boldsymbol{y}^d = \boldsymbol{A}\boldsymbol{h}^d + \boldsymbol{w}^d \tag{2.5}$$

where $\boldsymbol{h}^d \in \mathbb{C}^{N\times 1}$ denotes the downlink channel response, $\boldsymbol{w}^d \in \mathbb{C}^{T\times 1}$ is the received noise vector such that $\boldsymbol{w}^d \sim \mathcal{CN}(0, \mathbf{I})$. $\boldsymbol{A} \in \mathbb{C}^{T^d\times N}$ is the downlink pilots transmitted during the training period of T^d symbols, where $\|\boldsymbol{A}\|_F^2 = \rho^d T^d$ such that ρ^d measures the training SNR. Using conventional channel estimation technique such as *Least Square* (LS) channel estimation, the estimated channel is given by

$$\hat{\boldsymbol{h}}^d_{LS} = \boldsymbol{A}^\dagger \boldsymbol{y}^d \tag{2.6}$$

where $\boldsymbol{A}^\dagger$ is the Moore-Penrose pseudoinverse. Robust recovery of $\boldsymbol{h}^d$ by LS channel estimation requires $T^d \geq N$, which means the training period has to be larger than the number of antennas. In a massive MIMO system N is very large making this infeasible. Moreover, the UE needs to feed back channel information to the BS, which also requires feedback resources proportional to channel dimension N. The finite channel coherence time further exacerbates the situation.

In contrast to the downlink channel estimation, uplink channel estimation is relatively easy in a massive MIMO system. With the same assumption of N antennas at the BS and a single antenna at the UE, for K UEs the uplink training can be written as

$$\boldsymbol{Y}^u = \sum_{k=1}^{K} \boldsymbol{h}_k^u \sqrt{\rho_k^u T^u} \boldsymbol{s}_k^T + \boldsymbol{W}^u = \boldsymbol{H}^u \boldsymbol{C} \boldsymbol{S} + \boldsymbol{W}^u \tag{2.7}$$

where $\boldsymbol{H}^u = [\boldsymbol{h}_1^u, \ldots, \boldsymbol{h}_K^u] \in \mathbb{C}^{N \times K}$ is the uplink channel for K UEs, $\boldsymbol{Y}^u \in \mathbb{C}^{N \times T^u}$ denotes the received signal at the base station and $\boldsymbol{W}^u \in \mathbb{C}^{N \times T^u}$ is the received noise whose elements are assumed to be i.i.d Gaussian with zero mean and unit variance. $\boldsymbol{S} = [\boldsymbol{s}_1, \ldots, \boldsymbol{s}_K]^T \in \mathbb{C}^{K \times T^u}$ denotes the uplink pilots during training period T^u, where $\|\boldsymbol{s}_k\|_2^2 = 1$. ρ_k^u denotes the uplink training SNR for the k-th UE, which incorporates the transmit power, path loss and shadow fading, and is assumed to change slowly and known *a priori*. $\boldsymbol{C} = \text{diag}(\sqrt{\rho_1^u T^u}, \ldots, \sqrt{\rho_K^u T^u})$. Using LS channel estimation, we have

$$\hat{\boldsymbol{H}}_{LS}^u = \boldsymbol{Y}^u (\boldsymbol{C}\boldsymbol{S})^\dagger. \tag{2.8}$$

For the robust estimation, we only require $T^u \geq K$, i.e., the number of pilots to be greater than the number of users. In massive MIMO systems, it is common to assume the number of users is much smaller than the number of antennas. Comparing to $T^d \geq N$ for the downlink estimation, the uplink channel estimation task is simpler. Moreover, the uplink channel is estimated at the BS, incurring no feedback overhead.

The comparison of training and feedback overhead for uplink and downlink is summarized

Table 2.1: Comparison of overhead for uplink and downlink training and feedback

	Training	Feedback
Uplink (TDD)	$T^u \geq K$	No
Downlink (FDD)	$T^d \geq N$	$\propto N$

in Table 2.1. For a TDD system, only uplink training is required, since the downlink CSI can be directly obtained from uplink CSI by channel reciprocity. The uplink training overhead is only proportional to the number of UEs, and there is no feedback overhead. As a result, conventional massive MIMO system is assumed to be operated in TDD mode [1,2]. For FDD system, both the training and feedback overhead are proportional to the number of antennas at the BS, which is impractical for massive MIMO system. However, since FDD mode is widely deployed in current communication system, the adoption of massive MIMO would be much faster if it can be applied in FDD system. In the following section, we discuss how to reduce the downlink training and feedback overhead, such that they no longer scale with the number of antennas.

2.4 Compressive Sensing-Based Downlink Channel Estimation

In order to robustly estimate downlink channel with limited training overhead, compressive sensing-based channel estimation has been proposed in previous works [28,29,32]. In the compressive sensing framework, methods to measure a high-dimensional signal have been proposed with much smaller measurements, provided the original signal can be sparsely represented in some sparsifying matrix [6]. In our scenario, the high-dimensional signal is the channel vector $\boldsymbol{h}^d$, and the number of measurements corresponds to the number of downlink pilots T^d. By utilizing the compressive sensing, the goal is to robustly estimate $\boldsymbol{h}^d$ with reduced T^d such that T^d no longer scales with the dimension of $\boldsymbol{h}^d$.

2.4.1 Downlink Training

Assume there exists a *sparsifying matrix* $\boldsymbol{D}^d \in \mathbb{C}^{N \times M}$ $(M \geq N)$ such that $\boldsymbol{h}^d = \boldsymbol{D}^d \boldsymbol{\beta}^d$, where the representation vector $\boldsymbol{\beta}^d \in \mathbb{C}^{M \times 1}$ is sparse, i.e., $s = \|\boldsymbol{\beta}^d\|_0 \ll N$. Then the downlink channel estimation can be written as

$$\boldsymbol{y}^d = \boldsymbol{A}\boldsymbol{h}^d + \boldsymbol{w}^d = \boldsymbol{A}\boldsymbol{D}^d\boldsymbol{\beta}^d + \boldsymbol{w}^d. \tag{2.9}$$

Given $\boldsymbol{y}^d$, $\boldsymbol{A}$ and $\boldsymbol{D}^d$, if we are able to solve for $\boldsymbol{\beta}^d$, then the channel estimate is obtained as $\hat{\boldsymbol{h}}^d = \boldsymbol{D}^d\boldsymbol{\beta}^d$. However, (2.9) is an underdetermined system if we plan to use a small number of training samples $T^d < N$. The system will in general have an infinite number of solutions for $\boldsymbol{\beta}^d$ and the sparsity assumption provides a mechanism to regularize the problem. Consider the minimum sparsity assumption that $s \ll N$ and assuming $\|\boldsymbol{w}^d\|_2 \leq \epsilon$, then the problem, denoted as *compressive sensing-based downlink channel estimation*, is given as

$$\hat{\boldsymbol{\beta}}^d = \arg\min_{\boldsymbol{\beta}^d} \|\boldsymbol{\beta}^d\|_0 \quad \text{subject to} \quad \|\boldsymbol{y}^d - \boldsymbol{A}\boldsymbol{D}^d\boldsymbol{\beta}^d\|_2 \leq \epsilon \tag{2.10}$$

and $\hat{\boldsymbol{h}}^d_{CS} = \boldsymbol{D}^d\hat{\boldsymbol{\beta}}^d$. Notice that the optimization formula in (2.10) is non-convex, and a number of suboptimal but effective algorithms have been proposed to solve the problem [39]. One of the most widely used framework is to relax the ℓ_0 norm $\|\boldsymbol{\beta}^d\|_0$ to the ℓ_1 norm $\|\boldsymbol{\beta}^d\|_1$, which solves the following convex optimization problem

$$\hat{\boldsymbol{\beta}}^d = \arg\min_{\boldsymbol{\beta}^d} \|\boldsymbol{\beta}^d\|_1 \quad \text{subject to} \quad \|\boldsymbol{y}^d - \boldsymbol{A}\boldsymbol{D}^d\boldsymbol{\beta}^d\|_2 \leq \epsilon. \tag{2.11}$$

It has been shown that under certain conditions on $\boldsymbol{A}\boldsymbol{D}^d$, based on the ℓ_1 norm criteria a solution of $\boldsymbol{\beta}^d$ with bounded error can be obtained with $T^d \geq c \cdot s\log(N/s)$, where c is some constant [6]. Instead of using a training period proportional to the channel dimension N, we can compute good channel estimate with training period proportional to sparsity level s, which is assumed to be much less than N. This makes downlink channel estimation feasible in a limited training period.

The CS-based downlink channel estimation in (2.11) is for single antenna at the UE, and we show in the following how to extend it to scenario where UE has multiple antennas. Assume N_T antennas at BS and N_R antennas at UE, then the channel $\boldsymbol{H}^d = [\boldsymbol{h}_1^d, \ldots, \boldsymbol{h}_{N_R}^d] \in \mathbb{C}^{N_T \times N_R}$ where the column $\boldsymbol{h}_k^d$ denotes the channel from N_T BS antennas to the k-th UE antenna. Since the antenna aperture at UE is much smaller than the distance between the antenna and the scattering clusters in the environment, the scattering clusters that affect the signal transmission are the same for all antenna elements at the UE side. With the sparse representation $\boldsymbol{h}_k^d = \boldsymbol{D}^d \boldsymbol{\beta}_k^d, \forall k$, it implies the support of $\boldsymbol{\beta}_k^d$ is the same for all N_R antennas, i.e., supp$(\boldsymbol{\beta}_1^d) = \ldots =$ supp$(\boldsymbol{\beta}_{N_R}^d)$. Denoting $\boldsymbol{B}^d = [\boldsymbol{\beta}_1^d, \ldots, \boldsymbol{\beta}_{N_R}^d]$, then $\boldsymbol{H}^d = \boldsymbol{D}^d \boldsymbol{B}^d$ and the matrix $\boldsymbol{B}^d$ is row sparse. Similar observation can be made when applying the virtual channel model $\boldsymbol{H}^d = \boldsymbol{A}_T \tilde{\boldsymbol{H}}^d \boldsymbol{A}_R^H$ [29, 31], where $\boldsymbol{A}_T \in \mathbb{C}^{N_T \times N_T}$ and $\boldsymbol{A}_R \in \mathbb{C}^{N_R \times N_R}$ are orthogonal DFT matrices, $\tilde{\boldsymbol{H}}^d$ contains the virtual channel coefficients and is assumed to be sparse. Assume the i-th row $\tilde{\boldsymbol{H}}_{i\cdot}^d = \mathbf{0}_{1 \times N_R}$, then the whole i-th row of the combined matrix $\tilde{\boldsymbol{H}}^d \boldsymbol{A}_R^H$ (act similarly as $\boldsymbol{B}^d$) is zero, implying the row sparsity of the matrix $\tilde{\boldsymbol{H}}^d \boldsymbol{A}_R^H$. The downlink training can be written as

$$\boldsymbol{Y}^d = \boldsymbol{A}\boldsymbol{H}^d + \boldsymbol{W}^d = \boldsymbol{A}\boldsymbol{D}^d \boldsymbol{B}^d + \boldsymbol{W}^d \tag{2.12}$$

where $\boldsymbol{Y}^d \in \mathbb{C}^{T^d \times N_R}$. With respect to the row sparsity of $\boldsymbol{B}^d$, we cast the channel estimation into solving a multiple measurement vector (MMV) problem [40–44] such as

$$\hat{\boldsymbol{B}}^d = \arg\min_{\boldsymbol{B}^d} \|\boldsymbol{B}^d\|_{1,2} \text{ subject to } \|\boldsymbol{Y}^d - \boldsymbol{A}\boldsymbol{D}^d \boldsymbol{B}^d\|_F \leq \epsilon, \tag{2.13}$$

where $\|\boldsymbol{B}^d\|_{1,2} = \sum_{i=1}^{M} \|\boldsymbol{B}_{i\cdot}^d\|_2$, i.e., the summation of the ℓ_2 norm of each row in $\boldsymbol{B}^d$. The estimated channel is given by $\hat{\boldsymbol{H}}_{CS}^d = \boldsymbol{D}^d \hat{\boldsymbol{B}}^d$. For the sparse recovery, it has been shown that utilizing the row sparse property in the MMV formulation can achieve better recovery performance compared to the single measurement vector (SMV) formulation as in the form of (2.11) [40–43].

2.4.2 Downlink Feedback

By utilizing the compressive sensing, the number of downlink training pilots no longer scales with the number of antennas but is only proportional to the sparsity level of the channel, i.e., $||\boldsymbol{\beta}||_0$. As mentioned in Chapter 2.2, it is reasonable to assume that there exists a sparse representation which leads to small $||\boldsymbol{\beta}||_0$ for the massive MIMO channel due to the limited scattering effect and the large antenna array, so the downlink training overhead can be reduced. However, for traditional channel estimation scheme, the channel is estimated at UE side, and then UEs feed back the CSI to the BS through some quantization process. This scheme will cause large feedback overhead, since the feedback is proportional to the channel dimension, i.e., the number of antennas. To further reduce the feedback overhead, a new scheme has been proposed that the UE feeds back the received measurements $\boldsymbol{y}^d$ to the BS and the channel is estimated at the BS utilizing the compressive sensing-based channel estimation (2.10). This is different from the conventional channel estimation scheme where UEs estimate the channel and feed it back to the BS. The scheme of feeding back $\boldsymbol{y}^d$ has been proposed in previous works [28, 32, 45], which has several advantages: firstly the dimension of $\boldsymbol{y}^d$ is T^d, i.e., the number of training pilots. Since the CS is utilized for channel estimation, the required T^d is only proportional to $||\boldsymbol{\beta}||_0$ and is much less than the channel dimension N, so the feedback overhead is reduced. Moreover, the sparse recovery algorithms (channel estimation) can be complex so it is preferably done at the BS thus saving energy for UE. In this work, perfect uplink feedback is assumed for simplicity.

2.5 Sparse Recovery-Based Uplink Channel Estimation

As shown in Chapter 2.3, uplink channel estimation is relatively easy since the uplink training overhead is only proportional to the number of UEs K, which is typically much smaller than the number of antennas N. Furthermore there is no feedback overhead for uplink training since the channel is estimated at the BS. Interestingly, although the compressive sensing formulation (2.10) has been applied widely in the downlink channel estimation, utilizing sparse property for the uplink channel estimation has only received limited attention [33], partially due to the ease of the uplink training as shown in (2.8). However, given the channel is sparse, one can utilize such prior knowledge to further improve the performance. In the following, we show that the uplink channel can be accurately estimated even when $T^u < K$ by casting the channel estimation problem into a sparse recovery problem.

2.5.1 Uplink Training

Similar to the sparse representation for the downlink, in the uplink we assume each UE's channel $\boldsymbol{h}_k^u = \boldsymbol{D}^u \boldsymbol{\beta}_k^u, \forall k$, where $\boldsymbol{D}^u \in \mathbb{C}^{N \times M}$ is the *sparsifying matrix* and $\|\boldsymbol{\beta}_k^u\|_0 \ll N$. Denoting $\boldsymbol{B}^u = [\boldsymbol{\beta}_1^u, \ldots, \boldsymbol{\beta}_K^u]$, then the uplink training (2.7) can be written as

$$\boldsymbol{Y}^u = \boldsymbol{H}^u \boldsymbol{C} \boldsymbol{S} + \boldsymbol{W}^u = \boldsymbol{D}^u \boldsymbol{B}^u \boldsymbol{C} \boldsymbol{S} + \boldsymbol{W}^u. \tag{2.14}$$

Let $\boldsymbol{y}^u = \mathbf{vec}(\boldsymbol{Y}^u)$, then we have

$$\begin{aligned} \boldsymbol{y}^u &= \mathbf{vec}(\boldsymbol{Y}^u) \\ &= \mathbf{vec}(\boldsymbol{D}^u \boldsymbol{B}^u \boldsymbol{C} \boldsymbol{S}) + \mathbf{vec}(\boldsymbol{W}^u) \\ &= (\boldsymbol{S}^T \otimes \boldsymbol{D}^u) \mathbf{vec}(\boldsymbol{B}^u \boldsymbol{C}) + \mathbf{vec}(\boldsymbol{W}^u) \\ &= \boldsymbol{E} \boldsymbol{b}^u + \boldsymbol{w}^u \end{aligned} \tag{2.15}$$

where $\boldsymbol{E} = \boldsymbol{S}^T \otimes \boldsymbol{D}^u \in \mathbb{C}^{NT^u \times MK}$ denotes the equivalent sparsifying matrix, $\boldsymbol{b}^u = \mathbf{vec}(\boldsymbol{B}^u \boldsymbol{C}) = \left[(\sqrt{\rho_1^u T^u} \boldsymbol{\beta}_1^u)^T, \ldots, (\sqrt{\rho_K^u T^u} \boldsymbol{\beta}_K^u)^T\right]^T$ is the concatenated sparse coefficients. If $\boldsymbol{b}^u$ is a sparse vector, i.e., $\|\boldsymbol{b}^u\|_0 = \sum_{k=1}^K \|\boldsymbol{\beta}_k^u\|_0 \ll NT^u$ then we can form the sparse recovery problem as

$$\hat{\boldsymbol{b}}^u = \arg\min_{\boldsymbol{b}^u} \|\boldsymbol{b}^u\|_0 \quad \text{subject to} \quad \|\boldsymbol{y}^u - \boldsymbol{E} \boldsymbol{b}^u\|_2 \leq \epsilon \tag{2.16}$$

where $\boldsymbol{b}^u$ can be robustly estimated by many sparse recovery algorithms even when $T^u < K$. Once $\boldsymbol{b}^u$ is estimated, the uplink channel for the user k is given by $\hat{\boldsymbol{h}}_k^u = \boldsymbol{D}^u \boldsymbol{\beta}_k^u$ since ρ_k^u is assumed to be known. Notice that $T^u < K$ means the number of pilots is less than the number of users, which is underdetermined if using LS channel estimation (2.8). We denote the formulation in (2.15) as the *sparse recovery-based channel estimation*, in contrast to the downlink compressive sensing-based channel estimation (2.9) since there are no compressed measurements in the uplink.

In order to apply the sparse recovery algorithm to solve (2.16), columns in $\boldsymbol{E}$ are expected to be incoherent to each other, since two closely related columns may confuse any sparse recovery algorithm. Moreover, denoting $\Lambda = \text{supp}(\boldsymbol{b}^u)$ where $|\Lambda| = \|\boldsymbol{b}^u\|_0 < NT^u$, given Λ *a priori* the sparse recovery problem in (2.15) reduces to

$$\boldsymbol{y}^u = \boldsymbol{E}_\Lambda \boldsymbol{b}_\Lambda^u + \boldsymbol{w}^u \tag{2.17}$$

which can be solved by LS estimation. In this case, $\boldsymbol{E}_\Lambda$ is required to be a well conditioned matrix for the robust LS estimation. To summary, we hope columns in $\boldsymbol{E}$ and $\boldsymbol{E}_\Lambda$ to be as uncorrelated to each other as possible. In the following, we show how to decrease the correlation of columns in $\boldsymbol{E}$ and $\boldsymbol{E}_\Lambda$ by designing uplink training pilots $\boldsymbol{S}$ and performing uplink user scheduling.

2.5.2 Uplink Pilots Design

To quantitatively characterize the correlation between columns in a matrix $\boldsymbol{X}$, we utilize the *mutual coherence* [8]. Several other measures, e.g., null sparse property (NSP), restricted isometry property (RIP), etc., can provide better characterization of the geometry of a matrix. However those measures are difficult to evaluate explicitly [8]. The mutual coherence is defined as the largest absolute and normalized inner product between different columns. Formally,

$$\mu\{\boldsymbol{X}\} = \max_{i \neq j} \frac{|\boldsymbol{X}_{\cdot i}^H \boldsymbol{X}_{\cdot j}|}{\|\boldsymbol{X}_{\cdot i}\| \cdot \|\boldsymbol{X}_{\cdot j}\|}. \tag{2.18}$$

The mutual coherence provides a measure of the worst similarity between the columns of $\boldsymbol{X}$, which motivates us to minimize $\mu\{\boldsymbol{E}\}$ and $\mu\{\boldsymbol{E}_\Lambda\}$ to obtain a matrix with uncorrelated columns. Following this intuition, we first consider $\mu\{\boldsymbol{E}\}$, which is described in the following theorem [46]:

Theorem 1 ([46]) *Given $\boldsymbol{E} = \boldsymbol{S}^T \otimes \boldsymbol{D}^u$ and the mutual coherence defined in (2.18), $\mu\{\boldsymbol{E}\} =$ max$\{\mu\{\boldsymbol{S}^T\}, \mu\{\boldsymbol{D}^u\}\}$.*

Proof. To simplify the notation, denote $\boldsymbol{d}_i = \boldsymbol{D}^u_i, \boldsymbol{d}_j = \boldsymbol{D}^u_j$. For $1 \leq i, j \leq M$ and $1 \leq l, k \leq K$, denote

$$\begin{aligned} \boldsymbol{e}_{li} &= \boldsymbol{E}_{[(l-1)M+i]} = \boldsymbol{s}_l \otimes \boldsymbol{d}_i, \\ \boldsymbol{e}_{kj} &= \boldsymbol{E}_{[(k-1)M+j]} = \boldsymbol{s}_k \otimes \boldsymbol{d}_j. \end{aligned} \tag{2.19}$$

Then we have

$$\|\boldsymbol{e}_{li}\|_2^2 = \boldsymbol{e}_{li}^H \boldsymbol{e}_{li} = (\boldsymbol{s}_l \otimes \boldsymbol{d}_i)^H (\boldsymbol{s}_l \otimes \boldsymbol{d}_i) = (\boldsymbol{s}_l^H \boldsymbol{s}_l) \otimes (\boldsymbol{d}_i^H \boldsymbol{d}_i) = \|\boldsymbol{s}_l\|_2^2 \|\boldsymbol{d}_i\|_2^2. \tag{2.20}$$

So $\|\boldsymbol{e}_{li}\|_2 = \|\boldsymbol{s}_l\|_2 \|\boldsymbol{d}_i\|_2$, and similarly $\|\boldsymbol{e}_{kj}\|_2 = \|\boldsymbol{s}_k\|_2 \|\boldsymbol{d}_j\|_2$. Based on the same manipulation,

$$|\boldsymbol{e}_{li}^H \boldsymbol{e}_{kj}| = |(\boldsymbol{s}_l \otimes \boldsymbol{d}_i)^H (\boldsymbol{s}_k \otimes \boldsymbol{d}_j)| = |(\boldsymbol{s}_l^H \boldsymbol{s}_k) \otimes (\boldsymbol{d}_i^H \boldsymbol{d}_j)| = |\boldsymbol{s}_l^H \boldsymbol{s}_k| |\boldsymbol{d}_i^H \boldsymbol{d}_j|. \tag{2.21}$$

According to (2.18), the mutual coherence can be written as

$$\begin{aligned} \mu\{\boldsymbol{E}\} &= \max_{\substack{(l-1)M+i \neq (k-1)M+j \\ 1 \leq l,k \leq K, 1 \leq i,j \leq M}} \frac{|\boldsymbol{e}_{li}^H \boldsymbol{e}_{kj}|}{\|\boldsymbol{e}_{li}\|_2 \cdot \|\boldsymbol{e}_{kj}\|_2} \\ &= \max_{\substack{(l-1)M+i \neq (k-1)M+j \\ 1 \leq l,k \leq K, 1 \leq i,j \leq M}} \frac{|\boldsymbol{s}_l^H \boldsymbol{s}_k| |\boldsymbol{d}_i^H \boldsymbol{d}_j|}{\|\boldsymbol{s}_l\|_2 \|\boldsymbol{s}_k\|_2 \|\boldsymbol{d}_i\|_2 \|\boldsymbol{d}_j\|_2} \\ &= \begin{cases} \mu\{\boldsymbol{S}^T\} \mu\{\boldsymbol{D}^u\}, & i \neq j, l \neq k; \\ \mu\{\boldsymbol{D}^u\}, & i \neq j, l = k; \\ \mu\{\boldsymbol{S}^T\}, & i = j, l \neq k. \end{cases} \end{aligned} \tag{2.22}$$

Notice that the mutual coherence is always smaller or equal to 1, i.e., $\mu\{\boldsymbol{S}^T\} \leq 1, \mu\{\boldsymbol{D}^u\} \leq 1$, so we have $\mu\{\boldsymbol{E}\} = \max\{\mu\{\boldsymbol{S}^T\}, \mu\{\boldsymbol{D}^u\}\}$ for $1 \leq l, k \leq K, 1 \leq i, j \leq M$. ■

Theorem 1 indicates that to minimize $\mu\{\boldsymbol{E}\}$, the larger one of $\mu\{\boldsymbol{S}^T\}$ and $\mu\{\boldsymbol{D}^u\}$ needs to be minimized. Notice that $\boldsymbol{D}^u$ is the sparsifying matrix which models the channel, and it has been designed before the channel estimation. So during the channel estimation phase, $\mu\{\boldsymbol{D}^u\}$ is fixed and could be small depending on which $\boldsymbol{D}^u$ is used. The only way we can minimize $\mu\{\boldsymbol{E}\}$ is by minimizing $\mu\{\boldsymbol{S}^T\}$, which corresponds to *design uplink pilots* such that $\mu\{\boldsymbol{S}^T\}$ is small. We discuss different situations regarding to the length of the uplink training duration T^u:

- $T^u = 1$. when $T^u = 1$, $\boldsymbol{S}^T = [s_1, \dots, s_K] \in \mathbb{C}^{1\times K}$, so $\mu\{\boldsymbol{S}^T\} = 1$ for any $\boldsymbol{S}^T$. This is the worst case since even we pick sparsifying matrix $\boldsymbol{D}^u$ such that $\mu\{\boldsymbol{D}^u\} = 0$, we still have $\mu\{\boldsymbol{E}\} = 1$, i.e., there exist fully correlated columns. No sparse recovery algorithm can succeed in this situation.

- $T^u \geq K$. when $T^u \geq K$ we have

$$\min_{\boldsymbol{S}^T} \mu\{\boldsymbol{S}^T\} = 0 \tag{2.23}$$

  where the optimal $\boldsymbol{S}^T$ has orthogonal columns, i.e., $\boldsymbol{s}_l^H \boldsymbol{s}_k = 0, \forall l \neq k$. So the optimal uplink pilots design is $\boldsymbol{S}^* \boldsymbol{S}^T = \mathbf{I}_K$. The orthogonal pilots among users in the same cell are typically assumed for the uplink channel estimation in multiuser massive MIMO systems [26, 47].

- $1 < T^u < K$. when $1 < T^u < K$, $\boldsymbol{S}^T \in \mathbb{C}^{T^u \times K}$ is an overcomplete matrix. The famous welch bound indicates that

$$\mu\{\boldsymbol{S}^T\} \geq \sqrt{\frac{K - T^u}{T^u(K-1)}} \tag{2.24}$$

  where equality holds if and only if $\boldsymbol{S}^T = [\boldsymbol{s}_1, \dots, \boldsymbol{s}_K]$ forms an *equiangular tight frame* [8]. Unfortunately, equiangular tight frame does not exist for any pair $\{T^u, K\}$. In [48], the solution $\boldsymbol{S}^T$ to the problem $\min_{\boldsymbol{S}^T} \mu\{\boldsymbol{S}^T\}$ is called *Grassmannian frame*, and explicit construction of Grassmannian frame has been provided for some specific pairs $\{T^u, K\}$. In general, the design of Grassmannian frames is challenging. Not only is the associated optimization problem difficult, but there is no general procedure for deciding when a frame solves the optimization problem unless it meets the Welch bound [49]. In this work, we design $\boldsymbol{S}^T$ following the algorithm proposed in [50] which targets an average measure of the mutual coherence. The algorithm calculates the Gram matrix of $\boldsymbol{S}^T$ as $\boldsymbol{G} = \boldsymbol{S}^* \boldsymbol{S}^T$, and set the average mutual coherence $\mu_{t\%}\{\boldsymbol{S}^T\}$ such that the top $t\%$ of $|\boldsymbol{G}_{ij}|$ is greater than $\mu_{t\%}\{\boldsymbol{S}^T\}$. The algorithm then shrinks those large $|\boldsymbol{G}_{ij}|$ by some down-scaling factor γ to have $\tilde{\boldsymbol{G}}_{ij} = \gamma \boldsymbol{G}_{ij}$, and keeps the small ones unchanged. The estimated $\hat{\boldsymbol{S}}^T$ is the solution of $\min_{\boldsymbol{S}^T} \|\tilde{\boldsymbol{G}} - \boldsymbol{S}^* \boldsymbol{S}^T\|_F^2$, which is solved by SVD of $\tilde{\boldsymbol{G}}$. Then new $\boldsymbol{G}$ is calculated and such procedure is iteratively executed until some stopping rule is satisfied. By iterative shrinkage of those large $|\boldsymbol{G}_{ij}|$, the $\mu\{\boldsymbol{S}^T\}$ is also reduced. It has been shown in [50] that the algorithm practically converged and the resulted $\boldsymbol{S}^T$ can lead to better performance for the sparse recovery problem like (2.16). Interested readers are referred to [49, 50] for more details.

By designing the uplink pilots $\boldsymbol{S}$, a better structured sensing matrix $\boldsymbol{E}$ can be obtained, therefore improve the sparse recovery performance of the uplink channel estimation.

2.5.3 Uplink User Scheduling

Next we consider minimizing $\mu\{\boldsymbol{E}_\Lambda\}$. Denote $\Lambda_k = \text{supp}(\boldsymbol{\beta}_k)$, then $\boldsymbol{E}_\Lambda$ can be written as

$$\boldsymbol{E}_\Lambda = \begin{bmatrix} \boldsymbol{s}_1 \otimes \boldsymbol{D}^u_{\Lambda_1} & \boldsymbol{s}_2 \otimes \boldsymbol{D}^u_{\Lambda_2} & \dots & \boldsymbol{s}_K \otimes \boldsymbol{D}^u_{\Lambda_K} \end{bmatrix}. \tag{2.25}$$

We take a simple example in the following to see how Λ_k can affect the recovery performance when $T^u < K$. Assume $K = 2$, and both Λ_1 and Λ_2 are known *a priori* with $|\Lambda_1| = |\Lambda_2| = 1$.

Let $T^u = 1$, so s_1 and s_2 are scalars. If $\Lambda_1 \cap \Lambda_2 = \varnothing$, then $\text{rank}(\boldsymbol{E}_\Lambda) = 2$ and we can robustly recover $\boldsymbol{b}^u_\Lambda$ from $\boldsymbol{y}^u = \boldsymbol{E}_\Lambda \boldsymbol{b}^u_\Lambda + \boldsymbol{w}^u$ when the correlation of $\boldsymbol{D}^u_{\Lambda_1}$ and $\boldsymbol{D}^u_{\Lambda_2}$ is small. However, if Λ_1 is overlapped with Λ_2, which in this example means $\Lambda_1 = \Lambda_2$, then $\text{rank}(\boldsymbol{E}_\Lambda) = 1$ and we have $\boldsymbol{y}^u = \boldsymbol{D}^u_{\Lambda_1}(s_1 b^u_{\Lambda_1} + s_2 b^u_{\Lambda_2}) + \boldsymbol{w}^u$ making recovery of $b^u_{\Lambda_1}$ and $b^u_{\Lambda_2}$ impossible. In this case, $T^u \geq 2$ is required to estimate $b^u_{\Lambda_1}$ and $b^u_{\Lambda_2}$. This example motivates how the non-overlapping supports of different users can help sparse recovery when $T^u < K$, as formally shown in the following corollary.

Corollary 1. *Given $\boldsymbol{E}_\Lambda$ in (2.25) and the mutual coherence defined in (2.18), then $\mu\{\boldsymbol{E}_\Lambda\} = \mu\{\boldsymbol{D}^u\}$ if $\Lambda_l \cap \Lambda_k = \varnothing, \forall l \neq k$.*

Proof. Following the same steps as in the proof of Theorem 1, then the condition $\Lambda_l \cap \Lambda_k = \varnothing, \forall l \neq k$ implies $i \neq j$ for $\boldsymbol{e}_{li}$ and $\boldsymbol{e}_{kj}$. So $\mu\{\boldsymbol{E}_\Lambda\} = \max\{\mu\{\boldsymbol{S}^T\}\mu\{\boldsymbol{D}^u\}, \mu\{\boldsymbol{D}^u\}\} = \mu\{\boldsymbol{D}^u\}$ since $\mu\{\boldsymbol{S}^T\} \leq 1$ for any $\boldsymbol{S}^T$. ■

Comparing to $\mu\{\boldsymbol{E}\}$, $\mu\{\boldsymbol{E}_\Lambda\}$ is no longer depending on $\mu\{\boldsymbol{S}^T\}$ when the support sets of different users are *non-overlapping*. So even if $\mu\{\boldsymbol{S}^T\}$ is large [1], $\mu\{\boldsymbol{E}_\Lambda\}$ can still be small if $\mu\{\boldsymbol{D}^u\}$ is small. This result sheds light on how *user scheduling* can affect the performance of channel estimation. If given prior knowledge of $\Lambda_k = \text{supp}(\boldsymbol{\beta}_k)$, for example from some kind of control information or from previous estimate of $\boldsymbol{\beta}_k$ when users are slowly moving, we can schedule users whose supports satisfy $\Lambda_l \cap \Lambda_k = \varnothing, \forall l \neq k$, which will lead to smaller $\mu\{\boldsymbol{E}_\Lambda\}$ and better channel estimation. This result is consistent with [51], which shows that in a *multi-cell* network user interference can be eliminated by simple MMSE channel estimation when the AOA of the desired user has no overlap with AOAs of interfering users. Interestingly, authors in [28, 45] suggest to schedule users with overlapped supports for the *downlink* channel estimation, since it can be formulated into a joint sparse recovery problem which exploits the common support information among users. For the uplink training, in contrast, common support

[1] In the case when the number of users is much larger than the number of pilot symbols, i.e., $K \gg T^u$, we have $\mu\{\boldsymbol{S}^T\} \geq 1/\sqrt{T^u}$ from the welch bound in (2.24).

increases mutual coherence when $T^u < K$, causing decreased performance when applying sparse recovery algorithm for channel estimation.

2.6 Conclusion

In this chapter, we study the downlink and uplink channel estimation problem in massive MIMO systems. For conventional channel estimation algorithms, the downlink training and feedback overhead are proportional to the number of antennas at BS. To reduce such overhead, the sparse property of the massive MIMO channel is exploited and the compressive sensing-based channel estimation algorithm is utilized, which can robustly estimate the downlink channel with training and feedback overhead only proportional to the sparsity level of the channel. The sparse channel property is also utilized for uplink channel estimation, and we develop sparse recovery-based uplink channel estimation algorithm. The uplink channels from multiple UEs can be robustly estimated with the number of uplink pilots smaller than the number of UEs, which is an underdetermined problem when using the conventional channel estimation algorithm. To efficiently perform the sparse recovery algorithm, uplink pilots design and uplink user scheduling are required to construct a well structured sensing matrix.

Chapter 2, in part, is a reprint of the material as it appears in the paper: Y. Ding and B. D. Rao, “Dictionary learning-based sparse channel representation and estimation for FDD massive MIMO systems,” *IEEE Trans. Wireless Commun.*, in press. The dissertation author was the primary investigator and author of this paper.

Chapter 3

Sparse Channel Representation Using Dictionary Learning

To reduce the training and feedback overhead for the channel estimation in a massive MIMO system, the sparse structure of the massive MIMO channel is exploited, and compressive sensing methods and sparse recovery algorithms are utilized for efficient channel estimation. The success of such algorithms depends on the assumption that the channel can be sparsely represented under some sparsifying matrix. Previous works model the channel using some predefined sparsifying matrix. Although useful in some scenarios, such predefined sparsifying matrices are not efficient and robust enough for a specific cell or any antenna uncertainties, leading to performance loss in a practical system. In this chapter, we present a dictionary learning-based channel model such that a dictionary is learned from comprehensively collected channel measurements. The framework is further extended into a joint uplink/downlink dictionary learning by observing the reciprocity between the uplink and downlink transmission. Simulation results show that the learned dictionary can achieve efficient and robust sparse representation, thereby improving the channel estimation accuracy. Moreover, by utilizing the jointly learned dictionary, the downlink channel estimation performance can be improved by utilizing simpler uplink training.

3.1 Introduction

Channel estimation is challenging for the frequency-division duplexing (FDD) massive MIMO system. For downlink channel estimation, the base station (BS) transmits the pilot symbols, the user equipment (UE) estimates the channel and feeds back the channel state information (CSI) to the BS. This process causes training and feedback overhead proportional to the number of antennas at the BS, which is large in massive MIMO system. To alleviate the overhead of downlink channel training and feedback in a FDD massive MIMO system, sparse channel structure has been exploited and channel estimation algorithms based on compressive sensing and sparse recovery have been proposed which can estimate high-dimensional channel with reduced overhead. Those algorithms are based on the assumption that there exists a sparse representation such that the high-dimensional channel can be sparsely represented in some sparsifying matrix. Such sparsifying matrix can either be an orthonormal basis, or an overcomplete dictionary. The corresponding coefficient vector in the representation has only a limited number of nonzero elements, i.e., it is a sparse representation. With this sparse representation, the number of measurements which is required to robustly estimate the sparse coefficient is only proportional to the number of nonzero elements in the sparse coefficient, rather than the dimension of the channel. In other words, the training overhead only scales with the sparsity level of the channel rather than the number of antennas. As a result, when such sparsifying matrix indeed exists and leads to a very spare representation, the downlink training and feedback overhead can be greatly reduced.

Typically, the BS has high elevation and is far away from UEs, so the number of scattering clusters between the BS and the UE is limited, supporting the low dimensionality of the channel. Furthermore, the large antenna array leads to narrower beamwidth, resulting in less leakage effect and providing finer angular resolution to resolve the scattering clusters in the environment.

Consequently, it is reasonable to assume a low-dimensional representation of the large massive MIMO channel from a physical point of view [27–29, 32]. Notice that although the motivation is based on the limited scattering effect in the angular domain, from a theoretical point of view, we only need a sparsifying matrix which can lead to a sparse representation mathematically. In [30, 31], a *virtual channel model* is proposed where the discrete Fourier transform (DFT) matrix is used as the sparsifying matrix, when a uniform linear array (ULA) is assumed to be deployed at the BS. Many previous works based on compressive sensing utilize such virtual channel model. However, DFT matrix causes large leakage with practical channel and a moderate number of antennas, leading to a non-sparse representation. To alleviate the problem, overcomplete DFT matrix has been used as the sparsifying matrix [52–55]. The overcompleteness of the sparsifying matrix introduces the flexibility into the representation, leading to a more sparse coefficient vector. However, for both the DFT matrix and the overcomplete DFT matrix, they are predefined before the application. Therefore, they can not adapt to the specific cell properties. Moreover, with the strong assumption of ULA and far-field transmission, they are not robust to any antenna uncertainties beyond the assumed structure.

In this chapter, a new channel modeling framework based on the learning techniques is developed. We present a *dictionary learning-based channel model* (DLCM), where a learned *overcomplete* dictionary is used to represent the channel in some *specific cell*. To learn the dictionary, a large number of channel measurements need to be collected from different locations in a specific cell at the cell deployment stage, and used as the training samples for the dictionary learning algorithm. The learned dictionary is able to adapt to the cell characteristics as well as ensure a sparse representation of the channel. Since no structural constraints are placed on the dictionary, the approach is applicable to an arbitrary array geometry and does *not* require accurate array calibration. We demonstrate the improved channel estimation performance when applying the learned dictionary, compared to existing works which utilize some predefined basis. In [56], an aperture shaping scheme has been proposed that promotes sparse representation in the virtual channel model. Notice that the dictionary learning concept itself has been widely investigated in previous works [57–59], with many applications such as image denoising and feature extraction. But to the best of our knowledge, our work is the first to utilize the dictionary learning framework to model the massive MIMO channel.

By observing the reciprocity resides in the uplink and downlink channels, we further develop a general framework of *joint* uplink/downlink dictionary learning-based channel model (JDLCM) and channel estimation. Although in FDD systems the uplink and downlink are operated in different frequency band, the propagation environment is the same for the uplink and downlink transmission when the duplex distance is not large [60,61]. This motivates a joint sparse representation of uplink and downlink channels, and enables the use of information from the more easily obtained uplink training to help downlink channel estimation. In FDD systems, leveraging uplink channel information for the downlink use has been proposed, for example using uplink signals to compute direction of arrival (DOA) and construct downlink channel response [62], or utilizing uplink channel covariance matrix to estimate downlink channel covariance matrix [63]. To the best of our knowledge, our work is the first to explore the jointly sparse representation as an abstract model for the uplink and downlink channel reciprocity, and develop joint channel estimation algorithms to improve the channel estimation performance.

The chapter is organized as follows. In Section 3.2, we provide the background knowledge of the dictionary learning and review several dictionary learning algorithms. In Section 3.3, we present the predefined sparsifying matrices which have been used in previous compressive sensing-based channel estimation algorithms. The downlink dictionary learning framework is developed in Section 3.4, and the extension to the joint uplink/downlink dictionary learning is presented in Section 3.5. Numerical results are provided in Section 3.6 and we conclude the chapter in Section 3.7.

Notations used in this chapter are as follows. Upper (lower) bold face letters are used throughout to denote matrices (column vectors). $(\cdot)^T$, $(\cdot)^H$ $(\cdot)^\dagger$ denotes the transpose, Hermitian transpose, and the Moore-Penrose pseudo-inverse. $\boldsymbol{A}_{i\cdot}$ and $\boldsymbol{A}_{\cdot j}$ represents the i-th row and j-th column of $\boldsymbol{A}$, and for a set $\mathcal{S}$ we denote $\boldsymbol{A}_{\cdot\mathcal{S}}$ to be the submatrix of $\boldsymbol{A}$ that contains columns indexed by elements of $\mathcal{S}$, and $\boldsymbol{A}_{\mathcal{S}\cdot}$ to be the submatrix of $\boldsymbol{A}$ that contains rows indexed by elements of $\mathcal{S}$. For a vector $\boldsymbol{x}$, diag$(\boldsymbol{x})$ is a diagonal matrix with entries of $\boldsymbol{x}$ along its diagonal. $\|\boldsymbol{x}\|_1, \|\boldsymbol{x}\|_2$ denotes the ℓ_1 and ℓ_2 norm. $\|\boldsymbol{x}\|_0$ represents the number of nonzero entries in $\boldsymbol{x}$ and is referred to as the ℓ_0 norm. supp$(\boldsymbol{x})$ denotes the set of indices such that the corresponding entries of $\boldsymbol{x}$ are nonzero.

3.2 Dictionary Learning Methods

Consider a high dimensional signal $\boldsymbol{x} \in \mathbb{C}^N$, we are interested in finding a representation $\boldsymbol{x} \approx \boldsymbol{D}\boldsymbol{\beta}, \|\boldsymbol{\beta}\|_0 \ll N$, such that the signal can be well approximated by a limited number of columns in $\boldsymbol{D}$. The sparsifying matrix $\boldsymbol{D} \in \mathbb{C}^{N\times M}$ can either be a basis ($N = M$) or a dictionary ($N < M$), and it can either be chosen as a predefined matrix or learned by adapting to a given set of training samples. Choosing a predefined sparsifying matrix is appealing due to its simplicity, and many basis and dictionary, such as wavelets, DFT matrix, overcomplete DFT matrix, etc., have been shown to lead to a sparse representation for practical applications. However, those predefined sparsifying matrices are application-independent, meaning that they are generated beforehand and unable to exploit specific properties of signals. Moreover, the choice of which predefined sparsifying matrix to be used is mostly based on some assumed structure of the signal. As a result, when the true signal's structure deviates from the assumed one, those predefined sparsifying matrices can not fit to the true signal, and the resulted representation will no longer be sparse. In the following, we introduce a different route for designing the sparsifying matrix $\boldsymbol{D}$ based on the learning techniques. Given a set of signals $\boldsymbol{x}_l, l = 1, \dots, L$, the goal is to find a $\boldsymbol{D}$ such that every $\boldsymbol{x}_l$ can be sparsely represented as $\boldsymbol{x}_l \approx \boldsymbol{D}\boldsymbol{\beta}_l, \|\boldsymbol{\beta}_l\|_0 \ll N$. We will review several dictionary learning algorithms. Those algorithms are similar, in a sense that they all follow a two-step process which is based on the concept of block coordinate descent [64]. Specifically, the first step finds the sparse coefficient by fixing the dictionary, which actually solves a sparse recovery problem and is refer to as *sparse coding*. Then given the sparse coefficient, the dictionary is updated. Different algorithms apply different methods for sparse coding and dictionary updating. Since generally any sparse recovery algorithm can be used for sparse coding, we will focus on how the dictionary is updated in different algorithms.

3.2.1 ML Method

In [65, 66], a maximum likelihood (ML) method is used to learn $\boldsymbol{D}$ by assuming

$$\boldsymbol{x}_l = \boldsymbol{D}\boldsymbol{\beta}_l + \boldsymbol{v}_l, \;\; \forall l \tag{3.1}$$

where $\boldsymbol{v}_l \sim \mathcal{N}(\mathbf{0}, \sigma^2\mathbf{I})$ denotes the possible measurement noise in the signal or the model mismatch error. Given a set of independent signals $\boldsymbol{x}_l, l = 1, \ldots, L$ as the training samples, the likelihood function of $\boldsymbol{D}$ is given as

$$P(\boldsymbol{x}_1, \ldots, \boldsymbol{x}_l|\boldsymbol{D}) = \prod_{l=1}^{L} P(\boldsymbol{x}_l|\boldsymbol{D}) \tag{3.2}$$

and for each signal we have

$$\begin{aligned} P(\boldsymbol{x}_l|\boldsymbol{D}) &= \int P(\boldsymbol{x}_l, \boldsymbol{\beta}_l|\boldsymbol{D})\, d\boldsymbol{\beta}_l \\ &= \int P(\boldsymbol{x}_l|\boldsymbol{\beta}_l, \boldsymbol{D}) P(\boldsymbol{\beta}_l)\, d\boldsymbol{\beta}_l \end{aligned} \tag{3.3}$$

with the assumption that $\boldsymbol{D}$ is independent of $\boldsymbol{\beta}_l$. Based on (3.1), we have

$$P(\boldsymbol{x}_l|\boldsymbol{\beta}_l, \boldsymbol{D}) \sim \mathcal{N}(\boldsymbol{D}\boldsymbol{\beta}_l, \sigma^2\mathbf{I}). \tag{3.4}$$

Regarding to the sparse coefficient $\boldsymbol{\beta}_l$, each element of $\boldsymbol{\beta}_l$ is assumed to be zero-mean and identically independently distributed (i.i.d.), and is highly peaked around zero to promote the sparsity. For example, Cauchy distribution is used in [65] and Laplace distribution is used in [66]. However, the integration in (3.3) is difficult to be evaluated. In [65], it is assumed that $P(\boldsymbol{x}_l, \boldsymbol{\beta}_l|\boldsymbol{D})$ has a fairly tightly peaked maximum in $\boldsymbol{\beta}_l$ space, so the integral can be approximated by evaluating $P(\boldsymbol{x}_l, \boldsymbol{\beta}_l|\boldsymbol{D})$ at its maximum. As a result, the dictionary learning problem becomes [65]

$$\begin{aligned}\hat{\boldsymbol{D}} &= \arg\max_{\boldsymbol{D}} \log P(\boldsymbol{x}_1, \ldots, \boldsymbol{x}_l|\boldsymbol{D}) \\ &= \arg\max_{\boldsymbol{D}} \sum_{l=1}^{L} \log P(\boldsymbol{x}_l|\boldsymbol{D}) \\ &= \arg\max_{\boldsymbol{D}} \sum_{l=1}^{L} \max_{\boldsymbol{\beta}_l} \log P(\boldsymbol{x}_l, \boldsymbol{\beta}_l|\boldsymbol{D}) \\ &= \arg\min_{\boldsymbol{D}} \sum_{l=1}^{L} \min_{\boldsymbol{\beta}_l} \left\{ \|\boldsymbol{x}_l - \boldsymbol{D}\boldsymbol{\beta}_l\|_2^2 + \lambda\|\boldsymbol{\beta}_l\|_1 \right\}\end{aligned} \tag{3.5}$$

which is solved by a two separate phases. In the inner phase, for each $\boldsymbol{x}_l$, (3.5) is minimized with respect to $\boldsymbol{\beta}_l$ by fixing $\boldsymbol{D}$. Then in the outer phase, for all the signals $\boldsymbol{x}_l$, (3.5) is minimized with respect to $\boldsymbol{D}$. Notice that there is no regularization on $\boldsymbol{D}$, so the solution tends to increase the columns of $\boldsymbol{D}$ so the corresponding elements in $\boldsymbol{\beta}_l$ can be decreased, leading to a smaller cost function. To alleviate the problem, the ℓ_2 norm of each columns in $\boldsymbol{D}$ is constraint so that the output variance of the coefficients is kept at an appropriate level [65]. The dictionary is updated based on the gradient descent procedure in [65]:

$$\boldsymbol{D}^{(t+1)} = \boldsymbol{D}^{(t)} - \eta \sum_{l=1}^{L} (\boldsymbol{D}^{(t)}\boldsymbol{\beta}_l - \boldsymbol{x}_l)\boldsymbol{\beta}_l^T \tag{3.6}$$

where η is the learning rate.

3.2.2 MAP Method

In [58], the ML formulation in [65] is generalized to a maximum a-posteriori (MAP) formulation which considers the probability distribution of the dictionary $\boldsymbol{D}$. Specifically, the dictionary is assumed to belong to a compact submanifold $\mathcal{D}$ which is closed and bounded. The dictionary is further assumed to be uniformly distributed on this constraint submanifold as

$$P(\boldsymbol{D}) = c \cdot \mathbb{1}(\boldsymbol{D} \in \mathcal{D}) \tag{3.7}$$

where $\mathbb{1}(\cdot)$ is the indicator function and c is a constant which ensures $P(\boldsymbol{D})$ is a valid distribution function. Based on this, the MAP formulation aims to find $\boldsymbol{D}$ and $\boldsymbol{\beta}_l, \forall l$ by maximizing a-posteriori probability density $P(\boldsymbol{D}, \boldsymbol{\beta}_1, \ldots, \boldsymbol{\beta}_L | \boldsymbol{x}_1, \ldots, \boldsymbol{x}_L)$ as

$$\begin{aligned} & P(\boldsymbol{D}, \boldsymbol{\beta}_1, \ldots, \boldsymbol{\beta}_L | \boldsymbol{x}_1, \ldots, \boldsymbol{x}_L) \\ = & P(\boldsymbol{D}, \boldsymbol{\beta}_1, \ldots, \boldsymbol{\beta}_L, \boldsymbol{x}_1, \ldots, \boldsymbol{x}_L) / P(\boldsymbol{x}_1, \ldots, \boldsymbol{x}_L) \\ \propto & P(\boldsymbol{D}) \prod_{l=1}^{L} P(\boldsymbol{\beta}_l) P(\boldsymbol{x}_l | \boldsymbol{D}, \boldsymbol{\beta}_l). \end{aligned} \tag{3.8}$$

Denoting $\boldsymbol{X} = [\boldsymbol{x}_1, \ldots, \boldsymbol{x}_L]$ and $\boldsymbol{B} = [\boldsymbol{\beta}_1, \ldots, \boldsymbol{\beta}_L]$ and assume Laplace distribution on each element of $\boldsymbol{\beta}_l$, the MAP formulation is given by

$$\begin{aligned} \{\hat{\boldsymbol{D}}, \hat{\boldsymbol{\beta}}_1, \ldots \hat{\boldsymbol{\beta}}_L\} &= \underset{\boldsymbol{D}, \boldsymbol{\beta}_1, \ldots, \boldsymbol{\beta}_L}{\arg\max} \log P(\boldsymbol{D}, \boldsymbol{\beta}_1, \ldots, \boldsymbol{\beta}_L | \boldsymbol{x}_1, \ldots, \boldsymbol{x}_L) \\ &= \underset{\boldsymbol{D} \in \mathcal{D}, \boldsymbol{\beta}_1, \ldots, \boldsymbol{\beta}_L}{\arg\min} \|\boldsymbol{X} - \boldsymbol{D}\boldsymbol{B}\|_F^2 + \lambda \sum_{l=1}^{L} \|\boldsymbol{\beta}_l\|_1. \end{aligned} \tag{3.9}$$

Again, $\boldsymbol{\beta}_l, \forall l$ and $\boldsymbol{D}$ are iteratively updated. When no prior is chosen for $\boldsymbol{D}$, the same updating procedure as in [65] can be obtained. In [58], two types of constraint are considered. The first constraint enforces $\boldsymbol{D}$ to have the unit Frobenius norm, $\mathcal{D} = \{\boldsymbol{D} | \, \|\boldsymbol{D}\|_F = 1\}$. And the second constraint requires columns in $\boldsymbol{D}$ to have unit norm so $\mathcal{D} = \{\boldsymbol{D} | \, \|\boldsymbol{D}_{\cdot k}\|_2 = 1, k = 1, \ldots, M\}$.

Interested readers are referred to [58] for the updating rules and derivations.

3.2.3 MOD Method

In [57], method of optimal directions (MOD) algorithm is presented which provides a simple way to update the dictionary. Assume the sparse coefficients $\boldsymbol{B}$ have been calculated by any sparse recovery algorithm, then the $\boldsymbol{D}$ is calculated by minimizing the error for the representation of all signals

$$\begin{aligned} \hat{\boldsymbol{D}} &= \arg\min_{\boldsymbol{D}} \sum_{l=1}^{L} \|\boldsymbol{x}_l - \boldsymbol{D}\boldsymbol{\beta}_l\|_2^2 \\ &= \arg\min_{\boldsymbol{D}} \|\boldsymbol{X} - \boldsymbol{D}\boldsymbol{B}\|_F^2 \end{aligned} \tag{3.10}$$

where the optimal solution is given by

$$\boldsymbol{D} = \boldsymbol{X}\boldsymbol{B}^{\dagger} = \boldsymbol{X}\boldsymbol{B}^T(\boldsymbol{B}\boldsymbol{B}^T)^{-1}. \tag{3.11}$$

Then with the newly updated $\boldsymbol{D}$, $\boldsymbol{B}$ is calculated again. The update procedure has no regularization on $\boldsymbol{D}$, so after calculating $\boldsymbol{D}$, each of its columns is normalized to be 1. Notice that although the updated $\boldsymbol{D}$ given by (3.11) is optimal for fixed $\boldsymbol{B}$, the calculation complexity is prohibitive due to matrix inversion.

3.2.4 K-SVD Method

An appealing dictionary learning algorithm, named K-SVD algorithm, is presented in [59]. The algorithm is based on the concept of K-means algorithm for the vector quantization, but is generalized to represent the signal by a linear combination of multiple columns in $\boldsymbol{D}$. Furthermore, the columns in $\boldsymbol{D}$ is updated sequentially by fixing all the other columns, and the corresponding coefficients are simultaneously updated. Such update procedure is conducted by an efficient SVD operation.

In [59], the formulation of dictionary learning is

$$\{\hat{\boldsymbol{D}}, \hat{\boldsymbol{B}}\} = \underset{\boldsymbol{D},\boldsymbol{B}}{\arg\min} \|\boldsymbol{X} - \boldsymbol{D}\boldsymbol{B}\|_F^2 \quad s.t. \quad \|\boldsymbol{\beta}_l\|_0 \leq T_0, \forall l. \tag{3.12}$$

where T_0 constrains the number of nonzero elements in each $\boldsymbol{\beta}_l$. For the sparse coding stage, $\boldsymbol{D}$ is assumed to be fixed, and the cost function in (3.12) can be written as the sum of L terms, $\|\boldsymbol{X} - \boldsymbol{D}\boldsymbol{B}\|_F^2 = \sum_{l=1}^{L} \|\boldsymbol{x}_l - \boldsymbol{D}\boldsymbol{\beta}_l\|_2^2$. Then the problem can be decoupled into L individual sparse recovery problem of the form

$$\hat{\boldsymbol{\beta}}_l = \underset{\boldsymbol{\beta}_l}{\arg\min} \|\boldsymbol{x}_l - \boldsymbol{D}\boldsymbol{\beta}_l\|_2^2 \quad s.t. \quad \|\boldsymbol{\beta}_l\|_0 \leq T_0 \tag{3.13}$$

and can be solved efficiently by any sparse recovery algorithms. In [59], OMP algorithm is used. After solving for all $\boldsymbol{\beta}_l$, $\boldsymbol{B} = [\boldsymbol{\beta}_1, \ldots, \boldsymbol{\beta}_L]$ is fixed and the goal is to update $\boldsymbol{D}$ by minimizing $\|\boldsymbol{X} - \boldsymbol{D}\boldsymbol{B}\|_F^2$ similar to the MOD method. However, rather than calculating the whole $\boldsymbol{D}$ by (3.11) as in MOD method, only one column is updated at a time. Assume the k-th column will be updated, then the cost function can be written as

$$\begin{aligned} \|\boldsymbol{X} - \boldsymbol{D}\boldsymbol{B}\|_F^2 &= \|\boldsymbol{X} - \sum_{l=1}^{L} \boldsymbol{D}_{\cdot l}\boldsymbol{B}_{l\cdot}\|_F^2 \\ &= \|\boldsymbol{X} - \sum_{l \neq k} \boldsymbol{D}_{\cdot l}\boldsymbol{B}_{l\cdot} - \boldsymbol{D}_{\cdot k}\boldsymbol{B}_{k\cdot}\|_F^2 \\ &= \|\boldsymbol{E}^k - \boldsymbol{D}_{\cdot k}\boldsymbol{B}_{k\cdot}\|_F^2 \end{aligned} \tag{3.14}$$

where $\boldsymbol{E}^k = \boldsymbol{X} - \sum_{l \neq k} \boldsymbol{D}_{\cdot l}\boldsymbol{B}_{l\cdot}$ represents the residue of the signals by removing the contributions from all the other columns of $\boldsymbol{D}$ except the k-th column. Notice that not all the elements in $\boldsymbol{B}_{k\cdot}$ are nonzero, so not all the components of $\boldsymbol{E}^k$ can be reduced by adapting $\boldsymbol{D}_{\cdot k}$. Denoting Ω_k as the set of indexes corresponding to the nonzero elements in $\boldsymbol{B}_{k\cdot}$, then

$$\Omega_k = \{l \mid \boldsymbol{B}_{kl} \neq 0, 1 \leq l \leq L\} \tag{3.15}$$

which also represents the indexes of those signals that indeed utilize the k-th column of $\boldsymbol{D}$. Then (3.14) can be written as

$$\|\boldsymbol{X} - \boldsymbol{D}\boldsymbol{B}\|_F^2 = \|\boldsymbol{E}_{\Omega_k}^k - \boldsymbol{D}_{\cdot k}\boldsymbol{B}_{k\Omega_k}\|_F^2. \tag{3.16}$$

Unlike the other methods which do not change any of $\boldsymbol{\beta}_l$ during the update of $\boldsymbol{D}$, in the K-SVD algorithm both $\boldsymbol{D}_{\cdot k}$ and $\boldsymbol{B}_{k\Omega_k}$ can be updated simultaneously, which increases the convergence speed. As a result, the optimal solution to solve (3.16) is to perform the SVD to find the closed rank-1 matrix that approximates $\boldsymbol{E}_{\Omega_k}^k$. Denoting the SVD of $\boldsymbol{E}_{\Omega_k}^k$ as $\boldsymbol{E}_{\Omega_k}^k = \boldsymbol{U}\boldsymbol{\Sigma}\boldsymbol{V}^T$, then the solution of $\boldsymbol{D}_{\cdot k}$ and $\boldsymbol{B}_{k\Omega_k}$ are given by

$$\hat{\boldsymbol{D}}_{\cdot k} = \boldsymbol{U}_{\cdot 1}, \;\; \hat{\boldsymbol{B}}_{k\Omega_k} = \Sigma_{11}\boldsymbol{V}_{\cdot 1}^T. \tag{3.17}$$

After solving for $\hat{\boldsymbol{B}}_{k\Omega_k}$, $\hat{\boldsymbol{B}}_{k\cdot}$ is obtained by setting the elements whose indexes are in Ω_k as $\hat{\boldsymbol{B}}_{k\Omega_k}$ and the others as zeros. Note that in this solution, the columns in $\boldsymbol{D}$ are enforced to be normalized and the support of each $\boldsymbol{\beta}_l$ remain the same as the result of the sparse coding. The K-SVD algorithm sweeps through all the columns and for each column a SVD operation is used to update it. Also, the most updated sparse coefficients are used after the previous SVD step to increase the convergence speed of the algorithm. Due to its fast convergence and the efficiency in the sparse representation, we will utilized K-SVD method to learn the dictionary in this chapter.

3.3 Predefined Sparsifying Matrix

Now we consider the sparse representation of the massive MIMO channel. In Chapter 2, for both the compressive sensing-based downlink channel estimation and the sparse recovery-based uplink channel estimation, the key assumption is that the channel can be represented in the form of $\boldsymbol{h} = \boldsymbol{D}\boldsymbol{\beta}$, where $\boldsymbol{\beta}$ is a sparse vector. The existing works [28–32] which consider such a sparse representation typically use a normalized square DFT matrix as the sparsifying matrix when an ULA is employed, i.e., $\boldsymbol{h} = \boldsymbol{F}\boldsymbol{\beta}$, where

$$\begin{aligned}
\boldsymbol{F} &= \begin{bmatrix} \boldsymbol{f}(-\tfrac{1}{2}) & \boldsymbol{f}(-\tfrac{1}{2}+\tfrac{1}{N}) & \cdots & \boldsymbol{f}(\tfrac{1}{2}-\tfrac{1}{N}) \end{bmatrix} \in \mathbb{C}^{N\times N}, \\
\boldsymbol{f}(\psi) &= \frac{1}{\sqrt{N}}[1, e^{j2\pi\psi}, \ldots, e^{j2\pi\psi\cdot(N-1)}]^T.
\end{aligned} \tag{3.18}$$

Such a model is also known as the "virtual channel model" which transforms spatial channel response into the angular domain [29–31]. For a ULA, the array response with the antenna spacing d and the transmission wavelength λ is given as

$$\boldsymbol{a}(\theta) = [1, e^{j2\pi\frac{d}{\lambda}\sin(\theta)}, \ldots, e^{j2\pi\frac{d}{\lambda}\sin(\theta)\cdot(N-1)}]^T \tag{3.19}$$

where the θ denotes the AOA for the uplink and AOD for the downlink. Notice that the column $\boldsymbol{f}(\psi)$ has the same structure as the array response $\boldsymbol{a}(\theta)$, where ψ can be related to θ through $\psi = d\sin(\theta)/\lambda$, indicating the validity of the DFT matrix . However, in practice signals come from arbitrary directions, so $\psi = d\sin(\theta)/\lambda$ rarely resides on the DFT bins $\{-\frac{1}{2}, -\frac{1}{2}+\frac{1}{N}, \ldots, \frac{1}{2}-\frac{1}{N}\}$, leading to the "leakage" effect. Moreover, for each scattering cluster the signals' subpaths often span an angular spread, resulting even more leakage. So for practical channels, there will be a lot of nonzero elements in $\boldsymbol{\beta}$ when we apply the representation $\boldsymbol{h} = \boldsymbol{F}\boldsymbol{\beta}$, making the sparse assumption invalid.

To achieve a better sparse representation, our first suggestion in the same realm of "predefined matrix" for ULA is to apply the *overcomplete* DFT matrix $\tilde{\boldsymbol{F}}$, which has the form

$$\tilde{\boldsymbol{F}} = \begin{bmatrix} \boldsymbol{f}(-\frac{1}{2}) & \boldsymbol{f}(-\frac{1}{2}+\frac{1}{M}) & \dots & \boldsymbol{f}(\frac{1}{2}-\frac{1}{M}) \end{bmatrix} \in \mathbb{C}^{N\times M}. \tag{3.20}$$

The columns of $\tilde{\boldsymbol{F}}$ has the same structure $\boldsymbol{f}(\psi)$, but the angular domain is sampled (in the sense of ψ) more finely, i.e., $M > N$. The overcomplete DFT matrix introduces redundancy to the square DFT matrix, which improves the flexibility of representing the signal as well as the capability of inducing sparsity. When a uniform rectangular array (URA) with N_1 vertical antennas and N_2 horizontal antennas is applied, $\tilde{\boldsymbol{F}}$ is constructed as the kronecker product of two overcomplete DFT matrix such that

$$\tilde{\boldsymbol{F}} = \tilde{\boldsymbol{F}}_h \otimes \tilde{\boldsymbol{F}}_v \tag{3.21}$$

where $\tilde{\boldsymbol{F}}_h$ and $\tilde{\boldsymbol{F}}_v$ are $N_2 \times M_2$ and $N_1 \times M_1$ overcomplete DFT matrices as given in (3.20).

Although the overcomplete DFT matrix can alleviate the leakage effect to some extent, both $\boldsymbol{F}$ and $\tilde{\boldsymbol{F}}$ suffer from performance loss due to their inability to adapt to the real channels. Firstly, since $\tilde{\boldsymbol{F}}$ and $\boldsymbol{F}$ are predefined and independent of the specific cell properties, they lose the ability to more *efficiently* represent the channel by exploring *cell specific* characteristics. For example both $\tilde{\boldsymbol{F}}$ and $\boldsymbol{F}$ uniformly sample the ψ domain, but for a specific cell it is possible that no signals may be received from some directions, then the columns in $\tilde{\boldsymbol{F}}$ and $\boldsymbol{F}$ corresponding to those directions will never be used. On the other hand, for directions corresponding to those fixed location scattering clusters, finer angular sampling can lead to a reduced leakage. Since those fixed location scattering clusters can be seen by many different users, such finer sampling can lead to more sparse representation for many users. Secondly, predefined matrices also lose the ability to *robustly* represent the channel. They assume ideal mathematical models of channel responses, e.g., far-field plane wave, equal antenna gain and antenna spacing, etc., which are not robust to any propagation model mismatch or antenna array uncertainty.

3.4 Downlink Dictionary Learning

In this section, we propose a *dictionary learning-based channel model* (DLCM) which learns an overcomplete dictionary. During the learning process, the sparse representation is encouraged by the optimization function. Furthermore, the dictionary learning process adapts the channel model to the channel measurements collected in the cell, which contain the specific cell characteristics. The channel measurements describe the effect of scattering clusters on the transmitted electromagnetic waves and the antenna array. Therefore, the underlying structure of channel measurements collected in a specific cell can reflect the cell specific properties regarding to both the scattering clusters and the antenna array. Notice that when the knowledge of the underlying physical generation scheme of the channel is imperfect or even incorrect, e.g., antenna gains and locations are different from the nominal values, or there exist near-field scattering clusters, etc., the predefined matrix is no longer accurate and may cause severe performance degradation. However, the learned dictionary does not have any predefined structural constraints and is able to tune its own structure to adapt to the channel measurements, which leads to a more robust channel representation. The insight behind the sparse dictionary learning is that the high dimensional data (channel response in our case) usually has some structure correlated in some dimensions, and the true degrees of freedom that generate the data is usually small. So by learning from large amount of data, we are able to recover useful underlying structures or models, which make the representation of the data more efficient for the desired application. In our situation, one could view this as big data analytics applied to the physical layer.

3.4.1 Formulation of Dictionary Learning

From now, we denote $\boldsymbol{D} \in \mathbb{C}^{N \times M}$ as the learned dictionary from channel measurements. To benefit from the flexibility of overcompleteness, we let $N < M$. Assuming we collect L channel measurements as the training samples in a specific cell, the goal is to learn $\boldsymbol{D}$ such that for all the channel responses $\boldsymbol{h}_i, i = 1, \ldots, L$, they can be approximated as $\boldsymbol{h}_i \approx \boldsymbol{D}\boldsymbol{\beta}_i$. The algorithms should be able to address both model fitting $\|\boldsymbol{h}_i - \boldsymbol{D}\boldsymbol{\beta}_i\|_2$ (robustness), and encourage small $\|\boldsymbol{\beta}_i\|_0$ (efficiency) for the sparse representation. If we constrain the model mismatch error of each channel response to be bounded by η, then the dictionary learning can be formulated as

$$\min_{\substack{\boldsymbol{D}\in\mathcal{C} \\ \boldsymbol{\beta}_1,\ldots,\boldsymbol{\beta}_L}} \frac{1}{L}\sum_{i=1}^{L} \|\boldsymbol{\beta}_i\|_0 \quad s.t. \quad \|\boldsymbol{h}_i - \boldsymbol{D}\boldsymbol{\beta}_i\|_2 \leq \eta, \forall i \tag{3.22}$$

where the constraint set $\mathcal{C}$ is defined as

$$\mathcal{C} = \{\boldsymbol{D} \in \mathbb{C}^{N\times M},\ \text{s.t. } \|\boldsymbol{D}_{\cdot j}\|_2 \leq 1, \forall j = 1, \ldots, M\} \tag{3.23}$$

in order to prevent the scaling ambiguity between columns of $\boldsymbol{D}$ and corresponding elements in $\boldsymbol{\beta}$. as well as avoiding the trivial solution if we replace $\|\boldsymbol{\beta}\|_0$ to other norm, e.g., $\|\boldsymbol{\beta}\|_1$. The solved $\boldsymbol{D}$ in (3.22) leads to the sparsest representation in the sense of representing all collected channel measurements within the model mismatch tolerance η.

Two similar formulations could alternatively be used. If we know beforehand or want to constrain the sparsity level of each coefficient $\boldsymbol{\beta}_i$, then we solve:

$$\min_{\substack{\boldsymbol{D}\in\mathcal{C} \\ \boldsymbol{\beta}_1,\ldots,\boldsymbol{\beta}_L}} \frac{1}{L}\sum_{i=1}^{L} \frac{1}{2}\|\boldsymbol{h}_i - \boldsymbol{D}\boldsymbol{\beta}_i\|_2^2 \quad \text{subject to } \|\boldsymbol{\beta}_i\|_0 \leq T_0, \forall i \tag{3.24}$$

where T_0 constrains the number of non-zero elements in each $\boldsymbol{\beta}_i$. In other words, we expect every channel measurement can be approximately represented using *at most* T_0 atoms from the learned dictionary, and we solve the dictionary that minimizes the model mismatch given such constraint. Notice that T_0 is a cell specific parameter which trades off between the sparsity and the accuracy of the representation. When larger value of T_0 is used, it leads to smaller model mismatch error since more atoms participate in the channel representation. But larger T_0 also implies that more training pilots are needed in channel estimation. In practice, we can test several different values of T_0 and choose the smallest one that leads to the satisfied model mismatch error.

If we do not have any explicit constraints on model mismatch error or sparsity level, we can formulate the dictionary learning process in general form as

$$\min_{\substack{\boldsymbol{D}\in\mathcal{C}\\ \boldsymbol{\beta}_1,\ldots,\boldsymbol{\beta}_L}} \frac{1}{L}\sum_{i=1}^{L}\frac{1}{2}\|\boldsymbol{h}_i-\boldsymbol{D}\boldsymbol{\beta}_i\|_2^2+\lambda\|\boldsymbol{\beta}_i\|_0 \tag{3.25}$$

where λ is the parameter that trades off the data fitting and sparsity.

To solve the dictionary learning problems (3.22), (3.24), and (3.25), block coordinate descent framework has been applied where each iteration includes alternatively minimizing with respect to either $\boldsymbol{D}$ or $\boldsymbol{\beta}_i, \forall i$, while keeping the other fixed [57–59]. When $\boldsymbol{D}$ is fixed, optimizing $\boldsymbol{\beta}_i, \forall i$ is decoupled and each of them is a sparse recovery problem, which can be solved by any sparse recovery algorithm. When we fix $\boldsymbol{\beta}_i, \forall i$ and solve for $\boldsymbol{D}$, many dictionary learning algorithm can be applied [57–59]. The convergence of the iteration depends on the specific sparse recovery algorithm and dictionary update algorithm, and to the best of our knowledge, no general guarantees have been provided. Interested readers are referred to [59, 64] for some discussion about the convergence under specific assumptions. Notice that in our scenario, there exists *no* "true" dictionary that generates the channel. Because each channel response combines signals coming from both fixed location scattering clusters and user location dependent scattering clusters, where the latter depends on arbitrary user's location. So the goal of the dictionary learning here is not to identify any true dictionary [67], but to find an efficient and robust channel representation. For the purpose of this work, we will show experimentally that the learned dictionary can improve the performance in terms of both sparse representation and channel estimation.

3.4.2 Discussion

We make some comments relative to the practical implementation of the dictionary learning process. To learn a comprehensive dictionary for users located in any place of the cell, we need to collect channel measurements from all locations in a specific cell, i.e., *cell specific samples*, based on an extensive measurement campaign. The learned dictionaries will only be used for this specific cell. At this stage there is not much concern about reducing training and feedback overhead and one would like to collect channel measurements as accurately and as extensively as possible, since large amount of channel samples will prevent the learning algorithm from overfitting. For example, one can perform conventional channel estimation using more training pilots, larger transmitted power and more sophisticated equipment. Fortunately, such channel measurements collection and dictionary learning process is *offline*, and assumed to be done at the cell deployment stage. Another factor which will affect the convergence is the start pointing of the algorithm. Due to the non-convex learning process, it is possible that the learned dictionary converges to local optima. Starting from a reasonably good initial point, for example an overcomplete DFT matrix, can help avoid such local optima and promote quicker convergence.

The learned dictionary $\boldsymbol{D}^d$ and $\boldsymbol{D}^u$ are stored at the BS for use during downlink and uplink channel estimation. It is straightforward for the uplink since the channel estimation is performed at the BS, and we can directly applied $\boldsymbol{D}^u$ to estimate the uplink channel based on the sparse recovery. In the downlink channel estimation, users feed back the received measurements $\boldsymbol{y}^d$ to the BS and the channel is estimated at the BS using compressive sensing-based downlink channel estimation with the learned dictionary $\boldsymbol{D}^d$. This is different from the conventional channel estimation where users estimate the channel and feed back the channel state information to the base station. The scheme of feeding back $\boldsymbol{y}^d$ has been proposed in previous works [28, 32, 45], which has several advantages: firstly the compressive sensing algorithms used for channel estimation can be complex so it is preferably done at the BS thus saving energy for UE. Secondly, $\boldsymbol{y}^d$ has dimension T^d which is much less than the channel dimension N in massive MIMO system, so it also reduces feedback overhead which is now only proportional to the channel sparsity level. Furthermore, for the downlink channel estimation, making the learned dictionary available to all users involves significant overhead in storage at UE and also conveyance of dictionary. By feeding back $\boldsymbol{y}^d$ only the BS needs to know the dictionaries. For simplicity, we assume perfect uplink feedback.

3.5 Joint Uplink/Downlink Dictionary Learning

In compressive sensing-based downlink channel estimation, larger training period T^d leads to better recovery performance since more information about the downlink channel is collected. However, larger T^d also means more downlink resources for channel estimation and leaves less time for actual data transmission. This motivates our search for alternative information sources that can facilitate downlink channel estimation without increasing the downlink training overhead. In this section, we will discuss about how to use the uplink training information by exploiting the reciprocal structure between the uplink and downlink channels.

3.5.1 Motivation

For this we draw inspiration from TDD systems, where through channel reciprocity the uplink channel estimate provides downlink channel information [26,47]. In FDD system we do not have such channel reciprocity because uplink and downlink transmission are operated in different frequency bands. However, if the duplex distance is not large, i.e., the frequency difference between the uplink and the downlink is not large, a looser and more abstract form of reciprocity is possible and appropriate. For instance, it is reasonable to assume the AOA of signals in the uplink transmission is the same as the AOD of signals in the downlink transmission [35, 60–63]. In other words directions of signal paths are invariant to carrier frequency shift. Consider the spatial channel model proposed in Chapter 2

$$\begin{aligned} \boldsymbol{h}^u &= \sum_{i=1}^{N_c}\sum_{l=1}^{N_s} \alpha_{il}^u \boldsymbol{a}^u(\Omega_{il}^u) \\ \boldsymbol{h}^d &= \sum_{i=1}^{N_c}\sum_{l=1}^{N_s} \alpha_{il}^d \boldsymbol{a}^d(\Omega_{il}^d) \end{aligned} \tag{3.26}$$

This indicates that α_{il}^u in the uplink is different and uncorrelated from α_{il}^d in the downlink due to the frequency separation. However, both links share the same N_c, N_s and $\Omega_{il}^u = \Omega_{il}^d$. So when we treat $\boldsymbol{h}^u$ and $\boldsymbol{h}^d$ as a whole, they appear to be uncorrelated. But if we are able to resolve them finely in the angular domain, which indeed can be achieved by the large antenna array, they will show the common spatial structure which can be regarded as the reciprocity in the angular domain. In [61], congruence of the directional properties of the uplink and the downlink channel is observed experimentally, where the dominant uplink/downlink directions of arrival (DOA) show only a minor deviation, and the uplink/downlink azimuth power spectrums (APS) have a high correlation.

Furthermore, the directions in the angular domain are closely related to the locations of nonzero entries in the sparse coefficients. Consider the uplink and the downlink sparse channel model $\boldsymbol{h}^u = \boldsymbol{D}^u\boldsymbol{\beta}^u$ and $\boldsymbol{h}^d = \boldsymbol{D}^d\boldsymbol{\beta}^d$, the reciprocity in the angular domain translates to the same locations of nonzero entries in $\boldsymbol{\beta}^u$ and $\boldsymbol{\beta}^d$, i.e., supp$(\boldsymbol{\beta}^u) =$ supp$(\boldsymbol{\beta}^d)$. Consequently, if we know $\boldsymbol{h}^u$, and utilize for the downlink channel estimation the common support information supp$(\boldsymbol{\beta}^u) =$ supp$(\boldsymbol{\beta}^d)$, we have critical information about $\boldsymbol{h}^d$ and can obtain better downlink channel estimates without increasing the training overhead. Similar to the downlink dictionary learning, an uplink dictionary learning is needed for efficiently and robustly uplink channel representation. Moreover, the learned uplink dictionary should be able to encourage the support structure supp$(\boldsymbol{\beta}^u) =$ supp$(\boldsymbol{\beta}^d)$ motivated from the reciprocity between the uplink and downlink transmission.

3.5.2 Formulation of Joint Dictionary Learning

Based on the DLCM in the previous section, we propose a *joint* dictionary learning process where $\boldsymbol{D}^u$ and $\boldsymbol{D}^d$ are learned jointly with the constraint on the support, i.e., supp$(\boldsymbol{\beta}^u) =$ supp$(\boldsymbol{\beta}^d)$. In order to enforce such constraint, we collect channel samples $\{\boldsymbol{h}_i^u, \boldsymbol{h}_i^d\}$ in pair. Each pair of samples is measured at the *same* UE location, so the assumption of the same AOA/AOD is valid. The joint dictionary learning can be formulated as

$$\begin{aligned} \min_{\substack{\boldsymbol{D}^u\in\mathcal{C},\boldsymbol{\beta}_1^u,\ldots,\boldsymbol{\beta}_L^u\\ \boldsymbol{D}^d\in\mathcal{C},\boldsymbol{\beta}_1^d,\ldots,\boldsymbol{\beta}_L^d}} \quad & \frac{1}{L}\sum_{i=1}^{L}\|\boldsymbol{\beta}_i^u\|_0+\|\boldsymbol{\beta}_i^d\|_0 \\ \text{subject to} \quad & \|\boldsymbol{h}_i^u-\boldsymbol{D}^u\boldsymbol{\beta}_i^u\|_2\le\eta^u,\ \ \|\boldsymbol{h}_i^d-\boldsymbol{D}^d\boldsymbol{\beta}_i^d\|_2\le\eta^d, \\ & \text{supp}(\boldsymbol{\beta}_i^u)=\text{supp}(\boldsymbol{\beta}_i^d),\ \ \forall i \end{aligned} \tag{3.27}$$

which is very similar to the dictionary learning problem as shown in (3.22), except for the constraint supp$(\boldsymbol{\beta}_i^u) =$ supp$(\boldsymbol{\beta}_i^d)$. This constraint is important since it builds the connection between the uplink and downlink channel responses, which will be utilized in the joint channel estimation. Two alternative joint dictionary learning formulation can be extended from (3.24) and (3.25) straightforwardly.

To solve the joint dictionary learning, we minimize (3.27) iteratively similar to (3.22). We first fix $\boldsymbol{D}^u, \boldsymbol{D}^d$ and solve for $\boldsymbol{\beta}_i^u, \boldsymbol{\beta}_i^d, \forall i$, and then fix $\boldsymbol{\beta}_i^u, \boldsymbol{\beta}_i^d, \forall i$ and solve for $\boldsymbol{D}^u, \boldsymbol{D}^d$. Notice that when $\boldsymbol{\beta}_i^u, \boldsymbol{\beta}_i^d, \forall i$ are fixed, the solution of $\boldsymbol{D}^u$ and $\boldsymbol{D}^d$ are decoupled, and can be optimized independently using any of dictionary learning algorithms [57–59]. When $\boldsymbol{D}^u, \boldsymbol{D}^d$ are fixed, different pairs of $\{\boldsymbol{\beta}_i^u, \boldsymbol{\beta}_i^d\}$ are decoupled. But for each of the pair, they are coupled through the constraint supp$(\boldsymbol{\beta}_i^u) =$ supp$(\boldsymbol{\beta}_i^d)$, and need to be solved jointly. Algorithms aiming to solve joint sparse recovery have been proposed in previous works, such as OMP like algorithm [68], ℓ_1 norm algorithm [69], reweighted ℓ_p norm algorithm [70] and sparse Bayesian learning algorithm [71]. It has been shown that joint recovery can lead to more accurate results compared to the independent recovery.

In this work, we consider a group ℓ_1 formulation which is similar to the group-lasso in [69] to solve the joint sparse recovery problem. By forming

$$\boldsymbol{h} = \begin{bmatrix} \boldsymbol{h}_i^d \\ \boldsymbol{h}_i^u \end{bmatrix}, \boldsymbol{\beta} = \begin{bmatrix} \boldsymbol{\beta}_i^d \\ \boldsymbol{\beta}_i^u \end{bmatrix}, \boldsymbol{G} = \begin{bmatrix} \boldsymbol{D}^d & \boldsymbol{0}_{N \times M} \\ \boldsymbol{0}_{N \times M} & \boldsymbol{D}^u \end{bmatrix} \tag{3.28}$$

the joint sparse recovery of $\boldsymbol{\beta}_i^d, \boldsymbol{\beta}_i^u$ can be written as

$$\min_{\boldsymbol{\beta}} \sum_{j=1}^{M} \|\boldsymbol{\beta}\|_{\boldsymbol{K}_j} \quad \text{subject to } \|\boldsymbol{h} - \boldsymbol{G}\boldsymbol{\beta}\|_2 \leq \eta \tag{3.29}$$

where $\|\boldsymbol{\beta}\|_{\boldsymbol{K}_j} = (\boldsymbol{\beta}^H \boldsymbol{K}_j \boldsymbol{\beta})^{1/2}$, $\boldsymbol{K}_j = \text{diag}([\boldsymbol{e}_j^T \;\; \boldsymbol{e}_j^T]^T)$ is the group kernel, where $\boldsymbol{e}_j \in \mathbb{R}^{M \times 1}$ is the standard basis with 1 in the j-th location and 0 elsewhere. The group kernel gathers the j-th element in $\boldsymbol{\beta}_i^d$ and the j-th element in $\boldsymbol{\beta}_i^u$ into the same group. The cost function in (3.29) is a ℓ_2/ℓ_1 norm of $\boldsymbol{\beta}$ similar to the ℓ_p/ℓ_1 norm in [40], which encourages all the elements in the same group to be zero or nonzero simultaneously, and the total number of nonzero groups to be small. By applying this group ℓ_1 framework, we enforce the constraint of supp$(\boldsymbol{\beta}_i^u) =$ supp$(\boldsymbol{\beta}_i^d)$ and encourage a sparse representation.

3.5.3 Formulation of Joint Channel Estimation

After learning $\boldsymbol{D}^u, \boldsymbol{D}^d$, we have the joint uplink and downlink sparse channel representation as $\boldsymbol{h}^u \approx \boldsymbol{D}^u \boldsymbol{\beta}^u$ and $\boldsymbol{h}^d \approx \boldsymbol{D}^d \boldsymbol{\beta}^d$. The goal is to utilize uplink training to help improving the performance of the downlink channel estimation, by using the constraint supp$(\boldsymbol{\beta}^u) =$ supp$(\boldsymbol{\beta}^d)$. Consider the uplink training for a single user, we have

$$\boldsymbol{Y}^u = \boldsymbol{h}^u \sqrt{\rho^u T^u} \boldsymbol{s}^T + \boldsymbol{W}^u \tag{3.30}$$

where $\boldsymbol{s} \in \mathbb{C}^{T^u \times 1}$ denotes the uplink training pilots during T^u training duration, and $\|\boldsymbol{s}\|_2 = 1$. ρ^u includes the uplink training power and the large scale fading. Denote $\boldsymbol{y}^u = \boldsymbol{Y}^u(\sqrt{\rho^u T^u}\boldsymbol{s}^T)^\dagger$ and $\boldsymbol{w}^u = \boldsymbol{W}^u(\sqrt{\rho^u T^u}\boldsymbol{s}^T)^\dagger$, we have

$$\boldsymbol{y}^u = \boldsymbol{h}^u + \boldsymbol{w}^u = \boldsymbol{D}^u\boldsymbol{\beta}^u + \boldsymbol{w}^u. \tag{3.31}$$

Combined with the downlink training which is given by

$$\boldsymbol{y}^d = \boldsymbol{A}\boldsymbol{h}^d + \boldsymbol{w}^d = \boldsymbol{A}\boldsymbol{D}^d\boldsymbol{\beta}^d + \boldsymbol{w}^d \tag{3.32}$$

where $\boldsymbol{A} \in \mathbb{C}^{T^d \times N}$ denotes the downlink training pilots, the joint uplink/downlink channel estimation can be formulated as

$$\begin{aligned} \{\hat{\boldsymbol{\beta}}^u, \hat{\boldsymbol{\beta}}^d\} = \arg\min_{\boldsymbol{\beta}^u, \boldsymbol{\beta}^d} & \ \|\boldsymbol{\beta}^u\|_0 + \|\boldsymbol{\beta}^d\|_0 \\ \text{subject to} \quad & \|\boldsymbol{y}^u - \boldsymbol{D}^u\boldsymbol{\beta}^u\|_2 \leq \epsilon^u, \ \ \|\boldsymbol{y}^d - \boldsymbol{A}\boldsymbol{D}^d\boldsymbol{\beta}^d\|_2 \leq \epsilon^d, \\ & \text{supp}(\boldsymbol{\beta}^u) = \text{supp}(\boldsymbol{\beta}^d). \end{aligned} \tag{3.33}$$

where we seek the most sparse uplink and downlink representation that are consistent with the received uplink and downlink signal, which agree with the support constraint supp$(\boldsymbol{\beta}^u) =$ supp$(\boldsymbol{\beta}^d)$. After solving for $\boldsymbol{\beta}^u$ and $\boldsymbol{\beta}^d$, the uplink and downlink channel can be estimated as $\hat{\boldsymbol{h}}^u = \boldsymbol{D}^u\hat{\boldsymbol{\beta}}^u$ and $\hat{\boldsymbol{h}}^d = \boldsymbol{D}^d\hat{\boldsymbol{\beta}}^d$.

Again, we face the same joint sparse recovery problem with structure constraint supp$(\boldsymbol{\beta}^u) =$ supp$(\boldsymbol{\beta}^d)$ as in the joint dictionary learning problem. We utilize the same group ℓ_1 algorithm as in (3.29) as following

$$\min_{\boldsymbol{\beta}} \sum_{j=1}^{M} \|\boldsymbol{\beta}\|_{\boldsymbol{K}_j} \quad \text{subject to } \|\boldsymbol{y} - \boldsymbol{G}\boldsymbol{\beta}\|_2 \leq \epsilon \tag{3.34}$$

where now we have

$$\boldsymbol{y} = \begin{bmatrix} \boldsymbol{y}^d \\ \tau \boldsymbol{y}^u \end{bmatrix}, \boldsymbol{G} = \begin{bmatrix} \boldsymbol{A}\boldsymbol{D}^d & \mathbf{0}_{T \times M} \\ \mathbf{0}_{N \times M} & \tau \boldsymbol{D}^u \end{bmatrix} \tag{3.35}$$

and the same definition of $\boldsymbol{K}_j$. Notice that the norm of columns in $\boldsymbol{A}\boldsymbol{D}^d$ can be much larger than the norm of columns in $\boldsymbol{D}^u$ when ρ^d is large, which deemphasizes the role of uplink training in the noisy situation. So a constant τ is multiplied to make the columns of $\boldsymbol{G}$ to have similar norms. The solved $\boldsymbol{\beta}$ has the form of $\boldsymbol{\beta} = [(\boldsymbol{\beta}^d)^T (\boldsymbol{\beta}^u)^T]^T$. By joint sparse recovery of $\boldsymbol{\beta}^u, \boldsymbol{\beta}^d$, we are able to achieve improved downlink channel estimates with the help of uplink training measurements. Notice the dimension of $\boldsymbol{y}^u$ is N while dimension of $\boldsymbol{y}^d$ is T^d. In the massive MIMO system where $N \gg T^d$, the uplink training actually has larger number of measurements, which is beneficial for the sparse recovery algorithm. We can also improve the signal to noise ratio of the uplink received signal by increasing the uplink training period T^u. Due to the constraint supp($\boldsymbol{\beta}^u$) $=$ supp($\boldsymbol{\beta}^d$), $\boldsymbol{y}^u$ and $\boldsymbol{y}^d$ can regularize each other to achieve better recovery performance compared to independent recovery. More importantly, the performance of the downlink compressed channel estimation is improved without increasing the downlink training period T^d. In other words, we can reduce the downlink training overhead by leveraging the information from uplink training.

3.5.4 Discussion

Similar to the DLCM, there is a joint dictionary learning phase and a joint channel estimation phase. During the joint dictionary learning phase, a large amount of channel measurements need to be collected as training samples. Each pair of uplink/downlink channel measurements has to be collected at the *same user location*, in order to guarantee the same AOA/AOD for the uplink and downlink. This requirement is important since for each pair of $\{\boldsymbol{h}_i^u, \boldsymbol{h}_i^d\}$ the learning process has the constraint supp($\boldsymbol{\beta}_i^u$) $=$ supp($\boldsymbol{\beta}_i^d$). The joint dictionary learning is implemented when the cell is installed, and the learned $\boldsymbol{D}^u$, $\boldsymbol{D}^d$ are stored at the base station. In the channel estimation phase, the BS transmits downlink pilots while the UE transmits uplink pilots, then the UE feeds back the received signal. The joint channel estimation is performed at the BS, from which the uplink and downlink channel state information is obtained.

3.6 Numerical Results

In the simulation, we test both 2D and 3D channel model. For 2D channel, we assume the BS is equipped with an ULA with 100 antennas and each UE has a single antenna. The channel is generated using parameters from non line-of-sight (NLOS) urban macro scenario in [35]. Since the learned dictionary depends on the cell characteristics, we generate cell specific scattering clusters following the principles of Geometry-Based Stochastic Channel Model (GSCM) [38]. At the beginning of the simulation, 21 fixed location scattering clusters are uniformly generated in a cell with radius 900 meters and $\theta \in [-\frac{\pi}{2}, \frac{\pi}{2}]$, and then kept constant for the simulation of both dictionary learning and channel estimation. The user's location is also randomly and uniformly generated. For each channel response between the BS and the UE, it consists AOA/AOD of multi-paths from 3 fixed location scattering clusters which are closest to the UE, and 1 user-location dependent scattering cluster which is generated according to [35] based on the UE's location. All the other parameters, e.g., angular spread, delay spread, and path power, etc., are all generated following [35]. The AOA/AOD values are identical between the uplink and downlink, while the phases of subpaths are random and uncorrelated [35]. For 3D channel, the BS is assumed to be equipped with a 10×10 URA and the UE with a 3×3 URA. The channel is generated following the NLOS UMi-Street Canyon scenario in [37], where the carrier frequency is assumed to be 28 GHz. The generation of cell specific clusters is similar to the 2D model, except that the cell radius is 200 meters with $\theta \in [0, \pi]$, $\phi \in [0, \pi]$, and each cluster has a height $h \in [0.5, 30]$ while $h_{\mathrm{BS}} = 10$ m and $h_{\mathrm{UE}} = 1.5$ m, so elevation angles ZOA/ZOD can be calculated. Since the carrier frequency is 28 GHz, each channel response consists only 1 fixed location scattering cluster and 1

user-location dependent scattering cluster consistent with the small number of scattering clusters at the millimeter wave (mmWave) frequency [72].

Two kinds of antenna array are considered at the BS. The first is the perfectly calibrated antenna array, e.g., equal spacing $d = \lambda/2$ between antenna elements and equal antenna gains as 1. In the second case, there exist *antenna uncertainties* in the form of *unknown but fixed* calibration errors, where the antenna spacing and gains are deviating from the nominal values. We generate them as following: in 100 antennas, 20 antennas have gains $1 + e$ while the other 80 have gains 1. The $e \sim \mathcal{N}(0, 0.1)$, and if $1 + e > 1.2$ or $1 + e < 0.8$, then the gain is set to be 1.2 or 0.8. Among 99 antenna spacings, there are 20 having values $d = (1 + v)\lambda/2$ where $v \sim \mathcal{N}(0, 0.1)$. If $1 + v > 1.2$ or $1 + v < 0.8$, then the spacing is set to be $1.2\lambda/2$ or $0.8\lambda/2$. The rest of antenna spacings are $d = \lambda/2$. After the antenna gains and spacings are generated, they are fixed in the whole simulation of dictionary learning and channel estimation.

For the dictionary learning, $L = 10000$ channel responses are generated, and for each channel responses the UE is randomly and uniformly located in the cell with at least 300 meters (60 meters for the mmWave scenario) from the BS. K-SVD [59] combined with ℓ_1 or group ℓ_1 algorithm (implemented using SPGL1 toolbox [73]) are applied for the dictionary learning and sparse coding. There are many other dictionary learning and sparse recovery algorithms, which trade off between accuracy and speed. In this work our main objective is to demonstrate the usefulness and potential of dictionary learning-based channel modeling, and leave the problem of optimal algorithm design/selection for future work. Unless otherwise indicated, the dictionary is learned from the true channel responses without accounting for any measurement noise. We should emphasize that it is an ideal assumption and our results are only to prove the concept of using dictionary learning for channel estimation. In the simulation, we provide an experimental study to show the effect of inaccurate training channel measurements for the dictionary learning. We compare 100×400 learned dictionary $\boldsymbol{D}$ (DLCM) with 100×100 DFT matrix $\boldsymbol{F}$ (DFT) and 100×400 overcomplete DFT matrix $\tilde{\boldsymbol{F}}$ (ODFT).

3.6.1 Sparse Representation Using DLCM

The motivation of using DLCM is to find a dictionary which can (a) more efficiently represent the channel response, i.e., the sparse coefficient has fewer number of nonzero entries; and (b) more robustly represent the channel response, i.e., adapting to any model mismatches like antenna uncertainties. To compare the channel representation, we generate 1000 channel responses $\boldsymbol{h}_i$, normalize them to have unit norm and calculate the sparse coefficient using ℓ_1 framework:

$$\hat{\boldsymbol{\beta}}_i = \arg\min_{\boldsymbol{\beta}_i} \|\boldsymbol{\beta}_i\|_1 \text{ subject to } \|\boldsymbol{h}_i - \boldsymbol{D}\boldsymbol{\beta}_i\|_2 \leq \eta \tag{3.36}$$

where η is set to be 0.1, so the tolerance of model mismatch is 10%. Notice that the sparse representation can be obtained by any sparse recovery algorithm, where different algorithm may lead to different sparse coefficient. We use ℓ_1 framework here to be consistent with the algorithm applied in dictionary learning and channel estimation.

We then compute $\|\hat{\boldsymbol{\beta}}_i\|_0$ and plot its cumulative distribution function (CDF) using 1000 channel responses. Fig.3.1 (a) shows that for perfectly calibrated antenna array, the learned dictionary can represent channel responses using fewer number of nonzero entries. For example, 90% of channel responses can be represented using about 20 columns from the learned dictionary, while it requires about 27 or 100 columns if using overcomplete DFT matrix or square DFT matrix. In Fig.3.1 (b), we test antenna array with uncertainties. Both predefined sparsifying matrices are no longer able to sparsely represent the channel, since the assumed structure of ULA does not agree with the true antenna array whose gains and spacings deviate from nominal values. However, the learned dictionary can achieve efficient sparse representation similar to Fig.3.1 (a), due to its ability to adapt the dictionary to the channel measurements. So even there exist antenna array uncertainties, sparse representation can still be achieved given the limited scattering environment.

Since ℓ_1 norm is used in (3.36), we also compute $\|\hat{\boldsymbol{\beta}}_i\|_1$ and plot its CDF. Fig. 3.2 (a)

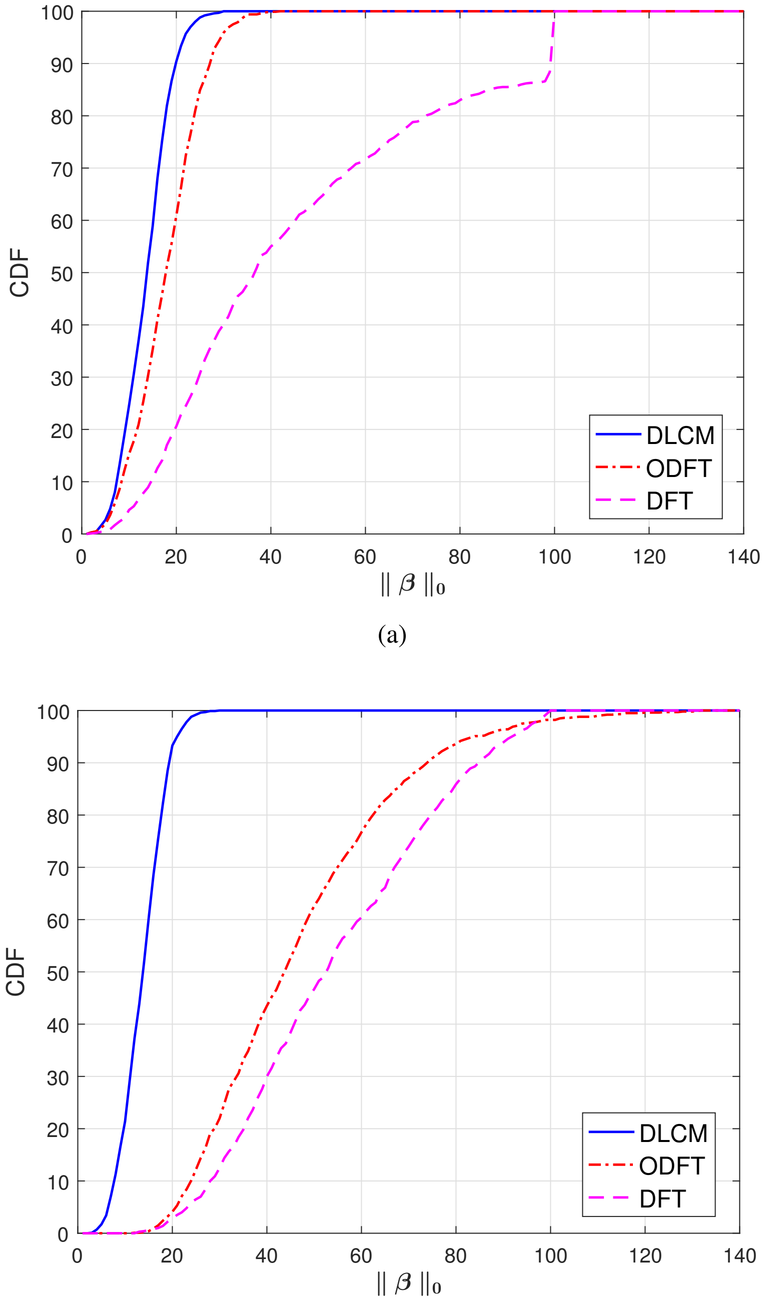

(a)

(b)

Figure 3.1: Cumulative distribution function of $\|\boldsymbol{\beta}\|_0$. (a) Perfectly calibrated antenna array. (b) Antenna array with uncertainties. $N = 100$, $\eta = 0.1$.

shows the result for perfectly calibrated antenna array, and Fig. 3.2 (b) tests antenna array with uncertainties. When the channel responses are represented using the learned dictionary, the

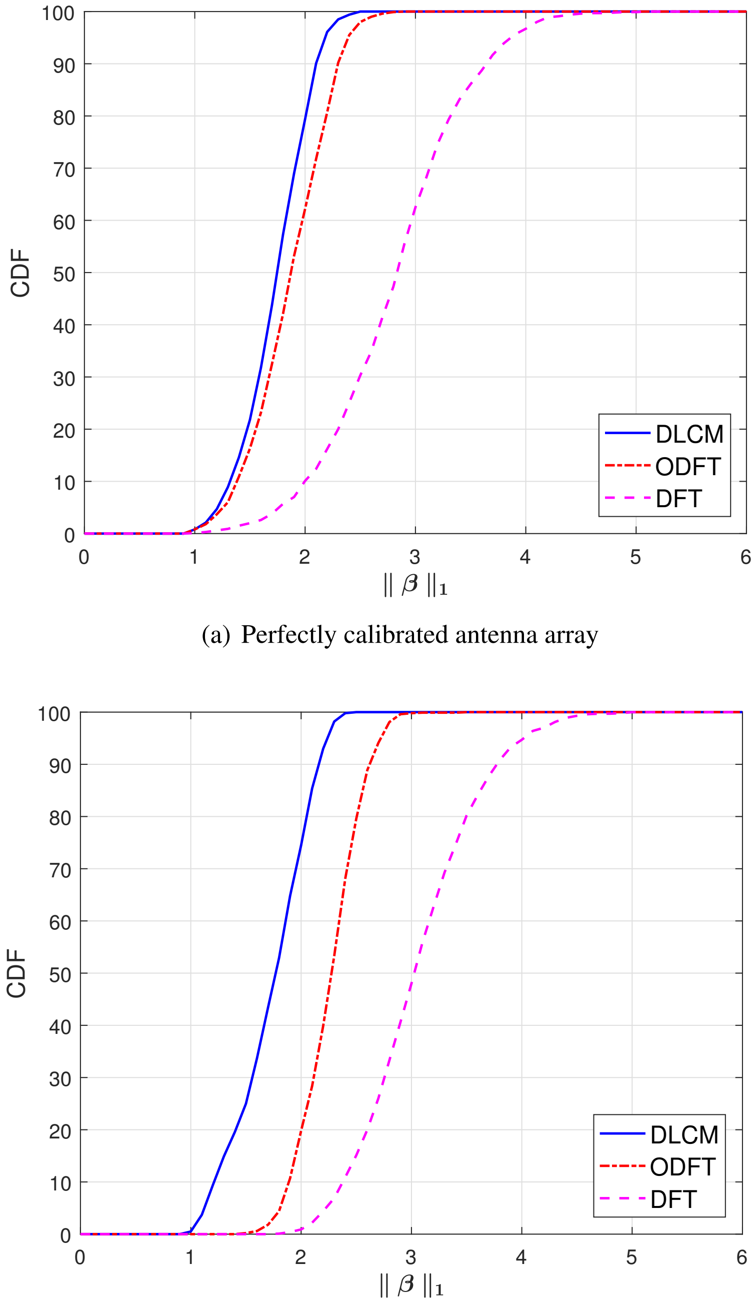

(a) Perfectly calibrated antenna array

(b) Antenna array with uncertainties

Figure 3.2: Cumulative distribution function of $\|\boldsymbol{\beta}\|_1$. (a) Perfectly calibrated antenna array. (b) Antenna array with uncertainties. $N = 100$, $\eta = 0.1$.

spare coefficient has smaller $\|\boldsymbol{\beta}\|_1$, indicating a more sparse representation since ℓ_1 norm is the convex relaxation of ℓ_0 norm. Similar to Fig. 3.1, the overcomplete DFT matrix can achieve comparable performance as the learned dictionary for perfectly calibrated antenna array, but has big performance loss when antenna array with uncertainties is used.

The results indicate that for a perfectly calibrated antenna array, the suggested overcomplete DFT matrix is a reasonably good sparsifying matrix with only a little inferior than the learned dictionary, since the columns of the overcomplete DFT matrix shares the same structure as the channel responses, and the overcompleteness brings much flexibility in representing the channel. However, when antenna array has uncertainties, predefined matrices degrades considerably due to the huge structure mismatches. In contrast, the learned dictionary leads to efficient and robust representation in both situations, since it is learned from the data without any structure constraint. In the following, we will show how this efficient and robust representation will lead to improved channel estimation performance in both downlink and uplink.

3.6.2 Downlink Channel Estimation

To evaluate how the channel representation affects the channel estimation, we compare the performance of compressive sensing-based downlink channel estimation when different sparsifying matrices are applied. The training pilots in $\boldsymbol{A}$ is generated as i.i.d. $\mathcal{CN}(0, \rho^d/N)$, so $\mathbb{E}\|\boldsymbol{A}\|_F^2 = \rho^d T^d$. The normalized mean square error (NMSE) is used as the performance metric and defined as

$$\text{NMSE} = \mathbb{E}\Big\{\frac{\|\boldsymbol{h} - \hat{\boldsymbol{h}}\|_2^2}{\|\boldsymbol{h}\|_2^2}\Big\} = \frac{1}{K}\sum_{i=1}^{K}\frac{\|\boldsymbol{h}_i - \hat{\boldsymbol{h}}_i\|_2^2}{\|\boldsymbol{h}_i\|_2^2}. \tag{3.37}$$

where K denotes the number of trials performed. We first consider the 2D channel model with ULA. Fig.3.3 (a) plots the NMSE performance with respect to the number of downlink pilot symbols T^d, when a perfectly calibrated antenna array is applied. We also include the LS channel estimation when $T^d = 100$ for comparison. To achieve the same NMSE, both DLCM and ODFT requires much less training pilots compared to DFT which is used in the virtual channel model, and the DLCM saves more than ODFT. Antenna array with uncertainties is tested in Fig.3.3 (b).

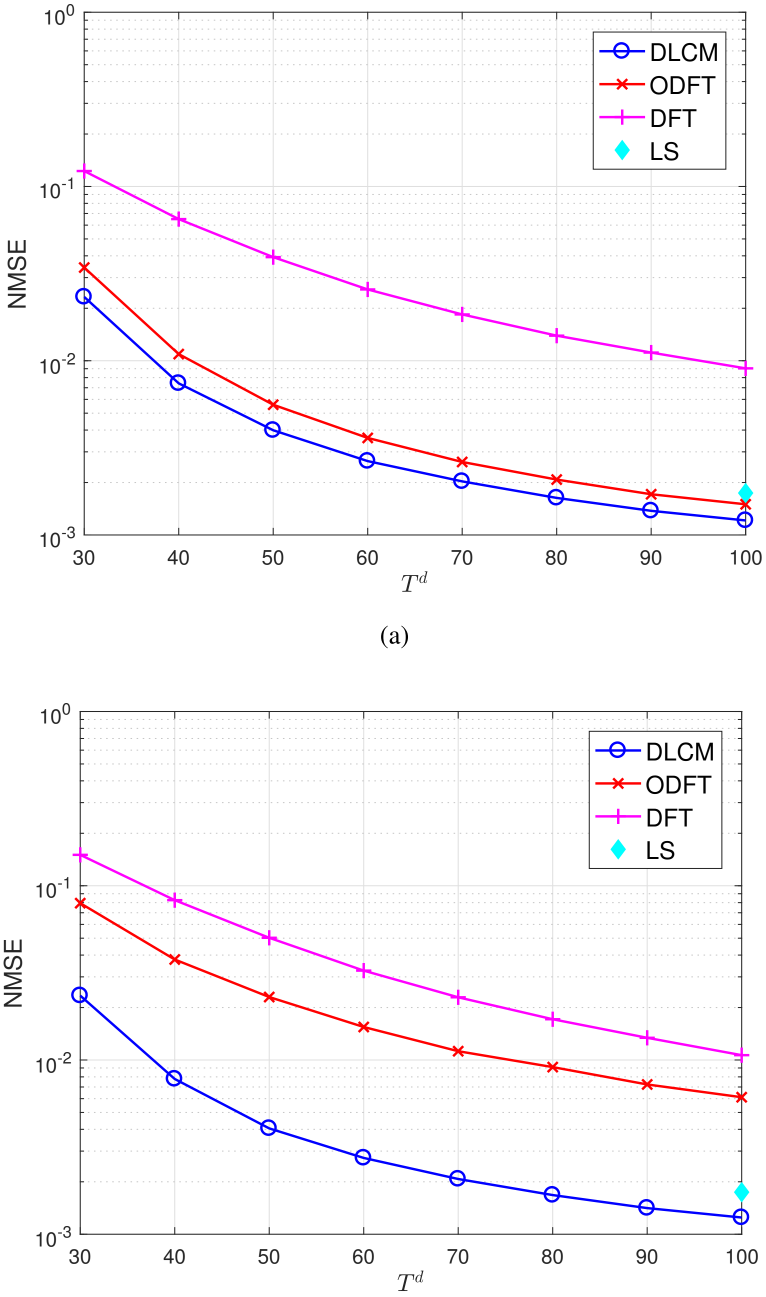

(a)

(b)

Figure 3.3: Normalized mean square error (NMSE) comparison of different sparsifying matrices for CS-based downlink channel estimation with ULA. (a) Perfectly calibrated antenna array. (b) Antenna array with uncertainties. SNR = 20dB.

It shows that the performance of ODFT degrades considerably, while the DLCM achieves almost the same accuracy as in Fig.3.3 (a). So when the antenna array is not perfectly calibrated, only the learned dictionary can achieve great savings on downlink training overhead.

In Fig. 3.4, we test mmWave 3D channel model with a 10×10 URA at the BS and a 3×3 URA at the UE. The MMV channel estimation

$$\hat{\boldsymbol{B}}^d = \arg\min_{\boldsymbol{B}^d} \|\boldsymbol{B}^d\|_{1,2} \text{ subject to } \|\boldsymbol{Y}^d - \boldsymbol{A}\boldsymbol{D}^d\boldsymbol{B}^d\|_F \leq \epsilon, \tag{3.38}$$

is applied with respect to multiple antennas at the UE (see Chapter 2 for details). Performance comparison with perfectly calibrated antenna array and antenna array with uncertainties are shown in Fig. 3.4 (a) and Fig. 3.4 (b). Similar to the 2D channel model with ULA, the DLCM achieves better performance than ODFT and DFT. The result demonstrates the applicability of the proposed DLCM framework to different antenna geometry and frequency band. Fig. 3.5 plots the performance with only a single antenna at the UE. Compared to Fig. 3.4 (a) where the UE has 9 antennas, the performance becomes worse. This shows the benefit of having multiple antennas at UE and utilizing the proposed MMV formulation (3.38) to estimate the channel. The joint sparse channel structure for different antennas at UE is exploited to improve the performance. To study the channel estimation in low SNR range, Fig.3.6 depicts the performance when SNR $= 5$dB. Compared to Fig.3.4 (a) where SNR $= 20$dB, the performances of all sparsifying matrices are worse, and the differences among them become small. The reason is that when the noise is large, the accuracy of the channel estimation is limited mostly by the noise, so the model mismatch error from applying different sparsifying matrices has only small influence on the performance. In a practical system, performance of channel estimation depends on many factors such as the noise level, model mismatch error, the number of antennas, etc., and more studies are required to show under what condition the DLCM can achieve the greatest improvement.

In previous experiments, perfect channel measurements are used for dictionary learning.

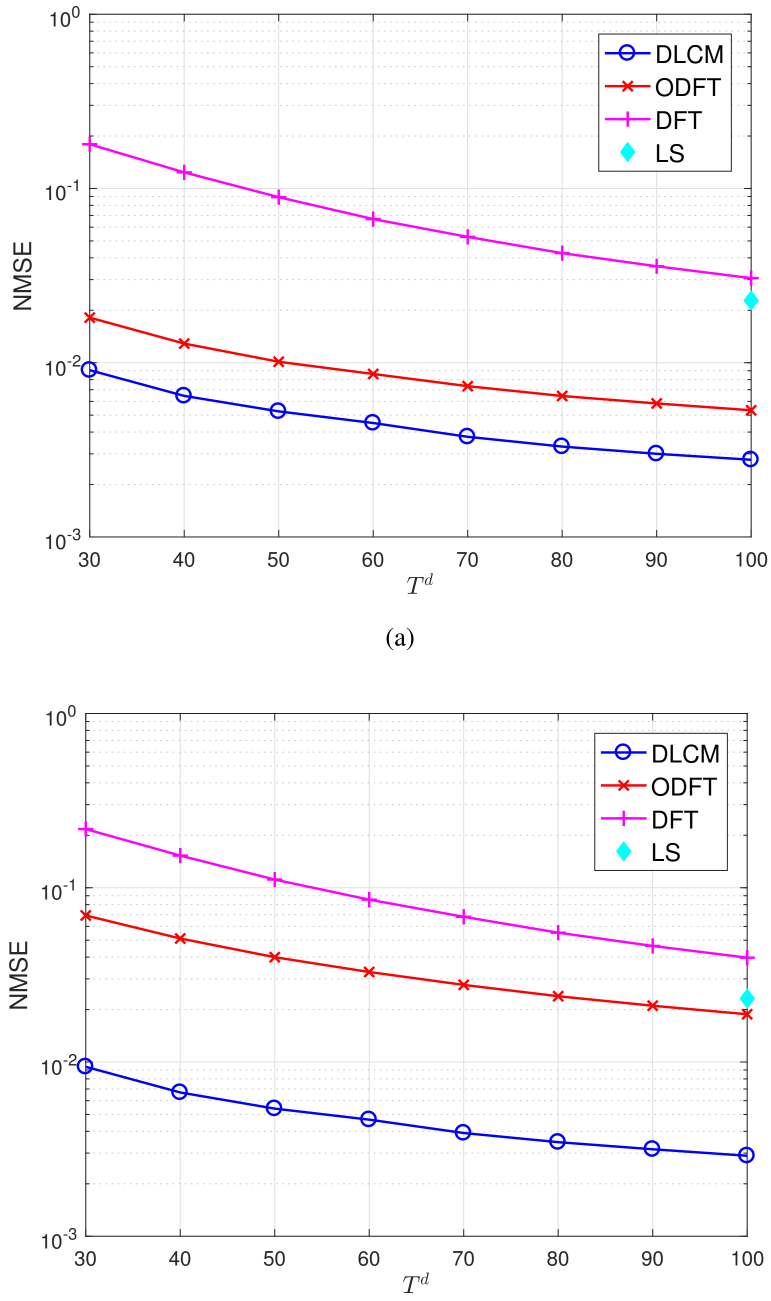

(a)

(b)

Figure 3.4: Normalized mean square error (NMSE) comparison of different sparsifying matrices for CS-based downlink channel estimation with URA in mmWave scenario. (a) Perfectly calibrated antenna array. (b) Antenna array with uncertainties. BS: 10×10, UE: 3×3, SNR = 20 dB.

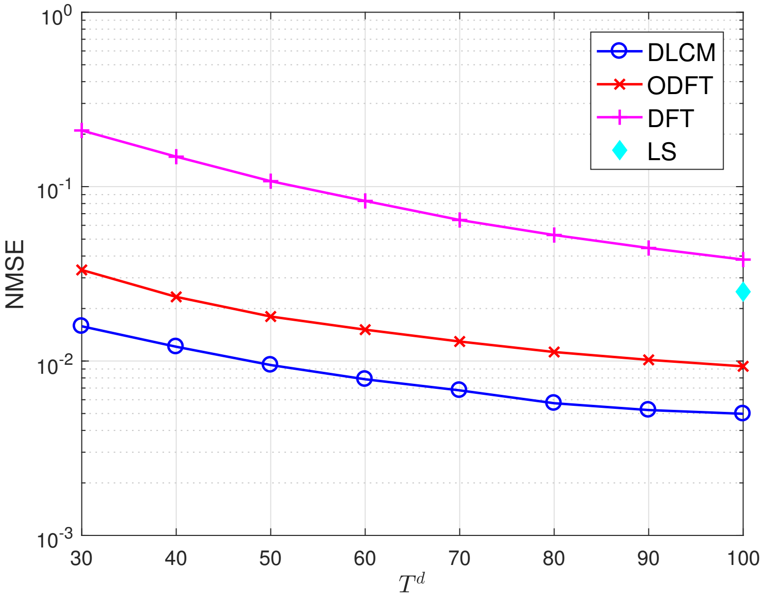

Figure 3.5: Normalized mean square error (NMSE) comparison of different sparsifying matrices for CS-based downlink channel estimation with URA in mmWave scenario. Perfectly calibrated antenna array. BS: 10×10, UE: 1×1, SNR = 20 dB.

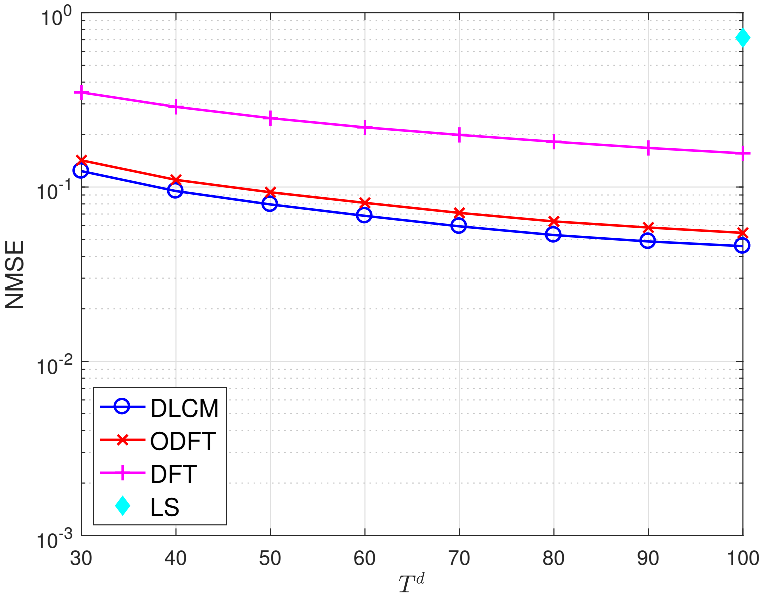

Figure 3.6: Normalized mean square error (NMSE) comparison of different sparsifying matrices for CS-based downlink channel estimation with URA in mmWave scenario. Perfectly calibrated antenna array. BS: 10×10, UE: 3×3, SNR = 5 dB.

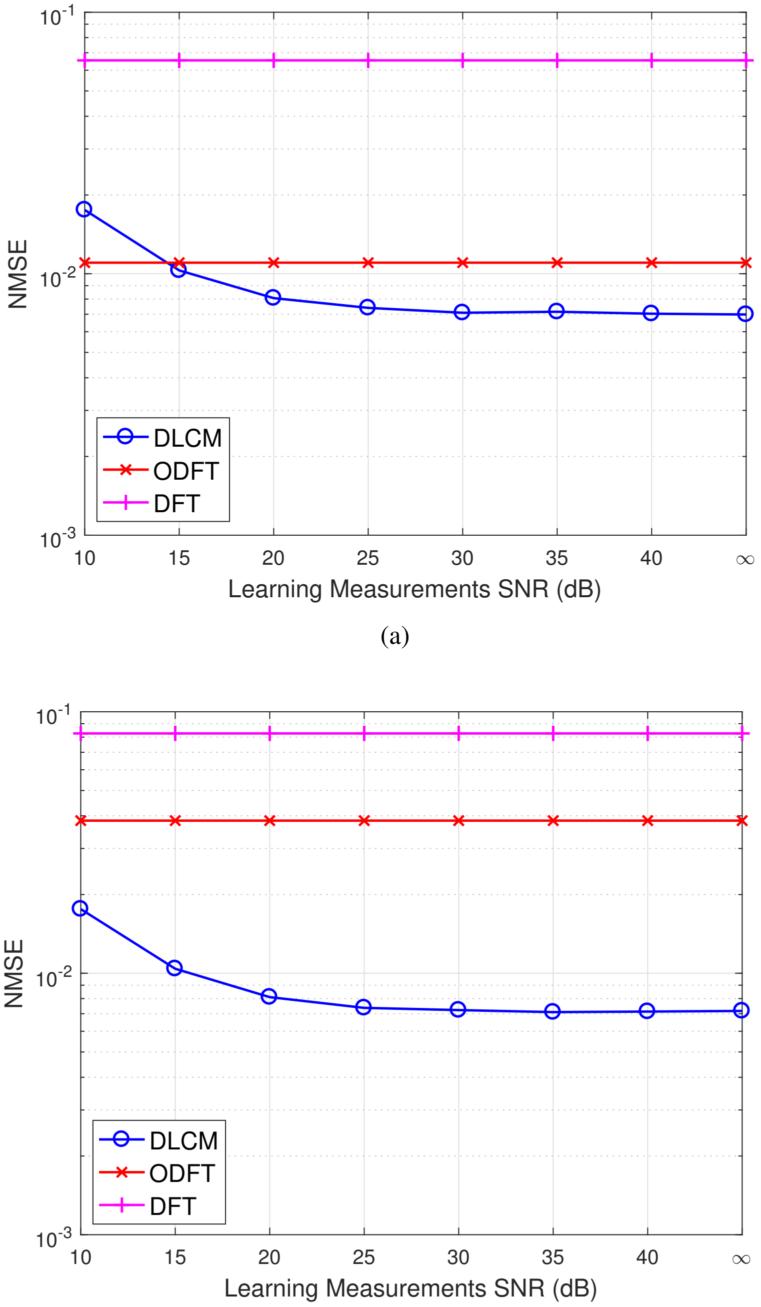

(a)

(b)

Figure 3.7: Normalized mean square error (NMSE) versus learning measurements SNR for CS-based downlink channel estimation with ULA. (a) Perfectly calibrated antenna array. (b) Antenna array with uncertainties. $T^d = 40$, SNR = 20dB.

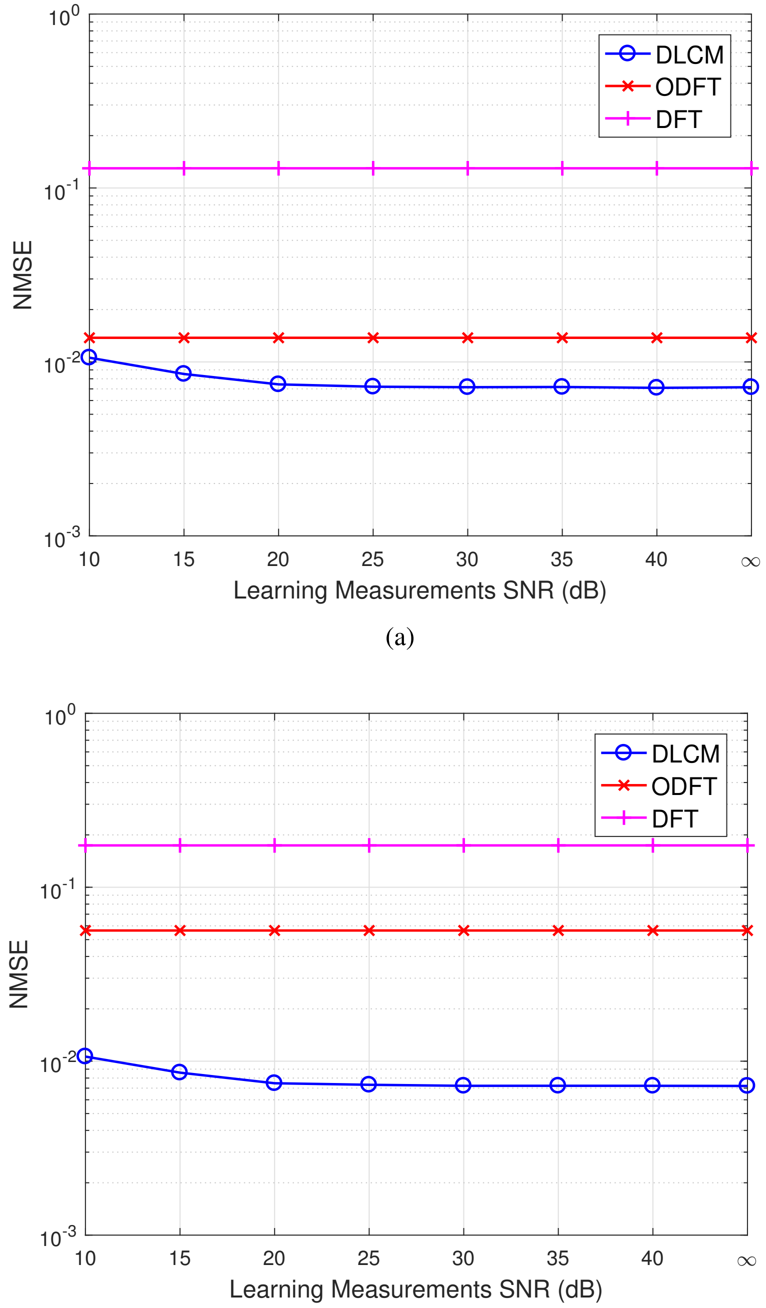

(a)

(b)

Figure 3.8: Normalized mean square error (NMSE) versus learning measurements SNR for CS-based downlink channel estimation with URA in mmWave scenario. (a) Perfectly calibrated antenna array. (b) Antenna array with uncertainties. $T^d = 40$, SNR = 20dB.

Next we investigate the performance of DLCM when the dictionary is learned from channel responses corrupted by the noise, since in practice channel measurements can have some estimation error in them. We consider the 2D channel model using ULA, and add noise $\tilde{\boldsymbol{n}}_i$ to the true channel response $\boldsymbol{h}_i$, where $\tilde{\boldsymbol{n}}_i \sim \mathcal{CN}(\mathbf{0}, \sigma_i^2 \mathbf{I})$ and σ_i is chosen according to the "learning measurements SNR" which is defined as

$$\text{Learning Measurements SNR} = \frac{\|\boldsymbol{h}_i\|_2^2}{\mathbb{E}\|\tilde{\boldsymbol{n}}_i\|_2^2} = \frac{\|\boldsymbol{h}_i\|_2^2}{N\sigma_i^2}. \tag{3.39}$$

Then the corrupted channel response is obtained as

$$\tilde{\boldsymbol{h}}_i = \boldsymbol{h}_i + \tilde{\boldsymbol{n}}_i \tag{3.40}$$

which is used as the training channel samples for the dictionary learning. Fig. 3.7 compares the NMSE of downlink channel estimation with respect to the learning measurements SNR, where for each learning measurements SNR a different dictionary is learned. We also include the performance when the true channel response $\boldsymbol{h}_i$ is used as the training samples, and denoted it as ∞ learning measurements SNR. When the learning measurements SNR is low, the performance of DLCM degrades since the dictionary learning process can not accurately capture the channel structure from too noisy channel measurements. As the learning measurements SNR increases, the performance of DLCM becomes better and approaches the performance of learning from noiseless measurements. Notice that when the antenna array is not perfectly calibrated, as shown in Fig. 3.7 (b), DLCM can obtain better performance than predefined sparsifying matrices even with dictionary learned from very noisy measurements, because the model mismatch error plays the dominant role for the channel representation when there exist antenna uncertainties. Similar observations can be made when consider the URA antenna array at mmWave scenario, which are shown in the Fig. 3.8. In this scenario, even the dictionary learned from highly noisy measurements can obtain better channel estimation performance compared to other predefined

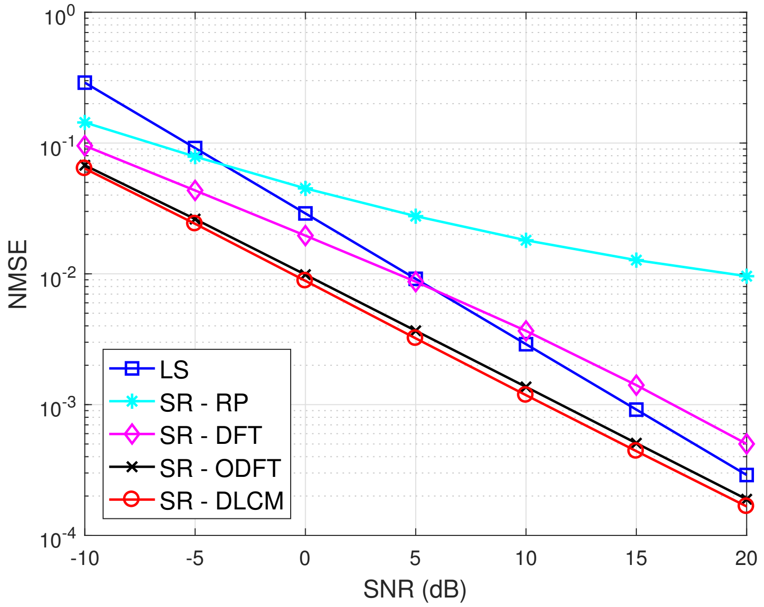

Figure 3.9: Normalized mean square error (NMSE) comparison of different sparsifying matrices, pilots design and user scheduling schemes for SR-based uplink channel estimation with ULA. Orthogonal users, perfectly calibrated antenna array. $K = 6, T^u = 6$.

sparsifying matrices. Since the dictionary learning is performed at the cell deployment stage, a high learning measurements SNR can be achieved by using more training pilots, higher transmitted power, and more sophisticated equipment. As a result, the learned dictionary is expected to efficiently represent the sparse channel and lead to a good channel estimation performance using DLCM.

3.6.3 Uplink Channel Estimation

We now evaluate performance of the sparse recovery-based (SR-based)uplink channel estimation using 2D channel model. Assume there are $K = 6$ users. In order to preserve fairness and evaluate the average NMSE performance for all users, we first assume the same ρ_k^u for all users and plot the average NMSE versus the SNR. In Fig. 3.9, the number of uplink pilots $T^u = K = 6$, so orthogonal pilots are used for both LS and SR with different sparsifying matrices.

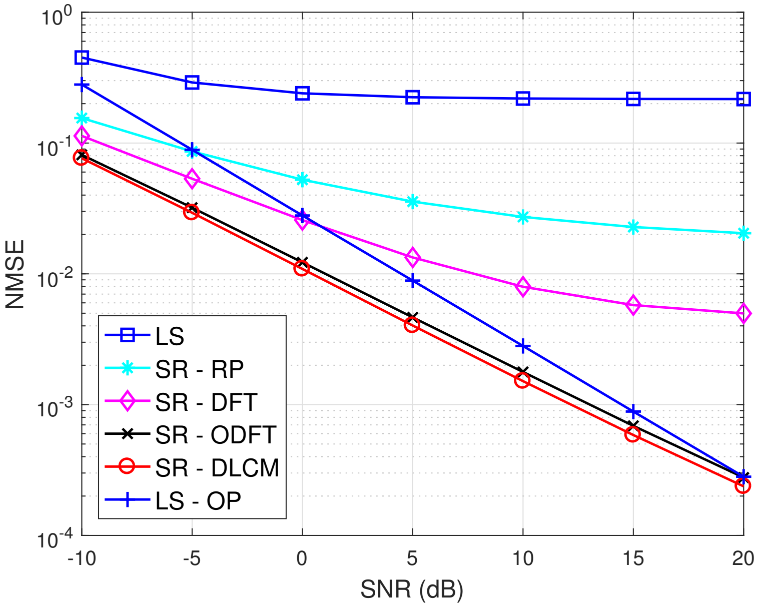

Figure 3.10: Normalized mean square error (NMSE) comparison of different sparsifying matrices, pilots design and user scheduling schemes for SR-based uplink channel estimation with ULA. Orthogonal users, perfectly calibrated antenna array. $K = 6, T^u = 5$.

We also compare SR with random pilots (SR-RP), which is possibly nonorthogonal. To encourage non-overlapping or limited overlapping sparse support, the locations of users are generated to be far away from each other, with each user's LOS AOA constrained in a distinct π/K range. For the whole SNR range, SR-DLCM and SR-ODFT are better than LS, while SR-DFT is worse than LS at high SNR. The result corroborates the conclusions made in the downlink channel estimation, such that when perfectly antenna array is used, the overcomplete DFT matrix can obtain similar performance as the learned dictionary. Furthermore, it shows that SR-RP can not achieve good performance, since random pilots can not lead to small $\mu\{\boldsymbol{E}\}$. So for SR-based uplink channel estimation, it is important to design UE's pilots to construct a well structured sensing matrix.

In Fig. 3.10, $T^u = 5$ is tested. Compared to Fig. 3.9, the performance of LS degrades a lot, since $T^u < K$ and the problem is underdetermined for LS estimation. On the other hand, SR with pilots design suggested in Chapter 2.5 has only little degradation. LS using orthogonal pilots

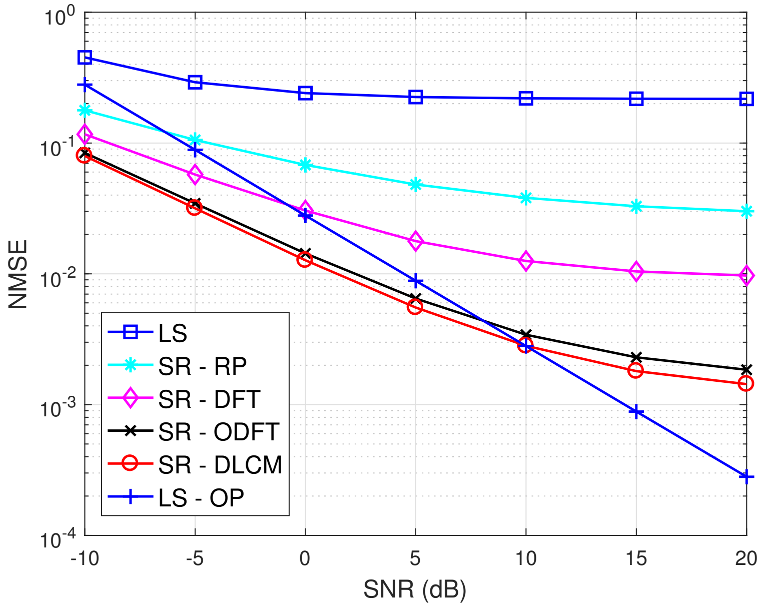

Figure 3.11: Normalized mean square error (NMSE) comparison of different sparsifying matrices, pilots design and user scheduling schemes for SR-based uplink channel estimation with ULA. Non-orthogonal users, perfectly calibrated antenna array. $K = 6, T^u = 5$.

(LS-OP, where $T^u = 6$) is also provided for comparison. Notably, SR-DLCM and SR-ODFT with $T^u = 5$ can achieve even better performance than LS with $T^u = 6$, showing the great benefit of using SR for uplink channel estimation.

In Fig. 3.11, users' locations are randomly and uniformly generated, so their supports can possibly be overlapped a lot. In this case the SR-based channel estimation degrades severely at high SNR, indicating the importance of minimizing $\mu\{\boldsymbol{E}_\Lambda\}$ in order to achieve good sparse recovery performance. In other words, it is important to perform uplink user scheduling when SR-based uplink channel estimation is performed with uplink training duration smaller than the number of UEs.

In Fig. 3.12, the antenna array with uncertainties is used to show the robustness of the learned dictionary. Comparing to Fig. 3.10, the learned dictionary can achieve the similar good NMSE, while the overcomplete DFT is no longer good. The reason is that only the

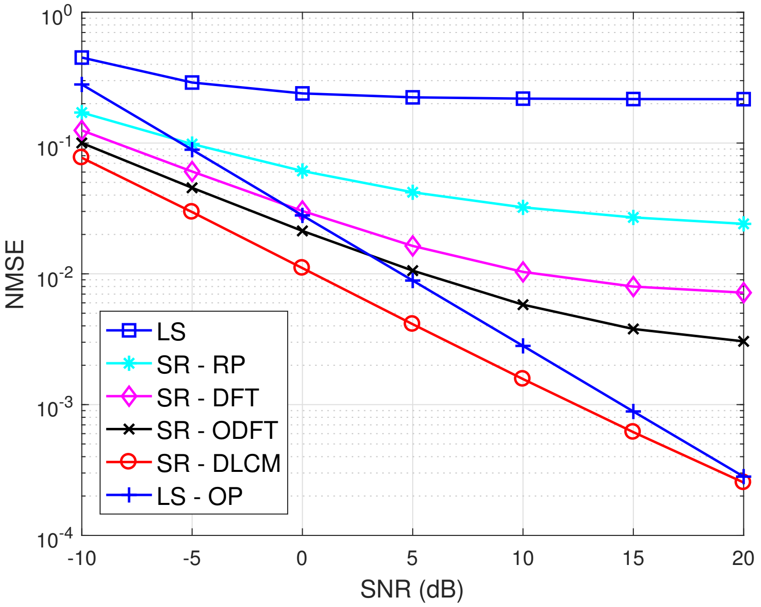

Figure 3.12: Normalized mean square error (NMSE) comparison of different sparsifying matrices, pilots design and user scheduling schemes for SR-based uplink channel estimation with ULA. Orthogonal users, antenna array with uncertainties. $K = 6, T^u = 5$.

learned dictionary can lead to an accurately sparse representation by adapting to the channel measurements.

The previous experiments assume the same SNR for all UEs, which can be done by user scheduling or power allocation. However, in practice, it may not be able to ensure that all UEs have exactly the same SNR. To show the performance when users have different SNR, we conduct similar experiments as shown in Fig. 3.9 to Fig. 3.12, but with different ρ_k^u assigned to each UE. The NMSE performance of each user is evaluated separately since each user has a different SNR and the results are plotted in Fig. 3.13 to Fig. 3.16. For UE1 to UE6, their SNRs are $-10, -4, 2, 8, 14, 20$ dB. As shown in the plots, UEs with higher SNR can achieve lower NMSE. And regarding to the performance comparison of different sparsifying matrices, pilots design, and user scheduling, similar conclusions can be drawn as in the scenario of same SNR for all UEs.

The experiments in this subsection show the benefits of utilizing sparse property to perform the uplink channel estimation, and the essential requirements are (a) sparsifying matrix which

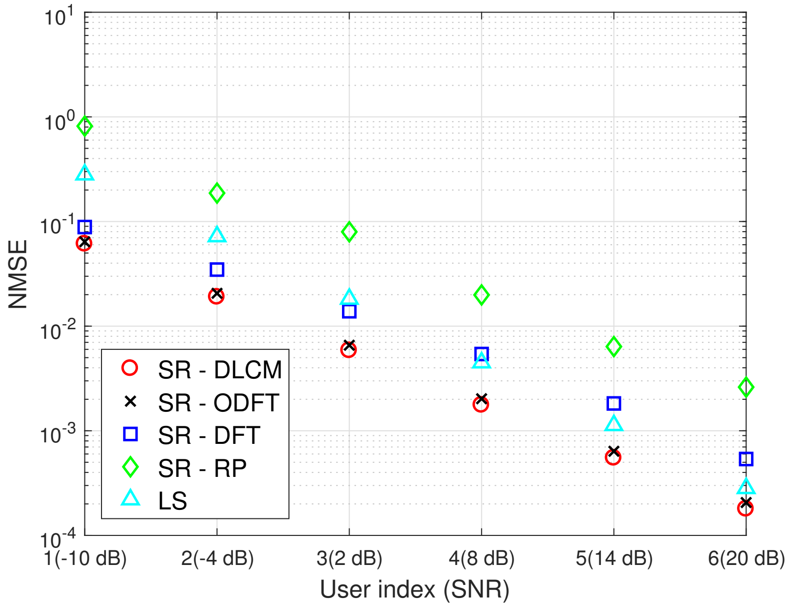

Figure 3.13: Normalized mean square error (NMSE) comparison of different sparsifying matrices, pilots design and user scheduling schemes for SR-based uplink channel estimation with ULA. Orthogonal users, perfectly calibrated antenna array. $K = 6, T^u = 6$.

can lead to efficient and robust sparse representation; (b) pilots design scheme which minimizes $\mu\{\boldsymbol{E}\}$; and (c) user scheduling scheme which decreases $\mu\{\boldsymbol{E}_\Lambda\}$. Even with $T^u < K$, SR-based channel estimation can still achieve good performance. Notice that all the experiments consider the single cell scenario, but can be easily extended to multi-cell scenario for pilot decontamination. For example, consider 6 cells and each of them has 6 users. Assume the total uplink training duration constraint $T^u = 30$. If LS channel estimation is applied, then each cell requires at least 6 training duration, so for all 6 cells their pilots can not be orthogonal to each other and pilot contamination occurs. However, by using SR-based channel estimation, each cell requires only 5 training duration to achieve the similar (even better) performance than LS. Training duration of 30 is enough for 6 cells to have orthogonal pilots, so there is no pilot contamination anymore.

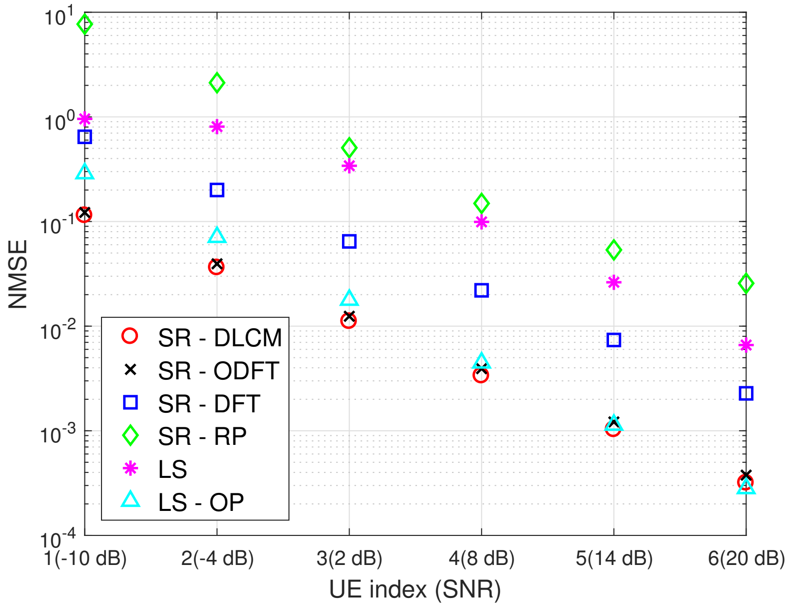

Figure 3.14: Normalized mean square error (NMSE) comparison of different sparsifying matrices, pilots design and user scheduling schemes for SR-based uplink channel estimation with ULA. Orthogonal users, perfectly calibrated antenna array. $K = 6, T^u = 4$.

3.6.4 Joint Uplink/Downlink Channel Estimation

For joint channel estimation, assume the uplink frequency is 1920 MHz and downlink frequency is 2110 MHz. The antenna spacing $d = \frac{c}{2f_0}$ where c denotes the light speed and $f_0 = 2010$ MHz. 10000 uplink/downlink channel responses pair $\{\boldsymbol{h}_i^u, \boldsymbol{h}_i^d\}$ are generated to perform the joint dictionary learning. During channel estimation, we set $T^u = 2$, and $\rho^u = \rho^d$. Fig. 3.17 (a) compares downlink joint and independent channel estimation performance. Besides the jointly learned dictionary (JDLCM), we consider the joint overcomplete DFT matrix (JODFT) obtained by setting $\psi^u = d\sin(\theta)/\lambda^u$, $\psi^d = d\sin(\theta)/\lambda^d$ and $\sin(\theta) \in [-1, -1 + \frac{2}{M}, \dots, 1 - \frac{2}{M}]$ as in (3.20). Smaller NMSE can be obtained by the joint channel estimation compared to their independent counterpart. Such improvement is most obvious when T^d is small, since the additional measurements from the uplink training help a lot. Fig. 3.17 (b) shows the robustness of JDLCM when there exist antenna uncertainties. The JODFT is no longer applicable in this

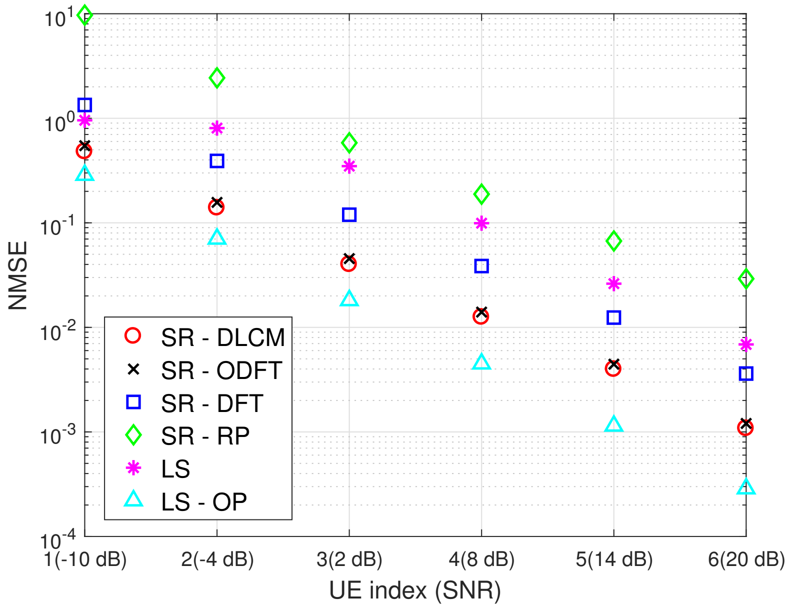

Figure 3.15: Normalized mean square error (NMSE) comparison of different sparsifying matrices, pilots design and user scheduling schemes for SR-based uplink channel estimation with ULA. Non-orthogonal users, perfectly calibrated antenna array. $K = 6, T^u = 4$.

case since the structure is incorrect, and for the large T^d it becomes even worse than the ODFT. With the help of small number of uplink training ($T^u = 2$ in the experiment), one can further improve the performance of downlink channel estimation therefore reduce the downlink training overhead. The simulation is conducted in the microwave scenario. More investigation, especially real experimental measurements, are needed to support the uplink/downlink angular reciprocity in a mmWave scenario.

3.7 Conclusion

In this chapter, we developed a dictionary learning-based channel model which learns a cell specific dictionary from comprehensively collected channel measurements from different locations in the cell. The learned dictionary is able to adapt to the cell characteristics and any antenna array uncertainties, leading to a more efficient and robust channel representation compared

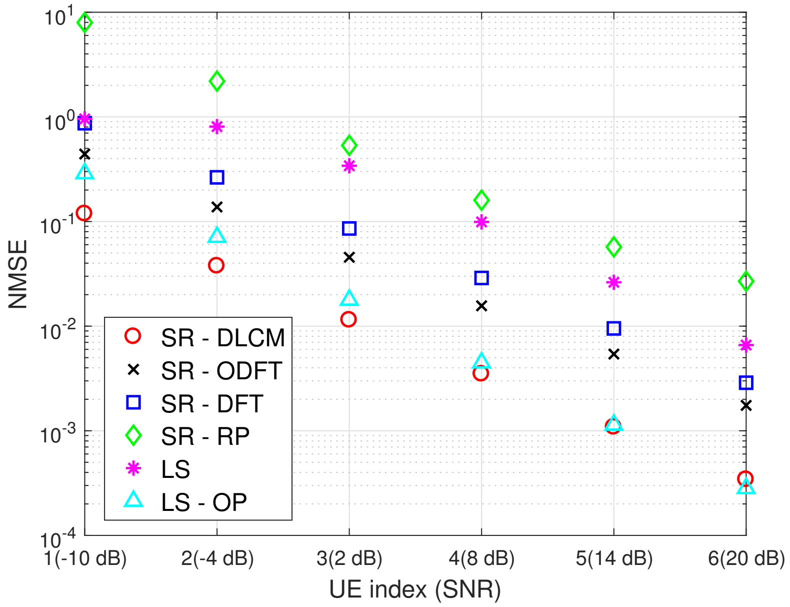

Figure 3.16: Normalized mean square error (NMSE) comparison of different sparsifying matrices, pilots design and user scheduling schemes for SR-based uplink channel estimation with ULA. Orthogonal users, antenna array with uncertainties. $K = 6, T^u = 4$.

to predefined sparsifying matrices. For both CS-based downlink and SR-based uplink channel estimation, the learned dictionary can improve the performance and reduce the training overhead. Motivated by the angular reciprocity between the uplink and downlink channel responses, we further develop a joint dictionary learning-based channel model in order to utilize the relatively simpler uplink channel training to help improving the downlink channel estimation. The results of this chapter show that concepts of utilizing sparse property and learning from the data can be useful for future communication systems. As the dimension of the channel vector increases, sparse representation provides an avenue to deal with the curse of dimensionality. Moreover, with the availability of more data and computational resources, learning from the data will bring new opportunities to improve performance.

As future work, several topics are under consideration. To learn the dictionary, extensive channel measurements are needed as the training samples. Besides using conventional drive tests to collect data, minimization of drive tests (MDT), specified in 3GPP release 10 [74], is a

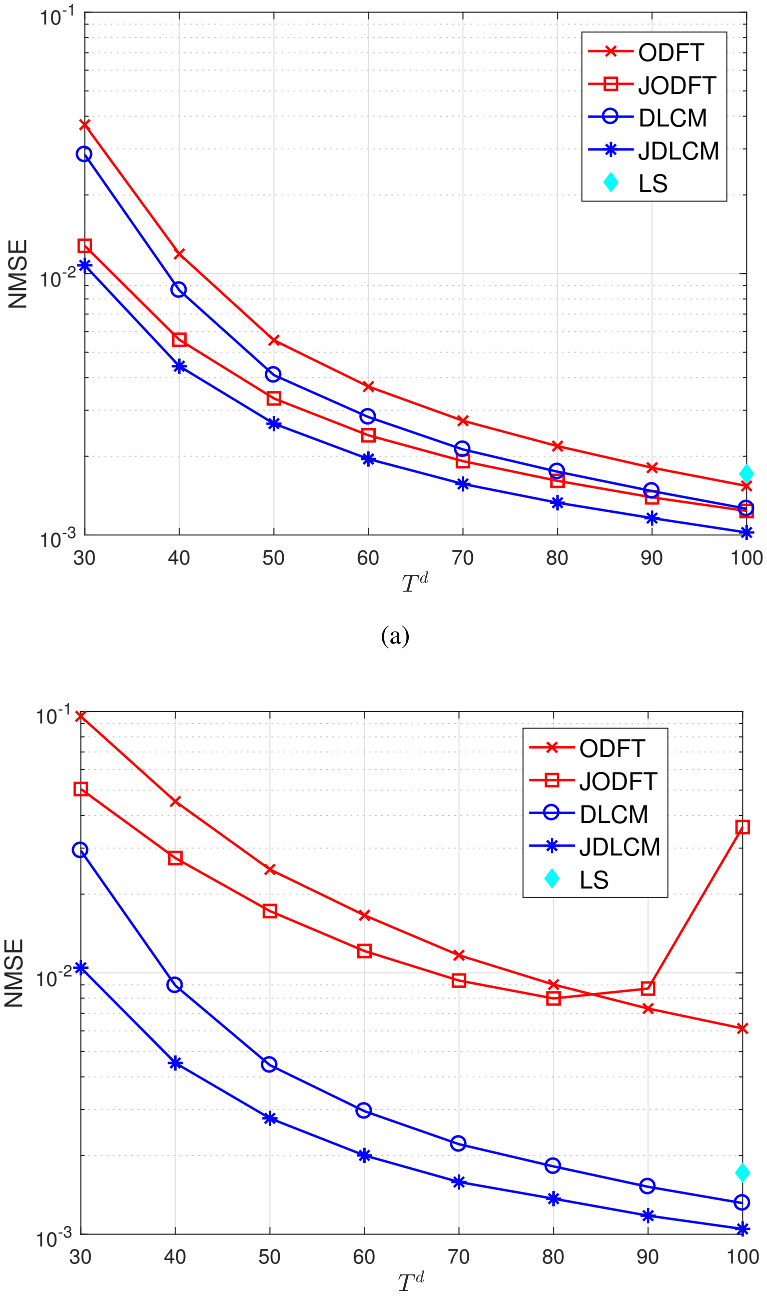

(a)

(b)

Figure 3.17: Normalized mean square error (NMSE) comparison of different sparsifying matrices for joint channel estimation with ULA. (a) Perfectly calibrated antenna array. (b) Antenna array with uncertainties. SNR = 20dB.

promising approach. The main concept is to exploit commercial user equipments, such as their measurement capabilities and geographically spread nature, for collecting radio measurements. Another option is to explore online dictionary learning [75], where an initial dictionary is first learned from limited training samples, and then updated as more training samples are obtained. Online dictionary learning can also be used to deal with the slowly changing cell and antenna characteristics, and adapt to specific user distribution properties in the cell, which is hard to be captured at cell deployment stage. For example, many users may appear in some specific area in the cell, while some areas may be rarely visited. This phenomenon can be measured only after the normal users perform real communication in the cell. Finally, for joint channel estimation, a looser relationship between the supports of the uplink and downlink sparse coefficients may be utilized instead of the strict constraint supp$(\boldsymbol{\beta}^u) = $ supp$(\boldsymbol{\beta}^d)$ to better model the angular reciprocity, for example allowing some mismatch between supp$(\boldsymbol{\beta}^u)$ and supp$(\boldsymbol{\beta}^d)$ through a Bayesian formulation.

Chapter 3, in part, is a reprint of the material as it appears in the papers: Y. Ding and B. D. Rao, “Compressed downlink channel estimation based on dictionary learning in FDD massive MIMO systems,” In *Proc. IEEE Global Commun. Conf. (GLOBECOM)*, Dec. 2015, pp. 1-6, Y. Ding and B. D. Rao, “Channel estimation using joint dictionary learning in FDD massive MIMO systems,” In *Proc. IEEE Glob. Conf. Signal Inf. Process. (GlobalSIP)* , Dec. 2015, pp. 185-189, and Y. Ding and B. D. Rao, “Dictionary learning-based sparse channel representation and estimation for FDD massive MIMO systems,” *IEEE Trans. Wireless Commun.*, in press. The dissertation author was the primary investigator and author of these papers.

Chapter 4

Massive MIMO System with Hardware-efficient Architecture

Conventional massive MIMO systems assume that each antenna element is connected to a dedicated RF chain and a high-resolution ADC, which will incur a large hardware and power cost when the number of antenna elements is large. To reduce the hardware and power cost, hardware-efficient architectures have been proposed where both hybrid analog-digital (AD) processing and low-resolution analog-to-digital converters (ADCs) are utilized [3, 4]. The hardware-efficient architecture is attractive from a power and cost point of view, but poses two significant challenges on the channel estimation. One is due to the smaller dimension of the measurement signal obtained from the limited number of RF chains, and the other is the coarser measurements from the low-resolution ADCs. We address this problem by utilizing two sources of information. Firstly, by exploiting the sparse nature of the massive MIMO channel, the channel estimate is enhanced and the required number of pilots is reduced. Secondly, by utilizing the transmitted data symbols as the "virtual pilots", the channel estimate is further improved without adding more pilot symbols. The constraints imposed by the architecture, the sparsity of the channel and the data aided channel estimation are treated in a unified manner by employing a Bayesian formulation. Simulation results show that the proposed algorithm can efficiently estimate the channel even with the architectural constraints, and that significant improvements are enabled by leveraging the transmitted data symbols.

4.1 Introduction

In massive MIMO system, the base station (BS) is equipped with a large scale antenna array to serve multiple user equipments (UEs), enabling significant gains in the capacity and the energy efficiency. However, conventional massive MIMO systems apply fully-digital architecture, where each antenna element is connected to a dedicated radio-frequency (RF) chain and a high-resolution analog-to-digital converters (ADC). Although the fully-digital architecture has more flexibility and can achieve the largest possible gain, such architecture increases considerably the hardware cost and power consumption of the RF circuits, due to the numerous usage of RF chains and high-resolution ADCs. To make the massive MIMO practical, two hardware efficient solutions have been proposed: hybrid analog-digital (AD) processing and low-resolution ADCs. For the hybrid AD processing, instead of dedicating a separate RF chain for each antenna, there is a limited number of RF chains each connected to all antenna elements through a network of analog phase shifters, therefore dividing the transceiver processing into the analog and digital domains. The power consumption can be further reduced by replacing the traditional high-resolution ADCs with low-resolution ADCs, for example, 1-4 bit ADCs. Moreover, the amount of data that has to be transferred from the RF sections to the baseband processor is reduced when coarser quantization is performed, lowering the burden on the fronthaul links and digital signal processing. However, despite their hardware effectiveness, such architectures also pose significant challenges to the channel estimation, since both the dimension and the precision of the received signal are reduced.

Channel estimation with hybrid AD processing has been previously studied for narrowband millimeter-wave (mmWave) systems [76], where the estimation is formulated as a sparse recovery problem by exploiting the sparse structure of mmWave channels in the angular domain. In [77], the dominant subspaces of the channel matrix are directly estimated through multiple iterations of amplify-and-forward transmission between the transmitter and receiver. Observing the large bandwidth in mmWave systems, a frequency domain channel estimation in an OFDM setting is proposed in [78], where the frequency selective channel model is dealt with by formulating the problem as distributed sparse recovery utilizing the joint sparse channel structure over different frequency bands. Recently, a wideband mmWave channel estimation scheme [54] has been proposed providing solutions for both frequency domain and time domain channel estimation, which utilizes the sparsity in the delay domain in addition to the angular domain.

Channel estimation with low-resolution ADCs, especially 1-bit ADCs, has been widely explored in previous works for both sub-6 GHz and mmWave scenarios. Also, many algorithms in the area of compressive sensing (CS) has been applied for channel estimation. Channel estimation using 1-bit ADCs [79,80] and multi-bit ADCs [4] are considered where the nonlinear quantization effect is transformed into a linear form and solved by linear minimum mean square error (LMMSE) estimation using the Bussgang decomposition. The correlation among the quantized received signals (for 1-bit ADCs) is further considered in [80] to improve the performance. In [81,82], an expectation-maximization (EM) algorithm is used to obtain the maximum likelihood (ML) channel estimation based on the quantized output, and a modified EM is proposed in [83] to account for the sparse structure of the channel. The maximum a posteriori (MAP) channel estimation is considered in [84], and formulated into a convex optimization problem similar to [85] in CS. The generalized approximate message passing (GAMP) algorithm, which has been proposed in CS [86] to deal with the quantized measurements, is also applied for the massive MIMO channel estimation [87] and mmWave sparse channel estimation [83]. There are several other algorithms in the area of quantized CS [88–90], which can be applied to the channel estimation problem when the sparse structure of the channel is considered.

In this chapter, we consider the multi-user massive MIMO channel estimation problem, and provides a *unified* treatment for a system that employs hybrid AD processing and low-resolution ADCs. The developed algorithm exploits the sparse property of the angular domain channel and incorporates the joint processing of pilots and data (JPD). The combined architecture of hybrid AD processing and low-resolution ADCs poses significant challenges on the channel estimation due to the reduced number of *effective* measurements from both the decreased dimension (limited number of RF chains) and reduced precision (limited number of quantization levels) of the received signal at the baseband. Conventional channel estimation requires more training pilots to compensate for the reduction in effective measurements, causing larger training overhead. Instead, the algorithm developed exploits the sparse structure of the massive MIMO channel in the angular domain, so that the *required* number of pilots is greatly reduced. In addition, a portion of the transmitted data is utilized as the *virtual* pilots to enhance the channel estimation. Previous works which apply the hardware efficient architectures either consider only the hybrid AD processing [54, 76–78], or consider only the low-resolution ADCs [4, 79–84, 87], but not both architectures simultaneously. As examples of past works which utilize data symbols for the channel estimation [87, 91–93], the sparse channel property is explored in [91, 92] but without considering low-resolution ADCs, while in [87, 93] low-resolution ADCs are assumed but without utilizing the sparse channel property.

All the mentioned components, such as hybrid AD processing, low-resolution ADCs, sparsity and data-aided estimation, are addressed using a Bayesian framework which is a robust and extensible inference framework. We formulate the problem into an sparse Bayesian learning (SBL) framework, where the sparse signal (angular domain channel in our case) is controlled by a hyper-parameter. Such a framework provides a robust hierarchical Bayesian model where the whole posterior distribution of the unknown variable can be learned from the data, rather than a point estimate. The variational Bayesian (VB) method is used to solve the quantized SBL problem, which aims to minimize the Kullback-Leibler (KL) divergence between the desired posterior density and the constrained family of distributions thereby enjoying the tractability and the guarantees of convergence to the local optimum. Furthermore, due to the VB-SBL framework, the approach is readily extensible to include the second order statistics of the channel and the transmitted data symbols when estimating the channel with JPD, which leads to improved performance and has not been considered in the previous works [91–93]. Our experimental study shows that in terms of the channel estimation accuracy, the low-resolution ADCs lead to a small performance gap compared to the high-resolution ADCs when the signal-to-noise ratio (SNR) is low. By utilizing JPD, one can achieve similar or even better performance with a smaller number of RF chains and low resolution ADCs, which is supportive of the proposed hardware-efficient architecture. Such benefit is obtained without increasing the training overhead.

The chapter is organized as follows. In Section 4.2, we formulate the quantized sparse channel estimation problem. In Section 4.3, we propose the VB-SBL algorithm to solve the problem of quantized channel estimation. The channel estimation with JPD is presented in Section 4.4. Numerical results are provided in Section 4.5, and we conclude the chapter in Section 4.6.

Notations used in this chapter are as follows. Upper (lower) bold face letters are used throughout to denote matrices (column vectors). $(\cdot)^T$, $(\cdot)^H$ $(\cdot)^\dagger$ denotes the transpose, Hermitian transpose, and the Moore-Penrose pseudo-inverse. $\boldsymbol{A}_{ij}$ represents the i, j-th element of the matrix $\boldsymbol{A}$, and $\boldsymbol{A}_{\cdot j}$ ($\boldsymbol{A}_{i\cdot}$) denotes the j-th column (i-th row) of $\boldsymbol{A}$. For a vector $\boldsymbol{x}$, diag$(\boldsymbol{x})$ is a diagonal matrix with entries of $\boldsymbol{x}$ along its diagonal. $\otimes$ represents the Kronecker product, and $\langle \boldsymbol{x} \rangle_{p(\boldsymbol{x})}$ denotes taking the expectation of $\boldsymbol{x}$ under the distribution $p(\boldsymbol{x})$. supp$(\boldsymbol{x})$ denotes an index set containing the indices of the nonzero entries of $\boldsymbol{x}$.

4.2 Quantized Sparse Channel Estimation

The hardware-efficient architecture of hybrid AD processing and low-resolution ADCs poses significant challenges on the channel estimation due to the reduced number of effective measurements. For conventional channel estimation algorithms, they require more training pilots to compensate it. By utilizing the sparse property of the massive MIMO channel, the channel estimation problem is formulated into a compressive sensing framework, so the required number of pilots is reduced. Due to the usage of low-resolution ADCs, the received signals at the baseband are highly quantized, leading to a quantized compressive sensing problem.

4.2.1 System Model

We consider a single-cell uplink massive MIMO system where the BS is assumed to have N antennas and there are K UEs, each equipped with a single antenna. The BS employs a hybrid AD architecture as shown in Fig. 4.1, which has R RF chains. Each RF chain connects to all the antenna elements through a network of phase shifters on one side, and links to a low-resolution ADC on the other side. Assuming a narrowband block fading channel model, the small-scale fading channel between the BS and K UEs is denoted as $\boldsymbol{H} \in \mathbb{C}^{N \times K}$. For the uplink transmission, let $\boldsymbol{s}[t] \in \mathbb{C}^{K \times 1}$ be the transmitted symbols from K UEs at the time instance t and $\mathbb{E}\{\boldsymbol{s}[t]\boldsymbol{s}[t]^H\} = \mathbf{I}_K$. For the k-th UE, denote $\rho_k = P_k \beta_k$, where P_k is the transmit power and β_k is the large-scale fading, which is assumed to change slowly over time and that an accurate estimate is available at the BS. Denoting $\boldsymbol{W}[t] \in \mathbb{C}^{N \times R}$ as the RF combining matrix at the receiver, the received signal $\boldsymbol{y}[t] \in \mathbb{C}^{R \times 1}$ after the combining by the phase shifters at the BS can be written as

$$\begin{aligned} \boldsymbol{y}[t] &= \boldsymbol{W}[t]^H \big(\boldsymbol{H}\boldsymbol{C}\boldsymbol{s}[t] + \boldsymbol{v}[t] \big) \\ &= \boldsymbol{W}[t]^H \tilde{\boldsymbol{H}} \boldsymbol{s}[t] + \boldsymbol{n}[t] \end{aligned} \tag{4.1}$$

where $\boldsymbol{C} = \mathrm{diag}(\sqrt{\rho_1}, \ldots, \sqrt{\rho_K})$, $\tilde{\boldsymbol{H}} = \boldsymbol{H}\boldsymbol{C}$, $\boldsymbol{v}[t] \sim \mathcal{CN}(\mathbf{0}, \sigma^2 \mathbf{I})$ denotes the measurement noise at the receiver antennas. $\boldsymbol{n}[t] = \boldsymbol{W}[t]^H \boldsymbol{v}[t] \in \mathbb{C}^{R \times 1}$ and $\boldsymbol{n}[t] \sim \mathcal{CN}(\mathbf{0}, \sigma^2 \boldsymbol{W}[t]^H \boldsymbol{W}[t])$ denotes the effective noise after combining using the phase shifters.

Each element of $\boldsymbol{W}[t]$ represents a realization of a phase shift which can be modeled as

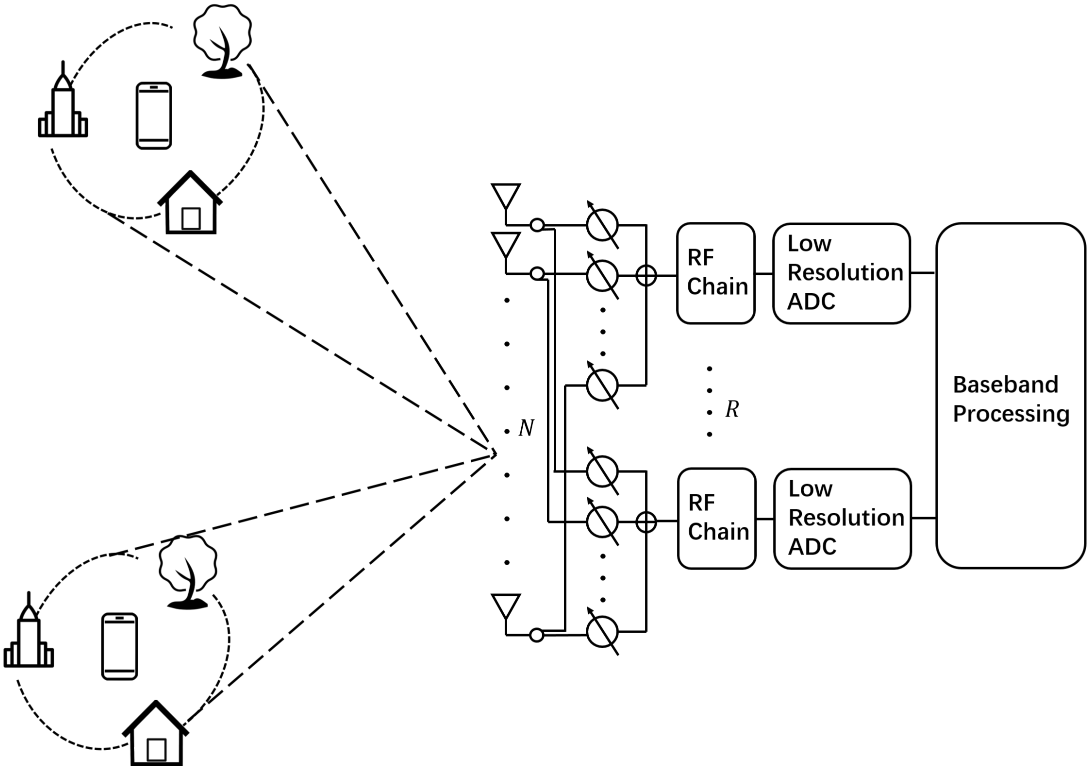

Figure 4.1: Illustration of the uplink quantized massive MIMO system model. Each UE has a single antenna, the BS utilizes the architecture of hybrid AD processing and low-resolution ADCs.

$c \cdot \exp(j\theta)$, where c is some constant which is the same for all phase shifters. We design columns of $\boldsymbol{W}[t] \in \mathbb{C}^{N \times R}$ to be cyclically shifted versions of a length N Zadoff-Chu sequence [94] with the k-th element as:

$$w_k = \begin{cases} \frac{1}{\sqrt{N}}\exp(j\frac{M\pi k^2}{N}), & N \text{ is even;} \\ \frac{1}{\sqrt{N}}\exp(j\frac{M\pi k(k+1)}{N}), & N \text{ is odd.} \end{cases} \tag{4.2}$$

where $k = 0, \dots, N-1$. M is an integer relatively prime to N. Since cyclically shifted versions of Zadoff-Chu sequences have zero correlation with each other, we have $\boldsymbol{W}[t]^H \boldsymbol{W}[t] = \mathbf{I}_R$. In some previous works [27, 95, 96], columns of the discrete Fourier transform (DFT) matrix are utilized to design precoding/combining matrices, which aims to *focus* the beam direction during the downlink data transmission to increase the beamforming gain and eliminate the multi-user interference. In contrast, at the uplink channel estimation stage, a broader beam direction is

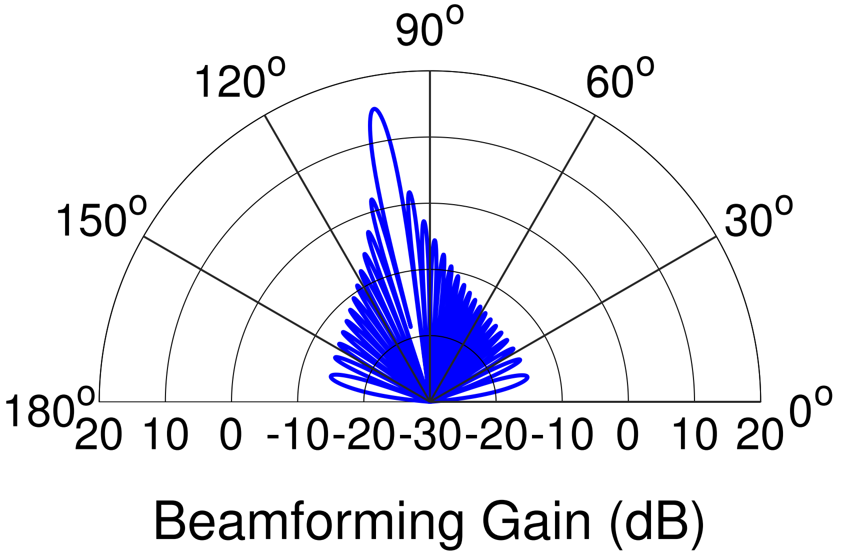

(a)

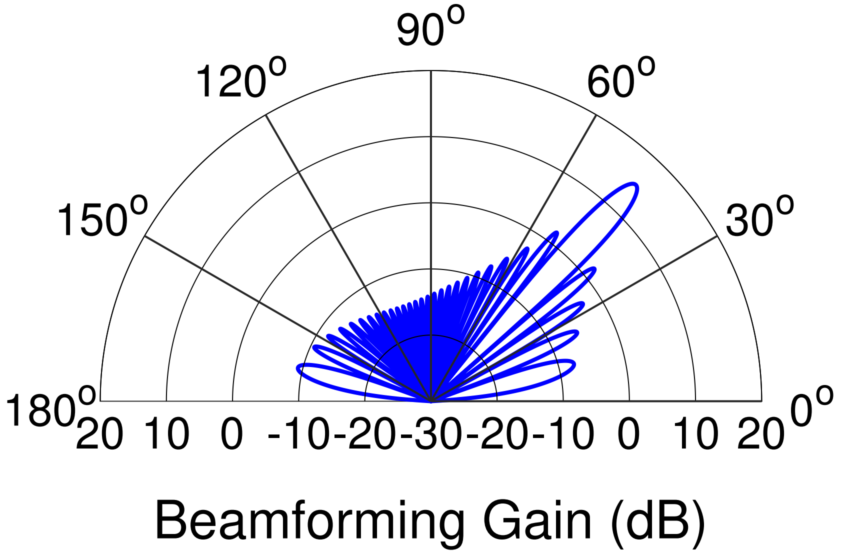

(b)

Figure 4.2: Beam pattern of one column of $\boldsymbol{W}[t]$, columns of $\boldsymbol{W}[t]$ are from DFT matrix.

preferred since the signal's angle of arrival (AOA) is unknown. Focusing a narrow beam may lead to very low SNR if the true AOA of the signal does not match the beamformer's main beam. Fig.

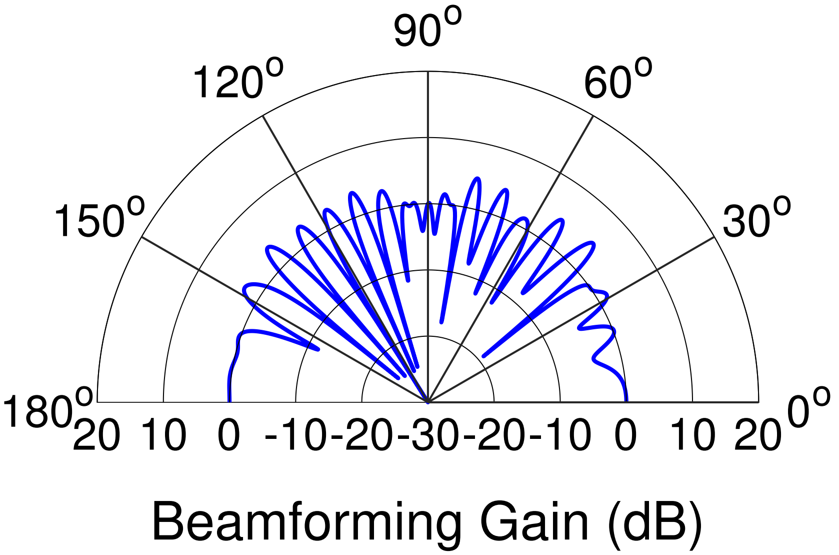

(a)

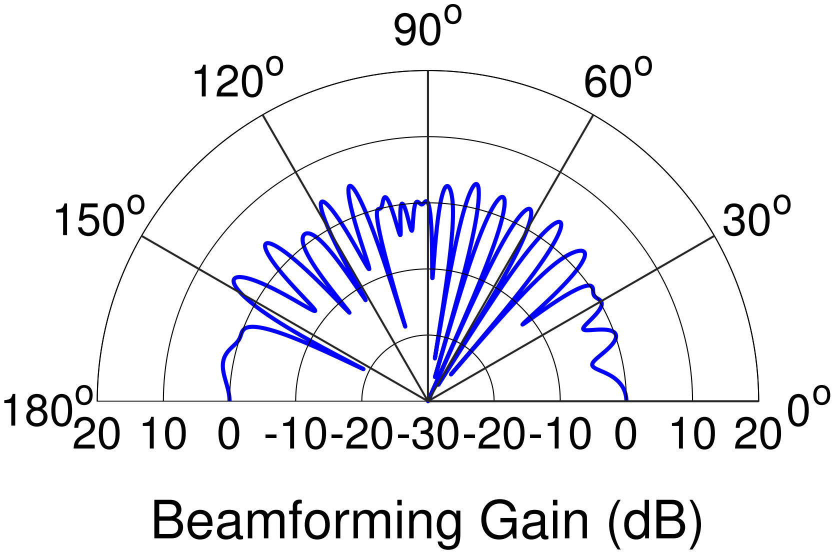

(b)

Figure 4.3: Beam pattern of one column of $\boldsymbol{W}[t]$, columns of $\boldsymbol{W}[t]$ are cyclically shifted Zadoff-Chu sequences.

4.2 and Fig. 4.3 compare the beam patterns of different $\boldsymbol{W}[t]$ whose columns are DFT matrix or cyclically shifter Zadoff-Chu sequences. Fig. 4.2 shows the narrow beam of the DFT matrix, and the beamforming gain towards directions other than the main beam direction are very small. In contrast, the wide beam of the Zadoff-Chu sequence can be seen in Fig. 4.3. The beam pattern shows no favor to any specific directions, and the beamforming gains are the same for almost all the directions. This property makes the Zadoff-Chu sequence more suitable for the channel estimation purpose. Notice that designing columns of $\boldsymbol{W}[t]$ as cyclically shifted Zadoff-Chu sequence is just one option and may not be optimal. For example, in [76], an adaptive algorithm based on *adaptive Compressive Sensing* is proposed to design $\boldsymbol{W}[t]$ using a multi-resolution codebook. Moreover, the combined matrix of $\boldsymbol{W}[t]$ and $\boldsymbol{s}[t]$ acts as the sensing matrix in the CS-based sparse channel estimation, therefore designing $\boldsymbol{W}[t]$ (jointly with $\boldsymbol{s}[t]$) can also be formulated as a *sensing matrix design* problem. Designing the optimal $\boldsymbol{W}[t]$ is beyond the scope of this chapter and is an interesting topic for the future work.

The received signal $\boldsymbol{y}[t]$ will be down-converted and then go through the ADCs to the baseband. Unlike the conventional high-resolution ADCs which are commonly assumed in conventional massive MIMO system, in this work we consider low-resolution ADCs, for example, 1-4 bit ADCs, and model the received signal at baseband as

$$\begin{aligned} \boldsymbol{z}[t] &= \mathcal{Q}(\boldsymbol{y}[t]) \\ &= \mathcal{Q}\big(\boldsymbol{W}[t]^H \tilde{\boldsymbol{H}} \boldsymbol{s}[t] + \boldsymbol{n}[t]\big) \end{aligned} \tag{4.3}$$

where $\mathcal{Q}(\cdot)$ is the quantizer that operates component-wise on $\boldsymbol{y}[t]$. For the k-th element in $\boldsymbol{y}[t]$, we have $z_k[t] = \mathcal{Q}(y_k[t]) = \mathcal{Q}(\Re\{y_k[t]\}) + j\mathcal{Q}(\Im\{y_k[t]\})$, i.e., the real and imaginary parts are quantized independently. A b-bit quantizer $\mathcal{Q}(y)$ for a scalar input $y \in \mathbb{R}$ is defined as

$$\mathcal{Q}(y) = \begin{cases} v_1, & y \in [u_0, u_1]; \\ v_2, & y \in (u_1, u_2]; \\ \ldots, & \ldots; \\ v_B, & y \in (u_{B-1}, u_B], \end{cases} \tag{4.4}$$

where $B = 2^b$ denotes the number of quantization levels, $u_0 < u_1 < \ldots < u_B$ are the quantization thresholds and $v_1, \ldots, v_B$ are the quantizer output value. In this work, we consider a simple mid-point uniform quantizer similar to [87] such that

$$\begin{aligned} u_k &= (-B/2 + k)\Delta, \;\; k = 0, \ldots, B, \\ v_k &= (u_{k-1} + u_k)/2, \;\; k = 1, \ldots, B \end{aligned} \tag{4.5}$$

where Δ is the quantization step size. In practice, the automatic gain control (AGC) can be ajusted to attain the desired step size Δ. Notice that we use mid-point uniform quantizer just for simplicity. The algorithm proposed in the following sections which solves the estimation problem given the quantized measurements can be applied to any quantizer given the thresholds $u_0, \ldots, u_B$, irrespective of the quantizer outputs $v_1, \ldots, v_B$.

4.2.2 Challenges of Channel Estimation

Assume the training duration is T_p, then for $t = 1, \ldots, T_p$, the UEs transmit the pilot symbols $\boldsymbol{s}[t]$ and the BS receives $\boldsymbol{z}[t]$ as (4.3). Given $\boldsymbol{s}[t], \boldsymbol{z}[t]$, $\boldsymbol{W}[t]$ and $\boldsymbol{C}$, the goal of channel estimation is to recover the uplink channel $\boldsymbol{H}$. Below we discuss the challenges of channel estimation due to the use of the hybrid AD processing and low-resolution ADCs.

Use of hybrid AD processing

For now we assume that the high-resolution ADCs are used, so $\boldsymbol{y}[t]$ can be obtained at the baseband. Since $\boldsymbol{W}[t]^H \tilde{\boldsymbol{H}} \boldsymbol{s}[t] \in \mathbb{C}^{R\times 1}$ is a column vector, we have $\boldsymbol{W}[t]^H \tilde{\boldsymbol{H}} \boldsymbol{s}[t] = \text{vec}(\boldsymbol{W}[t]^H \tilde{\boldsymbol{H}} \boldsymbol{s}[t])$. By noting that $\text{vec}(\boldsymbol{W}[t]^H \tilde{\boldsymbol{H}} \boldsymbol{s}[t]) = (\boldsymbol{s}[t]^T \otimes \boldsymbol{W}[t]^H)\text{vec}(\tilde{\boldsymbol{H}})$, and denoting $\boldsymbol{h} = \text{vec}(\tilde{\boldsymbol{H}}) \in \mathbb{C}^{NK\times 1}$, we reformulate (4.1) as

$$\boldsymbol{y}[t] = \boldsymbol{\Phi}[t]\boldsymbol{h} + \boldsymbol{n}[t] \tag{4.6}$$

where $\boldsymbol{\Phi}[t] = \boldsymbol{s}[t]^T \otimes \boldsymbol{W}[t]^H \in \mathbb{C}^{R \times NK}$. Notice that at each training time, only an R dimensional signal can be measured due to the utilization of hybrid AD processing with R RF chains. This makes a big difference compared to the conventional fully digital architecture where N dimensional measurements are obtained during each training slot. Collecting all T_p received signals $\boldsymbol{y}[t]$ together, and denote $\boldsymbol{y}_p = \left[\boldsymbol{y}[1]^T, \ldots, \boldsymbol{y}[T_p]^T\right]^T$, $\boldsymbol{\Phi}_p = \left[\boldsymbol{\Phi}[1]^T, \ldots, \boldsymbol{\Phi}[T_p]^T\right]^T$ and $\boldsymbol{n}_p = \left[\boldsymbol{n}[1]^T, \ldots, \boldsymbol{n}[T_p]^T\right]^T$, we obtain

$$\boldsymbol{y}_p = \boldsymbol{\Phi}_p \boldsymbol{h} + \boldsymbol{n}_p \tag{4.7}$$

where $\boldsymbol{\Phi}_p \in \mathbb{C}^{RT_p \times NK}$. To robustly estimate $\boldsymbol{h}$ from $\boldsymbol{y}_p$, for example using the least square (LS) estimation, one requires that $RT_p \geq NK$, which implies that $T_p \geq NK/R$. Compared to the fully digital architecture where one only requires that $T_p \geq K$, hybrid AD processing leads to an N/R times more training overhead. Since R is usually much smaller than N in order to lower the hardware cost, the required training overhead is largely increased in order to robustly estimate the channel.

Use of low-resolution ADCs

Now we consider the application of low-resolution ADCs where the received signal at the baseband is

$$\boldsymbol{z}_p = \mathcal{Q}(\boldsymbol{y}_p). \tag{4.8}$$

Notice that now each element of the received signal $z_{p,k}$ only provides the range in which $y_{p,k}$ lies. The use of low-resolution ADCs implies a very coarse indication, or in other words very large quantization noise $z_{p,k} - y_{p,k}$, making recovering of $\boldsymbol{h}$ from $\boldsymbol{z}_p$ challenging.

To handle the reduction of effective measurements in both the number and the quality, we consider two options: exploiting the sparsity of the channel and applying the data-aided channel estimation. We explore the sparse structure of the massive MIMO channel to reduce the required number of training pilots, and increase the dimension of the measured signal without sending more training pilots by utilizing the transmitted data symbols as "virtual pilots".

4.2.3 Formulation of Quantized Sparse Channel Estimation

As elaborated in Chapter 2, the low dimensionality of the massive MIMO channel in the angular domain has been widely observed in previous works [27–29, 32, 51] and can be modeled using the virtual channel model [30, 31]. Typically, the BS is far away from the UEs and mounted at a height with few scatterers around, while the UEs are located at low elevation with relatively rich local scatterers, as shown in Fig. 4.1. This leads to a small angular spread (AS) in the angular domain at the BS side, implying that only a small number of angular bins contain almost all the energy from the multipath signals. In the 3GPP spatial channel model [35], for an urban macrocell the mean AS at the BS can be $5°, 8°$ or $15°$ depending on different scenarios. Denoting the AS as σ_{AS}, we take $\sigma_{AS} = 10°$ as an example [32, 51] and assume a uniform linear array (ULA) at the BS. For a ULA with antenna spacing $d = \lambda/2$ (λ is the wavelength), the AOA $\theta \in [-90°, 90°]$, which corresponds to the angular bin $u = d/\lambda \sin(\theta) \in [-1/2, 1/2]$. For a specific user with $\sigma_{AS} = 10°$, if $\theta \in [-5°, 5°]$, it corresponds to $u \in [-0.0436, 0.0436]$, i.e., only 8.72% of the angular bins are occupied. If $\theta \in [80°, 90°]$ which corresponds to $u \in [0.4924, 0.5]$, then only 0.76% of the angular bins are occupied. So after transforming the spatial channel into the angular domain, it shows sparseness. Moreover, as the number of antennas increases, the resolution in the angular domain becomes finer. This leads to less power leakage and smaller residues in adjacent angular bins, which further promotes sparsity.

In this chapter, an ULA is used and we apply the sparse channel model

$$\boldsymbol{h}_k = \boldsymbol{A}\boldsymbol{x}_k \tag{4.9}$$

where $\boldsymbol{h}_k \in \mathbb{C}^{N\times 1}$ is the k-th column of $\boldsymbol{H}$ that corresponds to the channel between the k-th UE and the BS. $\boldsymbol{A}$ denotes the sparsifying matrix, which is defined below

$$\begin{aligned}\boldsymbol{A} &= \begin{bmatrix}\boldsymbol{a}(-\frac{1}{2}) & \boldsymbol{a}(-\frac{1}{2}+\frac{1}{M}) & \dots & \boldsymbol{a}(\frac{1}{2}-\frac{1}{M})\end{bmatrix} \in \mathbb{C}^{N\times M}, \\ \boldsymbol{a}(u) &= \frac{1}{\sqrt{N}}[1, e^{j2\pi u}, \dots, e^{j2\pi u\cdot(N-1)}]^T.\end{aligned} \tag{4.10}$$

In the virtual channel model [29–31], $N = M$ so $\boldsymbol{A}$ is an orthogonal DFT matrix that projects the spatial domain channel at equally spaced virtual angular domain coordinates. $\boldsymbol{A}$ can also be constructed as an overcomplete DFT matrix where $M > N$, which has more flexibility to encourage sparsity [52–54, 97]. $\boldsymbol{x}_k$ denotes the angular domain channel of the k-th UE, where each element represents the angular bin that is an aggregation of all the paths whose AOAs fall within the angular window. Based on the sparse assumption, most elements in $\boldsymbol{x}_k$ are close to zero, while only a small number of elements corresponding to AOAs of incoming multipath signals have non-negligible values. Denoting $\boldsymbol{X} = [\boldsymbol{x}_1, \dots, \boldsymbol{x}_k]$, we have $\boldsymbol{H} = \boldsymbol{A}\boldsymbol{X}$, so $\tilde{\boldsymbol{H}} = \boldsymbol{H}\boldsymbol{C} = \boldsymbol{A}\boldsymbol{X}\boldsymbol{C} = \boldsymbol{A}\tilde{\boldsymbol{X}}$, where $\tilde{\boldsymbol{X}} = \boldsymbol{X}\boldsymbol{C}$. As a result, $\boldsymbol{h} = \text{vec}(\tilde{\boldsymbol{H}}) = (\mathbf{I}_K \otimes \boldsymbol{A})\text{vec}(\tilde{\boldsymbol{X}}) = (\mathbf{I}_K \otimes \boldsymbol{A})\boldsymbol{x}$, where $\boldsymbol{x} = \text{vec}(\tilde{\boldsymbol{X}}) \in \mathbb{C}^{MK\times 1}$. Then (4.7) can be written as

$$\boldsymbol{y}_p = \boldsymbol{\Phi}_p(\mathbf{I}_K \otimes \boldsymbol{A})\boldsymbol{x} + \boldsymbol{n}_p \tag{4.11}$$

with $\|\boldsymbol{x}\|_0 \ll MK$, where $\|\boldsymbol{x}\|_0$ denotes the number of nonzero elements in $\boldsymbol{x}$. Notice that (4.11) is in the form of the sparse recovery in CS [6, 39], with $\boldsymbol{\Phi}_p$ as the sensing matrix, and $\mathbf{I}_K \otimes \boldsymbol{A}$ as the dictionary. From the theories of CS, the required number of measurements, i.e., the number of rows in $\boldsymbol{\Phi}_p$, needs to be proportional to $\|\boldsymbol{x}\|_0\text{log}(MK/\|\boldsymbol{x}\|_0)$ in order to robustly recover $\boldsymbol{x}$ [6]. In other words, $RT_p \geq c\|\boldsymbol{x}\|_0\text{log}(MK/\|\boldsymbol{x}\|_0)$ where c is some constant. Compared to the previous requirement of LS estimation that $RT_p \geq NK$, the required T_p is now scaling with $\|\boldsymbol{x}\|_0$ rather than NK. So the training overhead is greatly reduced when the channel is sparse, therefore easing the challenges posed by the hybrid AD processing. After estimating $\boldsymbol{x}$, we have $\tilde{\boldsymbol{X}}$ therefore obtain $\tilde{\boldsymbol{H}} = \boldsymbol{A}\tilde{\boldsymbol{X}}$. Finally, the estimated channel is given by $\boldsymbol{H} = \tilde{\boldsymbol{H}}\boldsymbol{C}^{-1}$ since $\boldsymbol{C}$

is assumed to be known at the BS.

However, unlike the conventional CS recovery problem where the unquantized (or quantized with high precision) measurements $\boldsymbol{y}_p$ are available, we only have the coarse quantized measurements

$$\boldsymbol{z}_p = \mathcal{Q}(\boldsymbol{y}_p) = \mathcal{Q}(\boldsymbol{\Phi}_p(\mathbf{I}_K \otimes \boldsymbol{A})\boldsymbol{x} + \boldsymbol{n}_p). \tag{4.12}$$

Many algorithms have been developed to solve this quantized CS problem, where $\mathcal{Q}(\cdot)$ is a 1-bit or multi-bit quantizer [85, 86, 88–90]. In this chapter, we develop an SBL framework [19–21] to solve (4.12) using a VB approach [90, 98–100].

4.2.4 Extension to Wideband System and Multi-antenna UE

In this work, we focus on the conventional massive MIMO system operated in sub-6 GHz, and assume narrowband channel and single-antenna UE for simplicity of illustration. However, the framework of quantized sparse channel estimation is general and the formulation can be readily extended to the wideband system and multi-antenna UE, which is of special interest for the mmWave communication system. To show this, we first formulate the wideband channel estimation where each UE is assumed to have multiple antennas and apply the hybrid AD architecture [54, 78]. Then the formulation is transformed into the quantized CS problem that shares the same form as (4.12). Due to the nonlinear nature of the operator $\mathcal{Q}(\cdot)$ which performs the quantization in the time domain, it is impossible to split the wideband channel into many parallel narrowband channel like in an OFDM system [80, 84]. Therefore, we develop the time domain wideband channel estimation similar to [54, 80, 84].

Assume the BS has N_r antennas and R_r RF chains, the UE has N_t antennas and R_t RF chains. Denote the receiver analog combiner at the BS as $\boldsymbol{W}[t] \in \mathbb{C}^{N_r \times R_r}$ and the transmitter analog precoder at the k-th UE as $\boldsymbol{F}^k[t] \in \mathbb{C}^{N_t \times R_t}$. The frequency selective channel is assumed to have N_d delayed taps, where the d-th tap of the k-th UE is denoted as $\boldsymbol{H}_d^k \in \mathbb{C}^{N_r \times N_t}$. Assume perfect synchronization and a sufficiently long cyclic prefix (CP) or zero prefix (ZP). After removal of the CP or ZP, the received signal after the phase shifters is given by

$$\begin{aligned}\boldsymbol{y}[t] &= \boldsymbol{W}[t]^H \big(\sum_{k=1}^{K} \sqrt{\rho_k} \sum_{d=0}^{N_d-1} \boldsymbol{H}_d^k \boldsymbol{F}^k[t-d] \boldsymbol{s}^k[t-d] + \boldsymbol{v}[t] \big) \\ &= \boldsymbol{W}[t]^H \big[\tilde{\boldsymbol{H}}_0^1 \, \tilde{\boldsymbol{H}}_1^1 \ldots \tilde{\boldsymbol{H}}_{N_d-1}^K \big] \boldsymbol{F}[t] \boldsymbol{s}[t] + \boldsymbol{n}[t]\end{aligned} \tag{4.13}$$

where $\boldsymbol{s}^k[t-d] \in \mathbb{C}^{R_t \times 1}$ is the transmitted symbols from the k-th UE at time $t-d$. $\boldsymbol{s}[t] = \big[\boldsymbol{s}^1[t]^T \;\; \boldsymbol{s}^1[t-1]^T \ldots \boldsymbol{s}^K[t-N_d+1]^T \big]^T$, $\boldsymbol{F}[t] = \operatorname{diag}\big(\boldsymbol{F}^1[t], \boldsymbol{F}^1[t-1], \ldots, \boldsymbol{F}^K[t-N_d+1] \big)$, and $\tilde{\boldsymbol{H}}_d^k = \sqrt{\rho_k} \boldsymbol{H}_d^k$. The received noise $\boldsymbol{v}[t] \sim \mathcal{CN}(\mathbf{0}, \sigma^2 \mathbf{I})$, and $\boldsymbol{n}[t] \sim \mathcal{CN}(\mathbf{0}, \sigma^2 \boldsymbol{W}[t]^H \boldsymbol{W}[t])$. Denoting $\boldsymbol{h} = \operatorname{vec}\Big(\big[\tilde{\boldsymbol{H}}_0^1 \, \tilde{\boldsymbol{H}}_1^1 \ldots \tilde{\boldsymbol{H}}_{N_d-1}^K \big] \Big) \in \mathbb{C}^{K N_r N_t N_d \times 1}$, with the same manipulation in (4.6) we have

$$\begin{aligned}\boldsymbol{y}[t] &= \big((\boldsymbol{s}[t]^T \boldsymbol{F}[t]^T) \otimes \boldsymbol{W}[t]^H \big) \operatorname{vec}\Big(\big[\boldsymbol{H}_0 \, \boldsymbol{H}_1 \ldots \boldsymbol{H}_{N_d-1} \big] \Big) + \boldsymbol{n}[t] \\ &= \boldsymbol{\Phi}[t] \boldsymbol{h} + \boldsymbol{n}[t]\end{aligned} \tag{4.14}$$

where $\boldsymbol{\Phi}[t] = (\boldsymbol{s}[t]^T \boldsymbol{F}[t]^T) \otimes \boldsymbol{W}[t]^H \in \mathbb{C}^{R_r \times K N_r N_t N_d}$. Notice that due to the existence of N_t antennas at each UE and N_d delayed taps, the dimension of $\boldsymbol{h}$ is augmented by $N_t N_d$ compared to (4.6). However, at each training time the dimension of the measured signal stays the same as R_r, which makes the estimation more difficult. Collecting $\boldsymbol{y}[t], \boldsymbol{\Phi}[t]$ in the whole training duration together, we have $\boldsymbol{y}_p = \boldsymbol{\Phi}_p \boldsymbol{h} + \boldsymbol{n}_p$ similar as (4.7). In [54], the whole training duration is divided into several frames where a ZP is appended to each frame. The $\boldsymbol{W}[t]$ and $\boldsymbol{F}[t]$ are kept the same when t belongs to the same frame, and reconfigured from one frame to the other during the ZP guard time. Our formulation above is general and does not assume any specific training scheme or transmission mode (single carrier or OFDM). The detailed development and comparison of different wideband schemes are left for the future work.

The sparse formulation for the frequency selective channel is similar to the narrowband one, where an additional domain, i.e., delay domain, can be explored [54, 78]. In [78], perfectly delay domain sampling is assumed, while in [54] the residue coming from sampling the raised cosine pulse shaping filter is considered. For each channel $\boldsymbol{H}_d^k$ in the delay domain, we have $\boldsymbol{H}_d^k = \boldsymbol{A}_r \boldsymbol{X}_d^k \boldsymbol{A}_t^H$, where $\boldsymbol{A}_r \in \mathbb{C}^{N_r \times M_r}$, $M_r \geq N_r$ and $\boldsymbol{A}_t \in \mathbb{C}^{N_t \times M_t}$, $M_t \geq N_t$ are sparsifying matrices which lead to the sparse coefficient $\boldsymbol{X}_d^k$, e.g., orthogonal DFT matrices [30, 31] or overcomplete DFT matrices [54]. Then the sparse channel representation can be formulated as

$$\begin{aligned}
\boldsymbol{h} &= \mathrm{vec}\Big(\big[\tilde{\boldsymbol{H}}_0^1\, \tilde{\boldsymbol{H}}_1^1 \ldots \tilde{\boldsymbol{H}}_{N_d-1}^K\big]\Big) \\
&= \mathrm{vec}\Big(\boldsymbol{A}_r \big[\tilde{\boldsymbol{X}}_0^1\, \tilde{\boldsymbol{X}}_1^1 \ldots \tilde{\boldsymbol{X}}_{N_d-1}^K\big] \big(\mathbf{I}_{KN_d} \otimes \boldsymbol{A}_t^H\big)\Big) \\
&= \big(\mathbf{I}_{KN_d} \otimes \boldsymbol{A}_t^* \otimes \boldsymbol{A}_r\big)\boldsymbol{x}
\end{aligned} \tag{4.15}$$

where $\tilde{\boldsymbol{X}}_d^k = \sqrt{\rho_k}\boldsymbol{X}_d^k$, and $\boldsymbol{x} = \mathrm{vec}\big([\tilde{\boldsymbol{X}}_0^1\, \tilde{\boldsymbol{X}}_1^1 \ldots \tilde{\boldsymbol{X}}_{N_d-1}^K]\big)$. Considering the effect of the low-resolution ADCs, the received signal can be written as

$$\boldsymbol{z}_p = \mathcal{Q}(\boldsymbol{y}_p) = \mathcal{Q}(\boldsymbol{\Phi}_p\big(\mathbf{I}_{KN_d} \otimes \boldsymbol{A}_t^* \otimes \boldsymbol{A}_r\big)\boldsymbol{x} + \boldsymbol{n}_p) \tag{4.16}$$

which has the same form as (4.12). It can be solved by the VB-SBL algorithm which will be proposed in this chapter. Notice that the combined sensing matrix $\boldsymbol{\Phi}_p\big(\mathbf{I}_{KN_d} \otimes \boldsymbol{A}_t^* \otimes \boldsymbol{A}_r\big)$ has the dimension $R_r T_p \times K M_r M_t N_d$, resulting in a very large problem size when large antenna arrays are applied at both the BS and the UE (large M_r and M_t), or there exists a large number of delayed taps N_d. Developing fast algorithm that can accommodate large-scale problems will be an interesting topic for the future work.

4.3 VB-SBL Channel Estimation Algorithm

In order to deal with both the sparse channel estimation and the data-aided channel estimation (elaborated in the next section), we adopt a Bayesian approach. A Bayesian framework, usually a MAP framework, for dealing with the unknown data symbols is natural as they are assumed to be selected uniformly from a chosen constellation. To deal with the sparse channel

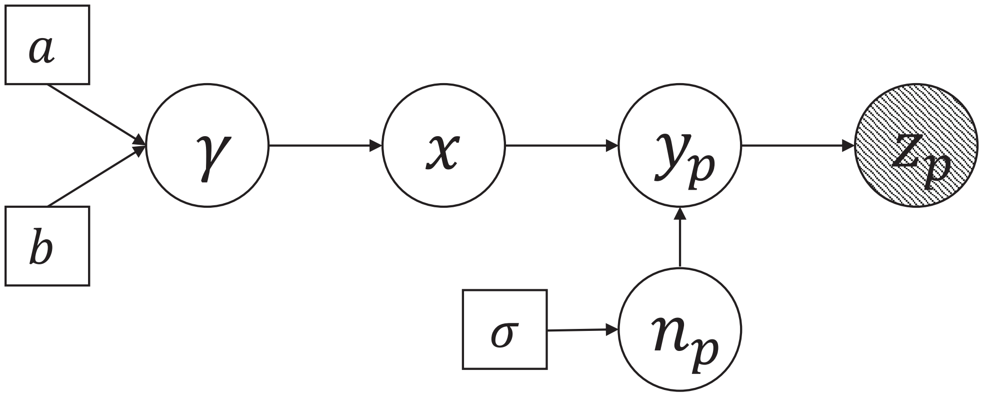

Figure 4.4: Graphical model for the quantized channel estimation using SBL.

in the same setting, i.e., solving the quantized sparse recovery problem (4.12), we utilize the SBL framework [19–21]. Conventional non-Bayesian approaches in sparse recovery or CS aim to estimate $\boldsymbol{x}$ directly from $\boldsymbol{z}_p$, i.e., the point estimation of $\boldsymbol{x}$. For example, ℓ_1 regularization is used on $\boldsymbol{x}$ to encourage its sparsity in [85]. In a Bayesian formulation, sparsity of $\boldsymbol{x}$ is promoted by utilizing a sparsity-promoting prior, usually a super-Gaussian density. For instance, when $\boldsymbol{x}$ is given a Laplace prior, the MAP estimation of $\boldsymbol{x}$ under the Gaussian noise reduces to the ℓ_1 regularized formulation. In SBL, $\boldsymbol{x}$ is further modeled by a hierarchical structure through an additional layer introducing hyperparameter $\boldsymbol{\gamma}$ as shown in Fig. 4.4. A MAP estimate of $\boldsymbol{\gamma}$ is sought and by utilizing the hierarchical structure, an approximation to the full posterior of $\boldsymbol{x}$ given the data is obtained as $p(\boldsymbol{x}|\boldsymbol{z}_p;\hat{\boldsymbol{\gamma}})$. Such an approach has been shown to yield a more robust estimate of $\boldsymbol{x}$ [101]. Also importantly, such a framework is easier to extend to other scenarios such as a temporally correlated channel model [32, 43] and integrate with data-aided channel estimation, providing a framework for dealing with all issues synergistically.

4.3.1 Sparse Bayesian Learning Framework

Based on (4.12), we depict the graphical structure of the data generation model in Fig. 4.4, where squares and circles are used to denote constants and hidden variables, and a shaded circle represents the observation. It is assumed that $\boldsymbol{x}$ conditioned on the hyperparameters is zero mean complex Gaussian such that

$$p(\boldsymbol{x}|\boldsymbol{\gamma}) = \mathcal{CN}(\mathbf{0}, \mathbf{\Gamma}^{-1}) \tag{4.17}$$

where $\mathbf{\Gamma} = \text{diag}(\boldsymbol{\gamma})$ denotes the precision matrix. The hyperparameter $\boldsymbol{\gamma} = [\gamma_1, \ldots, \gamma_{MK}]^T$, where each γ_i represents the reciprocal of the variance of the complex Gaussian distributed variable x_i, and is assumed to be Gamma distributed such that

$$\begin{aligned} p(\gamma_i) &= \text{Gamma}(\gamma_i; a, b) \\ &= \frac{b^a}{\Gamma(a)} \gamma_i^{a-1} \text{exp}\{-b\gamma_i\}, \ \ \gamma_i > 0, \ \ \forall i \end{aligned} \tag{4.18}$$

where $\Gamma(a)$ is the Gamma function, a, b are the constant parameters and $p(\boldsymbol{\gamma}) = \prod_{i=1}^{MK} p(\gamma_i)$. By choosing γ_i to be Gamma distributed, $p(\gamma_i)$ is the conjugate prior to the likelihood function $p(x_i|\gamma_i)$, which facilitates the calculation of the posterior distribution. Furthermore, by integrating out the hyperparameter γ_i, the marginal distribution of x_i can be obtained as

$$\begin{aligned} p(x_i) &= \int_0^\infty p(x_i|\gamma_i) p(\gamma_i) d\gamma_i \\ &= \frac{b^a \Gamma(a + \frac{1}{2})}{(2\pi)^{\frac{1}{2}} \Gamma(a)} (b + x_i^2/2)^{-(a+\frac{1}{2})} \end{aligned} \tag{4.19}$$

which is a Student-t distribution by setting $a = b$ [19]. With appropriate choice of a and b in the Gamma distribution, the Student-t distribution is strongly peaked about the origin $x_i = 0$, and has heavy tails thereby promoting the sparsity of $\boldsymbol{x}$. For example, the Student-t distribution with $a = b = 10^{-6}$ is plotted in Fig. 4.5. So, this hierarchical structure leads to a sparsity promoting distribution of $p(x_i)$, which is consistent with our assumption of a sparse angular domain channel $\boldsymbol{x}$.

Denoting $\boldsymbol{D}_p = \boldsymbol{\Phi}_p(\mathbf{I}_K \otimes \boldsymbol{A})$, the measurement equation (4.11) is given by $\boldsymbol{y}_p = \boldsymbol{D}_p\boldsymbol{x} + \boldsymbol{n}_p$, where $\boldsymbol{n}_p = \left[\boldsymbol{n}[1]^T, \ldots, \boldsymbol{n}[T_p]^T\right]^T$, $\boldsymbol{n}[t] \sim \mathcal{CN}(\mathbf{0}, \sigma^2 \boldsymbol{W}[t]^H \boldsymbol{W}[t])$ and is independent for

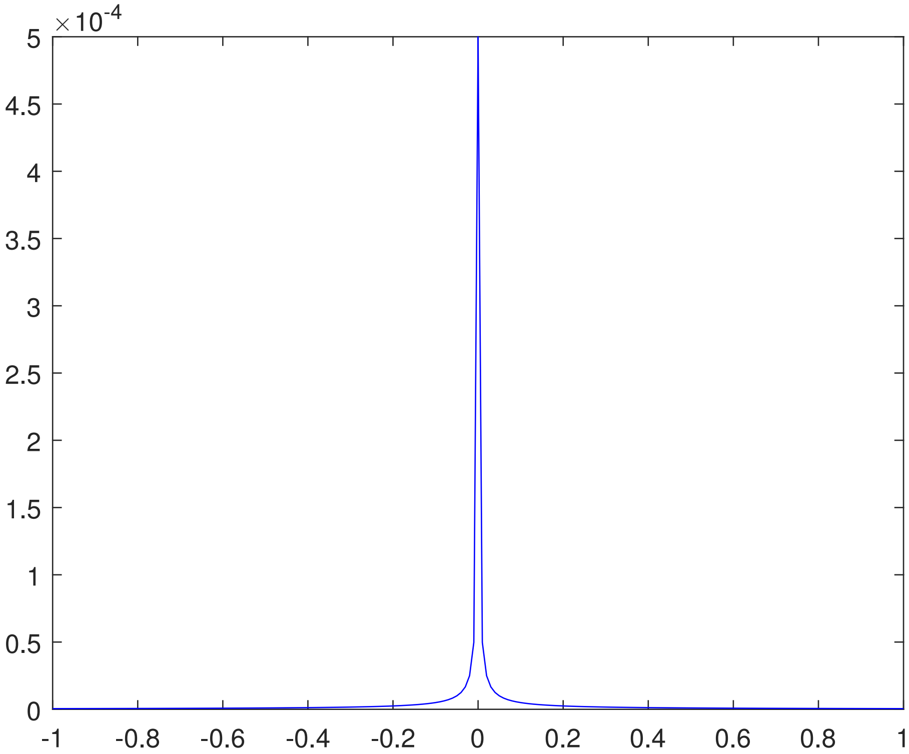

Figure 4.5: Student-t distribution

different t. Since columns of $\boldsymbol{W}[t]$ are designed to be the cyclically shifted Zadoff-Chu sequence, we have $\boldsymbol{W}[t]^H\boldsymbol{W}[t] = \mathbf{I}_R$. Consequently, $\boldsymbol{n}_p \sim \mathcal{CN}(\mathbf{0}, \sigma^2\mathbf{I}_{RT_p})$, and

$$p(\boldsymbol{y}_p|\boldsymbol{x}) = \mathcal{CN}(\boldsymbol{D}_p\boldsymbol{x}, \sigma^2\mathbf{I}_{RT_p}). \tag{4.20}$$

We assume that σ^2 is known to the BS, which is a reasonable assumption given σ^2 is a long term statistic. Finally, given $\boldsymbol{y}_p$ the observation data $\boldsymbol{z}_p$ is distributed as

$$p(\boldsymbol{z}_p|\boldsymbol{y}_p) = \mathbb{1}(\boldsymbol{y}_p \in (\boldsymbol{l}, \boldsymbol{u}]) \tag{4.21}$$

where $\mathbb{1}\big(\boldsymbol{y}_p \in (\boldsymbol{l}, \boldsymbol{u}]\big) := \mathbb{1}\big(\Re\{\boldsymbol{y}_p\} \in (\Re\{\boldsymbol{l}\}, \Re\{\boldsymbol{u}\}]\big) \cdot \mathbb{1}\big(\Im\{\boldsymbol{y}_p\} \in (\Im\{\boldsymbol{l}\}, \Im\{\boldsymbol{u}\}]\big)$, $\boldsymbol{l}$ and $\boldsymbol{u}$ denote the lower and upper limits of the range indicated by the quantizer output $\boldsymbol{z}_p$ when a specific quantizer $\mathcal{Q}(\cdot)$ is applied.

Considering the SBL model in Fig. 4.4, we denote all hidden (latent) variables as $\mathcal{H}$, i.e., $\mathcal{H} = \{\boldsymbol{\gamma}, \boldsymbol{x}, \boldsymbol{y}_p\}$, and the received signal $\boldsymbol{z}_p$ is denoted as the visible (observed) variable. Ideally, we would like to perform exact inference by finding the posterior marginal distribution $p(\boldsymbol{x}|\boldsymbol{z}_p)$. Unfortunately, this is intractable due to the high dimensional integration of $p(\boldsymbol{z}_p) = \int p(\boldsymbol{z}_p, \mathcal{H}) d\mathcal{H}$. In the following, we introduce an alternative method, i.e., VB method, to obtain a good and tractable approximation of this posterior density and conduct effective inference.

4.3.2 Variational Bayesian Method

We now provide a brief summary of the VB method that is utilized in this chapter. The goal in the VB inference is to find a tractable variational distribution $q(\mathcal{H})$ that closely approximates the true posterior distribution $p(\mathcal{H}|\boldsymbol{z}_p)$ [99, 100]. A starting point for this development is the identity given below

$$\begin{aligned} \ln p(\boldsymbol{z}_p) &= \mathcal{L}(q) + \mathrm{KL}(q||p) \\ \mathcal{L}(q) &= \int q(\mathcal{H}) \ln \frac{p(\boldsymbol{z}_p, \mathcal{H})}{q(\mathcal{H})} \, d\mathcal{H} \\ \mathrm{KL}(q||p) &= -\int q(\mathcal{H}) \ln \frac{p(\mathcal{H}|\boldsymbol{z}_p)}{q(\mathcal{H})} \, d\mathcal{H} \end{aligned} \tag{4.22}$$

where KL$(q||p)$ is the Kullback-Leibler divergence between the true posterior $p(\mathcal{H}|\boldsymbol{z}_p)$ and the variational approximation $q(\mathcal{H})$. Since KL$(q||p) \geq 0$, it follows that $\mathcal{L}(q)$ is a rigorous lower bound on ln $p(\boldsymbol{z}_p)$. Therefore we choose some family of distributions to represent $q(\mathcal{H})$ and seek a member from that family which maximizes $\mathcal{L}(q)$, hence minimizing KL$(q||p)$. The chosen distribution family should render a tractable evaluation and efficient optimization of $\mathcal{L}(q)$, even though ln $p(\boldsymbol{z}_p)$ is intractable.

Here we consider the mean field approximation [99] such that disjoint group of variables in $q(\mathcal{H})$ are independent. This is equivalent to choose $q(\mathcal{H})$ such that

$$q(\mathcal{H}) = \prod_i q(\mathcal{H}_i) \tag{4.23}$$

where $\{\mathcal{H}_i\}$ are the disjoint groups of variables. Within this fully factorized distribution family, $\mathcal{L}(q)$ can be written as

$$\begin{aligned}
&\mathcal{L}(q) \\
=& \int \prod_i q(\mathcal{H}_i) \Big\{ \ln p(\boldsymbol{z}_p, \mathcal{H}) - \sum_i \ln q(\mathcal{H}_i) \Big\}\, d\mathcal{H} \\
=& \int q(\mathcal{H}_i) \{ \int \ln p(\boldsymbol{z}_p, \mathcal{H}) \prod_{j \neq i} q(\mathcal{H}_j)\, d\mathcal{H}_{\sim i} \}\, d\mathcal{H}_i - \int q(\mathcal{H}_i) \ln q(\mathcal{H}_i)\, d\mathcal{H}_i + \text{const} \\
=& \int q(\mathcal{H}_i) \ln \tilde{p}(\boldsymbol{z}_p, \mathcal{H}_i)\, d\mathcal{H}_i - \int q(\mathcal{H}_i) \ln q(\mathcal{H}_i)\, d\mathcal{H}_i + \text{const} \\
=& - \text{KL}(q(\mathcal{H}_i) || \tilde{p}(\boldsymbol{z}_p, \mathcal{H}_i)) + \text{const}
\end{aligned} \tag{4.24}$$

where const denotes constants that are irrelevant with the interested random variables $\mathcal{H}_i$, and we have

$$\ln \tilde{p}(\boldsymbol{z}_p, \mathcal{H}_i) = \int \ln p(\boldsymbol{z}_p, \mathcal{H}) \prod_{j \neq i} q(\mathcal{H}_j)\, d\mathcal{H}_{\sim i} \tag{4.25}$$

where the integration is performed with respect to all $q(\mathcal{H}_j), j \neq i$. This leads to

$$\begin{aligned}
\tilde{p}(\boldsymbol{z}_p, \mathcal{H}_i) &= \frac{1}{Z} \exp\Big\{ \int \ln p(\boldsymbol{z}_p, \mathcal{H}) \prod_{j \neq i} q(\mathcal{H}_j)\, d\mathcal{H}_{\sim i} \Big\} \\
&= \frac{1}{Z} \exp\Big\{ \langle \ln p(\mathcal{H}, \boldsymbol{z}_p) \rangle_{\sim q(\mathcal{H}_i)} \Big\}
\end{aligned} \tag{4.26}$$

where $\langle \cdot \rangle$ denotes the expectation operator, and $\sim q(\mathcal{H}_i)$ means to take expectation with all $q(\mathcal{H})$ except $q(\mathcal{H}_i)$. Z is the normalization factor making $\tilde{p}(\boldsymbol{z}_p, \mathcal{H}_i)$ a valid probability distribution. To maximize $\mathcal{L}(q)$, the KL distance $\text{KL}(q(\mathcal{H}_i) || \tilde{p}(\boldsymbol{z}_p, \mathcal{H}_i))$ has to be minimized, so $q(\mathcal{H}_i)$ is chosen as

$$\begin{aligned} q(\mathcal{H}_i) &= \tilde{p}(\boldsymbol{z}_p, \mathcal{H}_i) \\ &= \frac{1}{Z}\,\text{exp}\Big\{\langle \ln p(\mathcal{H}, \boldsymbol{z}_p)\rangle_{\sim q(\mathcal{H}_i)}\Big\} \\ &\propto \text{exp}\Big\{\langle \ln p(\mathcal{H}, \boldsymbol{z}_p)\rangle_{\sim q(\mathcal{H}_i)}\Big\}. \end{aligned} \tag{4.27}$$

When the probabilistic model can be expressed as a directed acyclic graph as in Fig. 4.4, the solution for $q(\mathcal{H}_i)$ depends only on the distribution of variables which are in the Markov blankets of the node i. Note that the equations for all of the factors are coupled since the solution for each $q(\mathcal{H}_i)$ depends on expectations with respect to other factors $q(\mathcal{H}_j), j \neq i$. The variational optimization proceeds by cycling through each factor in turn replacing the current distribution with the updated one given by (4.27).

4.3.3 Solving SBL Using VB Method

Applying the mean field approximation, we have

$$q(\mathcal{H}) = q(\boldsymbol{\gamma}, \boldsymbol{x}, \boldsymbol{y}_p) = q(\boldsymbol{\gamma}) \cdot q(\boldsymbol{x}) \cdot q(\boldsymbol{y}_p). \tag{4.28}$$

Based on (4.27), we derive the posterior density update for each variable $\boldsymbol{\gamma}, \boldsymbol{x}, \boldsymbol{y}_p$ following [90, 98].

Derivation of $q(\boldsymbol{y}_p)$

Based on (4.20) and (4.21), $q(\boldsymbol{y}_p)$ can be derived from (4.27) as

$$\begin{aligned} q(\boldsymbol{y}_p) &\propto \exp\Big\{\ln p(\boldsymbol{z}_p|\boldsymbol{y}_p) + \big\langle \ln p(\boldsymbol{y}_p|\boldsymbol{x})\big\rangle_{q(\boldsymbol{x})}\Big\} \\ &\propto p(\boldsymbol{z}_p|\boldsymbol{y}_p) \exp\Big\{\big\langle \ln p(\boldsymbol{y}_p|\boldsymbol{x})\big\rangle_{q(\boldsymbol{x})}\Big\} \\ &\propto \mathbb{1}(\boldsymbol{y}_p \in (\boldsymbol{l}, \boldsymbol{u}]) \exp\Big\{\big\langle -\frac{1}{\sigma^2}\|\boldsymbol{y}_p - \boldsymbol{D}_p\boldsymbol{x}\|_2^2\big\rangle_{q(\boldsymbol{x})}\Big\} \\ &\propto \mathbb{1}(\boldsymbol{y}_p \in (\boldsymbol{l}, \boldsymbol{u}]) \exp\Big\{ -\frac{1}{\sigma^2}\|\boldsymbol{y}_p - \boldsymbol{D}_p\langle\boldsymbol{x}\rangle_{q(\boldsymbol{x})}\|_2^2\Big\} \end{aligned} \tag{4.29}$$

which indicates that $\boldsymbol{y}_p$ is distributed as a *truncated* multivariate complex Gaussian, and each element $y_{p,i}$ is independent of the others. Notice that to obtain $q(\boldsymbol{y}_p)$, $\langle\boldsymbol{x}\rangle_{q(\boldsymbol{x})}$ is needed, which will be evaluated when deriving $q(\boldsymbol{x})$. This shows how $q(\boldsymbol{y}_p)$ is coupled with the other distributions.

Similarly, $\langle\boldsymbol{y}_p\rangle_{q(\boldsymbol{y}_p)}$ will be needed in the later derivations. For the real part of $y_{p,i}$, i.e., $\Re\{y_{p,i}\}$, it is distributed as a real truncated Gaussian with mean $\Re\{[\boldsymbol{D}_p\langle\boldsymbol{x}\rangle_{q(\boldsymbol{x})}]_i\}$, variance $\sigma^2/2$, and lies within the interval $\Re\{l_i\} < \Re\{y_{p,i}\} \leq \Re\{u_i\}$. Define $\alpha = \sqrt{2}(\Re\{l_i\} - \Re\{[\boldsymbol{D}_p\langle\boldsymbol{x}\rangle_{q(\boldsymbol{x})}]_i\})/\sigma$, $\beta = \sqrt{2}(\Re\{u_i\} - \Re\{[\boldsymbol{D}_p\langle\boldsymbol{x}\rangle_{q(\boldsymbol{x})}]_i\})/\sigma$, then from [102] we have

$$\langle\Re\{y_{p,i}\}\rangle_{q(\boldsymbol{y}_p)} = \Re\{[\boldsymbol{D}_p\langle\boldsymbol{x}\rangle_{q(\boldsymbol{x})}]_i\} + \frac{\sigma}{\sqrt{2}} \cdot \frac{\phi(\alpha) - \phi(\beta)}{\Phi(\beta) - \Phi(\alpha)} \tag{4.30}$$

where $\phi(\cdot)$ is the probability density function of the standard normal distribution, and $\Phi(\cdot)$ is its cumulative distribution function. Similarly, by defining $\alpha = \sqrt{2}(\Im\{l_i\} - \Im\{[\boldsymbol{D}_p\langle\boldsymbol{x}\rangle_{q(\boldsymbol{x})}]_i\})/\sigma$, $\beta = \sqrt{2}(\Im\{u_i\} - \Im\{[\boldsymbol{D}_p\langle\boldsymbol{x}\rangle_{q(\boldsymbol{x})}]_i\})/\sigma$,

$$\langle\Im\{y_{p,i}\}\rangle_{q(\boldsymbol{y}_p)} = \Im\{[\boldsymbol{D}_p\langle\boldsymbol{x}\rangle_{q(\boldsymbol{x})}]_i\} + \frac{\sigma}{\sqrt{2}} \cdot \frac{\phi(\alpha) - \phi(\beta)}{\Phi(\beta) - \Phi(\alpha)}. \tag{4.31}$$

Combining the real and imaginary parts leads to

$$\langle y_{p,i}\rangle_{q(\boldsymbol{y}_p)} = \langle\Re\{y_{p,i}\}\rangle_{q(\boldsymbol{y}_p)} + \mathrm{j}\,\langle\Im\{y_{p,i}\}\rangle_{q(\boldsymbol{y}_p)}. \tag{4.32}$$

Applying the same approach, all $\langle y_{p,i}\rangle_{q(\boldsymbol{y}_p)}, i = 1, \ldots, T_p$ can be obtained, leading to

$$\langle \boldsymbol{y}_p\rangle_{q(\boldsymbol{y}_p)} = [\langle y_{p,1}\rangle_{q(\boldsymbol{y}_p)}, \langle y_{p,2}\rangle_{q(\boldsymbol{y}_p)}, \ldots, \langle y_{p,T_p}\rangle_{q(\boldsymbol{y}_p)}]^T. \tag{4.33}$$

Derivation of $q(\boldsymbol{x})$

Based on (4.17) and (4.20), we have

$$\begin{aligned} q(\boldsymbol{x}) &\propto \exp\Big\{\big\langle \ln p(\boldsymbol{y}_p|\boldsymbol{x})\big\rangle_{q(\boldsymbol{y}_p)} + \big\langle \ln p(\boldsymbol{x}|\boldsymbol{\gamma})\big\rangle_{q(\gamma)}\Big\} \\ &\propto \exp\Big\{\big\langle -\frac{1}{\sigma^2}\|\boldsymbol{y}_p - \boldsymbol{D}_p\boldsymbol{x}\|_2^2\big\rangle_{q(\boldsymbol{y}_p)} + \big\langle -\boldsymbol{x}^H\boldsymbol{\Gamma}\boldsymbol{x}\big\rangle_{q(\gamma)}\Big\} \\ &\propto \exp\Big\{-(\boldsymbol{x}-\boldsymbol{\mu})^H\boldsymbol{\Sigma}^{-1}(\boldsymbol{x}-\boldsymbol{\mu})\Big\} \end{aligned} \tag{4.34}$$

which indicates $q(\boldsymbol{x})$ is a Gaussian distribution with

$$\begin{aligned} \boldsymbol{\Sigma} &= \Big(\frac{1}{\sigma^2}\boldsymbol{D}_p^H\boldsymbol{D}_p + \big\langle\boldsymbol{\Gamma}\big\rangle_{q(\gamma)}\Big)^{-1}, \\ \boldsymbol{\mu} &= \frac{1}{\sigma^2}\boldsymbol{\Sigma}\boldsymbol{D}_p^H\langle\boldsymbol{y}_p\rangle_{q(\boldsymbol{y}_p)}. \end{aligned} \tag{4.35}$$

So we have $\langle\boldsymbol{x}\rangle_{q(\boldsymbol{x})}$ which is needed in deriving $q(\boldsymbol{y}_p)$ as

$$\langle\boldsymbol{x}\rangle_{q(\boldsymbol{x})} = \boldsymbol{\mu}. \tag{4.36}$$

Since $\boldsymbol{D}_p \in \mathbb{C}^{RT_p\times MK}$, the inversion of the matrix in (4.35) requires $\mathcal{O}(M^3K^3)$ operations. When $RT_p < MK$, we can apply the matrix inversion lemma to reduce the complexity such that

$$\boldsymbol{\Sigma} = \big\langle\boldsymbol{\Gamma}\big\rangle_{q(\gamma)}^{-1} - \big\langle\boldsymbol{\Gamma}\big\rangle_{q(\gamma)}^{-1}\boldsymbol{D}_p^H\big(\sigma^2\mathbf{I} + \boldsymbol{D}_p\big\langle\boldsymbol{\Gamma}\big\rangle_{q(\gamma)}^{-1}\boldsymbol{D}_p^H\big)^{-1}\boldsymbol{D}_p\big\langle\boldsymbol{\Gamma}\big\rangle_{q(\gamma)}^{-1} \tag{4.37}$$

where the inversion of the matrix $\big(\sigma^2\mathbf{I} + \boldsymbol{D}_p\big\langle\boldsymbol{\Gamma}\big\rangle_{q(\gamma)}^{-1}\boldsymbol{D}_p^H\big)^{-1}$ requires only $\mathcal{O}(R^3T_p^3)$ operations. Notice that to obtain $\langle\boldsymbol{x}\rangle_{q(\boldsymbol{x})}$, we need both $\langle\boldsymbol{y}_p\rangle_{q(\boldsymbol{y}_p)}$ and $\big\langle\boldsymbol{\Gamma}\big\rangle_{q(\gamma)}$. The former has been derived when we calculated $q(\boldsymbol{y}_p)$, and the latter will be given in the following.

Derivation of $q(\boldsymbol{\gamma})$

Based on (4.17) and (4.18), $q(\boldsymbol{\gamma})$ is derived as follows:

$$\begin{aligned} q(\boldsymbol{\gamma}) &\propto \exp\Big\{\big\langle \ln p(\boldsymbol{x}|\boldsymbol{\gamma})\big\rangle_{q(\boldsymbol{x})} + \ln p(\boldsymbol{\gamma})\Big\} \\ &\propto \exp\Big\{\big\langle -\boldsymbol{x}^H\boldsymbol{\Gamma}\boldsymbol{x}\big\rangle_{q(\boldsymbol{x})} + \ln|\boldsymbol{\Gamma}| + \sum_{i=1}^{MK} \ln p(\gamma_i)\Big\} \\ &\propto \prod_{i=1}^{MK} \exp\Big\{-\langle x_i^2\rangle_{q(\boldsymbol{x})}\gamma_i\Big\} \times \gamma_i \times p(\gamma_i) \\ &\propto \prod_{i=1}^{MK} \gamma_i^{(a+1)-1}\exp\{-(b+\langle x_i^2\rangle_{q(\boldsymbol{x})})\gamma_i\} \end{aligned} \tag{4.38}$$

which is the product of independent Gamma distribution, Gamma$(\gamma_i; \tilde{a}, \tilde{b})$ with $\tilde{a} = a+1, \tilde{b} = b + \langle x_i^2\rangle_{q(\boldsymbol{x})}$. From the property of the Gamma distribution, we have

$$\langle \gamma_i\rangle_{q(\boldsymbol{\gamma})} = \frac{\tilde{a}}{\tilde{b}} = \frac{a+1}{b+\langle x_i^2\rangle_{q(\boldsymbol{x})}} \tag{4.39}$$

where we set $a = b = 10^{-6}$ following [98], and $\langle x_i^2\rangle_{q(\boldsymbol{x})}$ is the i-th element in diag$(\boldsymbol{\mu}\boldsymbol{\mu}^H + \boldsymbol{\Sigma})$, with $\boldsymbol{\mu}$ and $\boldsymbol{\Sigma}$ given in (4.35). Finally, $\langle\boldsymbol{\Gamma}\rangle_{q(\boldsymbol{\gamma})}$ is obtained as

$$\langle\boldsymbol{\Gamma}\rangle_{q(\boldsymbol{\gamma})} = \text{diag}\Big(\big[\langle\gamma_1\rangle_{q(\boldsymbol{\gamma})}, \ldots, \langle\gamma_{MK}\rangle_{q(\boldsymbol{\gamma})}\big]\Big) \tag{4.40}$$

which is needed when deriving $\langle\boldsymbol{x}\rangle_{q(\boldsymbol{x})}$.

By iteratively updating between (4.29), (4.34) and (4.38), we obtain the variational distributions $q(\boldsymbol{y}_p)$, $q(\boldsymbol{x})$ and $q(\boldsymbol{\gamma})$, which approximate the posterior distributions $p(\boldsymbol{y}_p|\boldsymbol{z}_p)$, $p(\boldsymbol{x}|\boldsymbol{z}_p)$ and $p(\boldsymbol{\gamma}|\boldsymbol{z}_p)$ respectively. The VB method is guaranteed to converge to the *local* minimum of the KL divergence [99, 100]. As with many iterative algorithms, it is important to have a good initialization to ensure that the local minimum obtained is sufficiently close to the global minimum. In the simulations, we found that initializing all γ_i to the same constant, and initializing $\boldsymbol{y}_p = \boldsymbol{z}_p$ can lead to good results. In the iterative process, many γ_i tend to infinity (numerically indistinguishable from infinity), indicating those x_i having negligible values, which is equivalent to having $\boldsymbol{D}_p$ with corresponding columns excluded. So for those columns in $\boldsymbol{D}_p$ whose corresponding γ_i are larger than some threshold, we prune those columns from $\boldsymbol{D}_p$, which reduces the size of $\boldsymbol{D}_p$ and speeds up the convergence of the algorithm. Finally, the angular domain channel can be estimated as the posterior mean, i.e., $\hat{\boldsymbol{x}} = \langle \boldsymbol{x} \rangle_{q(\boldsymbol{x})}$, from which the spatial domain channel is obtained as $\hat{\boldsymbol{h}} = (\mathbf{I}_K \otimes \boldsymbol{A})\hat{\boldsymbol{x}}$.

4.4 Channel Estimation With Joint Processing of Pilots and Data

In the previous section, we developed the algorithm to exploit the sparse nature of the channel so that the required number of pilots is reduced. In this section, we develop a channel estimation scheme which involves the JPD. The motivation for this is the observation that the transmitted data symbols can be viewed as "virtual pilots" when they are jointly estimated with the channel, therefore increasing the number of effective measurements for the channel estimation.

4.4.1 Data-aided Channel Estimation

We denote the JPD duration as T, which includes the whole training duration T_p, and part of the data transmission duration $T - T_p$. During the channel training duration T_p, the received signal $\boldsymbol{z}_p$ is given by (4.12). By the similar manipulation, we can formulate the total received signal in duration T as being given by

$$\boldsymbol{z} = \mathcal{Q}(\boldsymbol{y}) = \mathcal{Q}(\boldsymbol{\Phi}(\mathbf{I}_K \otimes \boldsymbol{A})\boldsymbol{x} + \boldsymbol{n}). \tag{4.41}$$

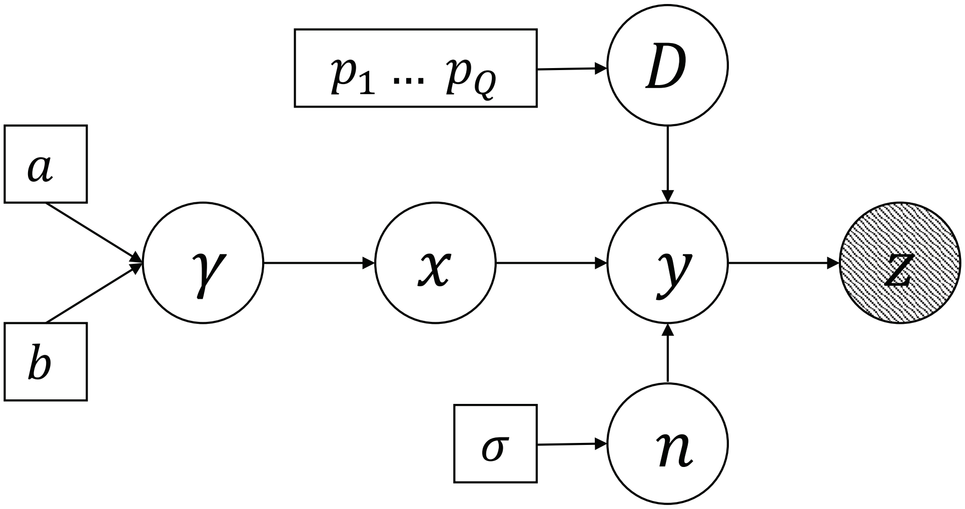

Figure 4.6: Graphical model for the channel estimation with JPD using SBL.

where $\boldsymbol{z} = \left[\boldsymbol{z}[1]^T, \dots, \boldsymbol{z}[T]^T\right]^T$, $\boldsymbol{y} = \left[\boldsymbol{y}[1]^T, \dots, \boldsymbol{y}[T]^T\right]^T$, $\boldsymbol{n} = \left[\boldsymbol{n}[1]^T, \dots, \boldsymbol{n}[T]^T\right]^T$. $\boldsymbol{\Phi} = [\boldsymbol{\Phi}_p^T \; \boldsymbol{\Phi}_d^T]^T$, where $\boldsymbol{\Phi}_p$ is given in (4.7) and $\boldsymbol{\Phi}_d = \left[\boldsymbol{\Phi}[T_p+1]^T, \dots, \boldsymbol{\Phi}[T]^T\right]^T$ is composed of the transmitted data symbols such that $\boldsymbol{\Phi}[t] = \boldsymbol{s}[t]^T \otimes \boldsymbol{W}[t]^H, t = T_p+1, \dots, T$. Notice that $\boldsymbol{\Phi} \in \mathbb{C}^{RT \times NK}$, $\boldsymbol{\Phi}_p \in \mathbb{C}^{RT_p \times NK}$, and $T > T_p$. So compared to (4.12), the number of measurements, i.e., the number of rows in $\boldsymbol{\Phi}$, is larger than $\boldsymbol{\Phi}_p$. As a result, it is expected to obtain a more accurate estimate of $\boldsymbol{x}$ if $\boldsymbol{\Phi}$ is known at the receiver.

However, the $\boldsymbol{s}[t], t = T_p+1, \dots, T$ in $\boldsymbol{\Phi}_d$ is the transmitted data which is unknown to the receiver, so the VB-SBL approach proposed in the previous section can not be directly applied to solve it. Therefore, we incorporate the unknown variable $\boldsymbol{D} = \boldsymbol{\Phi}(\mathbf{I}_K \otimes \boldsymbol{A})$ into the Bayesian framework as shown in Fig. 4.6. Notice that the actual random variable in $\boldsymbol{D}$ is the transmitted data $\boldsymbol{s}[t], t = T_p+1, \dots, T$, which are discrete random variables with probability mass function (pmf):

$$p(\boldsymbol{s}[t]) = \begin{cases} p_1, & \boldsymbol{s}[t] = \mathcal{S}_1; \\ \dots, & \dots; \\ p_Q, & \boldsymbol{s}[t] = \mathcal{S}_Q \end{cases} \tag{4.42}$$

where $\mathcal{S}_q$ is the K dimensional vector consisting of constellation points and p_q is the corresponding probability. Q is the total number of discrete points for K users. For example if $K = 4$ and BPSK is used, then $Q = 2^4 = 16$.

4.4.2 VB-SBL Algorithm For Channel Estimation With JPD

Similar to the previous section, we formulate the channel estimation with JPD into the SBL framework as shown in Fig. 4.6, and develop the VB method to solve it. Note the similarity between the structure of the graphical model in Fig. 4.4 and Fig. 4.6, we therefore omit the steps similar to those in the previous section and only highlight the differences.

Derivation of $q(\boldsymbol{y})$

This is similar to (4.29) except that $\boldsymbol{D}$ is now a random variable. We denote $\langle \boldsymbol{D} \rangle_{q(\boldsymbol{s})}$ to emphasize that the random variables that compose $\boldsymbol{D}$ are $\boldsymbol{s} = \{\boldsymbol{s}[T_p + 1], \ldots, \boldsymbol{s}[T]\}$. The $q(\boldsymbol{y})$ is given below:

$$\begin{aligned} q(\boldsymbol{y}) &\propto \exp\Big\{ \ln p(\boldsymbol{z}|\boldsymbol{y}) + \big\langle \ln p(\boldsymbol{y}|\boldsymbol{x}, \boldsymbol{D}) \big\rangle_{q(\boldsymbol{x})q(\boldsymbol{s})} \Big\} \\ &\propto \mathbb{1}(\boldsymbol{y} \in [\boldsymbol{l}, \boldsymbol{u}]) \exp\Big\{ -\frac{1}{\sigma^2} \|\boldsymbol{y} - \langle \boldsymbol{D} \rangle_{q(\boldsymbol{s})} \langle \boldsymbol{x} \rangle_{q(\boldsymbol{x})}\|_2^2 \Big\}. \end{aligned} \tag{4.43}$$

Compared to the derivation of $q(\boldsymbol{y}_p)$, we replace $\boldsymbol{D}_p$ with $\langle \boldsymbol{D} \rangle_{q(\boldsymbol{s})}$. For each component y_i, $\Re\{y_i\}$ is truncated Gaussian with mean $\Re\{[\langle \boldsymbol{D} \rangle_{q(\boldsymbol{s})} \langle \boldsymbol{x} \rangle_{q(\boldsymbol{x})}]_i\}$ and $\Im\{y_i\}$ is truncated Gaussian with mean $\Im\{[\langle \boldsymbol{D} \rangle_{q(\boldsymbol{s})} \langle \boldsymbol{x} \rangle_{q(\boldsymbol{x})}]_i\}$, while the other derivations are the same. The derivation of $\langle \boldsymbol{D} \rangle_{q(\boldsymbol{s})}$ is given in the Appendix 4.7.1. It involves the calculation of $\langle \boldsymbol{s}[t] \rangle_{q(\boldsymbol{s}[t])}$, i.e., the posterior mean of transmitted data symbols, which will be derived in the following. After those calculations we are able to obtain $\langle \boldsymbol{y} \rangle_{q(\boldsymbol{y})}$.

Derivation of $q(\boldsymbol{x})$

Similar to (4.34), we have

$$\begin{aligned} q(\boldsymbol{x}) &\propto \exp\Big\{\big\langle \ln p(\boldsymbol{y}|\boldsymbol{x},\boldsymbol{D})\big\rangle_{q(\boldsymbol{y})q(\boldsymbol{s})} + \big\langle \ln p(\boldsymbol{x}|\boldsymbol{\gamma})\big\rangle_{q(\boldsymbol{\gamma})}\Big\} \\ &\propto \exp\Big\{-(\boldsymbol{x}-\boldsymbol{\mu}_{\boldsymbol{x}})^H\boldsymbol{\Sigma}_{\boldsymbol{x}}^{-1}(\boldsymbol{x}-\boldsymbol{\mu}_{\boldsymbol{x}})\Big\}. \end{aligned} \tag{4.44}$$

And different from (4.35), we have

$$\begin{aligned} \boldsymbol{\Sigma}_{\boldsymbol{x}} &= \Big(\frac{1}{\sigma^2}\langle \boldsymbol{D}^H\boldsymbol{D}\rangle_{q(\boldsymbol{s})} + \big\langle \boldsymbol{\Gamma}\big\rangle_{q(\boldsymbol{\gamma})}\Big)^{-1} \\ \boldsymbol{\mu}_{\boldsymbol{x}} &= \frac{1}{\sigma^2}\boldsymbol{\Sigma}_{\boldsymbol{x}}\langle \boldsymbol{D}\rangle_{q(\boldsymbol{s})}^H\langle \boldsymbol{y}\rangle_{q(\boldsymbol{y})} \end{aligned} \tag{4.45}$$

where for $\boldsymbol{\Sigma}_{\boldsymbol{x}}$, the term $\langle \boldsymbol{D}^H\boldsymbol{D}\rangle_{q(\boldsymbol{s})}$ rather than $\boldsymbol{D}_p^H\boldsymbol{D}_p$ is required. The calculation of $\langle \boldsymbol{D}^H\boldsymbol{D}\rangle_{q(\boldsymbol{s})}$ is given in Appendix 4.7.1, where the second order statistics $\langle \boldsymbol{s}[t]^*\boldsymbol{s}[t]^T\rangle_{q(\boldsymbol{s}[t])}$ is needed and derived below. Finally, we have $\langle \boldsymbol{x}\rangle_{q(\boldsymbol{x})} = \boldsymbol{\mu}_{\boldsymbol{x}}$.

Derivation of $q(\boldsymbol{s}[t])$

Notice that when deriving $\langle \boldsymbol{D}\rangle_{q(\boldsymbol{s})}$ and $\langle \boldsymbol{D}^H\boldsymbol{D}\rangle_{q(\boldsymbol{s})}$ (in Appendix 4.7.1), $\langle \boldsymbol{s}[t]\rangle_{q(\boldsymbol{s}[t])}$ and $\langle \boldsymbol{s}[t]^*\boldsymbol{s}[t]^T\rangle_{q(\boldsymbol{s}[t])}$ are needed. To obtain $q(\boldsymbol{s}[t])$, we consider the form of the received signal as in (4.1), where $\boldsymbol{y}[t] \sim \mathcal{CN}(\boldsymbol{W}[t]^H\tilde{\boldsymbol{H}}\boldsymbol{s}[t], \sigma^2\mathbf{I})$, then

$$\begin{aligned} q(\boldsymbol{s}[t]) &\propto \exp\Big\{\big\langle \ln p(\boldsymbol{y}[t]|\tilde{\boldsymbol{H}},\boldsymbol{s}[t])\big\rangle_{q(\boldsymbol{x})q(\boldsymbol{y})} + \ln p(\boldsymbol{s}[t])\Big\} \\ &\propto \exp\Big\{\big\langle -\frac{1}{\sigma^2}\|\boldsymbol{y}[t]-\boldsymbol{W}[t]^H\tilde{\boldsymbol{H}}\boldsymbol{s}[t]\|_2^2\big\rangle_{q(\boldsymbol{x})q(\boldsymbol{y})}\Big\}p(\boldsymbol{s}[t]) \\ &\propto \exp\Big\{-(\boldsymbol{s}[t]-\boldsymbol{\mu}_{\boldsymbol{s}})^H\boldsymbol{\Sigma}_{\boldsymbol{s}}^{-1}(\boldsymbol{s}[t]-\boldsymbol{\mu}_{\boldsymbol{s}})\Big\}p(\boldsymbol{s}[t]) \\ &= \begin{cases} c\cdot w_1p_1, & \boldsymbol{s}[t]=\mathcal{S}_1; \\ \ldots, & \ldots; \\ c\cdot w_Qp_Q, & \boldsymbol{s}[t]=\mathcal{S}_Q \end{cases} \end{aligned} \tag{4.46}$$

where we apply the distribution of $p(\boldsymbol{s}[t])$ given in (4.42), and

$$\begin{aligned}\boldsymbol{\Sigma}_{\boldsymbol{s}} &= \Big(\frac{1}{\sigma^2}\big\langle \tilde{\boldsymbol{H}}^H \boldsymbol{W}[t]\boldsymbol{W}[t]^H\tilde{\boldsymbol{H}}\big\rangle_{q(\boldsymbol{x})}\Big)^{-1},\\ \boldsymbol{\mu}_{\boldsymbol{s}} &= \frac{1}{\sigma^2}\boldsymbol{\Sigma}_{\boldsymbol{s}}\big\langle \boldsymbol{W}[t]^H\tilde{\boldsymbol{H}}\big\rangle^H_{q(\boldsymbol{x})}\big\langle \boldsymbol{y}[t]\big\rangle_{q(\boldsymbol{y})},\end{aligned} \tag{4.47}$$

$w_i = \exp\Big\{-(\mathcal{S}_i-\boldsymbol{\mu}_{\boldsymbol{s}})^H\boldsymbol{\Sigma}_{\boldsymbol{s}}^{-1}(\mathcal{S}_i-\boldsymbol{\mu}_{\boldsymbol{s}})\Big\}$ and $c = 1/(w_1p_1+\ldots+w_Qp_Q)$ is the scaling constant. The pmf of $\boldsymbol{s}[t]$ is given by $q(\boldsymbol{s}[t])$. To obtain $\boldsymbol{\mu}_{\boldsymbol{s}}$ and $\boldsymbol{\Sigma}_{\boldsymbol{s}}$, both terms $\big\langle \boldsymbol{W}[t]^H\tilde{\boldsymbol{H}}\big\rangle_{q(\boldsymbol{x})}$ and $\big\langle \tilde{\boldsymbol{H}}^H \boldsymbol{W}[t]\boldsymbol{W}[t]^H\tilde{\boldsymbol{H}}\big\rangle_{q(\boldsymbol{x})}$ are needed, which are given in Appendix 4.7.2. Finally, the first and second order statistics $\langle \boldsymbol{s}[t]\rangle_{q(\boldsymbol{s}[t])}$ and $\langle \boldsymbol{s}[t]^*\boldsymbol{s}[t]^T\rangle_{q(\boldsymbol{s}[t])}$ which are needed before can be calculated as

$$\begin{aligned}\langle \boldsymbol{s}[t]\rangle_{q(\boldsymbol{s}[t])} &= \sum_{i=1}^{Q} c\cdot w_ip_i\mathcal{S}_i\\ \langle \boldsymbol{s}[t]^*\boldsymbol{s}[t]^T\rangle_{q(\boldsymbol{s}[t])} &= \sum_{i=1}^{Q} c\cdot w_ip_i\mathcal{S}_i^*\mathcal{S}_i^T.\end{aligned} \tag{4.48}$$

Derivation of $q(\boldsymbol{\gamma})$

The derivation is the same as (4.38).

Similar to the VB-SBL algorithm in the previous section, we iteratively update $q(\boldsymbol{y})$, $q(\boldsymbol{x})$, $q(\boldsymbol{s}[t]), t = T_p{+}1,\ldots,T$ and $q(\boldsymbol{\gamma})$. In terms of the initialization, it is found in the simulations that using pilots only update to obtain an initial estimate of $q(\boldsymbol{y})$ and $q(\boldsymbol{x})$, then updating together with $q(\boldsymbol{s}[t])$, can lead to a good performance. Notice that there is a trade-off between the performance and the complexity when applying the JPD. On one hand, the JPD can achieve better performance by using transmitted data symbols as the “virtual pilots”, which will be shown in the simulations. On the other hand, utilizing the transmitted data increases the problem size, thereby resulting in higher computational complexity. For pilots only channel estimation, each iteration of the VB-SBL algorithm requires $\mathcal{O}(R^2T_p^2MK)$ operations when $RT_p < MK$, and $\mathcal{O}(RT_pM^2K^2)$ operations when $RT_p > MK$. When JPD is applied, it requires $\mathcal{O}(M^3K^3)$ operations when $RT < MK$, and $\mathcal{O}(RTM^2K^2)$ operations when $RT > MK$. Taking an example of a small training duration T_p with a large JPD duration T such that $RT_p < MK < RT$, then utilizing JPD will cause $\frac{TMK}{T_p^2 R}$ times more operations compared to pilots only channel estimation.

4.4.3 Approximating the Distribution of Transmitted Data

In the previous derivation, $\boldsymbol{s}[t]$ is assumed to be a discrete random vector having pmf as in (4.42), where $Q = \bar{M}^K$ if $\bar{M}$-QAM is used. Notice that when either $\bar{M}$ or K is large, Q will be too large for the calculation of $q(\boldsymbol{s}[t])$ in (4.46). For example, when 64 QAM is used, even for 4 users, $Q = 64^4$ which is impossible to calculate. In such a case, we approximate $p(\boldsymbol{s}[t])$ as a Gaussian distribution such that $p(\boldsymbol{s}[t]) \sim \mathcal{CN}(\mathbf{0}, \sigma_s^2 \mathbf{I})$ where σ_s^2 is the average signal power. Then, the derivation of $q(\boldsymbol{s}[t])$ is modified to

$$\begin{aligned} q(\boldsymbol{s}[t]) &\propto \exp\Big\{ \big\langle \ln p(\boldsymbol{y}[t] | \tilde{\boldsymbol{H}}, \boldsymbol{s}[t]) \big\rangle_{q(\boldsymbol{x})q(\boldsymbol{y})} + \ln p(\boldsymbol{s}[t]) \Big\} \\ &\propto \exp\Big\{ \big\langle -\frac{1}{\sigma^2} \|\boldsymbol{y}[t] - \boldsymbol{W}[t]^H \tilde{\boldsymbol{H}} \boldsymbol{s}[t]\|_2^2 \big\rangle_{q(\boldsymbol{x})q(\boldsymbol{y})} - \frac{\|\boldsymbol{s}[t]\|_2^2}{\sigma_s^2} \Big\} \\ &\propto \exp\Big\{ -(\boldsymbol{s}[t] - \boldsymbol{\mu}_{\boldsymbol{s}}')^H (\boldsymbol{\Sigma}_{\boldsymbol{s}}')^{-1} (\boldsymbol{s}[t] - \boldsymbol{\mu}_{\boldsymbol{s}}') \Big\} \end{aligned} \tag{4.49}$$

where

$$\begin{aligned} \boldsymbol{\Sigma}_{\boldsymbol{s}}' &= \Big(\frac{1}{\sigma^2} \big\langle \tilde{\boldsymbol{H}}^H \boldsymbol{W}[t] \boldsymbol{W}[t]^H \tilde{\boldsymbol{H}} \big\rangle_{q(\boldsymbol{x})} + \frac{1}{\sigma_s^2} \mathbf{I} \Big)^{-1} \\ \boldsymbol{\mu}_{\boldsymbol{s}}' &= \frac{1}{\sigma^2} \boldsymbol{\Sigma}_{\boldsymbol{s}}' \big\langle \boldsymbol{W}[t]^H \tilde{\boldsymbol{H}} \big\rangle_{q(\boldsymbol{x})}^H \big\langle \boldsymbol{y}[t] \big\rangle_{q(\boldsymbol{y})}. \end{aligned} \tag{4.50}$$

Based on the derivations above, $q(\boldsymbol{s}[t])$ is also Gaussian distributed, and we have

$$\begin{aligned} \langle \boldsymbol{s}[t] \rangle_{q(\boldsymbol{s}[t])} &= \boldsymbol{\mu}_{\boldsymbol{s}}' \\ \langle \boldsymbol{s}[t]^* \boldsymbol{s}[t]^T \rangle_{q(\boldsymbol{s}[t])} &= \big(\boldsymbol{\mu}_{\boldsymbol{s}}' (\boldsymbol{\mu}_{\boldsymbol{s}}')^H + \boldsymbol{\Sigma}_{\boldsymbol{s}}' \big)^T. \end{aligned} \tag{4.51}$$

We will show the usefulness of this approximation in the simulations.

4.5 Numerical Results

In the simulation study, we consider an uplink single-cell massive MIMO system, and set the number of antennas at the BS as $N = 32$, with $R = 8$ RF chains. There are $K = 4$ single-antenna UEs. The training sequences of K UEs are cyclically shifted Zadoff-Chu sequences so they are orthogonal to each other. The transmitted data is randomly drawn from QPSK symbols unless otherwise indicated. We assume the same SNR for all UEs [51, 79, 80], i.e., $\rho_k = \rho, \forall k$, in order to compute the average performance of all UEs for ease of illustration, and define SNR $= 10\log_{10}(\rho/\sigma^2)$. In practice, equal SNR can be achieved by some type of power control or user scheduling, otherwise the channel estimation quality of the weaker users will be heavily degraded, especially when ADCs with very low-resolution (e.g., 1-bit) are used [79, 80]. The quantizer $\mathcal{Q}(\cdot)$ is a mid-point uniform quantizer described in Section 4.2, and for simplicity we set $B\Delta/2 = \max_{i,t}\big\{|\Re\{y_i[t]\}|, |\Im\{y_i[t]\}|\big\}, i = 1, \ldots, N, t = 1, \ldots T$, where $\max_{i,t}\big\{|\Re\{y_i[t]\}|, |\Im\{y_i[t]\}|\big\}$ is assumed to be obtained from AGC. Here we emphasize that the proposed VB-SBL algorithm does not have to be confined to any specific quantizer. It can be applied to any quantizer when the quantization thresholds $u_0, \ldots, u_B$ are given. The channel is generated following the spatial channel model (SCM) in 3GPP standard under Urban Macro Scenario [35], where each UE is randomly located with AOA $\theta \in [-90°, 90°]$ relative to the BS broadside. In the sparse channel representation (4.9) $\boldsymbol{A}$ is constructed as an overcomplete DFT matrix with $M = 64$. The performance metric is the normalized mean square error (NMSE) defined as

$$\text{NMSE} = \mathbb{E}\left\{\frac{\|\hat{\boldsymbol{h}} - \boldsymbol{h}\|_2^2}{\|\boldsymbol{h}\|_2^2}\right\} = \frac{1}{LK}\sum_{l=1}^{L}\sum_{k=1}^{K}\frac{\|\hat{\boldsymbol{h}}_k^l - \boldsymbol{h}_k^l\|_2^2}{\|\boldsymbol{h}_k^l\|_2^2} \tag{4.52}$$

where $L = 1000$ is the total number of experimental trials.

4.5.1 Comparing ADCs with Different Resolutions

In Fig. 4.7, we evaluate the channel estimation performance using VB-SBL algorithm, where hybrid AD processing is combined with ADCs of different resolutions. To compare, we also include the result where high resolution ADC is applied, i.e., the unquantized signal $\boldsymbol{y}$ is assumed to be available. It shows that for a specific resolution, there exists some *SNR range* where the quantized channel estimation performs similarly to the *unquantized* one (denoted as ∞-bit), and this range enlarges as the resolutions of ADCs increase. For example, 4-bit ADC can obtain the same performance as the ∞-bit ADC when SNR is below 0 dB, while the 8-bit ADC can achieve the same performance up to 20 dB SNR. So a decision on what resolution of ADC to be used indeed depends on the operating SNR range. In massive MIMO system, inexpensive low-power components can be used to improve the energy efficiency because the resulting distortions can be eliminated by processing a large number of received signals coherently [1,2]. Consequently, the operating SNR range in m1assive MIMO systems is expected to be low, especially as systems move to higher (e.g., millimeter wave) frequencies [80]. For channel estimation, we assume that our interested SNR range is from -10 dB to 10 dB. Fig. 4.7 shows that the performance of 4-bit ADCs is comparable to the performance of ∞-bit ADCs in this SNR range.

Unlike the *unquantized* channel estimate, the NMSE of the *quantized* channel estimate does not decrease monotonically with respect to the SNR. Above a certain SNR, the estimation performance degrades, which means proper intensity of noise can help the estimation of the signal. This phenomenon is known as the stochastic resonance or the dithering effect when dealing with such nonlinear threshold systems [103], and has been observed previously for 1-bit [83] and multi-bit (1-4 bits) [82] channel estimation using other algorithms. Fully exploring such effect is beyond the scope of this work, and would be an interesting topic for future research.

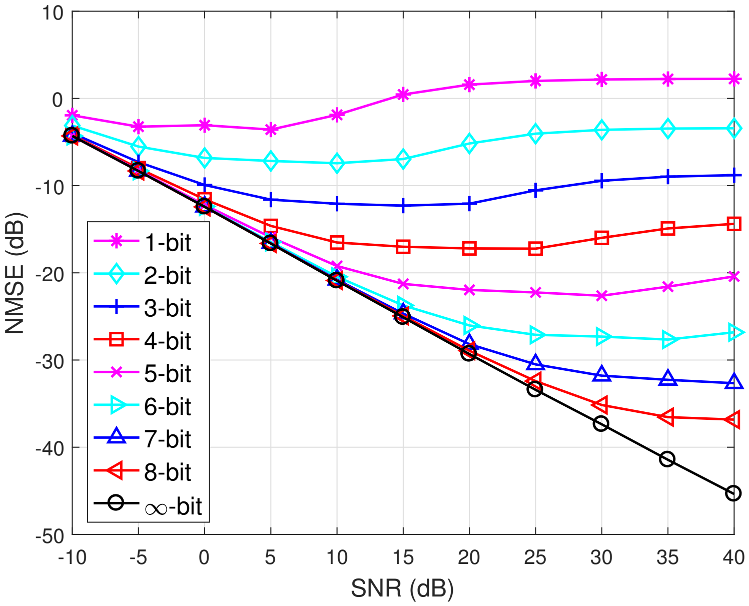

Figure 4.7: NMSE versus SNR for ADCs with different resolutions. $T_p = 10, N = 32, R = 8, K = 4$.

4.5.2 Comparing Different Algorithms

In this experiment, we compare the VB-SBL algorithm with several other channel estimation algorithms:

- EM-LS [81, 82]: this algorithm solves the ML channel estimation using EM algorithm. In the E step, the posterior mean $\hat{\boldsymbol{y}}_p = \mathbb{E}\{\boldsymbol{y}_p | \boldsymbol{z}_p, \hat{\boldsymbol{h}}\}$ is calculated, and in the M step the channel is given by the LS estimation $\hat{\boldsymbol{h}} = (\boldsymbol{\Phi}_p^H \boldsymbol{\Phi}_p)^{-1} \boldsymbol{\Phi}_p^H \hat{\boldsymbol{y}}_p$. where no channel statistic is assumed to be available. The LS estimation requires the number of rows in $\boldsymbol{\Phi}_p$ to be at least as large as the number of columns, i.e., $RT_p \geq NK$.

- EM-OMP [83]: this is a modified EM type algorithm which exploits the sparse property of the channel. The E step is the same as EM-LS, and in the M step the update of $\hat{\boldsymbol{h}}$ is given by $\hat{\boldsymbol{h}} = (\mathbf{I}_K \otimes \boldsymbol{A})\hat{\boldsymbol{x}}$ where $\hat{\boldsymbol{x}}$ is calculated by the orthogonal matching pursuit (OMP) algorithm.

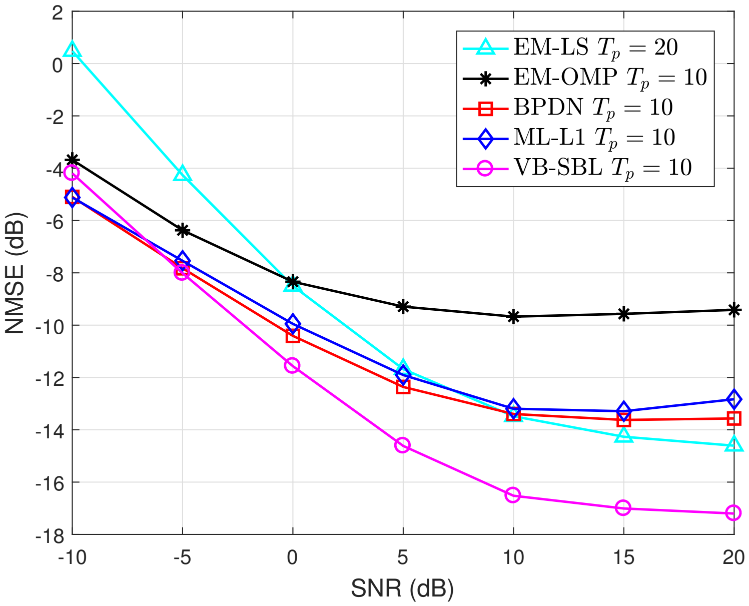

Figure 4.8: NMSE versus SNR for channel estimation using different algorithms. $N = 32, R = 8, K = 4, b = 4$ bit.

- BPDN [73]: we apply the basis pursuit denoise (BPDN) algorithm directly on the received signal $\boldsymbol{z}_p$, which inherently treats the quantization error as additive noise. The algorithm is implemented using SPGL1 toolbox [73].

- ML-L1 [84, 85]: this algorithm solves the ML channel estimation with ℓ_1 norm penalty on $\hat{\boldsymbol{x}}$ to promote the sparsity. The algorithm is implemented using the FASTA algorithm [104].

Except the EM-LS, all the other algorithms are based on CS algorithms and exploit the sparse property of the channel, which lead to a smaller number of training pilots T_p compared to the requirement of $T_p \geq NK/R$ for the EM-LS algorithm.

In Fig. 4.8, we compare the NMSE versus SNR for different algorithms when 4-bit ADCs are used. For EM-LS, it is required that $T_p \geq 16$, so we set $T_p = 20$. For the other CS-based algorithms, T_p is set to 10. In Fig. 4.8, all the CS-based algorithms achieve better performance than EM-LS at low SNR with even smaller T_p, showing the potential for reducing the number of pilots by exploiting the sparse property of the channel. Moreover, the proposed VB-SBL

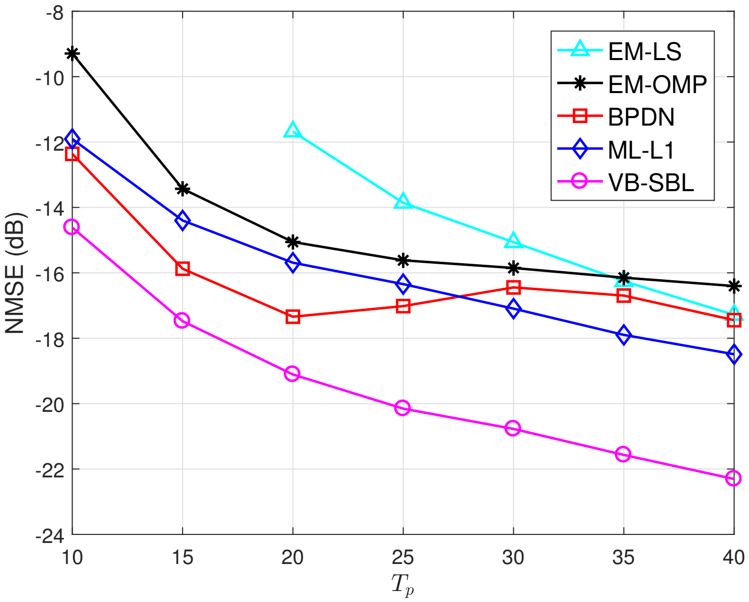

Figure 4.9: NMSE versus training duration T_p for channel estimation using different algorithms. $N = 32, R = 8, K = 4$, SNR $= 5$ dB, $b = 4$ bit.

algorithm can be seen to achieve the best performance among the various competing algorithms, with larger performance gap as the SNR increases. In Fig. 4.9, we compare the NMSE with respect to the number of training pilots T_p. Similarly, the results show that CS-based algorithms which utilize the sparse channel property can obtain better performance with smaller T_p compared to the EM-LS , and the VB-SBL algorithm is superior to the other algorithms.

With regards to complexity, since each algorithm requires different number of iterations to converge, we consider only the complexity of *each iteration* for different algorithms. The EM-LS can only be applied when $RT_p \geq NK$, and has complexity of $\mathcal{O}(RT_pN^2K^2)$. For all the CS-based algorithms, since the dimension of the sparsifying matrix $\boldsymbol{A}$ in (4.9) is $N \times M$, so the dimension of $\boldsymbol{D}_p$ is $RT_p \times MK$. The complexity of EM-OMP is dominant by correlating $\hat{\boldsymbol{y}}_p$ with every column of $\boldsymbol{D}_p$, which scales as $\mathcal{O}(RT_pMK)$. The complexities of SPGL1-based BPDN [73] and FASTA-based ML-L1 [104] are dominant by the matrix-vector operations $\boldsymbol{D}_p\hat{\boldsymbol{x}}$ and $\boldsymbol{D}_p^H\hat{\boldsymbol{y}}_p$, so their complexities also scale as $\mathcal{O}(RT_pMK)$. The complexity of VB-SBL is

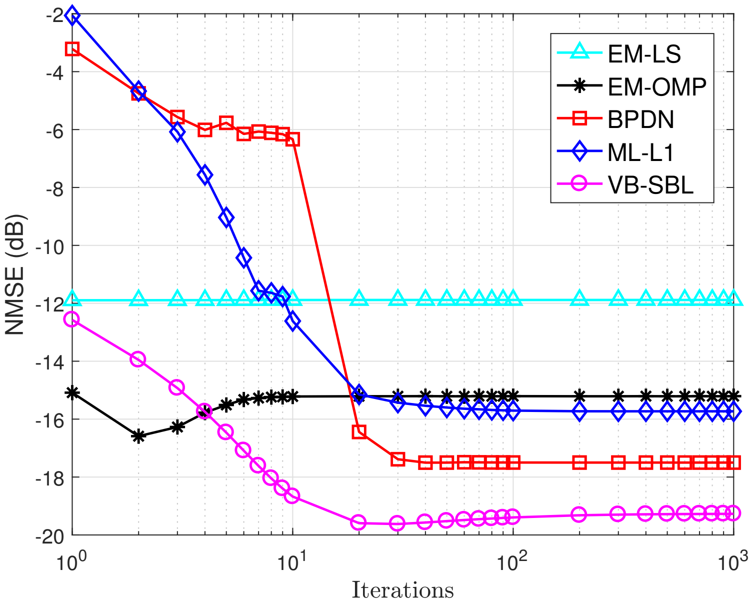

Figure 4.10: NMSE versus number of iterations for channel estimation using different algorithms. $N = 32, R = 8, K = 4$, SNR $= 5$ dB, $b = 4$ bit, $T_p = 20$.

$\mathcal{O}(R^2T_p^2MK)$ when $RT_p < MK$, and $\mathcal{O}(RT_pM^2K^2)$ when $RT_p > MK$. Compared to the other algorithms, VB-SBL has higher complexity. In Fig. 4.10, we plot the NMSE versus the number of iterations when different algorithms are applied. Fig. 4.10 shows that EM-LS and EM-OMP converge fast, while it takes more iterations for ML-L1, BPDN and VB-SBL to converge. However, with a few iterations, VB-SBL already obtains the smallest NMSE among all the algorithms. In summary, VB-SBL is superior in terms of the channel estimation performance, but it also has higher complexity. Some previous works have developed faster SBL algorithm for the conventional unquantized problem [105, 106]. Extending those algorithms to handle the quantized measurements would be an interesting topic for future work.

4.5.3 Comparing Different SNR

In previous simulations, we assume the same SNR for all UEs for ease of illustration of the plot. In this experiment, we set different ρ_k for each UE. When all UEs have the same SNR,

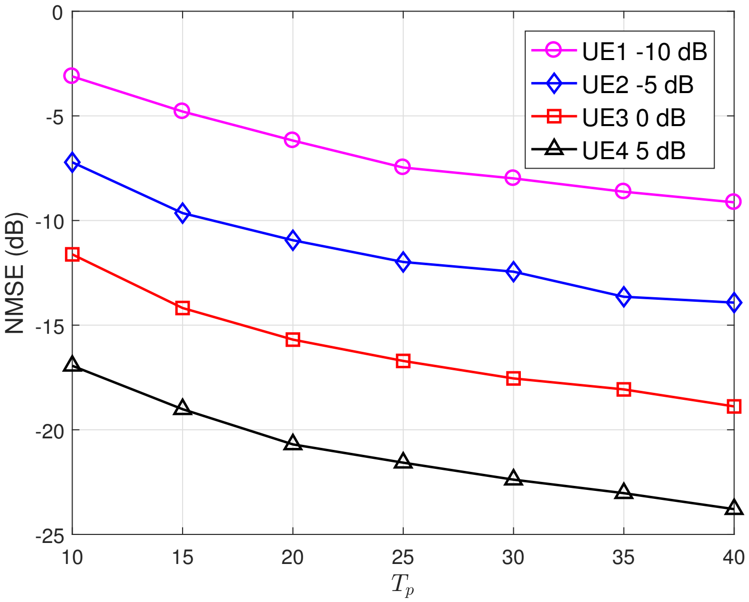

Figure 4.11: NMSE versus training duration T_p for VB-SBL algorithm with different SNR for each UE. $N = 32, R = 8, K = 4, b = 4$bit.

we can compute the average NMSE of all UEs as the performance metric. However, when each UE has different SNR, we need to plot the performance for each UE separately. Assume $K = 4$ UEs, and we set each UE's SNR as $\rho_1 = -10$ dB, $\rho_2 = -5$ dB, $\rho_3 = 0$ dB, $\rho_4 = 5$ dB. Fig. 4.11 plots the NMSE versus the training duration T_p for each UE using the proposed VB-SBL algorithm with 4-bit ADC. It shows that for all UEs, the NMSE decreases as the training duration T_p increases. Moreover, the UE with higher SNR has much better NMSE compared to UE with lower SNR. In practice, some type of power control or user scheduling should be done to make UEs having the similar SNR and avoid the weaker UEs.

4.5.4 Channel Estimation with JPD

In this experiment, we investigate the performance of channel estimation with JPD and compare it to the pilots only channel estimation (denoted as Pilot). Firstly, we compare the JPD and the Pilot when different number of RF chains are used. In Fig. 4.12, we test Pilot with 8, 16,

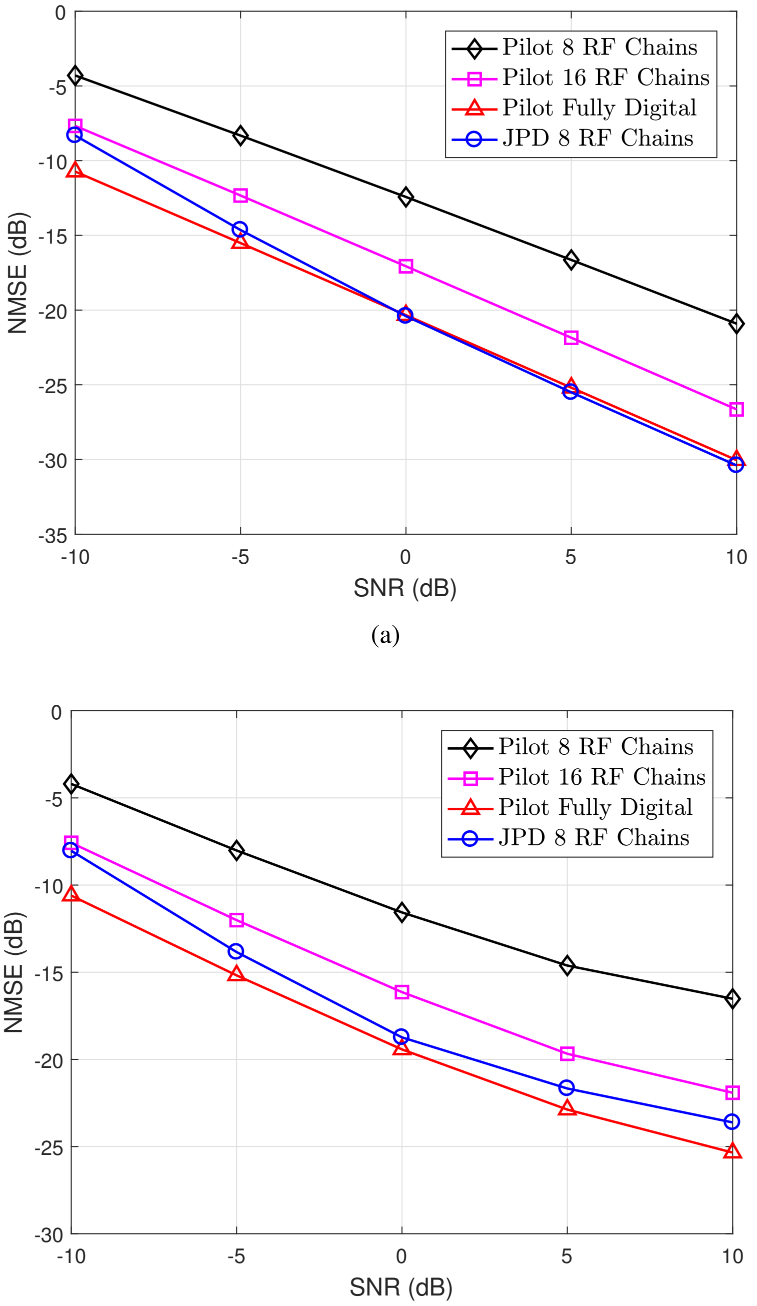

(a)

(b)

Figure 4.12: NMSE versus SNR for JPD and pilots only channel estimation with different number of RF chains. (a) ∞-bit ADCs. (b) 4-bit ADCs. For pilots only channel estimation, $T_p = 10$. For JPD, $T_p = 10, T = 50$. $N = 32, K = 4$.

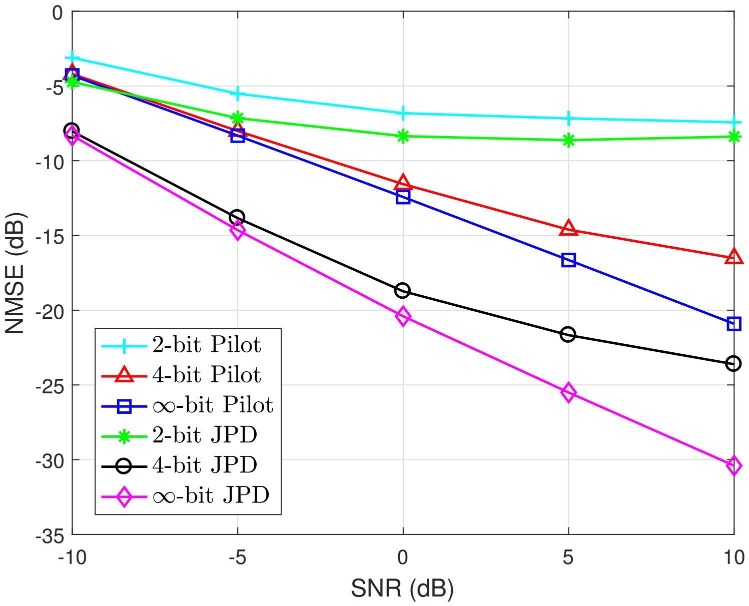

Figure 4.13: NMSE versus SNR for JPD and pilots only channel estimation with different resolution ADCs. For pilots only channel estimation, $T_p = 10$. For JPD, $T_p = 10, T = 50$. $N = 32, R = 8, K = 4$.

and 32 (fully digital) RF chains, and JPD with 8 RF chains. When both Pilot and JPD use 8 RF chains, JPD has much better performance than the Pilot. Moreover, JPD with 8 RF chains can obtain even smaller NMSE than Pilot with 16 RF chains. In Fig. 4.12 (b) where 4-bit ADCs are applied, JPD with 8 RF chains only has small performance loss compared to the Pilot with fully digital architecture. And in Fig. 4.12 (a) where ∞-bit ADCs are used, JPD with 8 RF chains can achieve the same performance as the Pilot with fully digital architecture from 0 to 10 dB. The results imply the benefits of using JPD when hybrid AD processing is applied, such that one can achieve better performance with reduced number of RF chains by utilizing JPD.

Next we compare the JPD and the Pilot when different resolution ADCs are used. Fig. 4.13 shows that for both high-resolution and low-resolution ADCs, JPD is better than the corresponding Pilot. Notice that more improvements can be achieved by JPD as the resolution of ADCs increases. Furthermore, with the help of JPD, better performance can be obtained using lower resolution ADCs. For instance, 4-bit JPD has smaller NMSE than ∞-bit Pilot from -10 dB to 10 dB

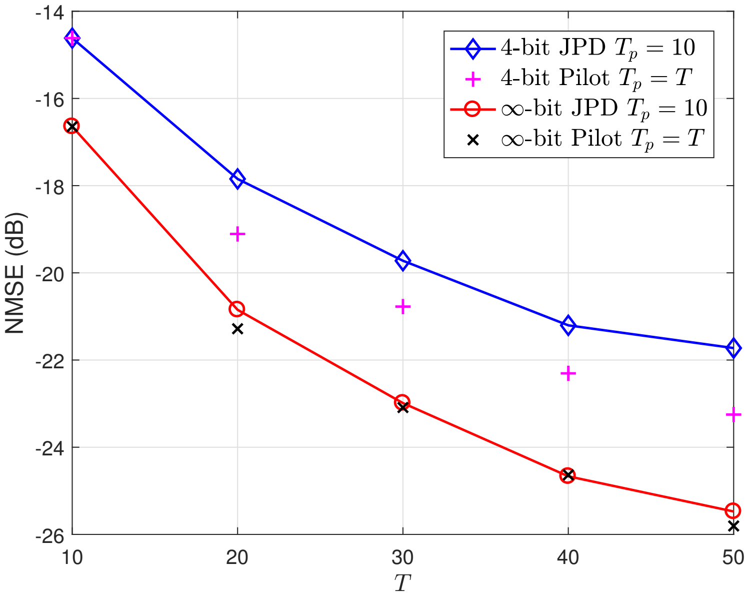

Figure 4.14: NMSE versus JPD duration T. For JPD, $T_p = 10$. For pilots only channel estimation, $T_p = T$. $N = 32$, $R = 8$, $K = 4$, SNR $= 5$ dB.

SNR. And even 2-bit JPD is better than ∞-bit Pilot at -10 dB SNR. This experiment shows the advantages of applying JPD when low-resolution ADCs are utilized.

In Fig. 4.14, we investigate the performance of JPD with different T, i.e., utilizing different number of data symbols. T_p in JPD is fixed as 10, and we gradually increase T from 10 to 50 (when $T = T_p = 10$, JPD is the same as Pilot). The performance of Pilot with $T_p = T$ is also provided as the benchmark, which can be treated as the best performance that JPD is able to achieve. Fig. 4.14 shows that for both 4-bit and ∞-bit ADCs, the performance of JPD improves as more transmitted data, i.e., larger T, is utilized for the channel estimation. However, the increment becomes slower as T increases, which means that most benefit of JPD can be achieved with a modest T. Notice that with $T_p = 10$, 4-bit JPD with $T = 20$ is already better than ∞-bit Pilot with $T_p = 10$, showing the benefit of JPD even with small T. Compared to Pilot with $T_p = T$, the NMSE of 4-bit JPD is only about 1 dB worse, while the ∞-bit JPD can achieve almost the same performance. Notice that the number of training pilots in JPD is only $T_p = 10$, in contrast to $T_p = T$ in Pilot. In other words, the training overhead can be reduced by using the

JPD scheme.

4.5.5 Effect of Gaussian Approximation

We now investigate the effects of Gaussian approximation for JPD as proposed in Section 4.4.3. In Fig. 4.15, we denote "constellation" when $p(\boldsymbol{s}[t])$ is set to be the true distribution of the transmitted data symbols as in (4.42), and "Gaussian" when the Gaussian approximation in Section 4.4.3 is used such that $p(\boldsymbol{s}[t]) \sim \mathcal{CN}(\mathbf{0}, \sigma_s^2 \mathbf{I}_K)$ with $\sigma_s^2 = 1$. As shown in Fig. 4.15 (a) and Fig. 4.15 (b), the performance of JPD Gaussian is close to the JPD Constellation when SNR $= -10$dB, which implies that the Gaussian approximation is useful at low SNR. However, the performance loss due to the Gaussian approximation becomes larger as the SNR increases. Specifically, the performance of JPD Gaussian with 4-bit ADC begins to saturate from SNR $= 5$ dB.

When higher order modulation is used, for example, 64 QAM as in Fig. 4.16, applying the true distribution to $p(\boldsymbol{s}[t])$ becomes infeasible, whereas the Gaussian approximation provides an simple alternative. Notice that even with the Gaussian approximation, for both ∞-bit and 4-bit ADCs there is about a 3 dB improvement when JPD is applied, especially for the SNR ranging from -10 dB to 5 dB.

4.6 Conclusion

In this chapter, we developed a VB-SBL-based channel estimation algorithm for the multi-user massive MIMO system where hybrid AD processing and low-resolution ADCs are utilized at the BS. To overcome the limitations imposed by the reduced number of effective measurements due to the hardware-efficient architecture, we exploit the sparse structure of the massive MIMO channel to reduce the training overhead. We further leverage the transmitted data symbols as "virtual pilots" to increase the measurement information. Experimental results show

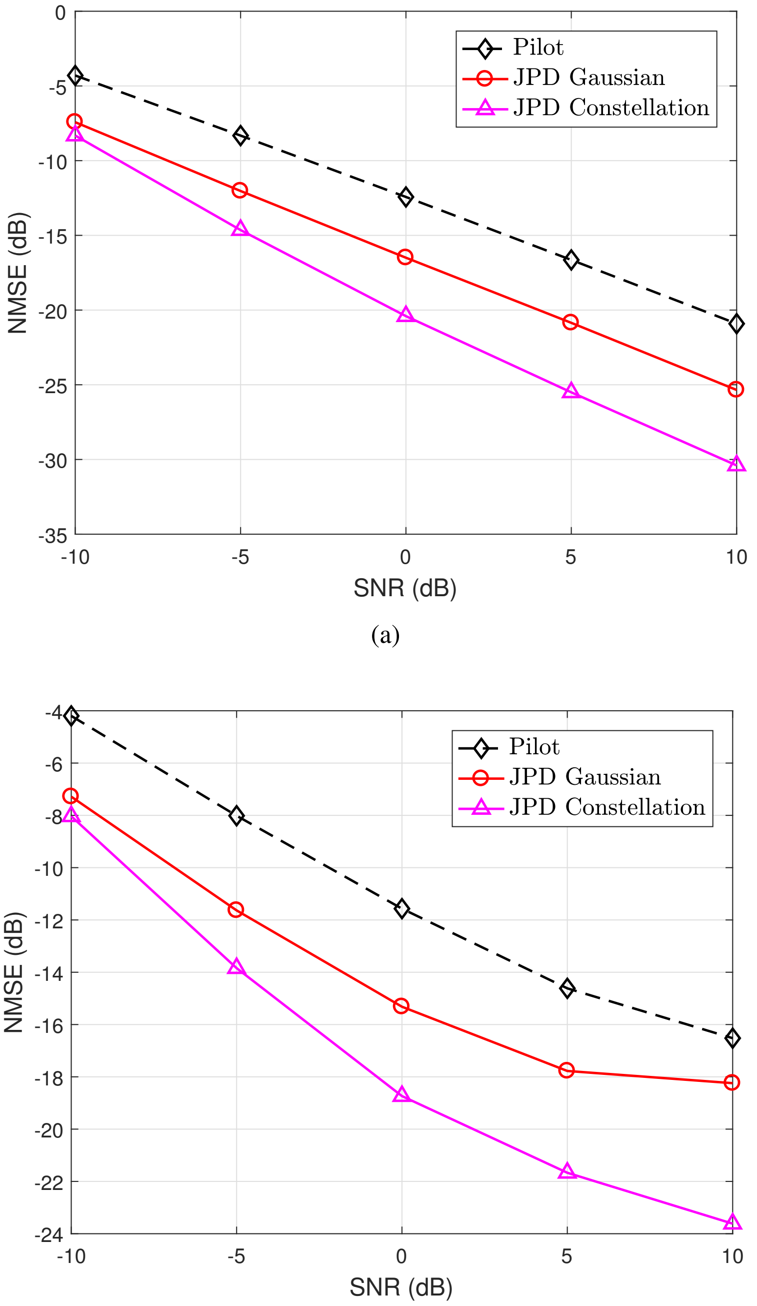

(a)

(b)

Figure 4.15: NMSE versus SNR for JPD with true distribution and Gaussian approximation to QPSK data symbols. (a) ∞-bit ADCs. (b) 4-bit ADCs. For pilots only channel estimation, $T_p = 10$. For JPD, $T_p = 10, T = 50$. $N = 32, R = 8, K = 4$.

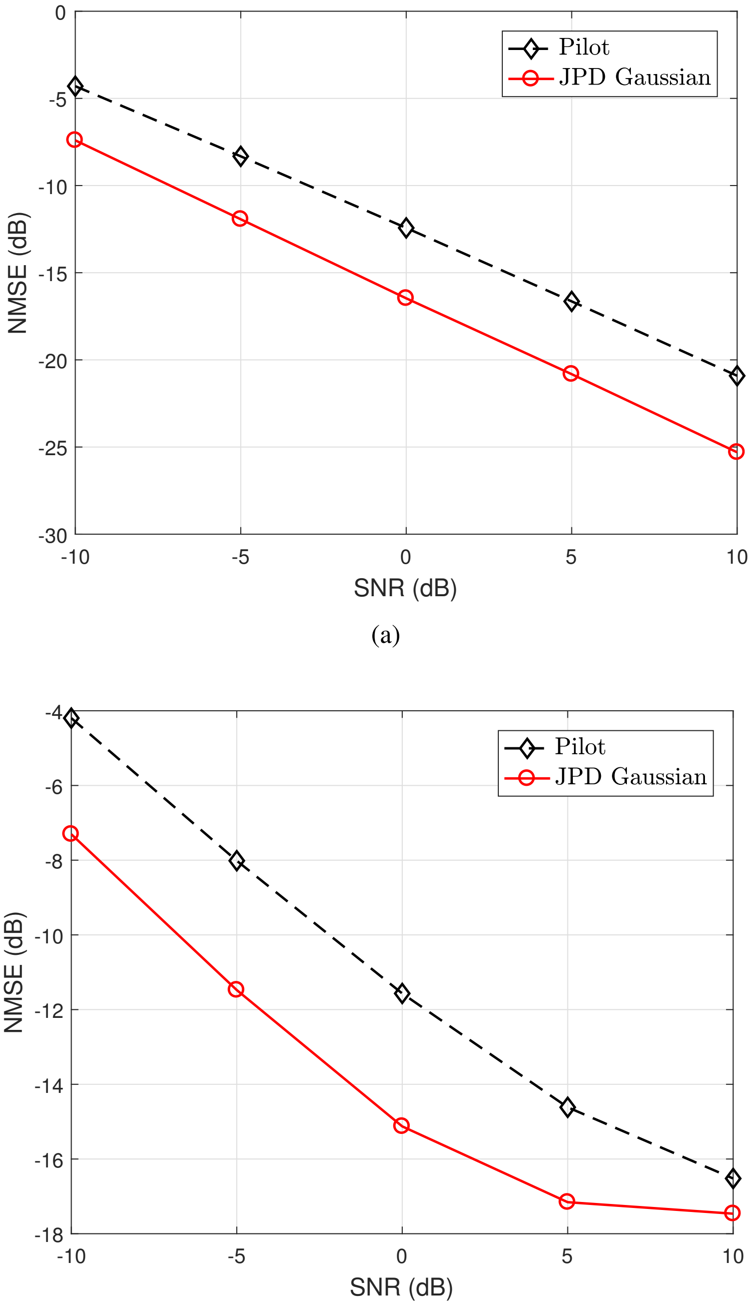

(a)

(b)

Figure 4.16: NMSE versus SNR for JPD with Gaussian approximation to 64 QAM data symbols. (a) ∞-bit ADCs. (b) 4-bit ADCs. For pilots only channel estimation, $T_p = 10$. For JPD, $T_p = 10, T = 50$. $N = 32, R = 8, K = 4$.

that the VB-SBL algorithm is superior than the other quantized channel estimation algorithms. At low SNR, channel estimation with low-resolution ADCs can achieve very similar performance as the high-resolution ADCs. Furthermore, the channel estimation using JPD can achieve better performance with smaller number of RF chains and coarser ADCs compared to the traditional pilots only channel estimation scheme, showing the significant benefits of applying JPD when the proposed hardware-efficient architecture is used. Future work of interest would be in adaptively designing the analog combining matrix based on previous channel estimate, developing faster algorithms that can accommodate very large problem size, and utilizing the dithering effect to improve the performance of low-resolution ADCs at high SNR.

Chapter 4, in part, is a reprint of the material as it appears in the paper: Y. Ding, S. Chiu, and B. D. Rao, "Bayesian channel estimation algorithms for massive MIMO systems with hybrid analog-digital processing and low resolution ADCs," *IEEE J. Sel. Topics Signal Process.*, vol. 12, no. 3, pp. 499-513, June 2018. The dissertation author was the primary investigator and author of this paper.

4.7 Appendices

4.7.1 Derivations About Transmitted Data

We present the derivation of $\langle \boldsymbol{D} \rangle_{q(\boldsymbol{s})}$ and $\langle \boldsymbol{D}^H \boldsymbol{D} \rangle_{q(\boldsymbol{s})}$ in this subsection. The term $\langle \boldsymbol{D} \rangle_{q(\boldsymbol{s})}$ is derived as following:

$$\langle \boldsymbol{D} \rangle_{q(\boldsymbol{s})} = \langle \boldsymbol{\Phi}(\mathbf{I}_K \otimes \boldsymbol{A}) \rangle_{q(\boldsymbol{s})} = \langle \boldsymbol{\Phi} \rangle_{q(\boldsymbol{s})}(\mathbf{I}_K \otimes \boldsymbol{A}) \tag{4.53}$$

where $\boldsymbol{\Phi} = [\boldsymbol{\Phi}_p^T \; \boldsymbol{\Phi}_d^T]^T$. $\boldsymbol{\Phi}_p$ contains known pilot symbols, and only $\boldsymbol{\Phi}_d$ contains unknown transmitted data $\boldsymbol{s}[t], t = T_p + 1, \dots, T$ which is random. So $\langle \boldsymbol{\Phi} \rangle_{q(\boldsymbol{s})} = [\boldsymbol{\Phi}_p^T \; \langle \boldsymbol{\Phi}_d \rangle_{q(\boldsymbol{s})}^T]^T$ and $\langle \boldsymbol{\Phi}_d \rangle_{q(\boldsymbol{s})} = \left[\langle \boldsymbol{\Phi}[T_p + 1] \rangle_{q(\boldsymbol{s}[T_p+1])}^T, \dots, \langle \boldsymbol{\Phi}[T] \rangle_{q(\boldsymbol{s}[T])}^T \right]^T$ where for each $\langle \boldsymbol{\Phi}[t] \rangle_{q(\boldsymbol{s}[t])}, t = T_p +$

$1, \ldots, T$ we have

$$\langle \boldsymbol{\Phi}[t] \rangle_{q(\boldsymbol{s}[t])} = \langle \boldsymbol{s}[t] \rangle_{q(\boldsymbol{s}[t])}^T \otimes \boldsymbol{W}[t]^H. \tag{4.54}$$

The term $\langle \boldsymbol{s}[t] \rangle_{q(\boldsymbol{s}[t])}$ needs to be calculated from the approximated posterior $q(\boldsymbol{s}[t])$, which is given in (4.48).

Since $\boldsymbol{D} = [\boldsymbol{D}_p^T \ \boldsymbol{D}_d^T]^T$, only $\boldsymbol{D}_d = \boldsymbol{\Phi}_d(\mathbf{I}_K \otimes \boldsymbol{A})$ contains the random variable $\boldsymbol{s}[t]$ in $\boldsymbol{\Phi}_d$. Similarly we have

$$\begin{aligned} \langle \boldsymbol{D}^H \boldsymbol{D} \rangle_{q(\boldsymbol{s})} &= \boldsymbol{D}_p^H \boldsymbol{D}_p + \langle \boldsymbol{D}_d^H \boldsymbol{D}_d \rangle_{q(\boldsymbol{s})} \\ &= \boldsymbol{D}_p^H \boldsymbol{D}_p + (\mathbf{I}_K \otimes \boldsymbol{A})^H \langle \boldsymbol{\Phi}_d^H \boldsymbol{\Phi}_d \rangle_{q(\boldsymbol{s})} (\mathbf{I}_K \otimes \boldsymbol{A}) \end{aligned} \tag{4.55}$$

where $\langle \boldsymbol{\Phi}_d^H \boldsymbol{\Phi}_d \rangle_{q(\boldsymbol{s})} = \sum_{t=T_p+1}^{T} \langle \boldsymbol{\Phi}[t]^H \boldsymbol{\Phi}[t] \rangle_{q(\boldsymbol{s}[t])}$. And for each $\langle \boldsymbol{\Phi}[t]^H \boldsymbol{\Phi}[t] \rangle_{q(\boldsymbol{s}[t])}$, we have

$$\begin{aligned} \langle \boldsymbol{\Phi}[t]^H \boldsymbol{\Phi}[t] \rangle_{q(\boldsymbol{s})} &= \Big\langle \big(\boldsymbol{s}[t]^T \otimes \boldsymbol{W}[t]^H\big)^H \big(\boldsymbol{s}[t]^T \otimes \boldsymbol{W}[t]^H\big) \Big\rangle_{q(\boldsymbol{s}[t])} \\ &= \Big\langle \big(\boldsymbol{s}[t]^* \otimes \boldsymbol{W}[t]\big) \big(\boldsymbol{s}[t]^T \otimes \boldsymbol{W}[t]^H\big) \Big\rangle_{q(\boldsymbol{s}[t])} \\ &= \langle \boldsymbol{s}[t]^* \boldsymbol{s}[t]^T \rangle_{q(\boldsymbol{s}[t])} \otimes \big(\boldsymbol{W}[t] \boldsymbol{W}[t]^H\big) \end{aligned} \tag{4.56}$$

where $\langle \boldsymbol{s}[t]^* \boldsymbol{s}[t]^T \rangle_{q(\boldsymbol{s}[t])}$ is given in (4.48).

4.7.2 Derivations About Angular Domain Channel

In this subsection, we derive $\big\langle \boldsymbol{W}[t]^H \tilde{\boldsymbol{H}} \big\rangle_{q(\boldsymbol{x})}$ and $\big\langle \tilde{\boldsymbol{H}}^H \boldsymbol{W}[t] \boldsymbol{W}[t]^H \tilde{\boldsymbol{H}} \big\rangle_{q(\boldsymbol{x})}$. The derivation of $\big\langle \boldsymbol{W}[t]^H \tilde{\boldsymbol{H}} \big\rangle_{q(\boldsymbol{x})}$ is straightforward such that

$$\big\langle \boldsymbol{W}[t]^H \tilde{\boldsymbol{H}} \big\rangle_{q(\boldsymbol{x})} = \boldsymbol{W}[t]^H \big\langle \tilde{\boldsymbol{H}} \big\rangle_{q(\boldsymbol{x})} = \boldsymbol{W}[t]^H \boldsymbol{A} \langle \tilde{\boldsymbol{X}} \rangle_{q(\boldsymbol{x})}. \tag{4.57}$$

The term $\langle \tilde{\boldsymbol{X}} \rangle_{q(\boldsymbol{x})}$ can be obtained by reshaping $\text{vec}(\langle \tilde{\boldsymbol{X}} \rangle_{q(\boldsymbol{x})})$, where $\text{vec}(\langle \tilde{\boldsymbol{X}} \rangle_{q(\boldsymbol{x})}) = \langle \boldsymbol{x} \rangle_{q(\boldsymbol{x})} = \boldsymbol{\mu}_{\boldsymbol{x}}$ as given in (4.45).

Similarly, regarding to the term $\big\langle \tilde{\boldsymbol{H}}^H \boldsymbol{W}[t]\boldsymbol{W}[t]^H \tilde{\boldsymbol{H}} \big\rangle_{q(\boldsymbol{x})}$, it can be reshaped from its vectorized form $\mathrm{vec}\Big(\big\langle \tilde{\boldsymbol{H}}^H \boldsymbol{W}[t]\boldsymbol{W}[t]^H \tilde{\boldsymbol{H}} \big\rangle_{q(\boldsymbol{x})}\Big)$, which is given below:

$$\begin{aligned}\mathrm{vec}\Big(\big\langle \tilde{\boldsymbol{H}}^H \boldsymbol{W}[t]\boldsymbol{W}[t]^H \tilde{\boldsymbol{H}} \big\rangle_{q(\boldsymbol{x})}\Big) &= \mathrm{vec}\Big(\big\langle \tilde{\boldsymbol{X}}^H \boldsymbol{A}^H \boldsymbol{W}[t]\boldsymbol{W}[t]^H \boldsymbol{A}\tilde{\boldsymbol{X}} \big\rangle_{q(\boldsymbol{x})}\Big) \\ &= \big\langle \tilde{\boldsymbol{X}}^T \otimes \tilde{\boldsymbol{X}}^H \big\rangle_{q(\boldsymbol{x})} \mathrm{vec}\big(\boldsymbol{A}^H \boldsymbol{W}[t]\boldsymbol{W}[t]^H \boldsymbol{A}\big).\end{aligned} \tag{4.58}$$

Notice that $\tilde{\boldsymbol{X}}^T \otimes \tilde{\boldsymbol{X}}^H$ consists of $K \times N$ blocks where each block is of size $K \times N$. For the (i,j)-th block of $\big\langle \tilde{\boldsymbol{X}}^T \otimes \tilde{\boldsymbol{X}}^H \big\rangle_{q(\boldsymbol{x})}$, its value is $\langle \tilde{x}_{j,i} \tilde{\boldsymbol{X}}^H \rangle_{q(\boldsymbol{x})}$, whose conjugate transpose is $\langle \tilde{\boldsymbol{X}} \tilde{x}^*_{j,i} \rangle_{q(\boldsymbol{x})}$. And the term $\langle \tilde{\boldsymbol{X}} \tilde{x}^*_{j,i} \rangle_{q(\boldsymbol{x})}$ can be further reshaped from $\mathrm{vec}\big(\langle \tilde{\boldsymbol{X}} \tilde{x}^*_{j,i} \rangle_{q(\boldsymbol{x})}\big) = \big[\boldsymbol{\mu}_{\boldsymbol{x}} \boldsymbol{\mu}_{\boldsymbol{x}}^H + \boldsymbol{\Sigma}_{\boldsymbol{x}}\big]_{\cdot,(i-1)N+j}$, which is the $((i-1)N+j)$-th column of $\boldsymbol{\mu}_{\boldsymbol{x}} \boldsymbol{\mu}_{\boldsymbol{x}}^H + \boldsymbol{\Sigma}_{\boldsymbol{x}}$, with both $\boldsymbol{\mu}_{\boldsymbol{x}}$ and $\boldsymbol{\Sigma}_{\boldsymbol{x}}$ given in (4.45). By forming all $K \times N$ blocks together, we obtain the matrix $\big\langle \tilde{\boldsymbol{X}}^T \otimes \tilde{\boldsymbol{X}}^H \big\rangle_{q(\boldsymbol{x})}$, thereby having $\big\langle \tilde{\boldsymbol{H}}^H \boldsymbol{W}[t]\boldsymbol{W}[t]^H \tilde{\boldsymbol{H}} \big\rangle_{q(\boldsymbol{x})}$.

Chapter 5

Sensing Matrix Design With Partial Knowledge of Support

In compressive sensing, it has been shown that a carefully designed sensing matrix is able to improve the performance of signal recovery, when the signal can be sparsely represented using an overcomplete dictionary. The designed sensing matrix is able to decrease the average coherence of the combined equivalent dictionary. In this chapter, we propose a new framework when partial knowledge of support is available. Observing that for an overcomplete equivalent dictionary, it is impossible to make the coherence between all pairs of atoms to be arbitrarily small, our algorithm leverages the partial knowledge of support and concentrates on minimizing coherence between atoms where at least one of the columns belongs to the preferred support set. In the noisy case, energy among atoms of the equivalent dictionary is non-uniformly distributed such that atoms in the preferred support set are emphasized. To solve the underlying optimization problem, we propose an algorithm for *sensing matrix design with partial knowledge on support* (SMPKS) based on the majorization-minimization (MM) framework. Experimental results show the superiority of the proposed SMPKS algorithm compared to other sensing matrix design algorithms. Since the compressive sensing algorithms have been widely applied for channel estimation in massive MIMO system, the proposed SMPKS algorithm can be utilized to design better pilot symbols to improve the channel estimation performance.

5.1 Introduction

In the framework of compressive sensing, the signal of interest $\boldsymbol{x} \in \mathbb{R}^{N \times 1}$, is assumed to have a sparse representation in a dictionary $\boldsymbol{D} \in \mathbb{R}^{N \times M}$, such that $\boldsymbol{x} = \boldsymbol{D}\boldsymbol{\beta}$. The sparse coefficient vector $\boldsymbol{\beta} \in \mathbb{R}^{M \times 1}$ is assumed to have only a few nonzero entries such that $\|\boldsymbol{\beta}\|_0 \ll M$. The signal $\boldsymbol{x}$ is measured by a *sensing matrix* $\boldsymbol{A} \in \mathbb{R}^{T \times N}$ such that

$$\boldsymbol{y} = \boldsymbol{A}\boldsymbol{x} = \boldsymbol{A}\boldsymbol{D}\boldsymbol{\beta} = \boldsymbol{E}\boldsymbol{\beta} \tag{5.1}$$

where $\boldsymbol{y} \in \mathbb{R}^{T \times 1}$ is the measured signal and $\boldsymbol{E} = \boldsymbol{A}\boldsymbol{D} \in \mathbb{R}^{T \times M}$ is the combined *equivalent dictionary*. The goal of compressive sensing is to recover $\boldsymbol{x}$ given $\boldsymbol{y}$, $\boldsymbol{A}$ and $\boldsymbol{D}$, even when the number of measurements is less than the dimension of the signal, i.e., $T < N$. In [6], it has been shown that when $\boldsymbol{D}$ is an *orthonormal* basis, by utilizing a *randomly* generated matrix $\boldsymbol{A}$ and with number of measurements $T \propto C \cdot s \log(N/s)$, the sparse coefficient $\boldsymbol{\beta}$ can be robustly recovered. Here the constant C depends on the property of the sensing matrix $\boldsymbol{A}$ and $s = \|\boldsymbol{\beta}\|_0$ represents the sparsity level. The signal $\boldsymbol{x}$ can then be computed as $\boldsymbol{x} = \boldsymbol{D}\boldsymbol{\beta}$. However in some applications, the signal $\boldsymbol{x}$ can not be sparsely represented in any orthonomal basis [107], or more generally a sparse representation of the signal is achieved using an *overcomplete* dictionary $\boldsymbol{D}$ which has more columns than rows $N < M$, and is possibly learned from the data [58, 59]. The utilization of an overcomplete dictionary $\boldsymbol{D}$ will alter the geometric structure induced by the random sensing matrix $\boldsymbol{A}$ and the equivalent dictionary $\boldsymbol{E}$ no longer satisfies the constraints required for robustly recovering $\boldsymbol{\beta}$. So a problem of interest is as follows: when given an overcomplete dictionary $\boldsymbol{D}$, rather than using a randomly generated $\boldsymbol{A}$ which is independent of $\boldsymbol{D}$, is it possible to design a better sensing matrix $\boldsymbol{A}$ that adapts to $\boldsymbol{D}$ such that the performance of sparse recovery algorithms can be improved?

Existing works which aim to optimize sensing matrix $\boldsymbol{A}$ can be generally categorized into two different types. The first type is to design $\boldsymbol{A}$ as a *whole*, which adapts to dictionary $\boldsymbol{D}$ such that the combined equivalent dictionary $\boldsymbol{E} = \boldsymbol{A}\boldsymbol{D}$ has good geometric properties [50, 108–111]. In [50], the author consider the "average" mutual coherence between atoms in $\boldsymbol{E}$, and try to decrease the large entries by a shrinkage process utilizing the Gram matrix $\boldsymbol{G} = \boldsymbol{E}^T\boldsymbol{E}$. In [108, 109], the sensing matrix is designed such that the distance between the Gram matrix and an identity matrix is minimized, which can be regarded as a way to minimize the average level of coherence. The work in [109] considers the application of measurement matrix design in MIMO radar, with optimality criterion depending on the coherence as well as the signal to interference ratio (SIR). In [110], the special case when the signal has a block sparse representation is considered, and the design of $\boldsymbol{A}$ is carried out by minimizing a weighted sum of sub-block coherence and inter-block coherence. Motivated by Grassmannian frame design, the work in [111] attempts to make the equivalent dictionary $\boldsymbol{E}$ to be an equiangular tight frame by using an alternating minimization algorithm.

In the second category, rows of $\boldsymbol{A}$ are *sequentially* designed, using previously collected measurements as guidance, see [21, 112, 113] and references therein. The sparse model assumes $\boldsymbol{D}$ to be an orthonormal basis or canonical coordinate. In [21], a Bayesian signal model is adopted and a new row of $\boldsymbol{A}$ is chosen to maximize the increment of differential entropy $h(\boldsymbol{y})$ as a means for making the new measurement most informative. In [112, 113], a constraint on the total sensing energy, i.e., $||\boldsymbol{A}||_F^2$, is considered and sequential measurement is designed to focus sensing energy towards the more probable non-zero elements based on knowledge from previous measurements. This adaptive sensing can decrease the required magnitude of the smallest element in $\boldsymbol{\beta}$ for a robust recovery [112, 113]. However, sequentially update rows of $\boldsymbol{A}$ such design requires the accessibility of the previous measurements in an *online* fashion, which may not be feasible in some applications.

In this chapter, we follow the concept in the first category to design $\boldsymbol{A} \in \mathbb{R}^{T \times N}$ as a whole with respect to a given overcomplete dictionary $\boldsymbol{D} \in \mathbb{R}^{N \times M}$. In order to guarantee the unique representation of $\boldsymbol{x}$, we assume spark$(\boldsymbol{D}) = N + 1$ and $\|\boldsymbol{\beta}\|_0 < T/2$ [7]. In the scenario of an overcomplete representation and compressed sensing such that $T < N < M$, we have $\|\boldsymbol{\beta}\|_0 <$ spark$(\boldsymbol{D})/2$. According to [16, 24], this condition implies that $\boldsymbol{\beta}$ is unique and sparsest given the representation of $\boldsymbol{x} = \boldsymbol{D}\boldsymbol{\beta}$. Moreover, we consider the situation where some partial knowledge about the support of $\boldsymbol{\beta}$ is available, for example a *prefered support set* $\mathcal{S}$. Defining the *true support* of $\boldsymbol{\beta}$ as $\mathcal{TS}(\boldsymbol{\beta})$ (or $\mathcal{TS}$ when $\boldsymbol{\beta}$ is clear from the context), then we have $\mathcal{S} = \Delta \cup \Delta_e$, where $\Delta = \mathcal{S} \cap \mathcal{TS}$ denotes the correct components in the preferred set, and $\Delta_e = \mathcal{S} \backslash \mathcal{TS}$ denotes the error in the preferred set. Similarly, $\mathcal{TS} = \Delta \cup \Delta_m$ where $\Delta_m = \mathcal{TS} \backslash \mathcal{S}$ represents the correct components that are missing from $\mathcal{S}$. To measure the quality of the the preferred support $\mathcal{S}$, we define the error rate as $p_e = |\Delta_e|/(|\Delta| + |\Delta_e|)$, and the missing rate as $p_m = |\Delta_m|/(|\Delta| + |\Delta_m|)$. We do not put any constraints on the size of preferred support, i.e., $|\mathcal{S}|$ can be smaller, equal, or larger than $|\mathcal{TS}|$.

Such partial information about the sparse support set exists in many applications. For example if $\boldsymbol{D}$ is an discrete wavelet transform frame and $\boldsymbol{\beta}$ represents the coefficient of an image, then the entries of $\boldsymbol{\beta}$ that correspond to the low frequency subbands are most likely to be nonzero and carry most of the energy, so $\mathcal{S}$ can be the set of location indices of those coefficients [114]. For the time series problem, $\mathcal{S}$ can be $\hat{\mathcal{TS}}$ which is the estimated support from the previous time slot. Then $\Delta_e = \mathcal{S} \backslash \mathcal{TS}$ corresponds to coefficients that were nonzero previously but are zero at the current time, while $\Delta_m = \mathcal{TS} \backslash \mathcal{S}$ is the newly added coefficients. Both Δ_e and Δ_m are typically much smaller than $|\mathcal{S}|$, following the empirical observation that sparsity patterns change slowly [115]. The channel estimation problem in massive MIMO systems is of particular interest to us, where the channel $\boldsymbol{x}$ can be sparsely represented in an overcomplete DFT dictionary or learned dictionary $\boldsymbol{D}$ as $\boldsymbol{x} = \boldsymbol{D}\boldsymbol{\beta}$ [97]. In a closed loop training, the user estimated the channel $\hat{\boldsymbol{x}} = \boldsymbol{D}\hat{\boldsymbol{\beta}}$ from the downlink training $\boldsymbol{y} = \boldsymbol{A}\boldsymbol{x} + \boldsymbol{n}$, and feeds back information such as the support of sparse coefficients $\mathcal{TS}(\hat{\boldsymbol{\beta}})$. Then the base station can utilize this information to design pilots $\boldsymbol{A}$ for the next training stage, i.e., $\mathcal{S} = \mathcal{TS}(\hat{\boldsymbol{\beta}})$. If the current channel is estimated correctly and the feedback is perfect, when the channel is slowly changing the $\mathcal{S}$ obtained during the current training stage would be a good indication for the next training stage. In the open loop training where there is no feedback, when the duplex distance (frequency difference between the uplink and downlink transmission) is small, it is reasonable to assume the uplink and downlink channel have similar sparse support due to the common scattering objects during uplink and downlink transmission, i.e., $\mathcal{TS}(\boldsymbol{\beta}^u) = \mathcal{TS}(\boldsymbol{\beta}^d)$ [97]. Then the base station can utilize uplink training to extract support information as the preferred support, $\mathcal{S} = \mathcal{TS}(\hat{\boldsymbol{\beta}}^u)$ and use it to design pilots $\boldsymbol{A}$ in the downlink channel estimation. When the uplink channel is correctly estimated, again $\mathcal{S}$ is a good indication of the sparse support of the downlink channel.

In [115], a similar concept of *partially known support* was proposed, and a modified basis pursuit algorithm was used to utilize such prior information and shown to require weaker conditions for exact reconstruction. Similarly in [114] a weighted ℓ_1 minimization was proposed where smaller weights are given to the elements in the preferred support. In our work, rather than designing for a specific *sparse recovery algorithm*, e.g., modified-BP in [115], we develop a framework to design a *sensing matrix*, and we demonstrate experimentally that for many sparse recovery algorithms the designed sensing matrix leads to an improved recovery performance. Designing sensing matrix with partial knowledge of support has also been considered in [116], in which spectral characteristics of underlying signal are assumed to be known, and colored Gaussian matrix with corresponding spectral shapes is used as sensing matrix to focus measurement energy. Our work generalizes this work in that we consider an overcomplete dictionary $\boldsymbol{D}$, rather than a Fourier transform matrix as used in [116] to extract spectral information. Also regarding the design of $\boldsymbol{A}$, we consider both structure optimization (decrease mutual coherence) as well as energy focussing (increase signal to noise ratio), where [116] only considers the energy focussing.

The chapter is organized as follows. In Section 5.2, we review two representative works on sensing matrix design. In Section 5.3, we introduce our motivation for utilizing the partial knowledge of support, and propose an efficient algorithm to solve the sensing matrix design problem. We then extend it to the noisy case in Section 5.4. Simulation results are presented in Section 5.5. Conclusions and future works are discussed in Section 5.6.

Notations used in this chapter are as follows. Upper (lower) bold face letters are used throughout to denote matrices (column vectors). $(\cdot)^T$, $(\cdot)^\dagger$ denotes the transpose and the Penrose-Moor pseudo-inverse. $\boldsymbol{x}_i$ is the i-th entry of the vector $\boldsymbol{x}$, and $\boldsymbol{A}_{ij}$ is the (i, j)-th entry of the matrix $\boldsymbol{A}$. $\boldsymbol{A}_{\cdot j}$ and $\boldsymbol{A}_{i\cdot}$ represents the j-th column and i-th row of $\boldsymbol{A}$. When $\mathcal{S}$ is an index set, $\boldsymbol{A}_{\cdot\mathcal{S}}$ and $\boldsymbol{A}_{\mathcal{S}\cdot}$ correspond to a submatrix collecting corresponding columns and rows of $\boldsymbol{A}$, respectively. For a vector $\boldsymbol{x}$, diag$(\boldsymbol{x})$ is a diagonal matrix with $\boldsymbol{x}$ being its diagonal. $\mathbf{I}_{N\times N}$ is an $N \times N$ identity matrix. For a given vector $\boldsymbol{x}$ and matrix $\boldsymbol{A}$, $\|\boldsymbol{x}\|_1$, $\|\boldsymbol{x}\|_2$ denotes the ℓ_1 and ℓ_2 norm, and $\|\boldsymbol{A}\|_F$ denotes the Frobenious norm. tr$(\boldsymbol{A})$ denotes the trace of a matrix $\boldsymbol{A}$. $\|\boldsymbol{x}\|_0$ represents the number of nonzero entries in $\boldsymbol{x}$ and is referred to as the ℓ_0 norm. For an integer M, $[M]$ is defined as the set $\{1, \ldots, M\}$. $|\cdot|$ denotes the absolute value of a scalar or cardinality of a set. $\lfloor x \rfloor$ rounds x to the nearest integer that is smaller than x.

5.2 Prior Work on Sensing Matrix Design

In this section we will introduce several basic concepts and terminologies which will be used later in the chapter. We review past work and two representative algorithms [50, 108] that motivate our work in some detail. These algorithms are used for comparison in the simulations.

5.2.1 The Basics

Mutual coherence plays an important role in compressive sensing to determine the recovery performance [7, 10, 24], which is defined as [50]:

Definition 1. *For a dictionary $\boldsymbol{E} \in \mathbb{R}^{T\times M}$, its mutual coherence is defined as the largest absolute* normalized inner product between different columns in $\boldsymbol{E}$, which is given by

$$\mu(\boldsymbol{E}) = \max_{1\leq i,j\leq M, i\neq j} \frac{|\boldsymbol{E}_{\cdot i}^T \boldsymbol{E}_{\cdot j}|}{\|\boldsymbol{E}_{\cdot i}\|_2 \cdot \|\boldsymbol{E}_{\cdot j}\|_2}. \tag{5.2}$$

Another way to understand mutual coherence is by the Gram matrix $\boldsymbol{G} = \boldsymbol{E}^T\boldsymbol{E}$. The diagonal elements $\boldsymbol{G}_{ii}$ is the squared norm of the i-th column of $\boldsymbol{E}$, i.e., $\boldsymbol{G}_{ii} = \boldsymbol{E}_{\cdot i}^T \boldsymbol{E}_{\cdot i} = \|\boldsymbol{E}_{\cdot i}\|_2^2$. The off-diagonal entries $\boldsymbol{G}_{ij}$ describes the coherence between $\boldsymbol{E}_{\cdot i}$ and $\boldsymbol{E}_{\cdot j}$ similar to (5.2), but without normalization and maximization. If we denote $\tilde{\boldsymbol{E}}$ as $\boldsymbol{E}$ with normalized columns and $\tilde{\boldsymbol{G}} = \tilde{\boldsymbol{E}}^T\tilde{\boldsymbol{E}}$, then

$$\mu(\boldsymbol{E}) = \max_{i\neq j} |\tilde{\boldsymbol{G}}_{ij}|. \tag{5.3}$$

We shall refer hereafter $|\boldsymbol{G}_{ij}|$ and $|\tilde{\boldsymbol{G}}_{ij}|$ as the *unnormalized coherence* and the *coherence* between the i-th column and the j-th column of the dictionary $\boldsymbol{E}$, to denote the similarity between two columns.

The mutual coherence provides a measure of the *worst* similarity between the dictionary columns, a value that exposes the dictionary's vulnerability, as two closely related columns may confuse any sparse recovery algorithm [50]. Suppose the signal $\boldsymbol{x}$ is sparse in the canonical coordinate basis, i.e., $\boldsymbol{D} = \mathbf{I}_{N\times N}$, then (5.1) becomes $\boldsymbol{y} = \boldsymbol{A}\boldsymbol{D}\boldsymbol{\beta} = \boldsymbol{A}\boldsymbol{\beta}$. It has been shown that if $\|\boldsymbol{\beta}\|_0 < \frac{1}{2}(1 + \frac{1}{\mu(\boldsymbol{A})})$, then $\boldsymbol{\beta}$ is the *uniquely sparsest* solution to $\boldsymbol{y} = \boldsymbol{A}\boldsymbol{\beta}$, and both basis pursuit (BP) and orthogonal matching pursuit (OMP) algorithms are guaranteed to recover $\boldsymbol{\beta}$ [7,10,24]. This result can be applied to (5.1) with a general overcomplete dictionary $\boldsymbol{D}$ such as $\|\boldsymbol{\beta}\|_0 < \frac{1}{2}(1 + \frac{1}{\mu(\boldsymbol{A}\boldsymbol{D})}) = \frac{1}{2}(1 + \frac{1}{\mu(\boldsymbol{E})})$, and we can see that a smaller $\mu(\boldsymbol{E})$ implies a wider range of solvable $\boldsymbol{\beta}$ ($\boldsymbol{\beta}$ whose sparse support has a larger cardinality). This is the motivation behind the idea of designing $\boldsymbol{A}$ such that $\boldsymbol{E} = \boldsymbol{A}\boldsymbol{D}$ possesses good geometric properties, e.g., a smaller $\mu(\boldsymbol{E})$.

However, as pointed in [50], mutual coherence $\mu(\boldsymbol{A}\boldsymbol{D})$ is the worst-case measure of the recoverability for a sparse recovery problem, which may be too pessimistic for practical problems.

If one allows a small fraction of signals with the same representation cardinality to fail (which relaxes the "guaranteed" essence in the proofs), then $\boldsymbol{\beta}$ with cardinality of support substantially beyond the above bound can still be recovered by the pursuit algorithms. This motivates one to consider properties of $\boldsymbol{E}$ that can lead to performance improvement in a more "average" sense, which will be introduced in the following subsection.

5.2.2 Some Representative Work

In [50], a "t-averaged mutual coherence" is proposed aiming to reflect average behavior of the dictionary:

Definition2. *For dictionary $\boldsymbol{E}$, it's t-averaged mutual coherence is defined as the average of all absolute and normalized inner products between different columns in $\boldsymbol{E}$ (denoted as $\tilde{\boldsymbol{G}}_{ij}$) that are above t. Formally*

$$\mu_t(\boldsymbol{E}) = \frac{\sum_{1\le i,j\le M, i\ne j} \mathbb{1}(|\tilde{\boldsymbol{G}}_{ij}| \ge t)\cdot|\tilde{\boldsymbol{G}}_{ij}|}{\sum_{1\le i,j\le M, i\ne j} \mathbb{1}(|\tilde{\boldsymbol{G}}_{ij}| \ge t)}. \tag{5.4}$$

The notation $\mathbb{1}(\cdot)$ denotes the indicator function, such that $\mathbb{1}(|\tilde{\boldsymbol{G}}_{ij}| \ge t) = 1$ if $|\tilde{\boldsymbol{G}}_{ij}| \ge t$, $\mathbb{1}(|\tilde{\boldsymbol{G}}_{ij}| \ge t) = 0$ if $|\tilde{\boldsymbol{G}}_{ij}| < t$. For $t = 0$, $\mu_t(\boldsymbol{E})$ is the average of the absolute off-diagonal entries of $\tilde{\boldsymbol{G}}$. As t grows, $\mu_t(\boldsymbol{E})$ grows and approaches $\mu(\boldsymbol{E})$ from below. Also from definition $\mu_t(\boldsymbol{E}) \ge t$. In [50], $\mu_t(\boldsymbol{E})$ was used as an "average" measure of coherence and the goal was to minimize $\mu_t(\boldsymbol{AD})$ with respect to $\boldsymbol{A}$ given $\boldsymbol{D}$. Notice that $\mu_t(\boldsymbol{E})$ is defined via the entries of the $\tilde{\boldsymbol{G}}$, and an iterative algorithm is proposed such that in each iteration all $\tilde{\boldsymbol{G}}_{ij}$ that are greater than t are shrunk by a factor $\gamma, 0 < \gamma < 1$, and $\boldsymbol{A}$ is recalculated according to the new $\tilde{\boldsymbol{G}}$. The iterations are carried out until some termination requirement is satisfied. Although no convergence proof is provided, it has been shown to achieve improved performance compared to the random sensing matrix using both BP and OMP as recovery algorithms. Similar iterative shrinkage approach has been applied to design Grassmanian frames that minimize the actual mutual coherence in (5.2) [49]. Another related work [111], constructs a relaxed equiangular tight frame (ETF) using a gradient-based alternating minimization approach.

In [108], $\boldsymbol{A}$ is designed such that the distance between the Gram matrix and the identity matrix is minimized. This formulation lead to the following design procedure.

$$\begin{aligned}\hat{\boldsymbol{A}} &= \arg\min_{\boldsymbol{A}} \|\boldsymbol{E}^T\boldsymbol{E} - \mathbf{I}\|_F^2 \\ &= \arg\min_{\boldsymbol{A}} \|\boldsymbol{D}^T\boldsymbol{A}^T\boldsymbol{A}\boldsymbol{D} - \mathbf{I}\|_F^2.\end{aligned} \tag{5.5}$$

Notice that (5.5) is the same as minimizing $\mu_t(\boldsymbol{E}), t = 0$ if columns of $\boldsymbol{E}$ are enforced to have unit norm. Rather than explicitly constraining columns of $\boldsymbol{E}$ to be unit norm, the diagonal terms of $\boldsymbol{D}^T\boldsymbol{A}^T\boldsymbol{A}\boldsymbol{D} - \mathbf{I}$ can be regarded as a penalty to encourage unit norm of columns of $\boldsymbol{E}$. By some manipulation, (5.5) can be transformed into $\|\boldsymbol{\Lambda} - \boldsymbol{\Lambda}\boldsymbol{\Gamma}^T\boldsymbol{\Gamma}\boldsymbol{\Lambda}\|_F^2$ where $\boldsymbol{V}\boldsymbol{\Lambda}\boldsymbol{V}^T$ is the eigen-decomposition of $\boldsymbol{D}\boldsymbol{D}^T$ and $\boldsymbol{\Gamma} = \boldsymbol{A}\boldsymbol{V}$. A K-SVD [59] like algorithm is used to progressively solve for $\boldsymbol{A}$ [108].

5.3 Sensing Matrix Design with Partial Knowledge of Support

5.3.1 Motivation

The cost function in (5.5) can also be written in terms of entries in Gram matrix $\boldsymbol{G} = \boldsymbol{E}^T\boldsymbol{E}$. As shown in [110], we have

$$\begin{aligned}\|\boldsymbol{E}^T\boldsymbol{E} - \mathbf{I}\|_F^2 &= \mathrm{Trace}(\boldsymbol{E}^T\boldsymbol{E}\boldsymbol{E}^T\boldsymbol{E} - 2\boldsymbol{E}^T\boldsymbol{E} + \mathbf{I}_M) \\ &= \mathrm{Trace}(\boldsymbol{E}\boldsymbol{E}^T\boldsymbol{E}\boldsymbol{E}^T - 2\boldsymbol{E}\boldsymbol{E}^T + \mathbf{I}_T) + (M - T) \\ &= \|\boldsymbol{E}\boldsymbol{E}^T - \mathbf{I}_T\|_F^2 + (M - T) \\ &\geq M - T\end{aligned} \tag{5.6}$$

since we have $\|\boldsymbol{E}\boldsymbol{E}^T - \mathbf{I}_T\|_F^2 \geq 0$. Also, (5.6) can be written using the Gram matrix $\boldsymbol{G}$ as given below:

$$\|\boldsymbol{E}^T\boldsymbol{E} - \mathbf{I}\|_F^2 = \sum_{i \neq j} |\boldsymbol{G}_{ij}|^2 + \sum_{i=j} |\boldsymbol{G}_{ij} - 1|^2 \geq M - T. \tag{5.7}$$

This means for an overcomplete equivalent dictionary $\boldsymbol{E}$, it is impossible to minimize coherence to be arbitrarily small between *all* pairs of columns. In other words, it is impossible to make all $|\boldsymbol{G}_{ij}|, i \neq j$ and $|\boldsymbol{G}_{ij} - 1|, i = j$ to be arbitrarily small at the same time. However, do we really need to minimize coherence between all pairs of columns? To address this question we draw some inspiration from past work.

In [7], it has been shown that for $\boldsymbol{y} = \boldsymbol{A}\boldsymbol{x} = \boldsymbol{A}\boldsymbol{D}\boldsymbol{\beta} = \boldsymbol{E}\boldsymbol{\beta}$, if $\|\boldsymbol{\beta}\|_0 < \frac{1}{2}(1 + \frac{1}{\mu(\boldsymbol{E})})$, then OMP is guaranteed to find it exactly. An examination of the proof reveals that only the coherence between two columns which are both in the true support, or the coherence between two columns of which only one belongs to the true support and the other is outside of the true support, are important. Coherence between columns which are both outside of the true support do not play a role in establishing the result. In other words, the OMP algorithm can always succeed if the sufficient condition in [7] is satisfied, no matter what value the coherence between two columns that are both outside the true support is. Another work that supports the above argument is [117], in which an *Exact Recovery Condition* (ERC) was proposed. With the same measurement system $\boldsymbol{y} = \boldsymbol{E}\boldsymbol{\beta}$ as above, assume $\mathcal{J}$ as the true support of $\boldsymbol{\beta}$, the ERC states that if $\max_{k \notin \mathcal{J}} \|\boldsymbol{E}_{\cdot\mathcal{J}}^\dagger \boldsymbol{E}_{\cdot k}\|_1 < 1$, then the sparsest representation of the signal is unique. Moreover, both OMP and BP identify the optimal atoms and their coefficients. Noting that $\boldsymbol{E}_{\cdot\mathcal{J}}^\dagger = (\boldsymbol{E}_{\cdot\mathcal{J}}^T \boldsymbol{E}_{\cdot\mathcal{J}})^{-1}\boldsymbol{E}_{\cdot\mathcal{J}}^T$, then the ERC becomes $\max_{k \notin \mathcal{J}} \|(\boldsymbol{E}_{\cdot\mathcal{J}}^T \boldsymbol{E}_{\cdot\mathcal{J}})^{-1}\boldsymbol{E}_{\cdot\mathcal{J}}^T \boldsymbol{E}_{\cdot k}\|_1 < 1$. Again in ERC, only coherence of columns that are both in the true support $\boldsymbol{E}_{\cdot\mathcal{J}}^T \boldsymbol{E}_{\cdot\mathcal{J}}$, or only one of them is in the true support $\boldsymbol{E}_{\cdot\mathcal{J}}^T \boldsymbol{E}_{\cdot k}$, are considered. It implies that when ERC is satisfied, the coherence of columns that are both outside the true support do not play a role. Moreover in both [7] and [117], by minimizing the coherence between pairs of columns when at least one belongs to the true support, one is able to achieve a more favorable bound for the recovery condition to be satisfied. In [7], this corresponds to minimize $|\boldsymbol{E}_{\cdot k}^T \boldsymbol{E}_{\cdot t}|, 1 \leq k, t \leq s$ and $|\boldsymbol{E}_{\cdot i}^T \boldsymbol{E}_{\cdot t}|, i > s, 1 \leq t \leq s$, and in [117] it corresponds to minimize $\|(\boldsymbol{E}_{\cdot \mathcal{J}}^T \boldsymbol{E}_{\cdot \mathcal{J}})^{-1}\|_{1,1}$ and $\|\boldsymbol{E}_{\cdot \mathcal{J}}^T \boldsymbol{E}_{\cdot k}\|_1, k \notin \mathcal{J}$. Minimizing those terms will give tighter bounds such that the required conditions tend to be more likely satisfied. Note that only the upper bounds but not the actual interested terms, i.e., $|\sum_{t=1}^s \boldsymbol{\beta}_t \boldsymbol{E}_{\cdot k}^T \boldsymbol{E}_{\cdot t}|, 1 \leq k \leq s$ and $|\sum_{t=1}^s \boldsymbol{\beta}_t \boldsymbol{E}_{\cdot i}^T \boldsymbol{E}_{\cdot t}|, i > s$ in [7] and $\|\boldsymbol{E}_{\cdot \mathcal{J}}^\dagger \boldsymbol{E}_{\cdot k}\|_1$ in [117], can be improved by minimizing those terms.

The above discussion reveals the benefit of reducing the coherence between columns when at least one of them belongs to $\mathcal{TS}(\boldsymbol{\beta})$, or formally

$$|\boldsymbol{G}_{ij}| = |\boldsymbol{E}_{\cdot i}^T \boldsymbol{E}_{\cdot j}|, \quad i \text{ or } j \in \mathcal{TS}(\boldsymbol{\beta}) \tag{5.8}$$

and we do not need to consider the coherence of columns when both are outside of the true support,

$$|\boldsymbol{G}_{ij}| = |\boldsymbol{E}_{\cdot i}^T \boldsymbol{E}_{\cdot j}|, \quad i \text{ and } j \notin \mathcal{TS}(\boldsymbol{\beta}). \tag{5.9}$$

Since $\boldsymbol{E} = \boldsymbol{A}\boldsymbol{D}$ where $\boldsymbol{D}$ is a given dictionary, we can only rely on designing $\boldsymbol{A}$ in order to minimize $|\boldsymbol{G}_{ij}| = |\boldsymbol{E}_{\cdot i}^T \boldsymbol{E}_{\cdot j}|$. Moreover, rather than requiring the equivalent dictionary $\boldsymbol{E} = \boldsymbol{A}\boldsymbol{D}$ to have a good geometric condition for every pair of atoms, which is demanding and potentially unnecessary, it motivates one to concentrate on pairs of atoms when at least one has a high chance of belonging to the true support $\mathcal{TS}(\boldsymbol{\beta})$. It is interesting to see that the previous works either minimize mutual coherence defined in (5.3), which focusses on the *maximum* of all $|\boldsymbol{G}_{ij}|$, or "t-averaged mutual coherence" defined in (5.4), which focusses on the *average* of all $|\boldsymbol{G}_{ij}|$. The above observations indicate that we should choose discriminatively the more important $|\boldsymbol{G}_{ij}|$ rather than considering them all.

However, we do not know the true support beforehand, otherwise (5.1) reduces to a trivial overdetermined linear inverse problem. In many practical applications, we may be able to gather some information on the support, potentially an approximation which we refer as the preferred support set $\mathcal{S}$. Observing the lower bound in (5.7), even if the $\mathcal{S}$ we obtain is only partially correct, it is useful to utilize it. The more confidence we have in this preferred support set $\mathcal{S}$, the more emphasis one should put on it.

5.3.2 Designing the Sensing Matrix

Based on the above discussion, we focuss on minimizing $|\boldsymbol{G}_{ij}|$ that at least i or j belongs to the preferred set $\mathcal{S}$. For a Gram matrix $\boldsymbol{G} = \boldsymbol{E}^T\boldsymbol{E} = (\boldsymbol{AD})^T(\boldsymbol{AD})$ with elements $\boldsymbol{G}_{ij}$, we aim to solve optimized sensing matrix $\boldsymbol{A}$ by minimizing $|\boldsymbol{G}_{ij}|^2$, corresponding to the unnormalized coherence between $\boldsymbol{E}_i$ and $\boldsymbol{E}_j$. Define sets that describe different conditions on $\{i, j\}$: $\mathcal{P}_1 = \{\{i, j\}|i = j, i, j \in \mathcal{S}\}$,$\mathcal{P}_2 = \{\{i, j\}|i = j, i, j \notin \mathcal{S}\}$, $\mathcal{P}_3 = \{\{i, j\}|i \neq j, i \in \mathcal{S} \text{ and } j \in \mathcal{S}\}$, $\mathcal{P}_4 = \{\{i, j\}|i \neq j, \text{only } i \text{ or } j \in \mathcal{S}\}$ $\mathcal{P}_5 = \{\{i, j\}|i \neq j, i \notin \mathcal{S} \text{ and } j \notin \mathcal{S}\}$, and

$$\begin{aligned} W_d &= \sum_{\{i,j\}\in\mathcal{P}_1} |\boldsymbol{G}_{ij} - 1|^2 + \sum_{\{i,j\}\in\mathcal{P}_2} |\boldsymbol{G}_{ij} - 1|^2, \\ W_s &= \sum_{\{i,j\}\in\mathcal{P}_3} |\boldsymbol{G}_{ij}|^2 + \sum_{\{i,j\}\in\mathcal{P}_4} |\boldsymbol{G}_{ij}|^2, \\ W_{ns} &= \sum_{\{i,j\}\in\mathcal{P}_5} |\boldsymbol{G}_{ij}|^2. \end{aligned} \tag{5.10}$$

Then the sensing matrix design problem is formulated as

$$\hat{\boldsymbol{A}} = \arg\min_{\boldsymbol{A}} \gamma W_d + \alpha W_s + W_{ns} \tag{5.11}$$

where γ and α are positive constants. In (5.11), we do not explicitly normalize columns of $\boldsymbol{E}$ to be unit norm, but implicitly encourage such constraint by minimizing W_d [108,110]. W_d controls the distance between the diagonal elements $\boldsymbol{G}_{ii}$ and 1, where $\boldsymbol{G}_{ii}$ represents the squared norm of the i-th column $\boldsymbol{E}_{\cdot i}$. If $W_d = 0$, then every column of the equivalent dictionary $\boldsymbol{E}$ is normalized, and the *unnormalized coherence* $\boldsymbol{G}_{ij}$ reduces to the the *coherence* $\tilde{\boldsymbol{G}}_{ij}$. W_s represents the summation of unnormalized coherence between two columns when at least one of them belongs to $\mathcal{S}$. W_{ns} represents the summation of unnormalized coherence between two columns that are both out of $\mathcal{S}$.

We use γ and α to trade off among W_d, W_s and W_{ns}. Typically we choose $\alpha > 1$ to emphasize W_s, which corresponds to the coherence of columns that are more important for successful recovery. Since usually the dimension of sparse coefficient $\boldsymbol{\beta}$ is much larger than the size of preferred support, i.e., $M \gg |\mathcal{S}|$, the value of W_{ns} is much larger than W_s, so we need a larger value α to favor minimizing W_s. Also we need a large value for γ, in order to guarantee every atom in $\boldsymbol{E}$ to be nearly normalized. Large γ avoids the situation that columns in $\mathcal{S}$ are driven to have too small norm. For example, assume $\alpha \gg \gamma$, and let $i \in \mathcal{S}$. By making $\boldsymbol{E}_{\cdot i}$ to be a vector with all zeros will lead to a smaller W_s since $\boldsymbol{G}_{ij} = 0, \forall j$. Due to $\alpha \gg \gamma$, the optimization process will favor this result. But it leads to a very large coherence after normalization. In other words, the process is favoring minimizing W_s by making $\boldsymbol{E}_{\cdot i}$ trivial rather than making $\boldsymbol{E}_{\cdot i}$ distinct with other columns, where the latter is the true purpose of minimizing W_s. In (5.11) we also minimize the term W_{ns} which only relates to columns outside $\mathcal{S}$. This is because $\mathcal{S}$ may only contain part of the correct indexes ($|\Delta_m| > 0$), there are still some columns belonging to the true support $\mathcal{TS}$ that are outside of $\mathcal{S}$, and minimizing coherence of those columns will give a better recovery performance. But since we have no idea about those columns, we can only treat them in an non-informative manner and use W_{ns} to minimize the summation of the unnormalized coherence corresponding to those columns.

5.3.3 SMPKS Algorithm

Although the cost function in (5.11) is in the quadratic form of entries in $\boldsymbol{G}$, the actual variable $\boldsymbol{A}$ that we are going to solve is coupled with $\boldsymbol{G}$ through the dictionary $\boldsymbol{D}$ such that $\boldsymbol{G} = \boldsymbol{E^T E} = \boldsymbol{D^T A^T A D}$, where $\boldsymbol{A} \in \mathbb{R}^{T \times N}, \boldsymbol{D} \in \mathbb{R}^{N \times M}$. With the assumption $T \leq N$ and

$N \leq M$, the Gram matrix $\boldsymbol{G}$ is rank T (assume generally $\boldsymbol{E} = \boldsymbol{AD}$ is full rank). Imposing such rank constraint makes the problem non-convex, and relaxation is often used to transform the problem into an approximate convex form. To solve (5.11), we can modify algorithms in the existing literatures to our specific setting. For example, rather than shrink all $\boldsymbol{G}_{ij}$ that are larger than some threshold, we can only shrink those $\boldsymbol{G}_{ij}$ if at least one of i or j belongs to $\mathcal{S}$, and then reduce the rank of $\boldsymbol{G}$ and update $\boldsymbol{A}$ following the same procedure as in [50]. However as mentioned in [50], such an algorithm does not have any convergence guarantees, although it works well in practice. Another possible approach is to follow [109], by setting $\boldsymbol{B} = \boldsymbol{A^T A}$, and treating $\boldsymbol{B}$ as the variable in $\boldsymbol{G} = \boldsymbol{D^T A^T A D} = \boldsymbol{D^T B D}$. This transforms the problem into convex form with respect to $\boldsymbol{B}$, and can be solved by many software packages. Once $\boldsymbol{B}$ is obtained, the eigenvalue decomposition is performed to reduce the rank and achieve $\boldsymbol{A}$. But notice the $\boldsymbol{B}$ is of size $N \times N$, and we need to constrain the norm of $\boldsymbol{E}$ to be one. Such a large number of variables and constraint functions greatly increases the complexity of the approach making it less suitable for large dimensional problems [109].

In this section, we propose an algorithm for *sensing matrix design with partial knowledge of support* (SMPKS) which applies the *majorization-minimization* (MM) framework to iteratively solve the problem [110, 118, 119]. In MM framework, the original cost function which is hard to minimize is upper bounded by a surrogate function which is easier to minimize. Since the MM approach is central to the SMPKS algorithm, we provide a brief background on the concept of MM algorithm in general for ease of understanding. Consider a real-valued function $f(\theta)$. Let $\theta^{(m)}$ represents a fixed value of the parameter θ, and let $g(\theta|\theta^{(m)})$ denote a real-valued function of θ whose form depends on $\theta^{(m)}$. Then the function $g(\theta|\theta^{(m)})$ is said to majorize $f(\theta)$ at the point $\theta^{(m)}$ if

$$\begin{aligned} &1.\ \ g(\theta|\theta^{(m)}) \geq f(\theta),\ \ \forall\theta, \\ &2.\ \ g(\theta^{(m)}|\theta^{(m)}) = f(\theta^{(m)}). \end{aligned} \tag{5.12}$$

In each iteration, $g(\theta|\theta^{(m)})$ rather than $f(\theta)$ is minimized. Denotes $\theta^{(m+1)}$ as the minimizer of

$g(\theta|\theta^{(m)})$ such that

$$\theta^{(m+1)} = \arg\min_{\theta} g(\theta|\theta^{(m)}). \tag{5.13}$$

Then the decrease of the original function $f(\theta)$ in the next iteration can be shown as follows:

$$\begin{aligned} f(\theta^{(m+1)}) &\leq g(\theta^{(m+1)}|\theta^{(m)}) \\ &\leq g(\theta^{(m)}|\theta^{(m)}) \\ &= f(\theta^{(m)}) \end{aligned} \tag{5.14}$$

where the first inequality comes from the property 1 in (5.12), the second inequality is from (5.13), and the last equality is from the property 2 in (5.12). By iteratively minimizing the surrogate function, it is able to achieve a stationary point of the original function. As the iteration goes on, the value of $f(\theta)$ keeps decreasing until a stationary point is achieved. The key point of the MM algorithm is to find the surrogate function $g(\theta|\theta^{(m)})$ such that properties in (5.12) are satisfied, and the surrogate function should be amenable to easy minimization in each iteration.

To solve for a good sensing matrix $\boldsymbol{A}$, we hope to write the cost function in (5.11) in the form of $\boldsymbol{G}$ rather than $\boldsymbol{G}_{ij}$, so it will be easier to incorporate the variable $\boldsymbol{A}$ by $\boldsymbol{G} = \boldsymbol{D}^{\boldsymbol{T}}\boldsymbol{A}^{\boldsymbol{T}}\boldsymbol{A}\boldsymbol{D}$. Similar to [110], we define matrix $\boldsymbol{H}^d(\boldsymbol{G}), \boldsymbol{H}^s(\boldsymbol{G}), \boldsymbol{H}^{ns}(\boldsymbol{G})$ as follows:

$$\begin{aligned} \boldsymbol{H}^d_{ij}(\boldsymbol{G}) &= \begin{cases} c_1 & i = j \text{ and } i,j \in \mathcal{S} \\ c_2 & i = j \text{ and } i,j \notin \mathcal{S} \\ \boldsymbol{G}_{ij} & \text{otherwise} \end{cases} \\ \boldsymbol{H}^s_{ij}(\boldsymbol{G}) &= \begin{cases} 0 & i \neq j, i \in \mathcal{S} \text{ or } j \in \mathcal{S} \\ \boldsymbol{G}_{ij} & \text{otherwise} \end{cases} \\ \boldsymbol{H}^{ns}_{ij}(\boldsymbol{G}) &= \begin{cases} 0 & i \neq j, i \notin \mathcal{S} \text{ and } j \notin \mathcal{S} \\ \boldsymbol{G}_{ij} & \text{otherwise} \end{cases} \end{aligned} \tag{5.15}$$

and build coefficient matrix $\mathbf{\Omega}$ as

$$\mathbf{\Omega} = \text{diag}(\boldsymbol{\omega}) \tag{5.16}$$

where $\boldsymbol{\omega} \in \mathbb{R}^{M\times 1}, \omega_i = \frac{1}{\sqrt{c_1}}, \forall i \in \mathcal{S}$ and $\omega_i = \frac{1}{\sqrt{c_2}}, \forall i \notin \mathcal{S}$. c_1 and c_2 are parameters that control the norm of the columns of $\boldsymbol{E}$ and will be elaborated in the next section when the noisy case is considered. For the noise free situation in this section, we just set $c_1 = c_2 = 1$, so $\Omega = \mathbf{I}$. Then the cost function in (5.11) can be written as

$$\begin{aligned} & f(\boldsymbol{G}) \\ &= \gamma W_d + \alpha W_s + W_{ns} \\ &= \gamma \|\mathbf{\Omega}(\boldsymbol{G} - \boldsymbol{H}^d(\boldsymbol{G}))\mathbf{\Omega}\|_F^2 + \alpha \|\mathbf{\Omega}(\boldsymbol{G} - \boldsymbol{H}^s(\boldsymbol{G}))\mathbf{\Omega}\|_F^2 + \|\mathbf{\Omega}(\boldsymbol{G} - \boldsymbol{H}^{ns}(\boldsymbol{G}))\mathbf{\Omega}\|_F^2. \end{aligned} \tag{5.17}$$

Note that (5.17) is in its general form. The noise free situation in this section can be regarded as a special case where $c_1 = c_2 = 1$ and $\Omega = \mathbf{I}$. To avoid unnecessary duplication, the derivations and proofs in the rest of the chapter are all based on this general form, and can be readily reduced to the noise free case by setting $\Omega = \mathbf{I}$.

It is common to use a quadratic function as the surrogate function due to the ease in minimization [110, 118, 119]. We build the surrogate function as follows:

Proposition 1. *$g(\boldsymbol{G}|\boldsymbol{G}^{(m)})$ is a valid surrogate function of $f(\boldsymbol{G})$ at the m-th iteration, where*

$$\begin{aligned} g(\boldsymbol{G}|\boldsymbol{G}^{(m)}) = {} & \gamma \|\mathbf{\Omega}(\boldsymbol{G} - \boldsymbol{H}^d(\boldsymbol{G}^{(m)}))\mathbf{\Omega}\|_F^2 \\ & + \alpha \|\mathbf{\Omega}(\boldsymbol{G} - \boldsymbol{H}^s(\boldsymbol{G}^{(m)}))\mathbf{\Omega}\|_F^2 \\ & + \|\mathbf{\Omega}(\boldsymbol{G} - \boldsymbol{H}^{ns}(\boldsymbol{G}^{(m)}))\mathbf{\Omega}\|_F^2 \end{aligned} \tag{5.18}$$

and $\boldsymbol{G}^{(m)} = \boldsymbol{D}^T \boldsymbol{A}^{(m)^T} \boldsymbol{A}^{(m)} \boldsymbol{D}$.

Proof. See Appendix 5.7.1. ■

Minimizing $g(\boldsymbol{G}|\boldsymbol{G}^{(m)})$ with respect to $\boldsymbol{A}$ leads to the solution of sensing matrix $\boldsymbol{A}^{(m+1)}$

in the next iteration, such that

$$\begin{aligned} \boldsymbol{A}^{(m+1)} &= \arg\min_{\boldsymbol{A}} g(\boldsymbol{G}|\boldsymbol{G}^{(m)}) \\ &= \arg\min_{\boldsymbol{A}} g(\boldsymbol{D^T A^T A D}|\boldsymbol{G}^{(m)}). \end{aligned} \tag{5.19}$$

The next proposition shows that the solution $\boldsymbol{A}^{(m+1)}$ has a closed form:

Proposition2. *The minimizer of the surrogate function $g(\boldsymbol{G}|\boldsymbol{G}^{(m)})$ at the m-th iteration is*

$$\boldsymbol{A}^{(m+1)} = \boldsymbol{\Delta}_T^{\frac{1}{2}} \boldsymbol{V}_T^T \boldsymbol{\Lambda}^{-\frac{1}{2}} \boldsymbol{U}^T \tag{5.20}$$

where $\boldsymbol{U}\boldsymbol{\Lambda}\boldsymbol{U}^T$ is the eigenvalue decomposition of $\boldsymbol{D}\Omega^2\boldsymbol{D}^T$, and $\boldsymbol{V}\boldsymbol{\Delta}\boldsymbol{V}^T$ is the eigenvalue decomposition of $\boldsymbol{H}'(\boldsymbol{G}^{(m)})$. $\boldsymbol{H}'(\boldsymbol{G}^{(m)})$ is defined as

$$\boldsymbol{H}'(\boldsymbol{G}^{(m)}) := \boldsymbol{\Lambda}^{-\frac{1}{2}} \boldsymbol{U}^T \boldsymbol{D} \boldsymbol{\Omega}^2 \boldsymbol{H}(\boldsymbol{G}^{(m)}) \boldsymbol{\Omega}^2 \boldsymbol{D}^T \boldsymbol{U} \boldsymbol{\Lambda}^{-\frac{1}{2}} \tag{5.21}$$

and $\boldsymbol{H}(\boldsymbol{G}^{(m)})$ is defined as

$$\boldsymbol{H}(\boldsymbol{G}^{(m)}) := \frac{\gamma \boldsymbol{H}^d(\boldsymbol{G}^{(m)})^T + \alpha \boldsymbol{H}^s(\boldsymbol{G}^{(m)})^T + \boldsymbol{H}^{ns}(\boldsymbol{G}^{(m)})^T}{\gamma + \alpha + 1}. \tag{5.22}$$

$\boldsymbol{\Delta}_T$ denotes the $T \times T$ diagonal matrix that contains the largest T eigenvalues in $\boldsymbol{\Delta}$, and $\boldsymbol{V}_T$ denotes the corresponding T eigenvectors.

Proof. See Appendix 5.7.2. ■

We iteratively solve for $\boldsymbol{A}^{(m+1)}$ and calculate the next $g(\boldsymbol{G}|\boldsymbol{G}^{(m+1)})$ using (5.18) until some stopping criterion is satisfied, and label the last $\boldsymbol{A}^{(m+1)}$ as $\hat{\boldsymbol{A}}$. Notice that the solution $\boldsymbol{A}^{(m+1)}$ is not unique. Actually multiplying any orthogonal matrix to the left side of $\boldsymbol{A}^{(m+1)}$ also leads to a valid solution. To see this, denote $\bar{\boldsymbol{A}} = \boldsymbol{Q}\boldsymbol{A}^{(m+1)}$ where $\boldsymbol{Q}$ is an orthogonal matrix, i.e., $\boldsymbol{Q}^T\boldsymbol{Q} = \mathbf{I}$. Then $\bar{\boldsymbol{G}} = \boldsymbol{D}^T\bar{\boldsymbol{A}}^T\bar{\boldsymbol{A}}\boldsymbol{D} = \boldsymbol{D}^T(\boldsymbol{Q}\boldsymbol{A}^{(m+1)})^T(\boldsymbol{Q}\boldsymbol{A}^{(m+1)})\boldsymbol{D} = \boldsymbol{D}^T\boldsymbol{A}^{(m+1)^T}\boldsymbol{A}^{(m+1)}\boldsymbol{D} = \boldsymbol{G}^{(m+1)}$.

5.3.4 Discussion

The goal of the sensing matrix design problem in (5.11) is to minimize the cumulative coherence discriminatively. For the coherence corresponding to pairs of columns where at least one of them belongs to the preferred support, it puts more weight on them. An important question in this connection is why coherence and not other measures as the criteria for designing the sensing matrix? Also, given that the performance bound in the form of coherence (or some descendants of coherence) provided in [7, 117] are only sufficient conditions, is there a need to justify that optimizing a sufficient condition provides a good sensing matrix?

The motivation of the sensing matrix design in this chapter is to design $\boldsymbol{A}$ such that the combined dictionary $\boldsymbol{E} = \boldsymbol{A}\boldsymbol{D}$ has good structure. Specifically, we expect the columns in $\boldsymbol{E}$ to be as distinct with each other as possible. Intuitively, if two columns are too alike to each other, then it will be hard for any recovery algorithm to distinguish them. In order to measure how distinct the columns in $\boldsymbol{E}$ are, this work utilizes coherence and tries to minimize them in a cumulative sense. The reason we choose coherence is a pragmatic one. It is easy to compute. There are some other measures that characterize the structure of the matrix, for example the spark, the restricted isometry property, the null space property, etc. But these measures are computationally intractable. On the other hand, when we deal with coherence in a cumulative sense the summation of coherence can be transformed into the Gram matrix form, and it facilitates the derivation of a closed form solution in each iteration by using the MM framework, which converges under fairly general conditions. There are also other options to deal with coherence, for example mutual coherence (largest among all coherence) and the t-averaged mutual coherence as proposed in [50]. However, the iterative algorithm in [50] has no convergence guarantees. In summary, the ultimate goal of minimizing coherence is not to achieve any sufficient conditions, but to obtain a combined dictionary with better structure. We take a pragmatic approach by utilizing an easy to compute metric, and develop a design algorithm that is easy to implement.

5.4 Designing the Sensing Matrix in Noisy Situation

5.4.1 Motivation

In the previous section, the noise free case (5.1) was considered. In this section, we will consider the case where there exists measurement noise such that

$$\boldsymbol{y} = \boldsymbol{A}\boldsymbol{x} + \boldsymbol{n} = \boldsymbol{A}\boldsymbol{D}\boldsymbol{\beta} + \boldsymbol{n} = \boldsymbol{E}\boldsymbol{\beta} + \boldsymbol{n} \tag{5.23}$$

where $\boldsymbol{n} \in \mathbb{R}^{T \times 1}$ is the random measurement noise and assumed to be Gaussian distributed as $\boldsymbol{n} \sim \mathcal{N}(\mathbf{0}, \sigma^2\mathbf{I})$. Furthermore, we put the norm constraint $\|\boldsymbol{A}\|_F \leq P$, where P represents the total power in the sensing matrix. Assumptions of the existence of measurement noise and constraints on the power of sensing matrix are more suitable for real practical problems. For example, for channel estimation in a wireless communication system, $\boldsymbol{A}$ represents the pilot signals sent by the base station, $\boldsymbol{x}$ is the channel vector that we aim to measure. $\boldsymbol{y}$ is the received signal at the user. Obviously $\boldsymbol{y}$ which will be contaminated by some noise and the total power in the pilot signals is constrained by the power limit imposed by the base station.

Stable reconstruction conditions similar to the exact reconstruction conditions as in [7] and [117] have been provided for OMP [120] and BP [121]. From the derivation steps in [120,121], similar conclusions can be drawn regarding the importance of different $|\boldsymbol{G}_{ij}|$. So when designing $\boldsymbol{A}$ in the noisy situation, once again it pays to focuss efforts on minimizing $|\boldsymbol{G}_{ij}|$ when either i or j belongs to $\mathcal{S}$, or both i and j belong to $\mathcal{S}$. One big difference compared to the noise free case is that now not only the structure of the combined dictionary $\boldsymbol{E}$, but also the noise term $\boldsymbol{n}$ will affect the performance of the recovery algorithm. We take the OMP algorithm as an example, and for simplicity we assume there is only one component in $\boldsymbol{\beta}$ that is nonzero, and its location is k. Then $\boldsymbol{y} = \boldsymbol{E}\boldsymbol{\beta} + \boldsymbol{n} = \boldsymbol{E}_{\cdot k}\boldsymbol{\beta}_k + \boldsymbol{n} = \tilde{\boldsymbol{E}}_{\cdot k}\|\boldsymbol{E}_{\cdot k}\|_2\boldsymbol{\beta}_k + \boldsymbol{n}$, where $\tilde{\boldsymbol{E}}_{\cdot k}$ denotes the normalized k-th column of $\boldsymbol{E}$, $\tilde{\boldsymbol{E}}_{\cdot k} = \boldsymbol{E}_{\cdot k}/\|\boldsymbol{E}_{\cdot k}\|_2$. At the first step of OMP, $\boldsymbol{y}$ is correlated with each column of

$\tilde{\boldsymbol{E}}$ and we determine the location of nonzero elements as $\hat{l} = \arg\max_l |\boldsymbol{y}^T \tilde{\boldsymbol{E}}_{\cdot l}|$. Notice that

$$
\begin{aligned}
|\boldsymbol{y}^T \tilde{\boldsymbol{E}}_{\cdot l}| &= |\ (\tilde{\boldsymbol{E}}_{\cdot k} \|\boldsymbol{E}_{\cdot k}\|_2 \boldsymbol{\beta}_k + \boldsymbol{n})^T \tilde{\boldsymbol{E}}_{\cdot l}\ | \\
&= \begin{cases} |\ \boldsymbol{\beta}_k \|\boldsymbol{E}_{\cdot k}\|_2 + \boldsymbol{n}^T \tilde{\boldsymbol{E}}_{\cdot l}\ |, & l = k; \\ |\ \boldsymbol{\beta}_k \|\boldsymbol{E}_{\cdot k}\|_2 (\tilde{\boldsymbol{E}}_{\cdot k}^T \tilde{\boldsymbol{E}}_{\cdot l}) + \boldsymbol{n}^T \tilde{\boldsymbol{E}}_{\cdot l}\ |, & l \neq k. \end{cases}
\end{aligned}
\tag{5.24}
$$

Even if $\boldsymbol{E}$ has a good structure, i.e., $\tilde{\boldsymbol{E}}_{\cdot k}^T \tilde{\boldsymbol{E}}_{\cdot l}$ is small, the existence of the term $\boldsymbol{n}^T \tilde{\boldsymbol{E}}_{\cdot l}$ can still make $|\ \boldsymbol{\beta}_k \|\boldsymbol{E}_{\cdot k}\|_2 (\tilde{\boldsymbol{E}}_{\cdot k}^T \tilde{\boldsymbol{E}}_{\cdot l}) + \boldsymbol{n}^T \tilde{\boldsymbol{E}}_{\cdot l}\ |$ greater than $|\ \boldsymbol{\beta}_k \|\boldsymbol{E}_{\cdot k}\|_2 + \boldsymbol{n}^T \tilde{\boldsymbol{E}}_{\cdot l}\ |$, thus leading to the incorrect estimation of $\hat{l}$. So handling of noise requires additional considerations. However, if $\|\boldsymbol{E}_{\cdot k}\|_2$ is large, then at least $|\ \boldsymbol{\beta}_k \|\boldsymbol{E}_{\cdot k}\|_2 + \boldsymbol{n}^T \tilde{\boldsymbol{E}}_{\cdot l}\ |$ is more likely to be large, in other words, less affected by the noise. This sheds light on how to make the recovery more robust in noisy case: with regards to the locations of nonzero entries in $\boldsymbol{\beta}$, making the corresponding columns in $\boldsymbol{E}$ to have large norm will combat the interference from noise. In our situation, this translates to designing a sensing matrix $\boldsymbol{A}$ such that the columns of $\boldsymbol{E} = \boldsymbol{A}\boldsymbol{D}$ which correspond to the locations of nonzero entries in $\boldsymbol{\beta}$ to have large norms, i.e., making $\|\boldsymbol{E}_{\cdot i}\|_2$ large if $i \in \mathcal{TS}(\boldsymbol{\beta})$. The goal is to tune $\boldsymbol{A}$, such that effects of columns in $\boldsymbol{D}$ that consist the signal $\boldsymbol{x}$ are enlarged after the application of the sensing matrix $\boldsymbol{A}$.

5.4.2 Sensing Matrix Design

Similar to the noise free case, we do not have the knowledge of $\mathcal{TS}$ and assume a preferred support set $\mathcal{S}$. To incorporate the ideas of producing larger norms to columns in $\mathcal{S}$, using the same definitions of $\mathcal{P}_1, \ldots, \mathcal{P}_5$ as before,we define

$$
\begin{aligned}
W_d &= \sum_{\{i,j\} \in \mathcal{P}_1} \frac{|\boldsymbol{G}_{ii} - c_1|^2}{c_1^2} + \sum_{\{i,j\} \in \mathcal{P}_2} \frac{|\boldsymbol{G}_{ii} - c_2|^2}{c_2^2} \\
W_s &= \sum_{\{i,j\} \in \mathcal{P}_3} \frac{|\boldsymbol{G}_{ij}|^2}{c_1^2} + \sum_{\{i,j\} \in \mathcal{P}_4} \frac{|\boldsymbol{G}_{ij}|^2}{c_1 c_2} \\
W_{ns} &= \sum_{\{i,j\} \in \mathcal{P}_5} \frac{|\boldsymbol{G}_{ij}|^2}{c_2^2}
\end{aligned}
\tag{5.25}
$$

where we use W_d to optimize norm of columns contained in $\mathcal{S}$ and columns out of $\mathcal{S}$. c_1 and c_2 can be regarded as "expected" squared norm of $\|\boldsymbol{E}_{\cdot i}\|_2^2$ for $i \in \mathcal{S}$ and $i \notin \mathcal{S}$. So as discussed above, we set c_1 to be a large number and c_2 to be a small number in order to focus the measurement energy to the parts where we believe the true nonzero elements are. If $\mathcal{S}$ is believed to contain a higher percentage of true locations, then a larger value should be given to c_1 in order to focus more energy to those columns in the $\mathcal{S}$. As opposite to c_1, c_2 should be set to a smaller number if $\mathcal{S}$ contains higher percentage of true locations, since we do not want to waste measurement energy on locations where entries of $\boldsymbol{\beta}$ are zero. W_s and W_{ns} are similar to the corresponding terms in (5.11), which control coherence between pairs. Since now the columns are optimized to have different norms, we normalize W_d, W_s and W_{ns} using the expected squared norm c_1 and c_2.

The optimization problem then becomes

$$
\begin{aligned}
\hat{\boldsymbol{A}}' &= \arg\min_{\boldsymbol{A}} \gamma W_d + \alpha W_s + W_{ns} \\
\hat{\boldsymbol{A}} &= \frac{\hat{\boldsymbol{A}}'}{\|\hat{\boldsymbol{A}}'\|_F} P.
\end{aligned}
\tag{5.26}
$$

In (5.26) the cost function does not enforce the constraint $\|\boldsymbol{A}\|_F \leq P$, since explicit enforcement of the constraint $\|\boldsymbol{A}\|_F \leq P$ requires solving (5.26) in a constrained set and is hard to be incorporated into the MM framework. Moreover, the cost function in (5.26) which uses $\boldsymbol{G}_{ij}$ to describe the coherence is just an *approximate* way since the columns in $\boldsymbol{E}$ are not strictly normalized. Actually once $\hat{\boldsymbol{A}}'$ is solved, scaling it with any positive constant does not change $\tilde{\boldsymbol{G}}_{ij}$, the *coherence* of columns in $\boldsymbol{E}$, as well as the ratio of two columns's norms, i.e., $\|\boldsymbol{E}_{\cdot i}\|_2/\|\boldsymbol{E}_{\cdot j}\|_2$ is preserved. So we first solve for $\hat{\boldsymbol{A}}'$ in (5.26) without the constraint $\|\boldsymbol{A}\|_F \leq P$, considering only the *coherence minimization* and *energy distribution*, using the SMPKS algorithm (with $c_1 \neq c_2$) proposed in last section. Then we scale it to the largest energy limitation such that $\hat{\boldsymbol{A}} = \frac{\hat{\boldsymbol{A}}'}{\|\hat{\boldsymbol{A}}'\|_F} P$, with respect to the energy limitation and the existence of noise. Since scaling up $\|\boldsymbol{E}_{\cdot i}\|_2$ will make the recovery algorithm more robust to the noise if $i \in \mathcal{TS}$ while make no difference if $i \notin \mathcal{TS}$. So we scale up $\|\boldsymbol{A}\|_F$ to its largest possible value to improve the performance.

5.4.3 Summary of the Algorithm

The detailed steps of the SMPKS algorithm is summarized in Algorithm 1, which is for the noisy case. To differentiate the noise free case from the noisy case, we denote it as SMPKS-NF. For SMPKS-NF, we do not have the norm constraint of $\|\boldsymbol{A}\|_F \leq P$, and we set $c_1 = c_2 = 1$. In the algorithm, the start point $\boldsymbol{A}^{(m)}, m = 1$ is set to be a random matrix, where we do not assume knowledge of any other $\boldsymbol{A}$. Since the MM framework can not guarantee to converge to global optimum, a good start point will help to avoid the algorithm being trapped in a local minimum. For example, we can initialize our algorithm with an $\boldsymbol{A}$ learned from other sensing matrix design algorithms. In the algorithm we set the stopping criterion by limiting the number of iterations by some chosen maximum number. We can also choose other stopping criterion such as when $\boldsymbol{A}^{(m+1)}$ does not change much compared to $\boldsymbol{A}^{(m)}$, or the value of cost function $f(\boldsymbol{G}^{(m+1)})$ does not change much as the iteration proceed.

5.5 Numerical Results

In this section, we evaluate the performance of the proposed algorithm experimentally. The goal is to show that when there exists a reasonable preferred support $\mathcal{S}$, the proposed algorithm

Algorithm 1 SMPKS Algorithm

```
Input: Use the following parameters:
    • $\boldsymbol{D}$ - the sparsifying dictionary,
    • $c_1$ - expected norm for columns belonging to $\mathcal{S}$,
    • $c_2$ - expected norm for columns out of $\mathcal{S}$,
    • $\gamma$ - weights for $W_d$,
    • $\alpha$ - weights for $W_s$,
    • MaxIter - maximal number of iterations,
    • $P$ - power constraint of sensing matrix.
Initialize:
    • Set $m = 1$,
    • Set $\boldsymbol{A}^{(m)}$ to a random matrix,
    • Calculate $\boldsymbol{G}^{(m)} = \boldsymbol{D}^T(\boldsymbol{A}^{(m)})^T\boldsymbol{A}^{(m)}\boldsymbol{D}$,
    • Calculate $\boldsymbol{\Omega}$ using (5.16),
    • Calculate $\boldsymbol{U\Lambda U}^T$ as eigenvalue decomposition of $\boldsymbol{D}\boldsymbol{\Omega}^2\boldsymbol{D}^T$.
Loop: until $m >$ MaxIter
    • Calculate $\boldsymbol{H}'(\boldsymbol{G}^{(m)})$ using (5.21),
    • Calculate $\boldsymbol{V\Delta V}^T$ as eigenvalue decomposition of $\boldsymbol{H}'(\boldsymbol{G}^{(m)})$,
    • Update $\boldsymbol{A}^{(m+1)} = \boldsymbol{\Delta}_T^{\frac{1}{2}}\boldsymbol{V}_T^T\boldsymbol{\Lambda}^{-\frac{1}{2}}\boldsymbol{U}^T$,
    • Update $\boldsymbol{G}^{(m+1)} = \boldsymbol{D}^T(\boldsymbol{A}^{(m+1)})^T\boldsymbol{A}^{(m+1)}\boldsymbol{D}$,
    • Update $m = m + 1$.
Output: $\boldsymbol{A} = \frac{\boldsymbol{A}^{(m)}}{\|\boldsymbol{A}^{(m)}\|_F}P$
```

that utilizes this information will lead to a more informative sensing matrix $\boldsymbol{A}$, which can improve the recovery performance. The basic setting of the experiment is as follows. $\boldsymbol{D} \in \mathbb{R}^{N\times M}$ is the dictionary consisting of i.i.d standard Gaussian variables. The signal of interest $\boldsymbol{x}$ is computed as $\boldsymbol{x} = \boldsymbol{D}\boldsymbol{\beta}$, where $\boldsymbol{\beta}_k, k \in \mathcal{TS}(\boldsymbol{\beta})$ are also i.i.d standard Gaussian variables with locations uniformly distributed. For $|\mathcal{TS}(\boldsymbol{\beta})|, |\mathcal{S}|, p_e, p_m$, given any three we can obtain the fourth, as well as $|\Delta|, |\Delta_m|, |\Delta_e|$ (recall that $|\mathcal{TS}(\boldsymbol{\beta})| = |\Delta| + |\Delta_m|, |\mathcal{S}| = |\Delta| + |\Delta_e|, p_e = |\Delta_e|/|\mathcal{S}|, p_m = |\Delta_m|/|\mathcal{TS}|$). Then the preferred support $\mathcal{S}$ is generated as $\mathcal{S} = \Delta \cup \Delta_e$, where $|\Delta|$ elements are randomly picked from $\mathcal{TS}$, and $|\Delta_e|$ elements are randomly picked form $[M]\backslash\mathcal{TS}$. Regarding sensing matrix $\boldsymbol{A}$, we compare: random sensing matrix, where the elements are i.i.d Gaussian with mean 0 and variance $1/\sqrt{T}$ (**random**), Elad's algorithm in [50] (**Elad**), Duarte-Carvajalino and Sapiro's algorithm [108] (**DS**) the proposed algorithm for noise free case (5.11) (**SMPKS-NF**) and noisy case (5.26) (**SMPKS**).

We run $L = 1000$ trials to compute an average measure of performance. In terms of performance metric, we use success rate and location distance [7, 50]:

- **Success rate**: after obtaining $\hat{\boldsymbol{x}}$, we calculate the relative ℓ_2 distance Dist_ℓ_2 as

$$\text{Dist\_}\ell_2(\boldsymbol{x}, \hat{\boldsymbol{x}}) = \frac{\|\boldsymbol{x} - \hat{\boldsymbol{x}}\|_2^2}{\|\boldsymbol{x}\|_2^2}. \tag{5.27}$$

  When Dist_ℓ_2 is smaller than some threshold, it is considered as a successful recovery. We calculate the percentage of successful recovery out of L experiments as the success rate. Notice that Dist_ℓ_2 is calculated using $\boldsymbol{x}$ rather than $\boldsymbol{\beta}$. Because $\boldsymbol{D}$ is an overcompleted dictionary, Dist_ℓ_2 calculated using $\boldsymbol{x}$ is different from using $\boldsymbol{\beta}$.

- **Location distance**: for some application, it is important that the locations of the nonzero entries in $\boldsymbol{\beta}$ are correctly detected. For example in a classification task, columns of dictionary $\boldsymbol{D}$ represent features. Given the measurement $\boldsymbol{y}$, classification of signal $\boldsymbol{x}$ is achieved by detecting which features contribute to $\boldsymbol{x}$, i.e., the location of nonzero entries in

$\boldsymbol{\beta}$. The location distance Dist_sup is defined as

$$\begin{aligned}&\text{Dist\_sup}(\mathcal{TS}(\boldsymbol{\beta}), \mathcal{TS}(\hat{\boldsymbol{\beta}})) = \\ &\frac{\max\{|\mathcal{TS}(\boldsymbol{\beta})|, |\mathcal{TS}(\hat{\boldsymbol{\beta}})|\} - |\mathcal{TS}(\boldsymbol{\beta}) \cap \mathcal{TS}(\hat{\boldsymbol{\beta}})|}{\max\{|\mathcal{TS}(\boldsymbol{\beta})|, |\mathcal{TS}(\hat{\boldsymbol{\beta}})|\}}.\end{aligned} \tag{5.28}$$

5.5.1 Comparing the Distribution of Coherence

In Fig. 5.1, we present the distribution of the coherence, i.e., $|\tilde{\boldsymbol{G}}_{ij}|, i \neq j$, obtained from combining the sensing matrix $\boldsymbol{A}$ designed using different sensing matrix design algorithms and the same dictionary $\boldsymbol{D}$. The distribution is calculated by the percentage of all $|\tilde{\boldsymbol{G}}_{ij}|, i \neq j$ which falls between the range $[0.05(l-1), 0.05l]$, where $l = 1, \dots, 20$. In Fig. 5.1 (a), the coherence is calculated using all pairs of columns in the equivalent dictionary $\boldsymbol{E} = \boldsymbol{AD}$. It shows that both the DS algorithm and the SMPKS-NF algorithm can reduce the percentage of large coherence and increase the percentage of small coherence compared to the random sensing matrix. Elad's algorithm also reduces the large coherence, but makes no more effort when the coherence becomes small enough. This is reason why there exists a peak at 0.175, where 40% of coherence values fall between 0.15 and 0.2. Fig. 5.1 (b) shows the distribution of coherence corresponding to columns where at least one of them belongs to $\mathcal{S}$, i.e., $|\tilde{\boldsymbol{G}}_{ij}|, i \in \mathcal{S}$ or $j \in \mathcal{S}$. It shows that except for the SMPKS-NF, the distributions of the coherences corresponding to the other three sensing matrices are very similar compared to Fig. 5.1 (a), implying that those sensing matrix design algorithms have to favor of column pairs which includes at least one column in the $\mathcal{S}$. For SMPKS-NF, the distribution of the coherence is more concentrated around small values compared to Fig. 5.1 (a), showing that more efforts have been put by the SMPKS-NF algorithm to reduce the coherences of those column pairs that contain columns from $\mathcal{S}$. In other words, although the coherence distributions for *all* columns are similar for DS and SMPKS-NF, when it comes to the coherence values of *interest* columns, SMPKS-NF is able to drive them smaller, which is exactly the goal of minimizing (5.11). In the following subsections, we will show how

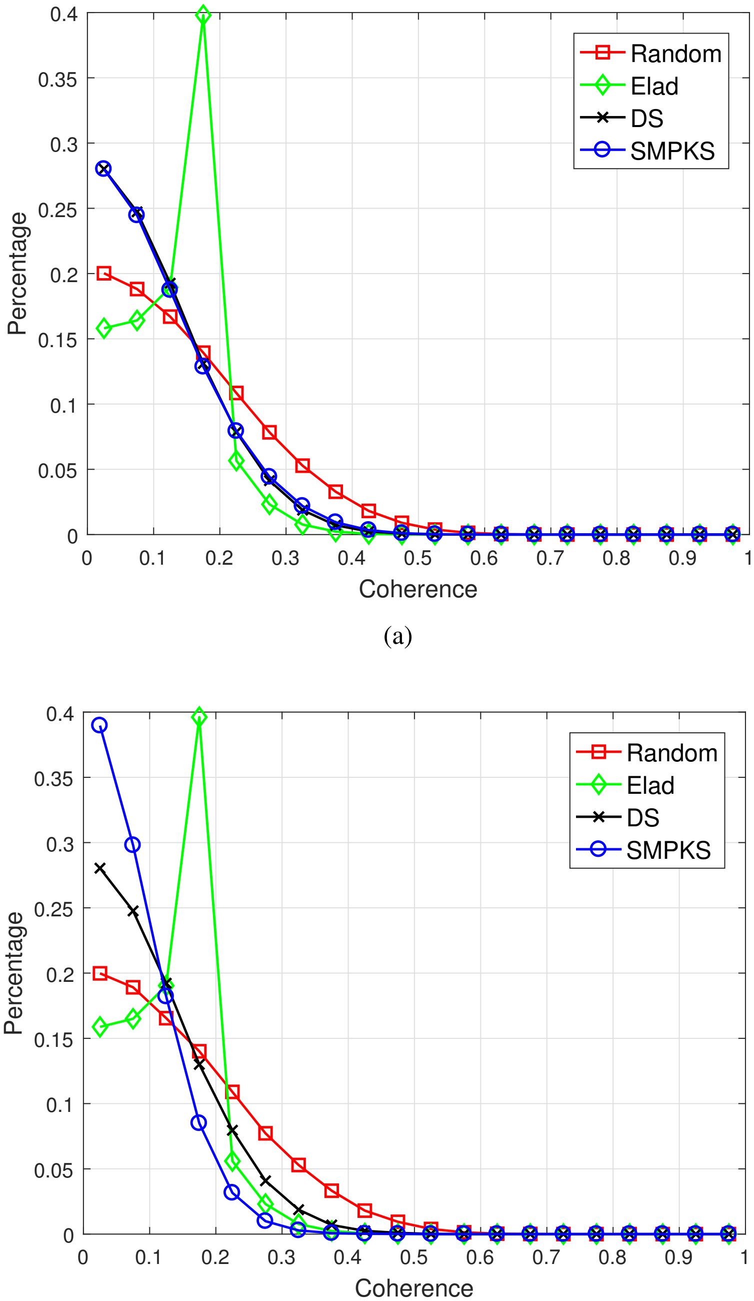

(a)

(b)

Figure 5.1: Distribution of the coherence between two columns in the equivalent dictionary. (a) All pairs of columns in the equivalent dictionary. (b) Pairs of columns that at least one column belongs to $\mathcal{S}$. $T = 40$, $N = 80$, $M = 160$, $|\mathcal{TS}| = |\mathcal{S}| = 12$.

such effect can improve the performance of compressive sensing algorithms.

5.5.2 Comparing Different Error Rate and Missing Rate

In this subsection, the OMP algorithm is applied to perform the sparse recovery, and the recovery performances using different sensing matrices are compared for different values of p_e and p_m in the noise free scenario. Setting $T = 40, N = 80, M = 160$, and $|\mathcal{TS}| = |\mathcal{S}| = 12$ (so $p_e = p_m$), we gradually increase $p_e(p_m)$ from 0 to 1 with step 0.1. Correspondingly, $\mathcal{TS}$ and $\mathcal{S}$ change from fully overlapped, to partially overlapped, until they are non-overlapping. Fig. 5.2 shows that the recovery performance of SMPKS-NF degrades as the $p_e(p_m)$ increases, indicating that large error rate and missing rate will make the recovery performance worse due to the incorrect prior knowledge of the support. The performances of other sensing matrices do not change with p_e and p_m, since the knowledge of preferred support is not used in those algorithms. When p_e (p_m) is less than 0.7 in this setting, the SMPKS-NF can achieve better performance than Elad and DS algorithm, and for all p_e (p_m) SMPKS-NF is much better than the random sensing matrices. Notice that $p_e = p_m = 0.7$ corresponds to $|\Delta| = 4, |\Delta_e| = |\Delta_m| = 8$, which means for a preferred set $\mathcal{S}$ containing 12 indices, only 4 of them are from the true support, and it contains 8 error indies and misses 8 true indices. The result shows that when the preferred support set is moderately accurate, the proposed sensing matrix leads to an improved recovery performance compared to other sensing matrices.

Next we examine the situation when the size of $\mathcal{S}$ is small and it is contained in $\mathcal{TS}$, or the size of $\mathcal{S}$ is large and it contains $\mathcal{TS}$. Notice that in practice we do not know whether $\mathcal{S}$ is large or small compared to the true support, or what p_e and p_m are. First we test $\mathcal{S} \subseteq \mathcal{TS}$ such that $p_e = 0$. $|\mathcal{TS}|$ is fixed to 12 in order to keep the difficulty of the recovery problem the same, and p_m changes from 0 to 0.9 with step 0.1, corresponding to $|\mathcal{S}|$ changing from 12 to 1. Fig. 5.3 shows that when $p_e = 0$ the SMPKS-NF can achieve better recovery performance for all p_m. Notice that the best performance is achieved at $p_m = 0.1$ rather than $p_m = 0$. When $p_m = 0.1$, $|\mathcal{S}| = \Delta = 11$ while $|\mathcal{S}| = \Delta = 12$ when $p_m = 0$. This shows that when $\mathcal{S} \subseteq \mathcal{TS}$, a relatively small preferred set may result in better performance, since it is easier for the SMPKS-NF algorithm to perform

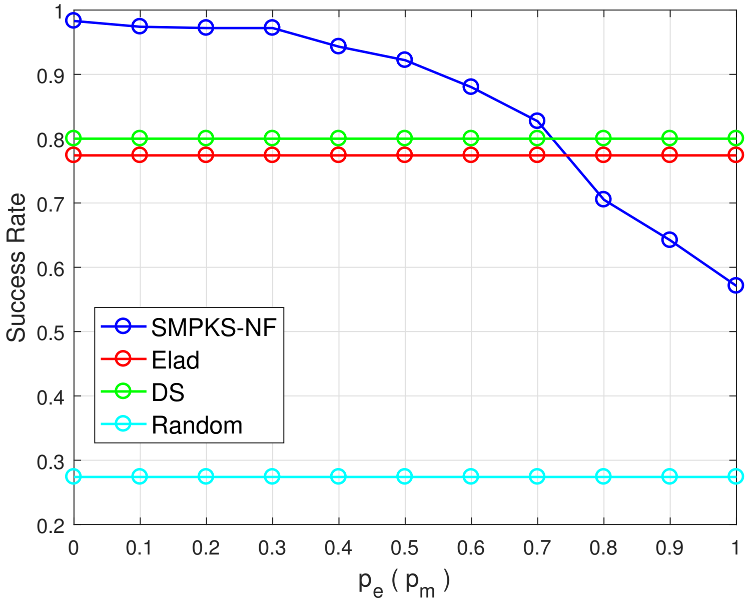

(a)

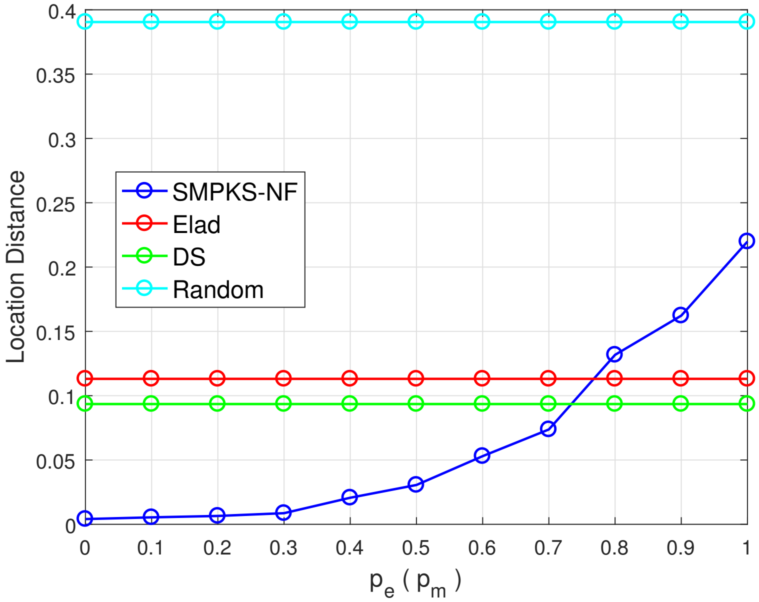

(b)

Figure 5.2: Performance comparison with different $p_e(p_m)$. $T = 40, N = 80, M = 160, |\mathcal{TS}| = |\mathcal{S}| = 12$.

the optimization process when $|\mathcal{S}|$ is small. However, $|\mathcal{S}|$ should not be too small compared to $\mathcal{TS}$, in which case there will be too many missing indices from $\mathcal{TS}$. The results show the benefits

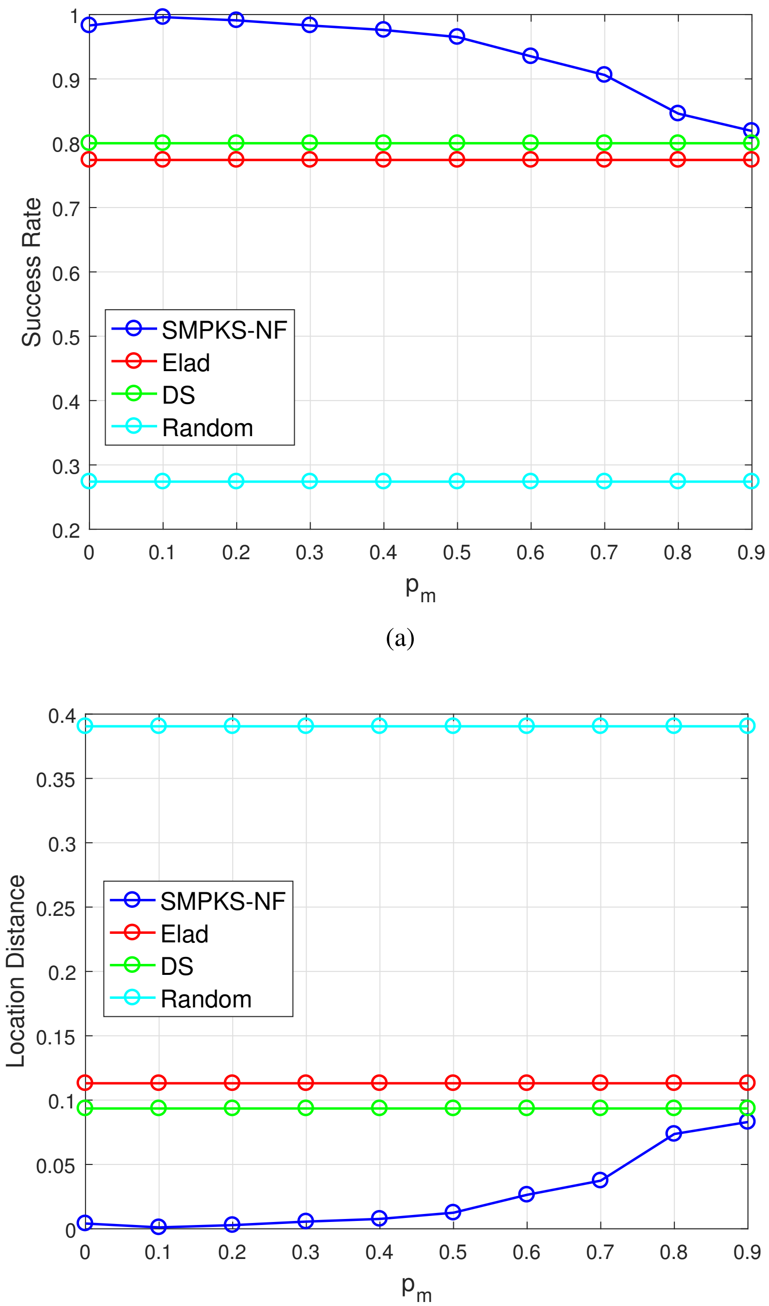

(a)

(b)

Figure 5.3: Performance comparison with different p_m. $T = 40, N = 80, M = 160, |\mathcal{TS}| = 12, p_e = 0$.

of utilizing the SMPKS-NF algorithm to explore the knowledge of the preferred support if we have high confidence on it, even a preferred support of small size would help to improve the

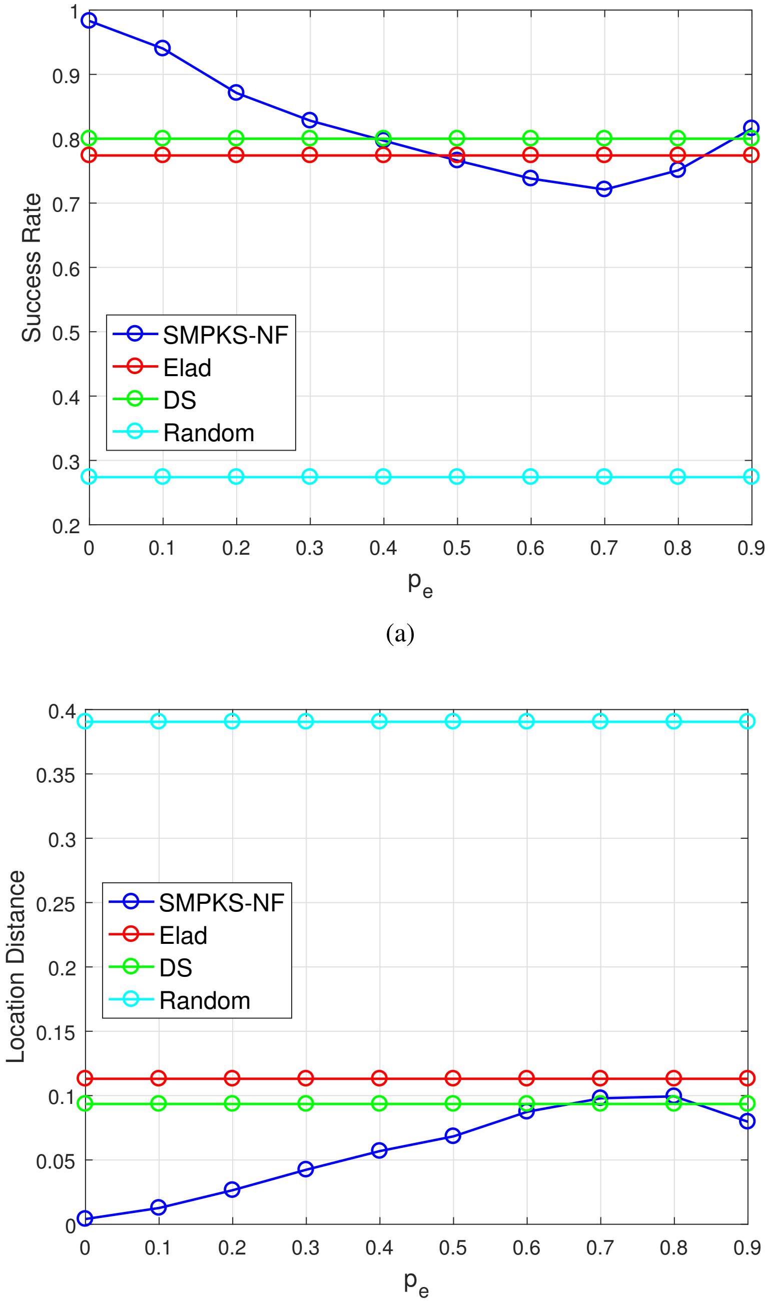

(a)

(b)

Figure 5.4: Performance comparison with different p_e. $T = 40, N = 80, M = 160, |\mathcal{TS}| = 12, p_m = 0$.

performance.

Lastly we consider the situation when $\mathcal{TS} \subseteq \mathcal{S}$, which means we have a preferred support with size larger than the true support. Again $|\mathcal{TS}|$ is set to 12 as in the previous simulations, and p_e changes from 0 to 0.9 with step 0.1. This results in a preferred support $\mathcal{S}$ with larger size, corresponding to $|\mathcal{S}| \in \{12, 13, 15, 17, 20, 24, 30, 40, 60, 120\}$. Fig. 5.4 shows that when p_e is smaller than 0.3, the SMPKS-NF has better performance than the other sensing matrices. Notice that when $p_e = 0.3$, $|\mathcal{S}| = 17$. Higher p_e results in larger $|\mathcal{S}|$ which contains many more error indices and degrades the recovery performance.

5.5.3 Comparing Different Levels of Noise

We now consider the noisy case where the sensing process is performed as in (5.23), $\boldsymbol{y} = \boldsymbol{A}\boldsymbol{x} + \boldsymbol{n}$ where $\boldsymbol{n} \sim \mathcal{N}(0, \sigma^2\mathbf{I})$. The signal to noise ratio (SNR) is defined as SNR $=$ $10\log_{10}(\frac{\|\boldsymbol{x}\|_2^2}{T\sigma^2})$. Again we use OMP for sparse recovery and compare different sensing matrix design algorithms. For the proposed SMPKS algorithm, we solve (5.26) with different norms for columns in and out of the preferred support, so $c_1 \neq c_2$. Notice that we only need to set the ratio c_1/c_2 rather than the specific values of c_1 and c_2, since after determining sensing matrix $\boldsymbol{A}$ using (5.26), it is normalized which changes the specific values of $\|\boldsymbol{E}_{\cdot i}\|_2^2, i \in \mathcal{S}$ and $\|\boldsymbol{E}_{\cdot j}\|_2^2, j \notin \mathcal{S}$, but not the ratio of $\|\boldsymbol{E}_{\cdot i}\|_2^2/\|\boldsymbol{E}_{\cdot j}\|_2^2$. The ratio c_1/c_2 determines how much preference to give to the columns in the preferred support. In the simulation, we set $c_1/c_2 = 2$, which means within the power constraint $\|\boldsymbol{A}\|_F \leq P$, the algorithm tries to achieve $\|E_{\cdot i}\|_2^2 = 2\|E_{\cdot j}\|_2^2, i \in \mathcal{S}, j \notin \mathcal{S}$. The SMPKS-NF algorithm which solves (5.11) in the noise free case is also included. The goal is to compare how unequally distributed energy will affect the recovery performance. All sensing matrices are normalized as $\|\boldsymbol{A}\|_F = P$, and the constrained power is set as $P = T$. Due to the existence of the noise, the previous threshold of 10^{-3} for determining the success rate in the noise free case is too strict for low SNR scenarios, so we set different thresholds for success rate with respect to different levels of noise. For many algorithms, the performance results show that the recovery error is at worst proportional to the noise level $\|\boldsymbol{n}\|_2$ [6, 11, 120], which motivates us to set thresholds according to the noise level. Specifically, we use $C \cdot \mathbb{E}(\|\boldsymbol{n}\|_2^2) = C \cdot T\sigma^2$ as the

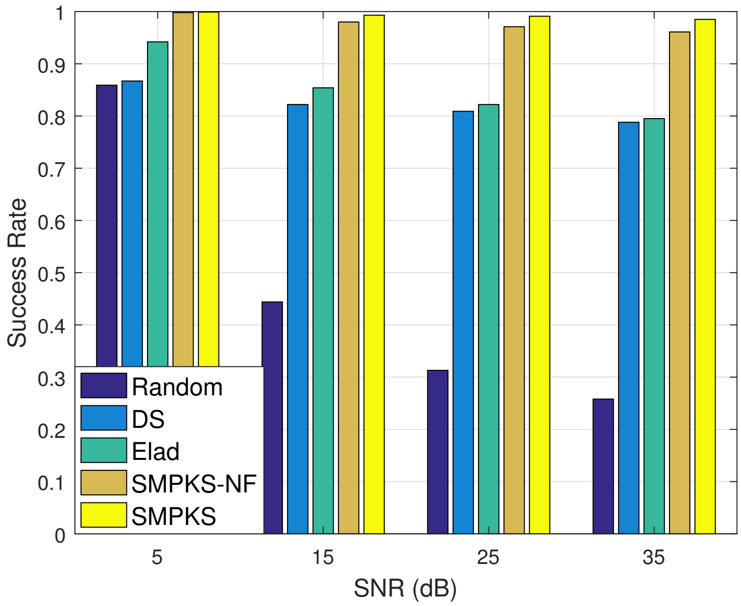

(a)

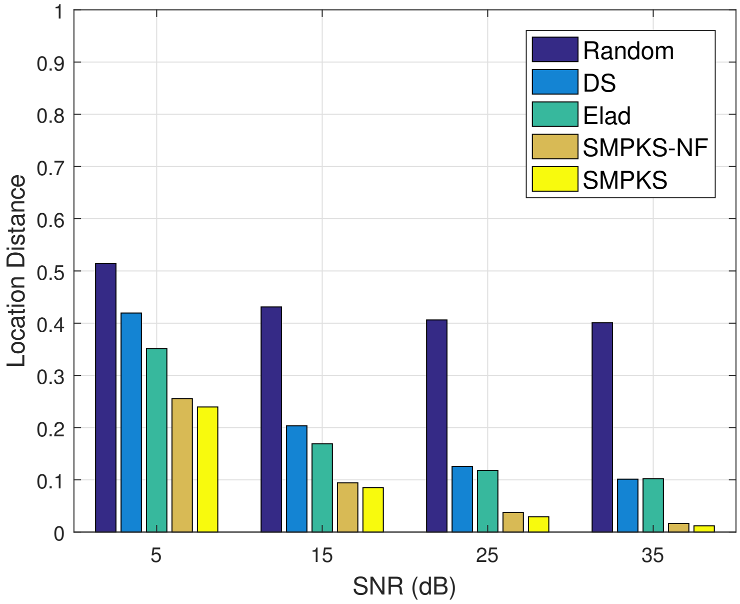

(b)

Figure 5.5: Performance comparison with different SNR. $T = 40, N = 80, M = 160, p_e = p_m = 0.2, |\mathcal{TS}| = |\mathcal{S}| = 12$.

threshold where $C = 2$ in the simulation.

In Fig. 5.5, we set $T = 40, N = 80, M = 160, p_e = 0.2$ and $|\mathcal{TS}| = |\mathcal{S}| = 12$. It shows the success rates for both SMPKS and SMPKS-NF are much higher than other algorithms, while the location distances are much lower. Also the SMPKS algorithm achieves better performance than SMPKS-NF, demonstrating the benefit of uneven energy distribution in the noisy situation. Notice that to compute success rate we set different thresholds for different SNRs, so it is not proper to compare performance across different SNR scenarios using theses plots. For example, in Fig. 5.5 (a) the success rate of all sensing matrices at SNR=5 dB is higher than other noise level. It does not mean that we can achieve better recovery performance at low SNR, and is just a result of larger threshold for higher noise. In Fig. 5.6, we increase the size of both the true support set and the preferred set to $|\mathcal{TS}| = |\mathcal{S}| = 16$ and perform the same experiment with different SNR level. Again both SMPKS and SMPKS-NF can achieve much better performance. Moreover the performance gap between the SMPKS-NF and SMPKS becomes larger compared to $|\mathcal{TS}| = |\mathcal{S}| = 12$ in Fig. 5.5, showing the ability of SMPKS to handle the more difficult recovery task in the noisy situation.

5.5.4 Comparing Different Recovery Algorithms

For both SMPKS and SMPKS-NF, the goal is to design sensing matrix that has better structure, i.e., the columns of the combined dictionary $\boldsymbol{E}$ are distinct from each other. Such design is expected to lead to an improved performance for different recovery algorithms. In previous simulations, we only evaluated the OMP algorithm and the results are consistent with our expectation. In this subsection, we compare the performance when different recovery algorithms are applied, such as compressive sampling matching pursuit (CoSaMP) [11], basis pursuit (BP) [12], re-weighted ℓ_2 (Rel2) algorithm [15] and sparse Bayesian learning algorithm [20, 43].

In Fig. 5.7, we test the noise-free situation. We set $|\mathcal{TS}| = |\mathcal{S}| = 12, p_e = 0.2$, and compare the performance of different sensing matrices when different recovery algorithms are utilized. It shows that for BP and Rel2, the SMPKS-NF can achieve the best success rate and locations distance. Especially for BP, there is a big advantage of SMPKS-NF over the other

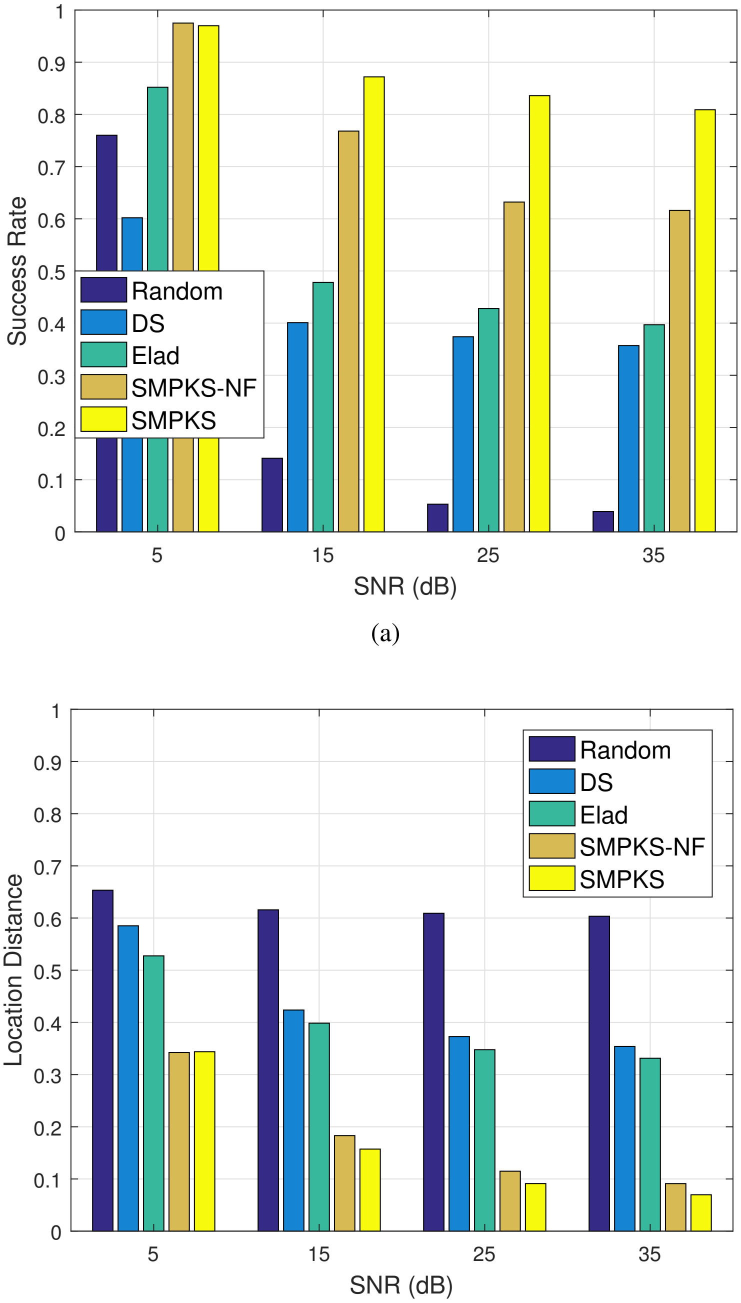

(a)

(b)

Figure 5.6: Performance comparison with different SNR. $T = 40, N = 80, M = 160, p_e = p_m = 0.2, |\mathcal{TS}| = |\mathcal{S}| = 16$.

algorithms. We also observe that for SBL, the SMPKS-NF does not show benefit compared to the other sensing matrices. And for CoSaMP, although the SMPKS-NF is better than DS and Elad,

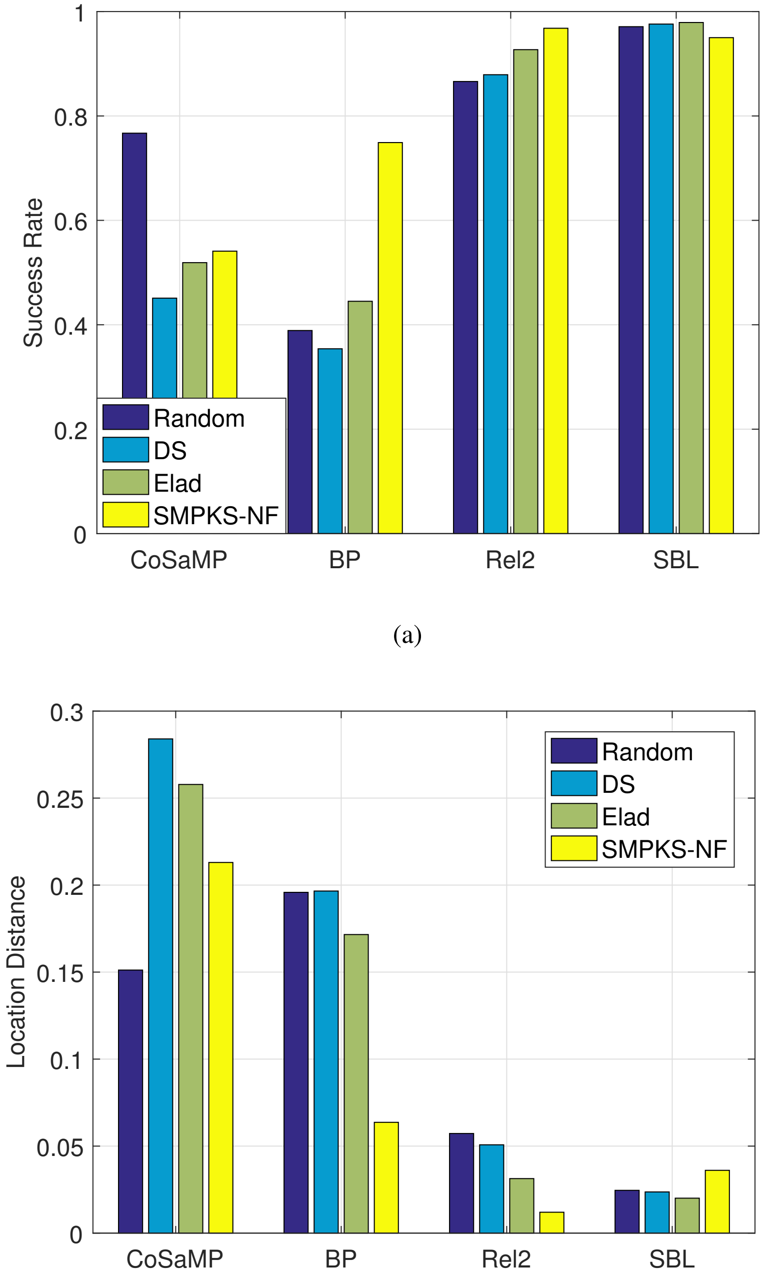

(a)

(b)

Figure 5.7: Performance comparison with different algorithms. $T = 40, N = 80, M = 160, |\mathcal{TS}| = |\mathcal{S}| = 12, p_e = p_m = 0.2$.

the random sensing matrix achieves the best performance. Fig. 5.7 implies that different recovery algorithms may take advantage of different properties of the sensing matrix, and the structure of the combined dictionary may not play a role in improving the performance for some algorithm. For example, all designed sensing matrices are worse than the random matrix for the CoSaMP algorithm.

Fig. 5.8 shows the performance in the noisy situation where we utilize SMPKS to obtain sensing matrix with unequally distributed energy. For all recovery algorithms, SMPKS can achieve the best performance with regards to both success rate and location distance, which demonstrates the benefit of unequally distributed energy in the noisy situation. Similar to the noiseless case, the benefit of SMPKS is much more obvious when BP and Rel2 are applied rather than SBL and CoSaMP. And for CoSaMP, although the random matrix is a little worse than SMPKS, it still achieves better performance than DS and Elad. In summary, both SMPKS-NF and SMPKS can achieve better performance when OMP, BP and Rel2 are applied for sparse recovery. There exist some algorithms for which SMPKS-NF does not obtain improved performance. Analysis of the specific properties of these algorithms is beyond the scope of this work, and we leave this for the future work.

5.5.5 Discussion

The simulations in the previous subsections show that by utilizing the preferred support set, we can achieve improved recovery performance by designing the sensing matrix. Such improvement can be obtained without increasing the number of measurements, i.e., the number of rows in $\boldsymbol{A}$, which is important for applications where performing additional measurements is expensive or infeasible. For example, in the channel estimation task of wireless communication, the number of measurements corresponds to the training duration. Given the limited channel coherence time in which one performs both channel estimation and data transmission, it is desirable to keep the training duration as small as possible, so that one can have more time for real data transmission. Then by designing pilots symbols $\boldsymbol{A}$, we can achieve improved performance without increasing the training duration. Practically, we do not know beforehand the missing rate

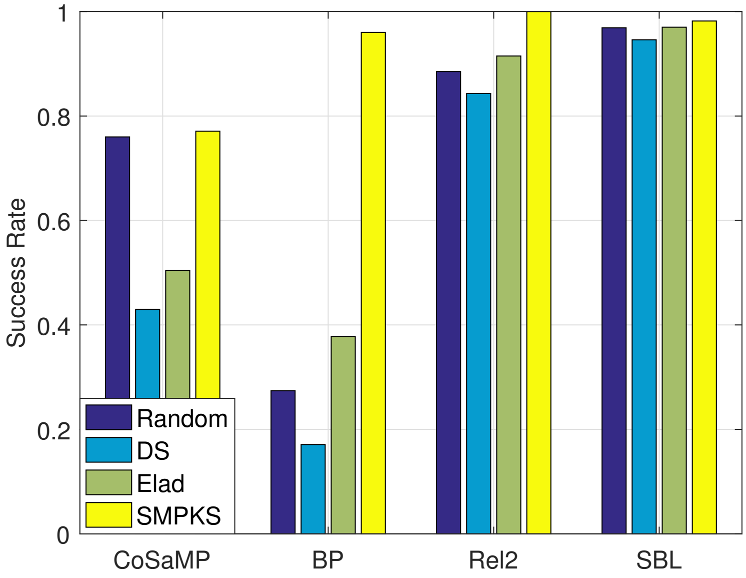

(a)

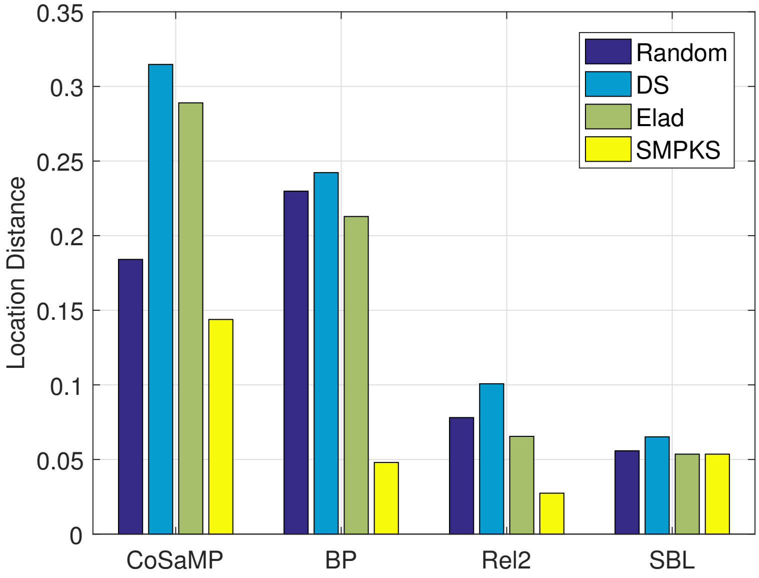

(b)

Figure 5.8: Performance comparison with different algorithms. $T = 40, N = 80, M = 160, |\mathcal{TS}| = |\mathcal{S}| = 12, p_e = p_m = 0.2, \text{SNR} = 25\text{dB}$.

p_m and error rate p_e, and so it is hard to tell whether it is beneficial to utilize the proposed sensing matrix or other sensing matrices. In the first experiment, it shows that when $p_e = p_m \leq 0.7$, the

SMPKS-NF can achieve better performance. For many applications, it is reasonable to assume a small p_e and p_m, for example in a time sequence problem mentioned in [115]. For the channel estimation task in wireless communication, if the channel changes relatively slowly, and the channel estimation is mostly correct in the current coherence block, then it is reasonable to assume p_e and p_m are small when utilizing the current support estimation as the preferred support for the channel estimation task in the next coherence block.

Also in the previous simulations, the sparse recovery algorithms are applied without utilizing the knowledge of the preferred support set. The focus of this work is at the sensing stage, aiming to design a better sensing matrix which can improve the recovery performance for various types of sparse recovery algorithms without any changes in exiting codes. Integrating the prior knowledge into the recovery algorithm would further improve the performance. This would require using recovery algorithm that can leverage prior knowledge effectively at the recovery stage, for example modified BP [115] and weighted ℓ_1 [114] algorithms. A more optimal approach is to design sensing matrix for a designated recovery algorithm, for example BP, by taking into account the specific properties of the recovery algorithm and utilizing the preferred support information both at the sensing and recovery stage. However, this topic would be more complex and beyond the scope of this chapter, and we will leave it for the future work.

5.6 Conclusion

In this chapter, we present a framework for designing sensing matrix with partial knowledge of support which is captured in the form of a preferred set. For a number of application scenarios, it is reasonable to have some partial knowledge of the sparse support. The framework in this chapter provides a way to utilize the preferred set to achieve improved performance. Motivated by the theoretical proofs of guaranteed recovery using OMP and BP, as well as the difficulty of decreasing the coherence of all pairs of columns to be arbitrarily small in an overcomplete dictionary, we propose a sensing matrix design process that concentrates on decreasing the coherence between pairs of columns where at least one of the columns belongs to the preferred support set. We further extend the algorithm to the noisy case, which focuses more sensing energy to the preferred support set. An algorithm based on majorization-minimization framework is utilized to solve the problem, which can converge under fairly general conditions.

The simulation results show the superiority of the proposed SMPKS algorithm in a wide range of scenarios. We test the performance with various error rate and missing rate, as well as different size of true support and preferred support. We also evaluate the performance in the noisy case, which again shows the advantages of the proposed algorithm. For different recovery algorithms, the proposed sensing matrix achieves the best performance for OMP, BP and Rel2, for both noise free and noisy case. This indicates that the proposed sensing matrix design algorithm leads to more informative measurements, which in turn results in an improvement in sparse recovery.

Although in this chapter we use an MM framework to solve for the sensing matrix, other algorithms can also be adjusted to solve the problem, such as the convex optimization framework in [109] and shrinkage procedure in [50]. It would be interesting to compare these different methods to see which one could lead to the best solution of (5.11) and (5.26). Also our focus in this work is only at the sensing stage, i.e., designing a good sensing matrix with the preferred support, rather than developing recovery algorithm that can benefit from the preferred support [114, 115]. Bridging the sensing stage and recovery stage, such that developing algorithm that utilizes the preferred support jointly for both sensing and recovery, would be another interesting topic for future work.

Chapter 5, in part is currently being prepared for submission for publication of the material. The dissertation author was the primary investigator and author of this material, and Bhaskar D. Rao supervised the research.

5.7 Appendices

5.7.1 Proof of Proposition 1

In proposition 1, we developed the surrogate function $g(\boldsymbol{G}|\boldsymbol{G}^{(m)})$ at the m-th iteration as following

$$\begin{aligned} g(\boldsymbol{G}|\boldsymbol{G}^{(m)}) &= \gamma\|\boldsymbol{\Omega}(\boldsymbol{G}-\boldsymbol{H}^{d}(\boldsymbol{G}^{(m)}))\boldsymbol{\Omega}\|_F^2 \\ &+ \alpha\|\boldsymbol{\Omega}(\boldsymbol{G}-\boldsymbol{H}^{s}(\boldsymbol{G}^{(m)}))\boldsymbol{\Omega}\|_F^2 \\ &+ \|\boldsymbol{\Omega}(\boldsymbol{G}-\boldsymbol{H}^{ns}(\boldsymbol{G}^{(m)}))\boldsymbol{\Omega}\|_F^2 \end{aligned}$$

Now we prove that it satisfies the two properties required in (5.12) to be a valid surrogate function.

Proof. We first prove that $g(\boldsymbol{G}|\boldsymbol{G}^{(m)})$ satisfies the first property in (5.12). Define sets that describe different conditions of $\{i,j\}$ as the same as in Section 5.3: $\mathcal{P}_1 = \{\{i,j\}|i=j, i,j \in \mathcal{S}\}$,$\mathcal{P}_2 = \{\{i,j\}|i=j, i,j \notin \mathcal{S}\}$, $\mathcal{P}_3 = \{\{i,j\}|i \in \mathcal{S} \text{ and } j \in \mathcal{S}, i \neq j\}$, $\mathcal{P}_4 = \{\{i,j\}|\text{only } i \text{ or } j \in \mathcal{S}, i \neq j\}$ $\mathcal{P}_5 = \{\{i,j\}|i \notin \mathcal{S} \text{ and } j \notin \mathcal{S}, i \neq j\}$. We now treat each term in the summation of (5.18) separately.

The first term is

$$\begin{aligned} &\|\boldsymbol{\Omega}(\boldsymbol{G}-\boldsymbol{H}^{d}(\boldsymbol{G}^{(m)}))\boldsymbol{\Omega}\|_F^2 \\ &= \sum_{\{i,j\}\in\mathcal{P}_1} \frac{|\boldsymbol{G}_{ij}-c_1|^2}{c_1^2} + \sum_{\{i,j\}\in\mathcal{P}_2} \frac{|\boldsymbol{G}_{ij}-c_2|^2}{c_2^2} + \sum_{\{i,j\}\in\mathcal{P}_3} \frac{|\boldsymbol{G}_{ij}-\boldsymbol{G}_{ij}^{(m)}|^2}{c_1^2} \\ &\quad + \sum_{\{i,j\}\in\mathcal{P}_4} \frac{|\boldsymbol{G}_{ij}-\boldsymbol{G}_{ij}^{(m)}|^2}{c_1c_2} + \sum_{\{i,j\}\in\mathcal{P}_5} \frac{|\boldsymbol{G}_{ij}-\boldsymbol{G}_{ij}^{(m)}|^2}{c_2^2} \\ &= W_d + \sum_{\{i,j\}\in\mathcal{P}_3} \frac{|\boldsymbol{G}_{ij}-\boldsymbol{G}_{ij}^{(m)}|^2}{c_1^2} + \sum_{\{i,j\}\in\mathcal{P}_4} \frac{|\boldsymbol{G}_{ij}-\boldsymbol{G}_{ij}^{(m)}|^2}{c_1c_2} + \sum_{\{i,j\}\in\mathcal{P}_5} \frac{|\boldsymbol{G}_{ij}-\boldsymbol{G}_{ij}^{(m)}|^2}{c_2^2} \\ &\geq W_d \end{aligned} \tag{5.29}$$

Similarly, the second term is

$$\begin{aligned}
&\|\boldsymbol{\Omega}(\boldsymbol{G} - \boldsymbol{H}^s(\boldsymbol{G}^{(m)}))\boldsymbol{\Omega}\|_F^2 \\
&= \sum_{\{i,j\}\in\mathcal{P}_3} \frac{|\boldsymbol{G}_{ij}|^2}{c_1^2} + \sum_{\{i,j\}\in\mathcal{P}_4} \frac{|\boldsymbol{G}_{ij}|^2}{c_1 c_2} \\
&\quad + \sum_{\{i,j\}\in\mathcal{P}_1} \frac{|\boldsymbol{G}_{ij} - \boldsymbol{G}_{ij}^{(m)}|^2}{c_1^2} + \sum_{\{i,j\}\in\mathcal{P}_2\cup\mathcal{P}_5} \frac{|\boldsymbol{G}_{ij} - \boldsymbol{G}_{ij}^{(m)}|^2}{c_2^2} \\
&= W_s + \sum_{\{i,j\}\in\mathcal{P}_1} \frac{|\boldsymbol{G}_{ij} - \boldsymbol{G}_{ij}^{(m)}|^2}{c_1^2} + \sum_{\{i,j\}\in\mathcal{P}_2\cup\mathcal{P}_5} \frac{|\boldsymbol{G}_{ij} - \boldsymbol{G}_{ij}^{(m)}|^2}{c_2^2} \\
&\geq W_s
\end{aligned} \tag{5.30}$$

And the third term is

$$\begin{aligned}
&\|\boldsymbol{\Omega}(\boldsymbol{G} - \boldsymbol{H}^{ns}(\boldsymbol{G}^{(m)}))\boldsymbol{\Omega}\|_F^2 \\
&= \sum_{\{i,j\}\in\mathcal{P}_5} \frac{|\boldsymbol{G}_{ij}|^2}{c_2^2} + \sum_{\{i,j\}\in\mathcal{P}_1\cup\mathcal{P}_3} \frac{|\boldsymbol{G}_{ij} - \boldsymbol{G}_{ij}^{(m)}|^2}{c_1^2} \\
&\quad + \sum_{\{i,j\}\in\mathcal{P}_2} \frac{|\boldsymbol{G}_{ij} - \boldsymbol{G}_{ij}^{(m)}|^2}{c_2^2} + \sum_{\{i,j\}\in\mathcal{P}_4} \frac{|\boldsymbol{G}_{ij} - \boldsymbol{G}_{ij}^{(m)}|^2}{c_1 c_2} \\
&= W_{ns} + \sum_{\{i,j\}\in\mathcal{P}_1\cup\mathcal{P}_3} \frac{|\boldsymbol{G}_{ij} - \boldsymbol{G}_{ij}^{(m)}|^2}{c_1^2} \\
&\quad + \sum_{\{i,j\}\in\mathcal{P}_2} \frac{|\boldsymbol{G}_{ij} - \boldsymbol{G}_{ij}^{(m)}|^2}{c_2^2} + \sum_{\{i,j\}\in\mathcal{P}_4} \frac{|\boldsymbol{G}_{ij} - \boldsymbol{G}_{ij}^{(m)}|^2}{c_1 c_2} \\
&\geq W_{ns}
\end{aligned} \tag{5.31}$$

Since $c_1 > 0, c_2 > 0$, the summation of squared terms are greater or equal to zero. Combine (5.29), (5.30) and (5.31), and notice that the coefficient $\gamma \geq 0$ and $\alpha \geq 0$, we have $\forall \boldsymbol{G}$

$$g(\boldsymbol{G}|\boldsymbol{G}^{(m)}) \geq \gamma W_d + \alpha W_s + W_{ns} = f(\boldsymbol{G})$$

which shows the first property in (5.12) holds with respect to $g(\boldsymbol{G}|\boldsymbol{G}^{(m)})$.

The satisfaction of second property follows by our construction of $g(\boldsymbol{G}|\boldsymbol{G}^{(m)})$ such that

$$\begin{aligned} & g(\boldsymbol{G}^{(m)}|\boldsymbol{G}^{(m)}) \\ & = \gamma \|\boldsymbol{\Omega}(\boldsymbol{G}^{(m)} - \boldsymbol{H}^{d}(\boldsymbol{G}^{(m)}))\boldsymbol{\Omega}\|_F^2 \\ & \quad + \alpha \|\boldsymbol{\Omega}(\boldsymbol{G}^{(m)} - \boldsymbol{H}^{s}(\boldsymbol{G}^{(m)}))\boldsymbol{\Omega}\|_F^2 \\ & \quad + \|\boldsymbol{\Omega}(\boldsymbol{G}^{(m)} - \boldsymbol{H}^{ns}(\boldsymbol{G}^{(m)}))\boldsymbol{\Omega}\|_F^2 \\ & = f(\boldsymbol{G}^{(m)}) \end{aligned} \tag{5.32}$$

which follows directly from the definition of $g(\boldsymbol{G}|\boldsymbol{G}^{(m)})$ in (5.18) and $f(\boldsymbol{G})$ in (5.17). Because the two properties in (5.12) are all satisfied, $g(\boldsymbol{G}|\boldsymbol{G}^{(m)})$ is a valid surrogate function used for MM algorithm ■

5.7.2 Proof of Proposition 2

We prove the surrogate function (5.18) is minimized at $\boldsymbol{A}^{(m+1)}$ in (5.20).

Proof. We rewrite the surrogate function $g(\boldsymbol{G}|\boldsymbol{G}^{(m)})$ as following [108, 110]

$$\begin{aligned} & g(\boldsymbol{G}|\boldsymbol{G}^{(m)}) \\ & = \gamma \|\boldsymbol{\Omega}(\boldsymbol{G} - \boldsymbol{H}^{d}(\boldsymbol{G}^{(m)}))\boldsymbol{\Omega}\|_F^2 + \alpha \|\boldsymbol{\Omega}(\boldsymbol{G} - \boldsymbol{H}^{s}(\boldsymbol{G}^{(m)}))\boldsymbol{\Omega}\|_F^2 \\ & \quad + \|\boldsymbol{\Omega}(\boldsymbol{G} - \boldsymbol{H}^{ns}(\boldsymbol{G}^{(m)}))\boldsymbol{\Omega}\|_F^2 \\ & = \text{Trace}\Big((\gamma + \alpha + 1)(\boldsymbol{\Omega}\boldsymbol{G}^T\boldsymbol{\Omega}^2\boldsymbol{G}\boldsymbol{\Omega}) - 2\boldsymbol{\Omega}\big[\gamma \boldsymbol{H}^{d}(\boldsymbol{G}^{(m)})^T \\ & \quad + \alpha \boldsymbol{H}^{s}(\boldsymbol{G}^{(m)})^T + \boldsymbol{H}^{ns}(\boldsymbol{G}^{(m)})^T\big]\boldsymbol{\Omega}^2\boldsymbol{G}\boldsymbol{\Omega}\Big) + \text{Const} \\ & \equiv \text{Trace}\Big(\boldsymbol{\Omega}\boldsymbol{G}^T\boldsymbol{\Omega}^2\boldsymbol{G}\boldsymbol{\Omega} - 2\boldsymbol{\Omega}\boldsymbol{H}(\boldsymbol{G}^{(m)})\boldsymbol{\Omega}^2\boldsymbol{G}\boldsymbol{\Omega}\Big) \end{aligned} \tag{5.33}$$

where Const denotes some constant term which is irrelevant to $\boldsymbol{G}$. $\boldsymbol{H}(\boldsymbol{G}^{(m)})$ is defined as

$$\boldsymbol{H}(\boldsymbol{G}^{(m)}) := \frac{\gamma \boldsymbol{H}^d(\boldsymbol{G}^{(m)})^T + \alpha \boldsymbol{H}^s(\boldsymbol{G}^{(m)})^T + \boldsymbol{H}^{ns}(\boldsymbol{G}^{(m)})^T}{\gamma + \alpha + 1}$$

and the equivalence symbol $\equiv$ is with respect to the same result of minimizing $g(\boldsymbol{G}|\boldsymbol{G}^{(m)})$, since $\gamma + \alpha + 1 > 0$ and Const is independent of $\boldsymbol{G}$. Substituting $\boldsymbol{G} = \boldsymbol{D^T A^T A D}$ into (5.33), we have

$$\begin{aligned} g(\boldsymbol{G}|\boldsymbol{G}^{(m)}) &= \operatorname{Trace}\left(\boldsymbol{\Omega}^2 \boldsymbol{G}^T \boldsymbol{\Omega}^2 \boldsymbol{G} - 2\boldsymbol{\Omega}^2 \boldsymbol{H}(\boldsymbol{G}^{(m)}) \boldsymbol{\Omega}^2 \boldsymbol{G}\right) \\ &= \operatorname{Trace}\left(\boldsymbol{\Omega}^2 \boldsymbol{D}^T \boldsymbol{A}^T \boldsymbol{A} \boldsymbol{D} \boldsymbol{\Omega}^2 \boldsymbol{D}^T \boldsymbol{A}^T \boldsymbol{A} \boldsymbol{D} - 2\boldsymbol{\Omega}^2 \boldsymbol{H}(\boldsymbol{G}^{(m)}) \boldsymbol{\Omega}^2 \boldsymbol{D}^T \boldsymbol{A}^T \boldsymbol{A} \boldsymbol{D}\right) \\ &= \operatorname{Trace}\left(\boldsymbol{A} \boldsymbol{D} \boldsymbol{\Omega}^2 \boldsymbol{D}^T \boldsymbol{A}^T \boldsymbol{A} \boldsymbol{D} \boldsymbol{\Omega}^2 \boldsymbol{D}^T \boldsymbol{A}^T - 2\boldsymbol{A} \boldsymbol{D} \boldsymbol{\Omega}^2 \boldsymbol{H}(\boldsymbol{G}^{(m)}) \boldsymbol{\Omega}^2 \boldsymbol{D}^T \boldsymbol{A}^T\right) \end{aligned} \tag{5.34}$$

Let $\boldsymbol{U} \boldsymbol{\Lambda} \boldsymbol{U}^T$ be the eigenvalue decomposition of $\boldsymbol{D} \boldsymbol{\Omega}^2 \boldsymbol{D}^T$, it is reasonable to assume $\boldsymbol{D}$ has full row rank such that $\boldsymbol{\Lambda}$ has nonzero diagonal elements. Define $\boldsymbol{\Gamma} = \boldsymbol{A} \boldsymbol{U} \boldsymbol{\Lambda}^{\frac{1}{2}}$, so $\boldsymbol{A} = \boldsymbol{\Gamma} \boldsymbol{\Lambda}^{-\frac{1}{2}} \boldsymbol{U}^T$ and is one-to-one with $\boldsymbol{\Gamma}$. Then we have

$$\begin{aligned} g(\boldsymbol{G}|\boldsymbol{G}^{(m)}) &= \operatorname{Trace}\left(\boldsymbol{A} \boldsymbol{U} \boldsymbol{\Lambda} \boldsymbol{U}^T \boldsymbol{A}^T \boldsymbol{A} \boldsymbol{U} \boldsymbol{\Lambda} \boldsymbol{U}^T \boldsymbol{A}^T - 2\boldsymbol{A} \boldsymbol{D} \boldsymbol{\Omega}^2 \boldsymbol{H}(\boldsymbol{G}^{(m)}) \boldsymbol{\Omega}^2 \boldsymbol{D}^T \boldsymbol{A}^T\right) \\ &= \operatorname{Trace}\left(\boldsymbol{\Gamma} \boldsymbol{\Gamma}^T \boldsymbol{\Gamma} \boldsymbol{\Gamma}^T - 2\boldsymbol{\Gamma} \boldsymbol{\Lambda}^{-\frac{1}{2}} \boldsymbol{U}^T \boldsymbol{D} \boldsymbol{\Omega}^2 \boldsymbol{H}(\boldsymbol{G}^{(m)}) \boldsymbol{\Omega}^2 \boldsymbol{D}^T \boldsymbol{U} \boldsymbol{\Lambda}^{-\frac{1}{2}} \boldsymbol{\Gamma}^T\right) \\ &= \operatorname{Trace}\left(\boldsymbol{\Gamma}^T \boldsymbol{\Gamma} \boldsymbol{\Gamma}^T \boldsymbol{\Gamma} - 2\boldsymbol{\Lambda}^{-\frac{1}{2}} \boldsymbol{U}^T \boldsymbol{D} \boldsymbol{\Omega}^2 \boldsymbol{H}(\boldsymbol{G}^{(m)}) \boldsymbol{\Omega}^2 \boldsymbol{D}^T \boldsymbol{U} \boldsymbol{\Lambda}^{-\frac{1}{2}} \boldsymbol{\Gamma}^T \boldsymbol{\Gamma}\right) \\ &\equiv \|\boldsymbol{\Gamma}^T \boldsymbol{\Gamma} - \boldsymbol{\Lambda}^{-\frac{1}{2}} \boldsymbol{U}^T \boldsymbol{D} \boldsymbol{\Omega}^2 \boldsymbol{H}(\boldsymbol{G}^{(m)}) \boldsymbol{\Omega}^2 \boldsymbol{D}^T \boldsymbol{U} \boldsymbol{\Lambda}^{-\frac{1}{2}}\|_F^2 \end{aligned} \tag{5.35}$$

where the symbol $\equiv$ is with respect to the same optimization result by omitting terms that are independent of $\boldsymbol{\Gamma}$.

Let $\boldsymbol{H}'(\boldsymbol{G}^{(m)}) := \boldsymbol{\Lambda}^{-\frac{1}{2}} \boldsymbol{U}^T \boldsymbol{D} \boldsymbol{\Omega}^2 \boldsymbol{H}(\boldsymbol{G}^{(m)}) \boldsymbol{\Omega}^2 \boldsymbol{D}^T \boldsymbol{U} \boldsymbol{\Lambda}^{-\frac{1}{2}}$. Since $\boldsymbol{A}$ and $\boldsymbol{\Gamma}$ has one-to-one correspondence, the original problem of minimizing $g(\boldsymbol{G}|\boldsymbol{G}^{(m)})$ to get $\boldsymbol{A}$ can be reformulated as

$$\begin{aligned} \boldsymbol{\Gamma}^{(m+1)} &= \arg\min_{\boldsymbol{\Gamma}} \|\boldsymbol{\Gamma}^T\boldsymbol{\Gamma} - \boldsymbol{H}'(\boldsymbol{G}^{(m)})\|_F^2 \\ \boldsymbol{A}^{(m+1)} &= \boldsymbol{\Gamma}^{(m+1)}\boldsymbol{\Lambda}^{-\frac{1}{2}}\boldsymbol{U}^T \end{aligned} \tag{5.36}$$

Notice that $\boldsymbol{H}'(\boldsymbol{G}^{(m)})$ is an $N \times N$ matrix, while $\boldsymbol{\Gamma}$ is with size $T \times N$. Let $\boldsymbol{V}\boldsymbol{\Delta}\boldsymbol{V}^T$ be the eigenvalue decomposition of $\boldsymbol{H}'(\boldsymbol{G}^{(m)})$, then (5.36) can be solved in closed form as

$$\begin{aligned} \boldsymbol{\Gamma}^{(m+1)} &= \arg\min_{\boldsymbol{\Gamma}} \|\boldsymbol{\Gamma}^T\boldsymbol{\Gamma} - \boldsymbol{V}\boldsymbol{\Delta}\boldsymbol{V}^T\|_F^2 \\ &= \boldsymbol{\Delta}_T^{\frac{1}{2}}\boldsymbol{V}_T^T \end{aligned} \tag{5.37}$$

where $\boldsymbol{\Delta}_T$ denotes the $T \times T$ diagonal matrix that contains the largest T eigenvalues in $\boldsymbol{\Delta}$, and $\boldsymbol{V}_T$ denotes the corresponding T eigenvectors. Based on $\boldsymbol{\Gamma}^{(m+1)}$, we have

$$\boldsymbol{A}^{(m+1)} = \boldsymbol{\Delta}_T^{\frac{1}{2}}\boldsymbol{V}_T^T\boldsymbol{\Lambda}^{-\frac{1}{2}}\boldsymbol{U}^T \tag{5.38}$$

which is the sensing matrix that minimizes the surrogate function $g(\boldsymbol{G}|\boldsymbol{G}^{(m)})$ at the m-th step. ■

Bibliography

[1] T. L. Marzetta, "Noncooperative cellular wireless with unlimited numbers of base station antennas," *IEEE Trans. Wireless Commun.*, vol. 9, no. 11, pp. 3590–3600, Nov. 2010.

[2] E. G. Larsson, O. Edfors, F. Tufvesson, and T. L. Marzetta, "Massive MIMO for next generation wireless systems," *IEEE Commun. Mag.*, vol. 52, no. 2, pp. 186–195, Feb. 2014.

[3] A. F. Molisch, V. V. Ratnam, S. Han, Z. Li, S. L. H. Nguyen, L. Li, and K. Haneda, "Hybrid beamforming for massive MIMO: A survey," *IEEE Commun. Mag.*, vol. 55, no. 9, pp. 134–141, Sept. 2017.

[4] S. Jacobsson, G. Durisi, M. Coldrey, U. Gustavsson, and C. Studer, "Throughput analysis of massive MIMO uplink with low-resolution ADCs," *IEEE Trans. Wireless Commun.*, vol. 16, no. 6, pp. 4038–4051, June 2017.

[5] R. G. Baraniuk, "Compressive sensing," *IEEE Signal Process. Mag.*, vol. 24, no. 4, pp. 118–121, July 2007.

[6] E. J. Candès and M. B. Wakin, "An introduction to compressive sampling," *IEEE Signal Process. Mag.*, vol. 25, no. 2, pp. 21–30, Mar. 2008.

[7] M. Elad, *Sparse and Redundant Representations: From Theory to Applications in Signal and Image Processing*. Springer-Verlag New York, 2010.

[8] S. Foucart and H. Rauhut, *A Mathematical Introduction to Compressive Sensing*. Birkhäuser Basel, 2013.

[9] Y. C. Eldar and G. Kutyniok, *Compressed Sensing: Theory and Applications*. Cambridge University Press, 2012.

[10] J. A. Tropp and A. C. Gilbert, "Signal recovery from random measurements via orthogonal matching pursuit," *IEEE Trans. Inf. Theory*, vol. 53, no. 12, pp. 4655–4666, Dec. 2007.

[11] D. Needell and J. Tropp, "Cosamp: Iterative signal recovery from incomplete and inaccurate samples," *Appl. Comput. Harmon. Anal.*, vol. 26, no. 3, pp. 301 – 321, 2009.

[12] S. S. Chen, D. L. Donoho, and M. A. Saunders, “Atomic decomposition by basis pursuit,” *SIAM J. Sci. Comput.*, vol. 20, no. 1, pp. 33–61, 1998.

[13] A. Beck and M. Teboulle, “A fast iterative shrinkage-thresholding algorithm for linear inverse problems,” *SIAM J. Imag. Sci.*, vol. 2, no. 1, pp. 183–202, 2009.

[14] E. J. Candès, M. B. Wakin, and S. P. Boyd, “Enhancing sparsity by reweighted ℓ_1 minimization,” *Journal of Fourier Analysis and Applications*, vol. 14, no. 5, pp. 877–905, Dec. 2008.

[15] R. Chartrand and W. Yin, “Iteratively reweighted algorithms for compressive sensing,” in *Proc. IEEE Int. Conf. Acoust., Speech, Signal Process. (ICASSP)*, Mar. 2008, pp. 3869–3872.

[16] I. F. Gorodnitsky and B. D. Rao, “Sparse signal reconstruction from limited data using focuss: a re-weighted minimum norm algorithm,” *IEEE Trans. Signal Process.*, vol. 45, no. 3, pp. 600–616, Mar. 1997.

[17] D. L. Donoho, A. Maleki, and A. Montanari, “Message-passing algorithms for compressed sensing,” *Proceedings of the National Academy of Sciences*, vol. 106, no. 45, pp. 18 914–18 919, Nov. 2009.

[18] S. Rangan, “Generalized approximate message passing for estimation with random linear mixing,” in *Proc. IEEE Int. Symp. Inf. Theory*, July 2011, pp. 2168–2172.

[19] M. E. Tipping, “Sparse Bayesian learning and the relevance vector machine,” *J. Mach. Learn. Res.*, vol. 1, pp. 211–244, Sept. 2001.

[20] D. P. Wipf and B. D. Rao, “Sparse Bayesian learning for basis selection,” *IEEE Trans. Signal Process.*, vol. 52, no. 8, pp. 2153–2164, Aug. 2004.

[21] S. Ji, Y. Xue, and L. Carin, “Bayesian compressive sensing,” *IEEE Trans. Signal Process.*, vol. 56, no. 6, pp. 2346–2356, June 2008.

[22] D. Shutin and B. H. Fleury, “Sparse variational Bayesian SAGE algorithm with application to the estimation of multipath wireless channels,” *IEEE Trans. Signal Process.*, vol. 59, no. 8, pp. 3609–3623, Aug. 2011.

[23] J. P. Vila and P. Schniter, “Expectation-maximization Gaussian-mixture approximate message passing,” *IEEE Trans. Signal Process.*, vol. 61, no. 19, pp. 4658–4672, Oct. 2013.

[24] D. L. Donoho and M. Elad, “Optimally sparse representation in general (nonorthogonal) dictionaries via ℓ_1 minimization,” *Proc. Nat. Acad. Sci.*, vol. 100, no. 5, pp. 2197–2202, 2003.

[25] E. J. Candes, J. Romberg, and T. Tao, “Robust uncertainty principles: exact signal reconstruction from highly incomplete frequency information,” *IEEE Trans. Inf. Theory*, vol. 52, no. 2, pp. 489–509, Feb. 2006.

[26] T. L. Marzetta, "How much training is required for multiuser MIMO?" in *Proc. 40th Asilomar Conf. Signals Syst. Comput.* IEEE, Oct. 2006, pp. 359–363.

[27] A. Adhikary, J. Nam, J. Y. Ahn, and G. Caire, "Joint spatial division and multiplexing — the large-scale array regime," *IEEE Trans. Inf. Theory*, vol. 59, no. 10, pp. 6441–6463, Oct. 2013.

[28] X. Rao and V. K. N. Lau, "Distributed compressive CSIT estimation and feedback for FDD multi-user massive MIMO systems," *IEEE Trans. Signal Process.*, vol. 62, no. 12, pp. 3261–3271, June 2014.

[29] W. U. Bajwa, J. Haupt, A. M. Sayeed, and R. Nowak, "Compressed channel sensing: A new approach to estimating sparse multipath channels," *Proc. IEEE*, vol. 98, no. 6, pp. 1058–1076, June 2010.

[30] A. M. Sayeed, "Deconstructing multiantenna fading channels," *IEEE Trans. Signal Process.*, vol. 50, no. 10, pp. 2563–2579, Oct. 2002.

[31] D. Tse and P. Viswanath, *Fundamentals of Wireless Communication.* Cambridge University Press, 2005.

[32] Z. Gao, L. Dai, Z. Wang, and S. Chen, "Spatially common sparsity based adaptive channel estimation and feedback for FDD massive MIMO," *IEEE Trans. Signal Process.*, vol. 63, no. 23, pp. 6169–6183, Dec. 2015.

[33] S. L. H. Nguyen and A. Ghrayeb, "Compressive sensing-based channel estimation for massive multiuser MIMO systems," in *Proc. IEEE Wireless Commun. Netw. Conf. (WCNC)*, Apr. 2013, pp. 2890–2895.

[34] Y. Ding, S. E. Chiu, and B. D. Rao, "Bayesian channel estimation algorithms for massive MIMO systems with hybrid analog-digital processing and low-resolution ADCs," *IEEE J. Sel. Topics Signal Process.*, vol. 12, no. 3, pp. 499–513, June 2018.

[35] 3GPP, "Spatial channel model for multiple input multiple output (MIMO) simulations," 3rd Generation Partnership Project (3GPP), TR 25.996 version 12.0.0 Release 12, Sep. 2014.

[36] D. Ying, F. W. Vook, T. A. Thomas, D. J. Love, and A. Ghosh, "Kronecker product correlation model and limited feedback codebook design in a 3D channel model," in *Proc. IEEE Int. Conf. Commun. (ICC)*, June 2014, pp. 5865–5870.

[37] 3GPP, "Study on channel model for frequencies from 0.5 to 100 GHz," 3rd Generation Partnership Project (3GPP), TR 38.901 version 14.0.0 Release 14, May 2017.

[38] A. F. Molisch, A. Kuchar, J. Laurila, K. Hugl, and R. Schmalenberger, "Geometry-based directional model for mobile radio channels—principles and implementation," *Eur. Trans. Telecommun.*, vol. 14, no. 4, pp. 351–359, 2003.

[39] J. W. Choi, B. Shim, Y. Ding, B. Rao, and D. I. Kim, “Compressed sensing for wireless communications: Useful tips and tricks,” *IEEE Commun. Surveys Tut.*, vol. 19, no. 3, pp. 1527–1550, Feb. 2017.

[40] S. F. Cotter, B. D. Rao, K. Engan, and K. Kreutz-Delgado, “Sparse solutions to linear inverse problems with multiple measurement vectors,” *IEEE Trans. Signal Process.*, vol. 53, no. 7, pp. 2477–2488, July 2005.

[41] J. A. Tropp, A. C. Gilbert, and M. J. Strauss, “Algorithms for simultaneous sparse approximation: Part I: Greedy pursuit,” *Signal Process.*, vol. 86, no. 3, pp. 572–588, Mar. 2006.

[42] D. P. Wipf and B. D. Rao, “An empirical bayesian strategy for solving the simultaneous sparse approximation problem,” *IEEE Trans. Signal Process.*, vol. 55, no. 7, pp. 3704–3716, 2007.

[43] Z. Zhang and B. D. Rao, “Sparse signal recovery with temporally correlated source vectors using sparse Bayesian learning,” *IEEE J. Sel. Topics Signal Process.*, vol. 5, no. 5, pp. 912–926, Sept. 2011.

[44] Y. Ding, S. E. Chiu, and B. D. Rao, “Sparse recovery with quantized multiple measurement vectors,” in *Proc. 51st Asilomar Conf. Signals Syst. Comput.*, Oct. 2017, pp. 845–849.

[45] A. Liu, F. Zhu, and V. K. N. Lau, “Closed-loop autonomous pilot and compressive CSIT feedback resource adaptation in multi-user FDD massive MIMO systems,” *IEEE Trans. Signal Process.*, vol. 65, no. 1, pp. 173–183, Jan. 2017.

[46] S. Jokar and V. Mehrmann, “Sparse solutions to underdetermined Kronecker product systems,” *Linear Algebra Appl.*, vol. 431, no. 12, pp. 2437–2447, Dec. 2009.

[47] J. Hoydis, S. ten Brink, and M. Debbah, “Massive MIMO in the UL/DL of cellular networks: How many antennas do we need?” *IEEE J. Sel. Areas Commun.*, vol. 31, no. 2, pp. 160–171, Feb. 2013.

[48] T. Strohmer and R. W. Heath, “Grassmannian frames with applications to coding and communication,” *Appl. Comput. Harmon. Anal.*, vol. 14, no. 3, pp. 257–275, May 2003.

[49] J. A. Tropp, I. S. Dhillon, R. W. Heath, and T. Strohmer, “Designing structured tight frames via an alternating projection method,” *IEEE Trans. Inf. Theory*, vol. 51, no. 1, pp. 188–209, Jan. 2005.

[50] M. Elad, “Optimized projections for compressed sensing,” *IEEE Trans. Signal Process.*, vol. 55, no. 12, pp. 5695–5702, Dec. 2007.

[51] H. Yin, D. Gesbert, M. Filippou, and Y. Liu, “A coordinated approach to channel estimation in large-scale multiple-antenna systems,” *IEEE J. Sel. Areas Commun.*, vol. 31, no. 2, pp. 264–273, Feb. 2013.

[52] Y. Ding and B. D. Rao, “Compressed downlink channel estimation based on dictionary learning in FDD massive MIMO systems,” in *Proc. IEEE Global Commun. Conf. (GLOBECOM)*, Dec. 2015, pp. 1–6.

[53] ——, “Channel estimation using joint dictionary learning in FDD massive MIMO systems,” in *Proc. IEEE Glob. Conf. Signal Inf. Process. (GlobalSIP)*, Dec. 2015, pp. 185–189.

[54] K. Venugopal, A. Alkhateeb, N. G. Prelcic, and R. W. Heath, “Channel estimation for hybrid architecture-based wideband millimeter wave systems,” *IEEE J. Sel. Areas Commun.*, vol. 35, no. 9, pp. 1996–2009, Sept. 2017.

[55] Y. Han, J. Lee, and D. J. Love, “Compressed sensing-aided downlink channel training for FDD massive MIMO systems,” *IEEE Trans. Commun.*, vol. 65, no. 7, pp. 2852–2862, July 2017.

[56] P. Schniter and A. Sayeed, “Channel estimation and precoder design for millimeter-wave communications: The sparse way,” in *Proc. 48th Asilomar Conf. Signals Syst. Comput.*, Nov. 2014, pp. 273–277.

[57] K. Engan, S. O. Aase, and J. H. Husoy, “Method of optimal directions for frame design,” in *Proc. IEEE Int. Conf. Acoust., Speech, Signal Process. (ICASSP)*, Mar. 1999, pp. 2443–2446.

[58] K. Kreutz-Delgado, J. F. Murray, B. D. Rao, K. Engan, T.-W. Lee, and T. J. Sejnowski, “Dictionary learning algorithms for sparse representation,” *Neural Comput.*, vol. 15, no. 2, pp. 349–396, 2003.

[59] M. Aharon, M. Elad, and A. Bruckstein, “K-SVD: An algorithm for designing overcomplete dictionaries for sparse representation,” *IEEE Trans. Signal Process.*, vol. 54, no. 11, pp. 4311–4322, Nov. 2006.

[60] A. J. Paulraj and C. B. Papadias, “Space-time processing for wireless communications,” *IEEE Signal Process. Mag.*, vol. 14, no. 6, pp. 49–83, 1997.

[61] K. Hugl, K. Kalliola, and J. Laurila, “Spatial reciprocity of uplink and downlink radio channels in FDD systems,” in *Proc. COST 273 Technical Document TD (02) 066*, May 2002.

[62] P. Zetterberg and B. Ottersten, “The spectrum efficiency of a base station antenna array system for spatially selective transmission,” *IEEE Trans. Veh. Technol.*, vol. 44, no. 3, pp. 651–660, Aug. 1995.

[63] K. Hugl, J. Laurila, and E. Bonek, “Downlink beamforming for frequency division duplex systems,” in *Proc. IEEE Global Commun. Conf. (GLOBECOM)*. IEEE, Dec. 1999, pp. 2097–2101.

[64] P. Tseng, “Convergence of a block coordinate descent method for nondifferentiable minimization,” *J. Optim. theory Appl.*, vol. 109, no. 3, pp. 475–494, June 2001.

[65] B. A. Olshausen and D. J. Field, “Sparse coding with an overcomplete basis set: A strategy employed by v1?” *Vision Res.*, vol. 37, no. 23, pp. 3311 – 3325, 1997.

[66] M. S. Lewicki and B. A. Olshausen, “Probabilistic framework for the adaptation and comparison of image codes,” *J. Opt. Soc. Am. A*, vol. 16, no. 7, pp. 1587–1601, Jul 1999.

[67] R. Remi and K. Schnass, “Dictionary identification — sparse matrix-factorization via ℓ_1-minimization,” *IEEE Trans. Inf. Theory*, vol. 56, no. 7, pp. 3523–3539, July 2010.

[68] M. F. Duarte, S. Sarvotham, D. Baron, M. B. Wakin, and R. G. Baraniuk, “Distributed compressed sensing of jointly sparse signals,” in *Proc. 39th Asilomar Conf. Signals Syst. Comput.*, Oct. 2005, pp. 1537–1541.

[69] M. Yuan and Y. Lin, “Model selection and estimation in regression with grouped variables,” *J. Roy. Statist. Soc. B, Statist. Methodol.*, vol. 68, no. 1, pp. 49–67, 2006.

[70] Y. Ding and B. D. Rao, “Joint dictionary learning and recovery algorithms in a jointly sparse framework,” in *Proc. 49th Asilomar Conf. Signals Syst. Comput.*, Nov 2015, pp. 1482–1486.

[71] S. Ji, D. Dunson, and L. Carin, “Multitask compressive sensing,” *IEEE Trans. Signal Process.*, vol. 57, no. 1, pp. 92–106, 2009.

[72] M. K. Samimi and T. S. Rappaport, “3-D millimeter-wave statistical channel model for 5G wireless system design,” *IEEE Trans. Microw. Theory Techn.*, vol. 64, no. 7, pp. 2207–2225, July 2016.

[73] E. van den Berg and M. P. Friedlander, “Probing the Pareto frontier for basis pursuit solutions,” *SIAM J. Sci. Comput.*, vol. 31, no. 2, pp. 890–912, 2008.

[74] W. A. Hapsari, A. Umesh, M. Iwamura, M. Tomala, B. Gyula, and B. Sebire, “Minimization of drive tests solution in 3GPP,” *IEEE Commun. Mag.*, vol. 50, no. 6, pp. 28–36, June 2012.

[75] J. Mairal, F. Bach, J. Ponce, and G. Sapiro, “Online dictionary learning for sparse coding,” in *Proc. 26th Annu. Int. Conf. Mach. Learn. (ICML).* ACM, June 2009, pp. 689–696.

[76] A. Alkhateeb, O. E. Ayach, G. Leus, and R. W. Heath, “Channel estimation and hybrid precoding for millimeter wave cellular systems,” *IEEE J. Sel. Topics Signal Process.*, vol. 8, no. 5, pp. 831–846, Oct. 2014.

[77] H. Ghauch, T. Kim, M. Bengtsson, and M. Skoglund, “Subspace estimation and decomposition for large millimeter-wave MIMO systems,” *IEEE J. Sel. Topics Signal Process.*, vol. 10, no. 3, pp. 528–542, Apr. 2016.

[78] Z. Gao, C. Hu, L. Dai, and Z. Wang, "Channel estimation for millimeter-wave massive MIMO with hybrid precoding over frequency-selective fading channels," *IEEE Commun. Lett.*, vol. 20, no. 6, pp. 1259–1262, June 2016.

[79] C. Mollén, J. Choi, E. G. Larsson, and R. W. Heath, "Uplink performance of wideband massive MIMO with one-bit ADCs," *IEEE Trans. Wireless Commun.*, vol. 16, no. 1, pp. 87–100, Jan. 2017.

[80] Y. Li, C. Tao, G. Seco-Granados, A. Mezghani, A. L. Swindlehurst, and L. Liu, "Channel estimation and performance analysis of one-bit massive MIMO systems," *IEEE Trans. Signal Process.*, vol. 65, no. 15, pp. 4075–4089, Aug. 2017.

[81] T. M. Lok and V. K. W. Wei, "Channel estimation with quantized observations," in *Proc. IEEE Int. Symp. Inf. Theory (ISIT)*, Aug. 1998, p. 333.

[82] A. Mezghani, F. Antreich, and J. A. Nossek, "Multiple parameter estimation with quantized channel output," in *Proc. Int. ITG Workshop on Smart Antennas (WSA)*, Feb. 2010, pp. 143–150.

[83] J. Mo, P. Schniter, N. G. Prelcic, and R. W. Heath, "Channel estimation in millimeter wave MIMO systems with one-bit quantization," in *Proc. 48th Asilomar Conf. Signals Syst. Comput.*, Nov. 2014, pp. 957–961.

[84] C. Studer and G. Durisi, "Quantized massive MU-MIMO-OFDM uplink," *IEEE Trans. Commun.*, vol. 64, no. 6, pp. 2387–2399, June 2016.

[85] A. Zymnis, S. Boyd, and E. Candès, "Compressed sensing with quantized measurements," *IEEE Signal Process. Lett.*, vol. 17, no. 2, pp. 149–152, Feb. 2010.

[86] U. S. Kamilov, V. K. Goyal, and S. Rangan, "Message-passing de-quantization with applications to compressed sensing," *IEEE Trans. Signal Process.*, vol. 60, no. 12, pp. 6270–6281, Dec. 2012.

[87] C. K. Wen, C. J. Wang, S. Jin, K. K. Wong, and P. Ting, "Bayes-optimal joint channel-and-data estimation for massive MIMO with low-precision ADCs," *IEEE Trans. Signal Process.*, vol. 64, no. 10, pp. 2541–2556, May 2016.

[88] L. Jacques, J. N. Laska, P. T. Boufounos, and R. G. Baraniuk, "Robust 1-bit compressive sensing via binary stable embeddings of sparse vectors," *IEEE Trans. Inf. Theory*, vol. 59, no. 4, pp. 2082–2102, Apr. 2013.

[89] Y. Plan and R. Vershynin, "Robust 1-bit compressed sensing and sparse logistic regression: A convex programming approach," *IEEE Trans. Inf. Theory*, vol. 59, no. 1, pp. 482–494, Jan. 2013.

[90] Z. Yang, L. Xie, and C. Zhang, "Variational Bayesian algorithm for quantized compressed sensing," *IEEE Trans. Signal Process.*, vol. 61, no. 11, pp. 2815–2824, June 2013.

[91] R. Prasad, C. R. Murthy, and B. D. Rao, “Joint approximately sparse channel estimation and data detection in OFDM systems using sparse Bayesian learning,” *IEEE Trans. Signal Process.*, vol. 62, no. 14, pp. 3591–3603, July 2014.

[92] ——, “Joint channel estimation and data detection in MIMO-OFDM systems: A sparse Bayesian learning approach,” *IEEE Trans. Signal Process.*, vol. 63, no. 20, pp. 5369–5382, Oct. 2015.

[93] S. Jacobsson, G. Durisi, M. Coldrey, U. Gustavsson, and C. Studer, “One-bit massive MIMO: Channel estimation and high-order modulations,” in *Proc. IEEE Int. Conf. Commun. Workshop (ICCW)*, June 2015, pp. 1304–1309.

[94] D. Chu, “Polyphase codes with good periodic correlation properties,” *IEEE Trans. Inf. Theory*, vol. 18, no. 4, pp. 531–532, July 1972.

[95] A. Liu and V. Lau, “Phase only RF precoding for massive MIMO systems with limited RF chains,” *IEEE Trans. Signal Process.*, vol. 62, no. 17, pp. 4505–4515, Sept. 2014.

[96] O. E. Ayach, S. Rajagopal, S. Abu-Surra, Z. Pi, and R. W. Heath, “Spatially sparse precoding in millimeter wave MIMO systems,” *IEEE Trans. Wireless Commun.*, vol. 13, no. 3, pp. 1499–1513, March 2014.

[97] Y. Ding and B. D. Rao, “Dictionary learning-based sparse channel representation and estimation for FDD massive MIMO systems,” *IEEE Trans. Wireless Commun.*, in press.

[98] C. Bishop and M. E. Tipping, “Variational relevance vector machines,” in *Proc. 16th Conference on Uncertainty in Artificial Intelligence*, Jan. 2000, pp. 46–53.

[99] M. J. Beal, *Variational algorithms for approximate Bayesian inference*. University of London, London, 2003.

[100] J. Winn and C. M. Bishop, “Variational message passing,” *J. Mach. Learn. Res.*, vol. 6, pp. 661–694, Apr. 2005.

[101] D. J. C. MacKay, “Bayesian interpolation,” *Neural Comput.*, vol. 4, no. 3, pp. 415–447, May 1992.

[102] N. Johnson, S. Kotz, and N. Balakrishnan, *Continuous Univariate Probability Distributions*. John Wiley & Sons Inc., 1994.

[103] L. Gammaitoni, “Stochastic resonance and the dithering effect in threshold physical systems,” *Phys. Rev. E*, vol. 52, pp. 4691–4698, Nov. 1995.

[104] T. Goldstein, C. Studer, and R. Baraniuk, “A field guide to forward-backward splitting with a FASTA implementation,” *arXiv preprint arXiv:1411.3406*, 2014.

[105] M. E. Tipping and A. C. Faul, “Fast marginal likelihood maximisation for sparse Bayesian models,” in *Proc. 9th Int. Workshop Artif. Intell. Statist.*, 2003, pp. 3–6.

[106] M. Al-Shoukairi, P. Schniter, and B. D. Rao, "A GAMP-based low complexity sparse Bayesian learning algorithm," *IEEE Trans. Signal Process.*, vol. 66, no. 2, pp. 294–308, Jan. 2018.

[107] E. J. Candes, Y. C. Eldar, D. Needell, and P. Randall, "Compressed sensing with coherent and redundant dictionaries," *Appl. Comput. Harmon. Anal.*, vol. 31, no. 1, pp. 59–73, 2011.

[108] J. M. Duarte-Carvajalino and G. Sapiro, "Learning to sense sparse signals: Simultaneous sensing matrix and sparsifying dictionary optimization," *IEEE Trans. Image Process.*, vol. 18, no. 7, pp. 1395–1408, July 2009.

[109] Y. Yu, A. P. Petropulu, and H. V. Poor, "Measurement matrix design for compressive sensing-based MIMO radar," *IEEE Trans. Signal Process.*, vol. 59, no. 11, pp. 5338–5352, Nov. 2011.

[110] L. Zelnik-Manor, K. Rosenblum, and Y. C. Eldar, "Sensing matrix optimization for block-sparse decoding," *IEEE Trans. Signal Process.*, vol. 59, no. 9, pp. 4300–4312, Sept. 2011.

[111] V. Abolghasemi, S. Ferdowsi, and S. Sanei, "A gradient-based alternating minimization approach for optimization of the measurement matrix in compressive sensing," *Signal Process.*, vol. 92, no. 4, pp. 999 – 1009, 2012.

[112] M. L. Malloy and R. D. Nowak, "Near-optimal adaptive compressed sensing," *IEEE Trans. Inf. Theory*, vol. 60, no. 7, pp. 4001–4012, July 2014.

[113] J. Haupt, R. Baraniuk, R. Castro, and R. Nowak, "Sequentially designed compressed sensing," in *Proc. IEEE Statist. Signal Process. Workshop (SSP)*, Aug. 2012, pp. 401–404.

[114] M. P. Friedlander, H. Mansour, R. Saab, and O. Yilmaz, "Recovering compressively sampled signals using partial support information," *IEEE Trans. Inf. Theory*, vol. 58, no. 2, pp. 1122–1134, Feb. 2012.

[115] N. Vaswani and W. Lu, "Modified-CS: Modifying compressive sensing for problems with partially known support," *IEEE Trans. Signal Process.*, vol. 58, no. 9, pp. 4595–4607, Sept 2010.

[116] Z. Wang, G. R. Arce, and J. L. Paredes, "Colored random projections for compressed sensing," in *Proc. IEEE Int. Conf. Acoust., Speech, Signal Process. (ICASSP)*, vol. 3, Apr. 2007, pp. 873–876.

[117] J. A. Tropp, "Greed is good: algorithmic results for sparse approximation," *IEEE Trans. Inf. Theory*, vol. 50, no. 10, pp. 2231–2242, Oct. 2004.

[118] D. R. Hunter and K. Lange, "A tutorial on MM algorithms," *Am. Statist.*, vol. 58, no. 1, pp. 30–37, 2004.

[119] M. A. T. Figueiredo, J. M. Bioucas-Dias, and R. D. Nowak, “Majorization-minimization algorithms for wavelet-based image restoration,” *IEEE Trans. Image Process.*, vol. 16, no. 12, pp. 2980–2991, Dec. 2007.

[120] D. L. Donoho, M. Elad, and V. N. Temlyakov, “Stable recovery of sparse overcomplete representations in the presence of noise,” *IEEE Trans. Inf. Theory*, vol. 52, no. 1, pp. 6–18, Jan. 2006.

[121] J. A. Tropp, “Just relax: convex programming methods for identifying sparse signals in noise,” *IEEE Trans. Inf. Theory*, vol. 52, no. 3, pp. 1030–1051, Mar. 2006.